Gas and Plasma structures

Aldo Conti

August 2004

Contents

1 Gas and plasma structures 5
- 1.1 Natural and artificial gas structures on our planet 7
  - 1.1.1 Mirages 9
- 1.2 Structures in the Solar System 15
- 1.3 Space structures 22
- 1.4 Shocks 22
- 1.5 Gas clouds 24
- 1.6 Explosions 26
  - 1.6.1 Novas 26
  - 1.6.2 Supernovas 28
  - 1.6.3 Hypernovas 35
  - 1.6.4 Planetary nebulae 37
- 1.7 Galaxies 45
- 1.8 Gas and plasma structures in laboratories 46
  - 1.8.1 Magnetically confined plasmas 47

2 Particle acceleration in plasmas 54
- 2.1 Beat wave accelerator 57
  - 2.1.1 Experimental results 59
- 2.2 Laser wake field accelerator 60
  - 2.2.1 Experimental results 62
- 2.3 Self Modulated Laser Wake Field Accelerator (SMLWF) . . . 62
  - 2.3.1 Experimental results 63
- 2.4 Laser guiding 63
  - 2.4.1 Experimental results 66
  - 2.4.2 Improved laser guiding 66
- 2.5 Conclusion 68

3 Experimental setup **70**
3.1 Production . . . 71
3.1.1 Spherical shocks . . . 71
3.1.2 Cylindrical shocks . . . 73
3.2 Propagation . . . 77
3.3 The image acquisition system . . . 79
3.4 The optical setup . . . 82
3.5 The circuit . . . 83

4 Gas pipes **89**
4.1 Electron density gradient . . . 91
4.2 Experimental set up . . . 94
4.2.1 Cylindrical shocks . . . 95
4.2.2 Different foci . . . 100
4.3 The cylindrical gas pipe . . . 104
4.4 Experimental problems . . . 109
4.4.1 Debris . . . 109
4.5 Conclusions . . . 124

5 Colliding shock lenses **127**
5.1 Experimental set-up . . . 133
5.1.1 Speed measurement . . . 143
5.2 Experimental results . . . 144
5.2.1 Laser anomaly . . . 168
5.3 Applications . . . 168

6 The nitrogen laser **169**
6.0.1 The classic laser . . . 170
6.0.2 The parabolic laser . . . 173
6.1 Experimental results . . . 178
6.2 Multilayer laser . . . 184

7 Simulations **188**
7.1 Ray tracing . . . 190
7.2 Shock shape . . . 193

8 Conclusions **197**

List of Figures

1.1 Two spectacular images of lighting. They produce powerful shock waves, that degenerate quickly into acoustic waves. (Author unknown) 8

1.2 The inferior mirage produces the well known water effect on a hot surface, like asphalt in a sunny day. (Author unknown) . . 10

1.3 The cold seas of the northern Europe are ideal places to observe superior mirages. In spring there is very often a layer of warm air coming from the land above the still icy cold waters. These two pictures where obtained in Sweden. (Author unknown) 12

1.4 A spectacular example of a superior mirage. (Author unknown) 13

1.5 Another example of a superior mirage, observed in Antarctica.(Picture thanks to Jack Stephens) 14

1.6 The solar wind flowing around the magnetic field of the Earth and the van Allen belts. (Image European Space Agency) . . . 16

1.7 Jupiter and its famous Great Red Spot, in this picture obtained by the Hubble Space Telescope (www.stsci.edu). 18

1.8 A composite image of our Sun obtained by the SOHO probe (sohowww.estec.esa.nl). The left part shows the surface of the Sun as it appears in visible light, the right part in the Hydrogen α line. Some protuberances are visible, large fountains (structures) of plasma that erupt from the surface pushed by powerful magnetic fields. 21

1.9 A picture of the central part of the famous Orion nebula. It is a very big nebula relatively close to our planet. The centre of the nebula is hidden by another cloud of dust and is visible only in radio waves (www.stsci.edu). 25

1.10 An image of the Nova Velorum 1999. This nova was perfectly visible with the naked eye from Durban during the month of may 1999. I estimated the brightness to magnitude 4.5 only a few days after the explosion, but the nova had reached magnitude 3. 27
1.11 This picture shows the Crab Nebula, a remnant of a supernova which exploded in the year 1054 and was observed by Chinese astronomers. The picture was taken with one of the 8.2 m telescopes of the Very Large Telescope of the European Southern Observatory. 29
1.12 Four images of the evolution of the supernova SN1987a during the first ten years since the explosion. 33
1.13 Eta Carinae, a good supernova candidate imaged by the Hubble Space Telescope. 34
1.14 Two hypernova remnants observed by the Hubble Space Telescope in the galaxy M101. 36
1.15 Hen-1357, the youngest known planetary nebula. 38
1.16 MyCn18, known as the Hourglass nebula for obvious reasons. . 40
1.17 Another interesting example of planetary nebula. 41
1.18 The Cygnus Veil. 43
1.19 The famous double spiral M51, in the constellation of Canes Venatici. It is clearly visible the bridge of matter that joins the two interacting galaxies. (Image Hubble Space Telescope) 45
1.20 Schematic of a toroidal magnetic confinement system showing the basic magnetic geometry. The major and minor radii (R and r) are labelled together with the poloidal and toroidal magnetic field $\vec{B}_{pol}$ and $\vec{B}_{tor}$. A toroidal plasma current may also be present. 48
1.21 Schematic of the Stellarator Wendelstein VII-A. 52

2.1 This graph from A. Ogata of the National Laboratory for High Energy Physics, Japan, explains clearly the generation of plasma waves in different accelerators. The background intensity shows the plasma density, the balls show the particle bunches and the solid lines show the laser intensity. 61

3.1 Shock wave production by means of facing pins. It can be noted that all but the first and the last pins are left floating. The voltage is applied between the first and the last pin by mean of an inductor or a resistor (see figure 3.10 on page 88). The voltage propagates by induction to the other pins. The pairs could be driven in parallel, but this makes more difficult to synchronise the discharges. When the discharge is very fast, each arc is like a small explosion and produces a shock wave. . 72

3.2 An oscilloscope trace of one of our pipe experiments. The actual explosion is the second peak from the left in the top trace. It is interesting to note that, despite our wire was made with an unknown alloy, the explosion time is comparable with the calculated ones. 77

3.3 The "detector" used during our experiments. The photographic paper is placed into the box. On the right, a lens focuses the beam into a little hole and the light is then filtered through a UV filter. In this way, we avoid the light from the explosion of the wire. 81

3.4 The diagnostic nitrogen laser used in our experiment. We had to put a small shutter in front of it because it often self triggers. 83

3.5 The simple optics of the experiment. The two lenses of the beam collimator, on the right, have a focal length of 5 cm and 50 cm respectively. The lens used for the filter has a focal length of 10 cm. 84

3.6 The main remote controls of the experiment. The orange box is our delay box and, above it, there are the power supply of the optical trigger and the controls of the power supply. 85

3.7 The main circuit of the experiment. 86

3.8 The circuit used in most of our experiment. The power supply is in the top right corner of the picture. It can be seen that the power supply is connected to the capacitor through two resistors and a "pan cake" inductor used as protection. The spark gap is above the capacitor and the high voltage probe (red) can be seen. 87

3.9 The High Voltage circuit of the pipe experiment. The inductor and the resistor are there only to protect the power supply from the high voltage spikes generated during the discharge. Their value is not important and has not been recorded. The value of the capacity was 1 μF. 88

3.10 The High Voltage circuit of the CSL experiment. It can be noted this circuit is almost identical to the pipe experiment circuit (figure 3.9 on page 88) and, as in that case, the values of the resistor an the inductor has not been recorded. The only difference is that in this case there is a coil connected in parallel to the CSL. The coil carries the voltage across the device, that otherwise would be an open circuit. For the capacity we used values of 1, 4 and 8 μF 88

4.1 The diagnostic setup for the pipe experiment. From the left, the two lenses used for the telescope have a focal length of 5 cm and 50 cm. The lens used for the "spatial filter" has a focal length of 10 cm. 96

4.2 A SEM image of a piece of the wire used during the experiment. It can be noted that the wire has a thickness of about 130 μm. In order to be sure that the thickness of the wire was uniform, we took several images of different pieces of wire. . . 97

4.3 The single strong shock coming from the coil, due probably to the jumping of the arc across the coils. The shock is travelling toward the top of the picture. Turbulence left behind by the shocks is clearly visible. This is a clear sign of the energy being too high. The white circle is the cylinder of paper used to hold the wire, that is usually blown away by the explosion. It should be noted that all our pictures have a negative grayscale, so the highest light intensity corresponds to the blackest parts of the image. 99

4.4 The line focus with two shocks. The shocks have already collided in the centre. Many secondary shocks are visible. 101

4.5 Four pictures of the square pipe. a) the four shocks coming to the centre; b) the short side of this square pipe is about 5 mm long. c) The moment of the collision; the pipe is not visible, as the shocks collide in the centre at the same time. d) The moment immediately after the collision. The square pipe focusing the light; the light is refracted to the centre of the image, which appears darker. Between the first and the last image, the delay is about 6 μs.Though square pipes are unlikely to be useful, this demonstrates the ability of colliding shocks to produce channels. 103
4.6 The wire holder used for the experiment. The two disks on both sides protect the optics from the debris ejected by the exploding wire. 104
4.7 Four pictures of an early series of experiments with eight wires. All these images were obtained before the shock waves collided in the centre. This pictures were obtained with too much energy (265 J) and it was never possible to observe a pipe after collision. The delay between (a) and (d) about 5 μs. . . . 106
4.8 Four more pictures from an earlier series of experiments performed with too much energy (265 J). (a) was taken just before collision, whilst (b) during and (c) and (d) after. It is clear that there is no channel formation after collision, because of the turbulence. The delay between the first and the last image is about 5 μs. 107
4.9 Image of a circle well before the collision of the shocks. The delay between the explosion and the diagnostic laser is 49.8 μs. This picture is a good example of Mach addition, because the shocks are creating a uniform common shock with a circular shape. The uneven background is due to defects of the lens used to collimate the laser. $W_{bank} = 180$ J. 110
4.10 Image of a gas pipe before the collision of the shocks in the centre. The delay between the explosion and the diagnostic laser is 52.8 μs. The circle is not perfect, probably due to small errors in the position of the wire. It can be noted that there is no turbulence behind the shocks. $W_{bank} = 180$ J. . . . 111
4.11 Image of a big pipe before the collision of the shocks. The delay between the explosion and the diagnostic laser is 56.6 μs. The pipe has now a diameter of about 1 mm. $W_{bank} = 180$ J. . . . 112

4.12 An example of a quasi perfect pipe, with a delay of 61.2 μs. Only two shots are arriving later, without affecting the shape of the pipe too much. The inset shows a schematic drawing of the shock waves. One can see that six shocks are almost perfectly on time. It is not clearly understandable what the two on the right are doing. Probably, distortions like this one are smoothed by Mach addition after collision. Indeed, we noted that the pictures after collision tend to show more regular shapes than the ones before. $W_{bank} = 180$ J. 113

4.13 A fast shot. Despite the delay of 57.4 μs the inner diameter of the pipe is now smaller. As the time between the explosion and the firing of the laser is measured on the oscilloscope, this can only mean that the shocks were faster. Indeed, from shot to shot the residual energy left in the capacitor, and therefore the energy gone into the shock, is different. $W_{bank} = 180$ J. . . 114

4.14 An even faster shot. After 55.8 μs the shocks have already merged through Mach addition. Despite the delay is smaller than in picture vrefpict:s32, the circle is smaller, which means the shock waves travelled faster. The circle is now smooth and the single shocks cannot be recognised anymore. $W_{bank} = 180$ J.115

4.15 This picture with a delay of 57.0 μs shows the smallest pipe we have observed before collision. It can be noted that the pipe is not perfectly circular but has an elongated shape. The line shows the path of the densitometry in graph 4.4 on page 117. $W_{bank} = 180$ J. 116

4.16 In this picture with a delay of 62.2 μs the shock are colliding in the centre. In the centre there might be a solid column of gas or a very small and slightly misaligned pipe, so that no light is getting through. $W_{bank} = 180$ J. 118

4.17 This picture, obtained with a delay of 54.6 μs shows the smallest pipe we obtained after collision. The pipe is not perfect because of some turbulence, but the size is very small. The central black dot should be noted. This corresponds to light refracted inward by the rebounding shock waves. Is is the desired result for colliding shock lenses. It may also be the optimum time for colliding pipe formation. $W_{bank} = 180$ J. . . 119

4.18 Another shot immediately after the collision of the shock in the centre. The circle has already a diameter of about 5 mm. Unfortunately, the delay is unknown because the oscilloscope did not record the trace. The small dots close to the centre are foci created by the intersection of the shock waves. W_{bank} = 180 J. 121
4.19 In this fast shot after collision with a delay of 65.2 μs the shocks have expanded more. Now the circle has expanded up to more than one centimetre in diameter and no focus is observed in the centre. It is interesting to notice in any case that there is no light in the centre. W_{bank} = 180 J. 122
4.20 SEM pictures of copper droplets from the melted wire on the lens surface. 123

5.1 The working principle of a colliding shock lens. A hot cigar of air left behind after the collision of the shock wave focuses the light inward. 128
5.2 The fringes produced by a single shock wave. If there is a steep pressure gradient in air, light is refracted toward the denser medium. Steeper gradients bend the light more. In a single shock we have a front, with a very steep gradient and a tail, which is less steep. Both, the front and the tail refract light that interferes with the unperturbed light propagating on the side of the shock to create fringes. The fringes produced by the tail, visible in the pictures in front of the shock, are finer[64][50].129
5.3 Evolution of a CSL with the corresponding images. In a), before collision, the light is refracted both by the head and by the tail of the shock, producing a sharp focus in the centre and a weaker ring focus. In b), at collision time, the light is refracted only toward the centre, creating a sharp focus. After collision, in c), the shocks are smoother, the pressure gradient is similar on both side of a shock and a sharp ring focus is produced. 131
5.4 The lens used in the experiments. The frame is made out of plastic because the pins have to be insulated from each other. 134

5.5 Two pictures of the lens during a shot. It is possible to see the light coming from all the pairs of pin. The sparks leaving the pins are debris from the electrodes, a clear sign of the erosion of them taking place. 135
5.6 An image of a lens in which part of the shocks are completely missing. In this case, the resulting structure is a circle with a missing part. Such a lens can still work, but of course the optical quality is very poor and the focus is not circular. . . . 136
5.7 Connection of the pins (only 10 are shown for sake of simplicity). It can be noted that the middle segments of the circuit are all floating. This is the reason why we had to put a coil in parallel to the lens, in order to carry the voltage to the spark gap. As in the drawing, each pair has a flat surface in front of a semi-spherical one 138
5.8 Oscilloscope trace of a normal experiment. The top trace shows the noise from a coil close to the device. The first high peak from the left is the breakdown of the pins; the second is the firing of the laser. The bottom trace is the signal from the optical trigger. 139
5.9 Oscilloscope trace of the experiment when the pins do not break down. In this case most of the energy is radiated as electromagnetic noise. This noise can be seen in channel 1, at the top. It should be noted that the oscilloscope settings were the same as in in figure 5.8 on page 139. The bottom trace shows that the optical trigger is activated by this noise. 140
5.10 The figure on top represents the connection that we used to put two high voltage capacitors in series without increasing the impedance of the circuit very much. It should be noted that the two capacitors do not have a polarity. Normally the electrode in the centre (labelled +) is connected to the high voltage and the case to ground, for safety reasons. Having used the capacitors this way, both the cases where at half the charging voltage. Two resistors, not shown in this diagram, were put in parallel to each capacitor to divide the voltage. . . 141
5.11 An actual picture of the capacitors connected as described in figure 5.10 on page 141. The resistors (a few hundreds kiloohms) partitioning the voltage are clearly visible, as well as other components of the circuit. 142

5.12 The two picture used to measure the speed of the shock waves. The reference object on the bottom has a size of 6 mm and the two lenses have a radius of 1.9 mm and 3.9 mm and the delay between them is 5 μs. 143
5.13 The scheme of the first experiment with the CSL. The telescope was adjusted in order to have the beam focused 5 m after the CSL. In this case it is like having two lenses in series and when the CSL works the focus moves closer to the laser. . 144
5.14 An image of the lens and of the corresponding focus, obtained in a different shot. The diameter of the lens is 7.2 mm. It should be noticed that the two images were taken in different shots (we can not simultaneously image the shocks and the laser spot in the far field). The photographic paper was 3 m far from the CSL and the densitometry (see figure 5.1 on page 149) shows that the focus is still rather large. Later experiments showed that the focal length of our CSL is around 15 m, which means that the focus was probably 3.75 m from the lens. A comparison between an actual experiment and an image showing only the laser can be seen in figure 5.15 on page 146. 145
5.15 A comparison of a blank image (left), obtained firing only the laser and one firing the CSL too. It is clear that the CSL is really focusing the beam. The image on the right is the same as in figure 5.14 on page 145 146
5.16 An image of a 9.0 mm lens and the corresponding focus, 3 m far from the CSL. It should be noticed that the images were taken in different shots. 150
5.17 One of the best foci obtained during our experiment. The diameter of the lens was in this case 10 mm. The focus is smaller than 1 mm. As in the previous case, the focus is probably better than this, but our detector, the photographic paper, was too close to the lens. 152
5.18 Two images of the shock obtained before the collision in the centre. It is interesting to note how all the images before collision show an irregular shape, which is smoothed into a circle after the collision due to the Mach addition. 154

5.19 Two images of small lenses (i.e. with a short focal length) obtained immediately after collision, when the lens has still a very small diameter. Such lenses have a much shorter focal length, but their size does not make them interesting for practical applications. 155
5.20 Two images of lenses of good quality, obtained with an energy of 600 J. In this case the lens has an almost perfect circular shape. Many refraction fringes are observable. 156
5.21 Two images of lenses of good quality, obtained with an energy of 600 J. In the bottom image a part of the lens is missing. Such an incomplete lens might be expected to give a poor focus. 157
5.22 Image of the lens obtained in the near field, 91 cm far from the device. The diameter of the lens is 9.0 mm. At the bottom is reported the oscilloscope trace. In this image, and in the following ones, the telescope was adjusted in order to have a parallel laser beam. 158
5.23 Another image of the lens obtained in the near field, 91 cm far from the device. The diameter of the lens is 10.3 mm. At the bottom is reported the oscilloscope trace. 159
5.24 Image of the converging beam of a 10 millimetres CSL at a distance of 3.3 m. From our measurements we know that such a large (as far as CSLs go) lens has a focal length of around 10 m. This means that the darker circle in the centre is light converging into a focus that is still far away. 160
5.25 Another image of the focus obtained on the far field at more than 10 m from the lens. The size of the focus can be compared with the 0.5 mm expected for a diffraction limited beam. It must be considered that our beam has a very low optical quality. Moreover, in order to image the laser beam at such distances we had to use two mirrors (respectively at 4 and 8 metres from the CSL) to relay the beam. 161
5.26 Image of the focus obtained in the far field, about 15 m far from the lens. Part of the poor quality of the focus derives from the fact that our laboratory was not long enough and we had to use two mirrors to be able to take images so far from the lens. 162

5.27 Image of the focus obtained 15 m far from the CSL. The bottom image shows a magnification of the centre, processed, increasing the contrast, in order to make visible the Airy rings. . 163
5.28 Image of the focus obtained 15 m far from the CSL. Despite the fact that the delay and all the other parameters of the experiment were the same as in the previous one, in this case the focus has a poorer quality, i.e., size. 164
5.29 Densitometry of image 5.28 on page 164. In this case, the lens did not work very well and the focus is larger than 5 mm. . . . 165
5.30 Image of a good focus, obtained in the same conditions of the previous ones. 166
5.31 Densitometry of image 5.30 on page 166, taken across a vertical path. 167

6.1 One of our square nitrogen lasers, in this picture without both the electrodes and the spark gap. 172
6.2 Cross section of the nitrogen laser. 173
6.3 One of our parabolic nitrogen lasers. It is clearly visible the slope of the electrodes, included in a Plexiglas frame. In this case, the spark gap is of the pressurised triggerable type. . . . 174
6.4 The rectangular nitrogen laser. 175
6.5 Calculation of the angle of the discharge pipe for a parabolic nitrogen laser. 177
6.6 The parabolic nitrogen laser. 178
6.7 Cross section of the multilayer nitrogen laser. 185

7.1 The simple optical scheme used for the ray tracing. 189
7.2 The results of the simulation, for a shock 1 mm wide and a grid of 10 mm. In this case, the profile of the shock is the first one of the graph 7.1 on page 194, with the steeper front. The picture on the left is the input matrix of the refractive index, the one on the right shows the result of the ray tracing 50 0cm after the pipe. The shock is travelling from the top to the bottom. 195
7.3 The results of the simulation with the other shapes for the shock. Clockwise, the shapes are the second, third and fourth of the graph 7.1 on page 194 196

List of Tables

3.1 Elements data 78

List of graphs

2.1 These two graphs show the behaviour of the intensity onto the target and the Rayleigh length for a typical laser pulse of 3 J, with a duration of 400 fs and a wavelength of 1 μm. 65

3.1 Resistance of three materials vs wire diameter. 74

4.1 Electron density gradient in a Helium plasma as a function of the shock tail thickness (see equation 4.5 on page 94) for different ionisation states of the plasma. A peak pressure of 500 kPa is assumed. From this graph and the following one, it is clear that by preforming a channel by means of shock waves it is possible to achieve a gradient of electron density suitable for laser guiding. 92

4.2 Electron density gradient in a Helium plasma as a function of the peak pressure of the shock (see equation 4.5 on page 94) for different ionisation state of the plasma. A tail thickness of .1 mm is assumed. 93

4.3 Densitometry of the smallest channel obtained during the pipe experiment (see picture 4.15 on page 116). This picture was obtained before the collision of the shocks, therefore the channel does not have the right density profile for particle acceleration. 108

4.4 Densitometries of the picture 4.15 on page 116. The top graph shows the densitometry along the longest side of the pipe, the other one along the shortest side. The density, obtained with a computer scanner, is in arbitrary units. $W_{bank} = 180$ J. . . . 117

4.5 A densitometry of the picture in figure 4.17 on page 119. It can be noted that the bright spot in the centre has a size of $\sim$ 100 μm (FWMH). In order to have a focus reasonably close to the lens, the laser beam was not parallel, but converging 5 m after the device, by means of a quartz lens. $W_{bank} = 180$ J. 120
5.1 Horizontal and vertical densitometry of figure 5.14 on page 145. It can be seen that the actual size of the focus is quite large in the horizontal direction. The difference between the horizontal and vertical profiles might be due to the asymmetry of the laser beam or to the multiple laser beams described in subsection 5.2.1 on page 168. In any case, it cannot be due to the lens itself, which is quite symmetric. 149
5.2 Horizontal and vertical densitometry of figure 5.16 on page 150. It can be noted that the focus size on the vertical axis is less than two millimetres. 151
5.3 Horizontal and vertical densitometry of figure 5.17 on page 152. 153
6.1 Geometrical divergence for a nitrogen laser with an electrodes separation of 2 mm. 171
6.2 Energy versus nitrogen flux in a parabolic nitrogen laser. The flux was measured with a flux-meter connected between the gas cylinder and the laser. 180
6.3 Energy versus nitrogen flux in the big parabolic nitrogen laser 182
6.4 Energy versus electrodes separation for a big parabolic laser . 183
6.5 Output for a multilayer square laser. 186
7.1 Shocks shapes used for the simulation. 194

Acknowledgements

My first sound "thank you" goes to my supervisor, Prof Max Michaelis. He gave me the opportunity to finish the interesting project described in this thesis. Furthermore, I want to thank him for his outstanding welcome and for his friendship.

The whole workshop of the Physics Department, where I found the friendliest people and the kindest welcome and help. Every time, despite the fact that I must have been in many people's nightmares. A particular thought goes to Robert Piasecky, for the time he spent looking after the equipment of our laboratory, making sure that we could perform our experiments. I want to mention Willem de Beer, former chief of the workshop, mainly for being the way he was.

Dr Nicola Lisi, who came first to this place, put me in contact with Max Michaelis and opened the way for me.

All the fellow members of the Laser Group, in particular Conrad Mahalase and Edric McEnzie, who helped me run experiments which I was not allowed to run on my own, for high voltage safety reasons. Without their help or

their presence, these experiments would have never been done.

My friend Ino Scribani, who accepted the boring task of helping me with my English.

All the secretaries of the department, both stable and temporary.

Our man in Pretoria, Geoff Turner, whose useful suggestions often got things moving again.

All the past members of the Laser Group, whose work made mine possible.

All my friends, some of them I have already mentioned, who very often did not have anything to do with the actual work, but helped me in living in a place that could have been far more alien. Among them, the late Bartolomeo Ribero, who taught me many things about life, South Africa and living in South Africa.

My parents, who shared my enthusiasm for what I was doing and where I was living.

My most sincere apologies to whoever I have forgotten. I am aware this list should be much longer.

Introduction

The title of this thesis might seem inappropriate. After all, everyone has been told at school that gases don't have a defined shape, but expand until they fill all the available space. But gas can indeed form structures, both dynamic, as in the case of explosions, and stable, as in the case of planetary atmospheres. Moreover, the same argument is true for plasmas, which are by far more common than gases in the universe. This is particulary true in space, where clouds of gas can be held together by their own gravitational pull.

A short look at the definition of structure on the *Webster's Revised Dictionary* can remove any doubt about the applicability of the word "structure" to a gas:

> Arrangement of parts, of organs, or of constituent particles, in a substance or body; as, the structure of a rock or a mineral; the structure of a sentence.

Italian dictionaries report similar definitions.

The only difference with the normal solid structures that we experience in our normal life is that the single particles that form gas structures are not bound in a particular position. In solid structures, single atoms or molecules only vibrate around a fixed position. In a gas, or a plasma, single particles are free to move, with a mean free path much smaller than the structure they form.

Gas and plasma structures are indeed very important. For example, the big structures formed by the cosmic explosions known as supernovas can affect the chemical evolution of the universe. We would not exist without them. For this reason, the first chapter of this thesis is a review of many different gas and plasma structures, from the earthly laboratories to the heavenly spaces.

But gas structures can have applications too. With shock waves it is possible to create three-dimensional distributions of temperature and pressure, and therefore refractive index, turning a bit of air into an optical element, a lens or a light guide. The rest of the thesis describes two particular gas structures that we studied in our laboratory. One structure, a gas pipe with the walls of compressed air and the core at a low pressure, might be useful in experiments of particle acceleration in plasmas, hopefully.

Chapter 1

Gas and plasma structures

Most of the matter in the universe, up to more than 99% of it, is in the form of gas or plasma. In fact, we live on a rocky planet, a small piece of solid material, that represents an exception, and not the rule. Stretching the matter even further, we could say that the universe itself is a large lump of dusty plasma. The key is in the word structure. On the Earth, in our experience, this word refers to a certain amount of solid matter organised in a shape. A house is a structure, a bridge, but even a pen, a box. In our experience, gases do not form structures: we are told that they expand until they have used the whole available space. This is not always true on our planet, but becomes even more incorrect when we leave our small environment and go into space. Even when leaving our planet, we can see that the pressure and the density of our atmosphere become lower, until we are in a space virtually empty (in reality, even the

space between galaxies is never completely empty, but it contains at least two or three hydrogen atoms per cubic meter). This pressure change means that the gases of our atmospheres are somehow organised, they form a structure. As we shall soon see, gas structures are very common in our universe, and often they affect our lives. The situation is even more complicated when we extend our attention to plasmas, which can form even more complex structures, due to the fact that they are affected by electromagnetic fields.

But how can gas and plasma structures form naturally in our cosmos? And how can we copy the way nature creates them? Gas structures in the universe can be created by means of big explosions of different kinds, and this is something that we can reproduce in our laboratories. But other structures take place when big clouds of gas are held together by their own gravitational pull. Plasma structures form when charged particles are trapped by a magnetic field, as in the Van Allen belts around the Earth; these structures are very similar to the ones used in Tokamaks and other similar devices.

The only difference between solid structures and gas (and plasma) ones is in the movement of the particles they are made from. In a gas (or plasma) structure, single particles are free to move within the structure. In a solid structure, single particles only oscillate around a resting point.

1.1 Natural and artificial gas structures on our planet

On the Earth gas structures are very rare and can be formed only by means of explosions, of shock waves. Unfortunately, structures from artificial explosions, from bombs, are very common. This kind of shock is very well studied, especially by the military people, who want to maximise the damages to obtain a more efficient mean of destruction. We shall not consider this topic.

On our planet, natural explosions occur, but they are not usually very important. One good example is lightning (see picture 1.1 on the next page), which can produce a very sharp shock. This shock decays quickly into a normal acoustic wave, the thunder we can hear. It happens often that a lightning next to a building breaks at least the glass of windows. But lightning can be interesting even for another reason, which does not concern gas structures. In our laboratory we observed sometimes our nitrogen lasers lasing even if we had forgotten to open the nitrogen cylinder. This means that given enough energy a laser can be built in air. But this means also that lightning might be a good source of well collimated ultraviolet beams. For the time being, no one has ever observed this emission, but it seems that no one has searched for it.

Other natural explosions on the Earth can come from volcanoes. In the past there have been some very powerful ones, which affected the course

Figure 1.1: Two spectacular images of lighting. They produce powerful shock waves, that degenerate quickly into acoustic waves. (Author unknown)

of our civilisation. We can mention the explosion that destroyed Santorini, or the Vesuvius eruption that killed all the inhabitants of Pompei. Despite their importance for mankind, these explosions do not produce any kind of interesting gas structure.

Leaving for a while the realm of nature, other kind of shocks are produced by airplanes flying faster than the sound. This shock is very well known as the "supersonic boom", even if very few people have heard it. Being very loud explosions, planes are normally not allowed to reach the speed of sound over land, but they have to be over the sea. Very similar to that, at least in principle, are the shocks associated with the Cherenkov radiation, which is emitted when a particle travels through a medium faster than the light. In this case, the energy of the shock is dissipated as a typical blue light, called Cherenkov radiation, that can be seen in the pools of nuclear reactors.

1.1.1 Mirages

A whole series of natural gas structures are very interesting, because they turn our own atmosphere into a gas lens. The most basic effect is the refraction that allows us to see objects that are below the horizon. This is normally due to the fact that our atmosphere becomes less dense with increasing altitudes. But light rays are refracted toward the denser medium. This refraction is the reason why we can usually see objects that are in principle below the geometric horizon. But refraction moves not only earthly objects, it changes the position of objects in the sky. This can sometimes be

Figure 1.2: The inferior mirage produces the well known water effect on a hot surface, like asphalt in a sunny day. (Author unknown)

a problem for positional astronomers and has to be taken into account. It is also a source of turbulence that can lower the quality of astronomical images and therefore reduce the amount of obtainable information. This problem has been solve by the use of adaptive optics[5].

But the atmosphere can also have an irregular temperature and pressure profile, and this irregularity produces more interesting phenomena, mirages[33][38]. The word mirage comes from the French *se mirer*, to be reflected, to see one's image in a mirror. This is due to the fact that mirages involve the presence of many inverted images of the same object. There are many different kind of mirages, depending on the thermal structure present in the atmosphere. The inferior mirage is the most common one and does not owe the name to the fact that it is a poor example. In this mirage, the inverted image lies below the erect real one. This is the same kind of mirage that is usually seen when driving on a very hot day and produces images of water pools on the asphalt. In this mirage, the surface of the Earth, heated by the Sun, produces a layer of hot air of lower density just on the surface. Grazing rays bend back up in the denser air above and what we see is not water, but an image of the sky.

The superior mirage happens when there is a thermal inversion in the atmosphere. In this case, the refracting layer is higher than the observer. This happens quite often in spring in northern Europe, because of the warm air that comes from inland and goes above the still icy water. The mirage is an inverted image above the normal one, and this is the reason for the name.

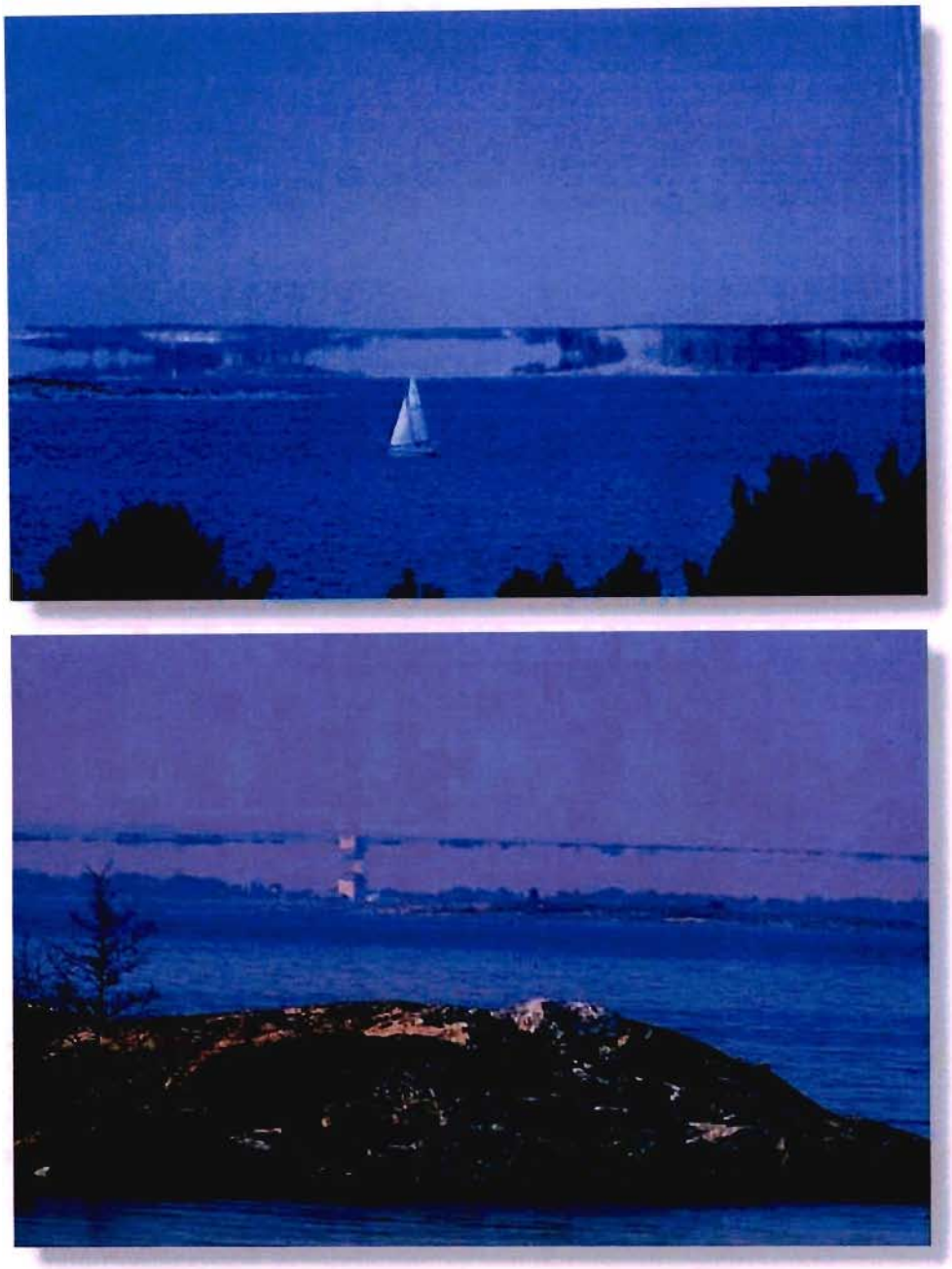

Figure 1.3: The cold seas of the northern Europe are ideal places to observe superior mirages. In spring there is very often a layer of warm air coming from the land above the still icy cold waters. These two pictures where obtained in Sweden. (Author unknown)

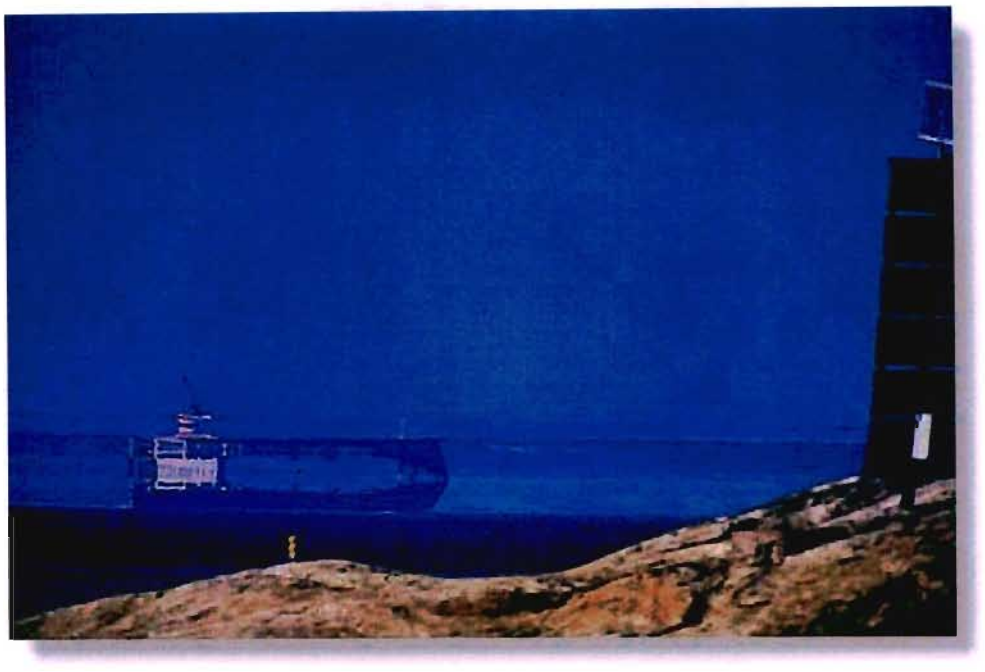

Figure 1.4: A spectacular example of a superior mirage. (Author unknown)

But mirages can even be used in a laboratory, and a good example of that is the spinning pipe gas lens[56], in which a quasi static gas structure is created by heating and spinning a pipe. Inside the pipe, the gas has a gradient of temperature and pressure, and so of refractive index, and works as a lens that can be used to make a small telescope[57]. As in the case of the hot asphalt mirage, the air is hotter close to the walls of the pipe and so the light is refracted toward the centre. In our group such a lens was used to take pictures of the Moon and of some feature on the hills surrounding the university. The lens is not really useful as a telescope, because convection

Figure 1.5: Another example of a superior mirage, observed in Antarctica.(Picture thanks to Jack Stephens)

does not allow one to make a lens larger than 2 cm, but it can be very useful to focus a laser beam[47][55][36].

But even our atmosphere can be considered as a gas structure on its on, even without considering winds and other local phenomena. The atmosphere, in fact, changes with altitude, getting thinner, until it dissolves into space. And even considered as a whole, our atmosphere has some optical properties, but not really good ones. As a window, for instance, it is very bad for astronomy, because it blurs all the images and it absorbs selected wavelengths, not allowing the view of the universe over the whole electromagnetic spectrum. In order to avoid this window, many observatories are now sent into space,

like the Hubble Space Telescope and many others that observe at different wavelengths, like gamma and X-rays.

As far as plasma structures are concerned, on our planet we can find only lightning, already described. Plasmas are very common in the universe, but luckily not on this tiny piece of rock we live on.

1.2 Structures in the Solar System

Just outside our planet there is an interesting plasma structure, the Van Allen belt, discovered by James Van Allen and his colleagues in the year 1958 (see figure 1.6 on the following page). The discovery was made thanks to an instrument designed by Van Allen himself and installed on Explorer 1, the first American satellite, and on the Explorer 3. This belt is made of charged particles that come from the Sun and are trapped by the magnetic field of the Earth. The Van Allen Belt is located a few thousands kilometres above the surface, where many satellites orbit our planet. These structures are very important because of the threat they pose to these satellites, but they were also a major concern for the astronauts who went to the Moon. They had to travel through the belt and, despite this they did not suffer from any apparent radiation damage. They did however report flashes of light in their eyes. These were later explained as Cerenkov radiation of the electrons travelling through the liquid medium of the eye. To make the matter worse, but nevertheless more interesting, it has been recently discovered that the

Figure 1.6: The solar wind flowing around the magnetic field of the Earth and the van Allen belts. (Image European Space Agency)

Van Allen belt work as a particles accelerator. The solar wind alone in fact does not account for all the observed high energy electrons. The true mechanisms of the acceleration have not been fully understood, unfortunately, though it is at least partly due to the magnetic mirror mechanism. It is in fact possible that the same mechanism could be used in laboratories to make more powerful particles accelerators based on plasma confinement.

As our planet has an atmosphere, most of the planets in the Solar System

are surrounded by a layer of gas. This is true for Mercury, with its thin atmosphere formed by hydrogen atoms trapped from the solar wind. Venus has a very thick atmosphere, rich in carbon dioxide, that is very unusual among the inner rocky planets. This means that as an optical element it is even more powerful than the Earth's atmosphere. This was observed by the few Russian probes Venera that managed to survive for a few minutes on the surface of the planet, in temperatures up to 400° centigrade. The dense atmosphere allows to see far below the geometric horizon. According to many scientists, this might be a scary looking picture of the future of our planet. Many scientists claim that Venus was once very similar to the Earth, until a series of powerful volcano eruptions increased dramatically the carbon dioxide level in the atmosphere, triggering a runaway greenhouse effect. If that is true, the arguable mounting evidence of global warming on the Earth might be only the beginning of the process; in our case, the carbon dioxide comes from human activities, but the result could be the same.

Skipping Mars, with its very thin atmosphere, and the asteroids, which are not relevant in our discussion, we find some very impressive gas structures. The four giant gaseous planets are a fine example of gas structures. These planets are surrounded by a very thick atmosphere and they do not have a solid surface, like the inner rocky planets. Especially the atmosphere of Jupiter is rich in interesting phenomena, due to its size (it is the biggest planet in the solar system) and its relatively small distance from the Sun. Jupiter's atmosphere is reach of features, from its belts to the famous Great

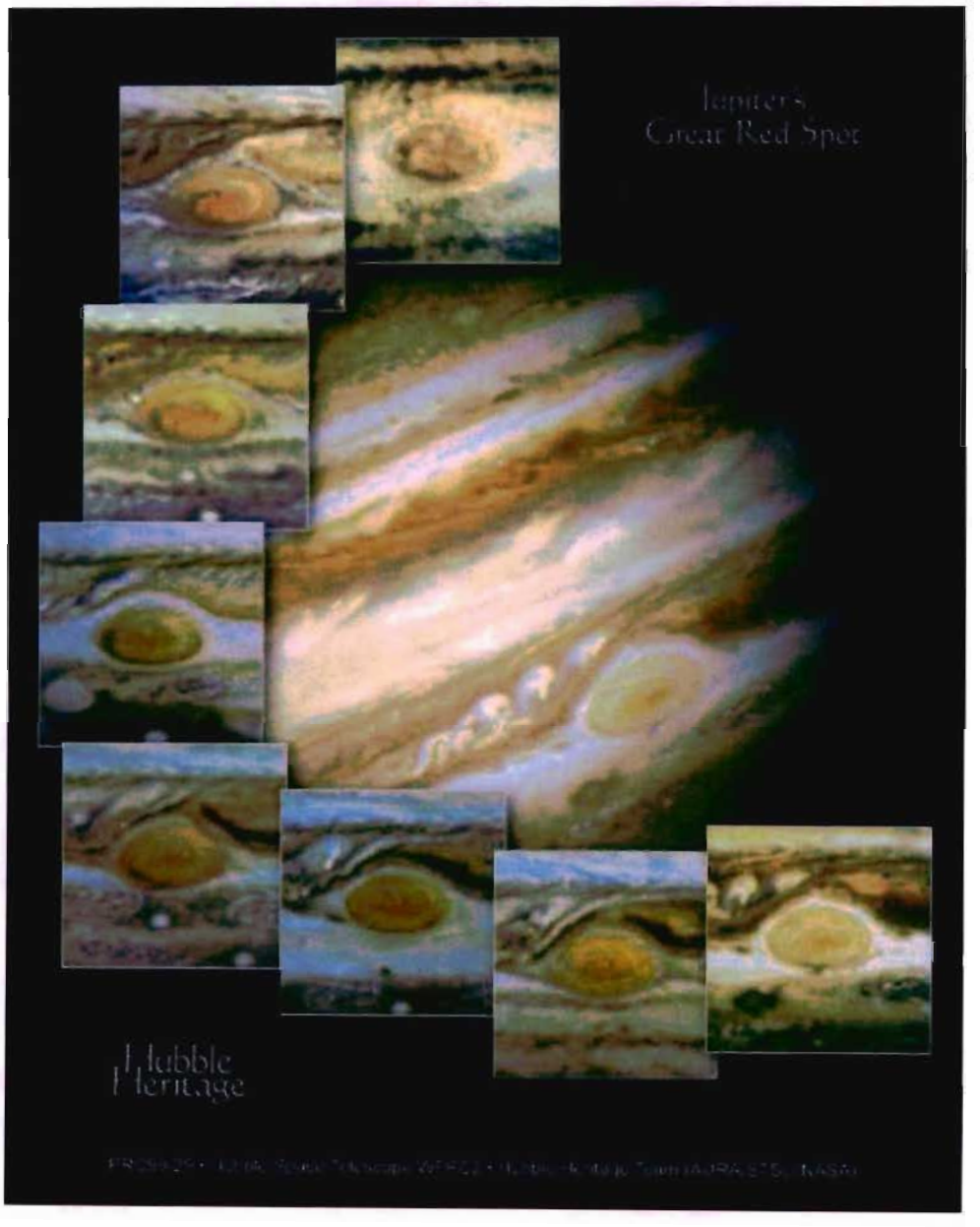

Figure 1.7: Jupiter and its famous Great Red Spot, in this picture obtained by the Hubble Space Telescope (www.stsci.edu).

Red Spot, an ancient hurricane with winds up to 600 m/s. In the space around Jupiter there is a magnetosphere similar to the one of the Earth, but within it there is a powerful flux of charged particles that links electrically Io, one of Jupiter satellites, with the poles of the planet. This current of some millions of amperes produces the brightest auroras in the solar system, imaged by the Space Telescope in ultraviolet light.

Among the gaseous giants, Jupiter is the closest one to the Sun, and the still vast amount of energy it receives from our star is the reason of its hectic atmosphere. Saturn is in fact more quiet, with some very stable dark belts and a few spots that appear every few years. But going farther away, the core of Uranus might have a very precious surprise. Deep in the planet atmosphere, some scientists speculate that there is a real hail of diamonds. At something like 12000 km deep, the temperature is high enough to dissociate the methane molecules in their atoms. Then, the pressure is high enough to condense the carbon into a diamond. Unfortunately, the severe conditions do not allow a simple trip to the planet to collect this treasure.

If we consider the solar system as a whole, it is included in a big cocoon made by the particles of the solar wind. These particles are guided by the magnetic field of the Sun, and this heliosphere is really important, even for our life. This structure extends well beyond the orbit of Pluto, but scientists still don't know exactly where the influence of the Sun ends. At the moment, the two Voyager spacecraft are looking for the edge of this structure, that Voyager 1 should meet within not more than four years. The Voyager mis-

sion, once the tour of the solar system was concluded, is now called Voyager Interstellar Mission. The boundaries of the magnetosphere are where the solar wind become sub-sonic. Just as our magnetosphere protects the Earth from the solar wind, so the heliosphere protects the whole solar system from the high energy cosmic rays coming from the interstellar space. Some scientists speculate that this structure was blown away a few times, in the history of the solar system, when the Sun went through a dense interstellar cloud. They think that this is the reason for the extinction of the dinosaurs, and maybe for some other mass extinctions in the past. This theory is intriguing, because the extinction of the dinosaurs was followed by a real explosion of new species, that can be explained quite well with the mutations due to the high level of radiation.

At the centre of the solar system there is an interesting plasma structure, a star, our Sun (see picture 1.8 on the next page). A star is in fact nothing else but a very complex plasma structure. The Sun has in its core a temperature and a pressure which are high enough for some thermonuclear reaction to take place. This is the source of energy of most of the solar system, the fusion of four hydrogen atoms into one helium atom. In the outer layer of the Sun the temperature is much lower, but still a few thousands of degrees, enough to make the star very bright. The outer atmosphere of the Sun is very important, because it is the source of the solar wind, already described earlier, where particles are accelerated up to 1000 km/s. There are incredible gas structures here, like the solar protuberances, fountains of hot gas that rises

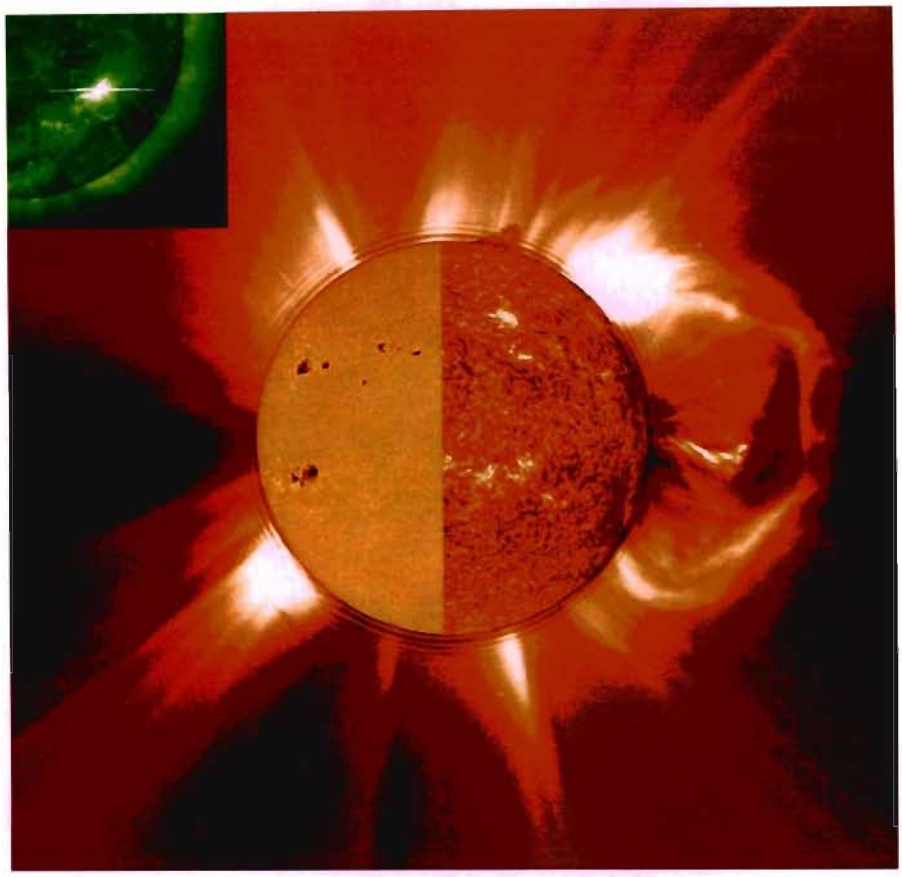

Figure 1.8: A composite image of our Sun obtained by the SOHO probe (sohowww.estec.esa.nl). The left part shows the surface of the Sun as it appears in visible light, the right part in the Hydrogen α line. Some protuberances are visible, large fountains (structures) of plasma that erupt from the surface pushed by powerful magnetic fields.

above the surface pushed by powerful magnetic fields. The real mechanism of most of these processes has not been fully understood, despite centuries of observations, starting from the ancient Chinese. More recently, the SOHO probe has studied the Sun for a few years, giving some clues to the scientists.

One of the most intriguing mysteries is the temperature of the solar corona, a few million degrees, that lies above a surface with only a few thousand. The energy, SOHO discovered, is transferred by a magnetic field, but most of the details are still unknown.

Sometimes the Sun emits large amounts of material in what are called coronal mass emissions. When this happens, the Earth is bathed in a much denser solar wind with velocities up to million kilometres per hour. This huge flux of charged particles can affect the communication on the surface and can also disrupt the power distribution lines. To try to prevent this damage, the new science of the space meteorology is being developed all around the world.

1.3 Space structures

As we leave our solar system completely, the number of gas and plasma structures increases dramatically. There are stars similar to our Sun, but also big stable clouds of gas and plasma. But the most impressive structures are those associated with shock waves.

1.4 Shocks

Shock waves in space can be created in many different ways. In particular, the shocks from dying stars are very spectacular, either when they come from a very sharp explosion (supernovas), a weaker one (novas) or from stars going

through the last phase of their existence and dissipating their most external layers into space. These phenomena, even if they are somehow related, come from completely different processes, but they have many things in common. They come from plasma structures, stars, and produce other gas structures, the shocks themselves. Even more interesting is the fact that, in all this phenomena stars emit part of their material into the space. This is a very important aspect. When the universe, which is in its own a very complicated gas and plasma structure, dotted by some pieces of solids and liquids, was created, there where only light chemical elements in it. Then, in the furnaces of stars where created all the heavier elements. So, most of the elements that sustain life on the Earth where created in a star and ejected during one of the explosions described above. Gold, in particular, can be created only during the explosion of a supernova. But the shock coming from a supernova can trigger the creation of many more stars: we are children of a shock wave.

Some very large shocks, even if in this case they are very far from the topic of this thesis, can be created even in solid matter. A good example of that is the Weird Terrain on Mercury. This structure, called from the way it looks, strange, was created when a big object collided with Mercury, creating the impact basin Caloris and shocks which propagated all the way through the body, meeting on the other side and giving birth to the strange terrain. Of course, an interaction of shocks is very unlikely in the Universe, where explosion occur usually at different times.

1.5 Gas clouds

Some very important and numerous structures are the big gas clouds, like the Orion nebula (see picture 1.9 on the following page). These are huge clouds of gas held together by their own gravity. These clouds are usually stable structures, but when they are perturbed they can collapse into a star or, more frequently, a star cluster. The perturbation is normally a shock wave from a supernova (see section 1.6.2 on page 28).

What happens is that the shock increases the density in a small portion of the cloud, that then pulls more and more material, until it lights up as a star. Then, the first thing a star does is to blow away all the gas left behind by its formation. Though this process is not yet well understood, it seems to be very important because planets form very soon around new stars.

The formation of new stars in nebulae goes sometimes through some sort of avalanche effect. Among the stars formed in a nebula, there are some very massive ones. These are very likely to become supernovas on their own, when there is still enough material to form more stars. This process goes on until all the gas has been sucked into a star or blown away.

A particular kind of cloud, the molecular clouds, is very important for another reason. Astronomers have discovered in these clouds over fifty organic compounds and the Orion nebula is a powerful factory of water. And most clouds contain ethylic alcohol too, even if probably not as structured as a well aged wine. Some astronomers think that the first organic molecules,

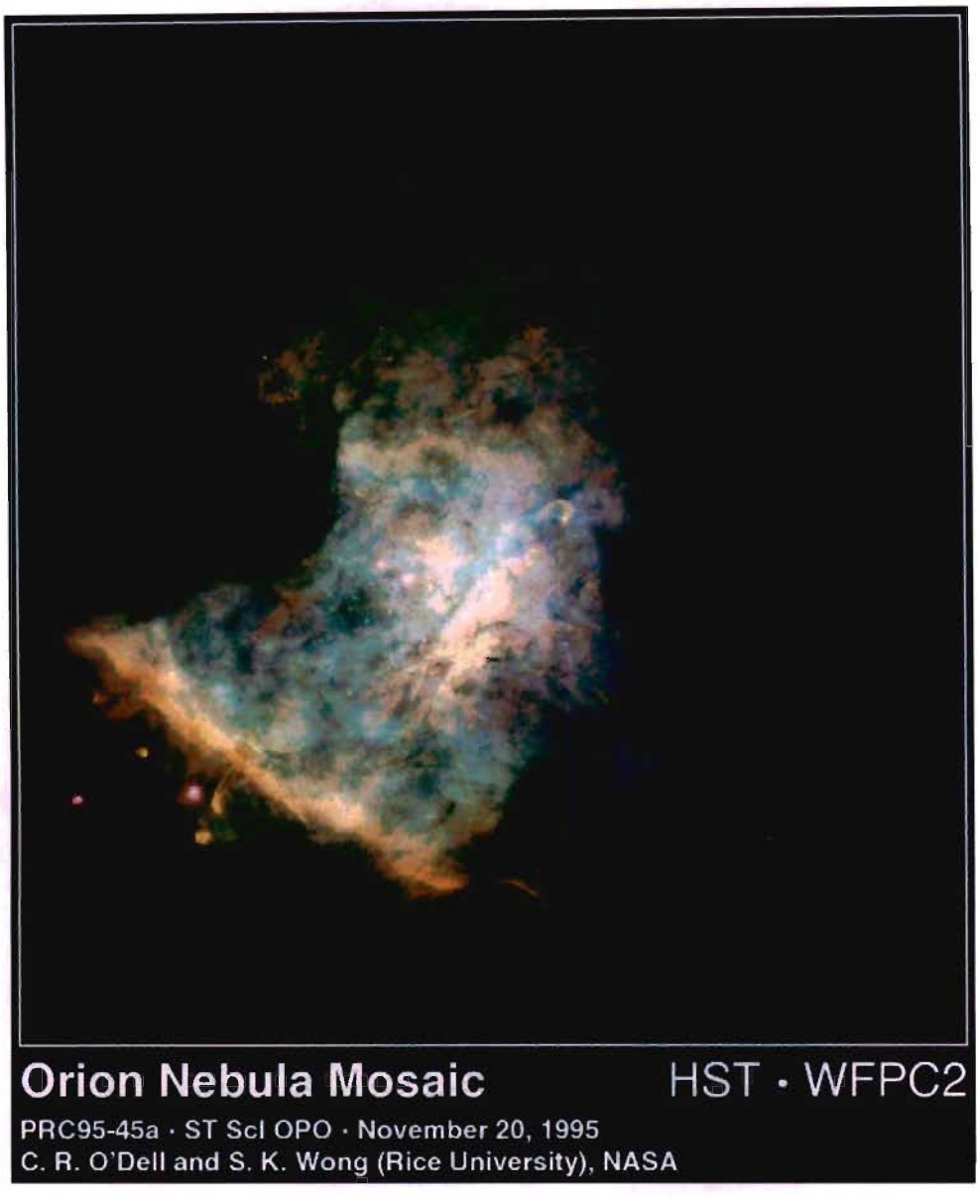

Figure 1.9: A picture of the central part of the famous Orion nebula. It is a very big nebula relatively close to our planet. The centre of the nebula is hidden by another cloud of dust and is visible only in radio waves (www.stsci.edu).

that started life on the Earth, arrived here from space, from these clouds. But, as described earlier, these clouds might have wiped out many times most of the creatures living on the Earth.

1.6 Explosions

The most amazing gas and plasma structures in the universe are originated by many different kind of powerful explosions. Even if the universe might look like a quiet place, during the timescale of our lives, many objects find their end in catastrophic processes. All these explosions result in shock waves, that can create beautiful structures when they are disturbed by the presence of another body.

1.6.1 Novas

The smallest possible explosions in space are the kind known as novas. The name, the Latin for *new*, comes from the fact that these explosions increase the brightness of a star by a factor of a few hundred. This makes the star appear in the sky, apparently from nowhere. Modern astronomers, with their telescopes, can identify the star that exploded in the picture taken before the event, but antique astronomers were puzzled by these newcomers.

Novas are always double systems, in which there is usually a red giant and a normal and smaller star. What happens is that the normal star steals material from the under-dense red giant. This material falls on the star and

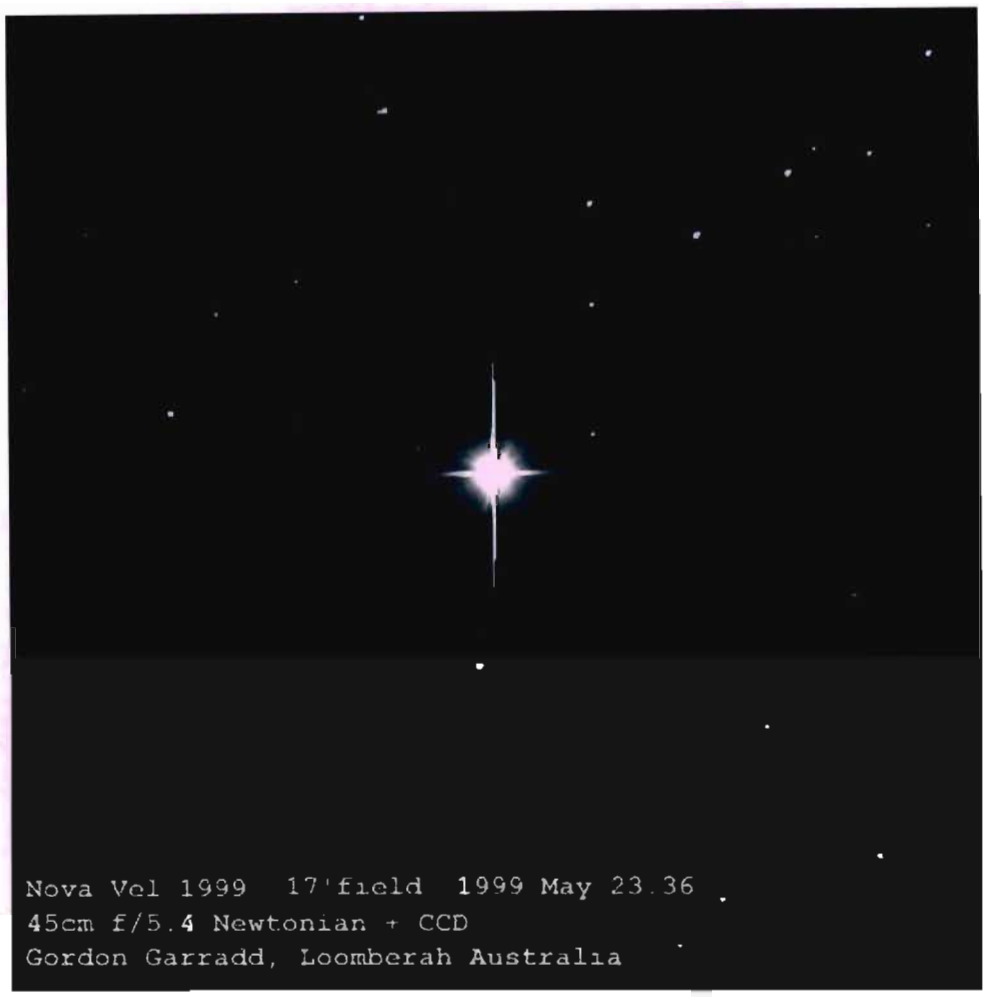

Figure 1.10: An image of the Nova Velorum 1999. This nova was perfectly visible with the naked eye from Durban during the month of may 1999. I estimated the brightness to magnitude 4.5 only a few days after the explosion, but the nova had reached magnitude 3.

accumulates on its surface. If there is too much material, the outer layer of the star can become so hot as to ignite the same nuclear reactions that take place in the centre of every star. The sudden release of energy blows away the outer layer at once, cooling down the star and stopping the nuclear reactions.

Novas are quite frequent even within our own galaxy and in a normal year several are observed. Most of them are visible with normal binoculars or a small telescope and so are very often discovered by amateur astronomers.

1.6.2 Supernovas

Supernovas are the second kind of explosions that we consider. The name is misleading, because they are not just more powerful novas. The physical processes of the explosion are completely different.

Supernovas are very young stars, which were far too greedy at the moment of their formation. What happens is that these stars burn quickly their hydrogen in order to avoid a gravitational collapse. After the hydrogen, these stars burn helium and carbon and so on, until they get to iron. When they burn iron there is a sudden burst of energy that triggers the explosion.

Supernovas are so impressive that the first records we have come from the Chinese astronomers. A good example is the supernova that exploded in the year 1054, creating the Crab Nebula (see picture 1.11 on the following page) in the constellation of Taurus. Luckily, the Chinese astronomers recorded the position of the supernova so carefully that modern astronomers

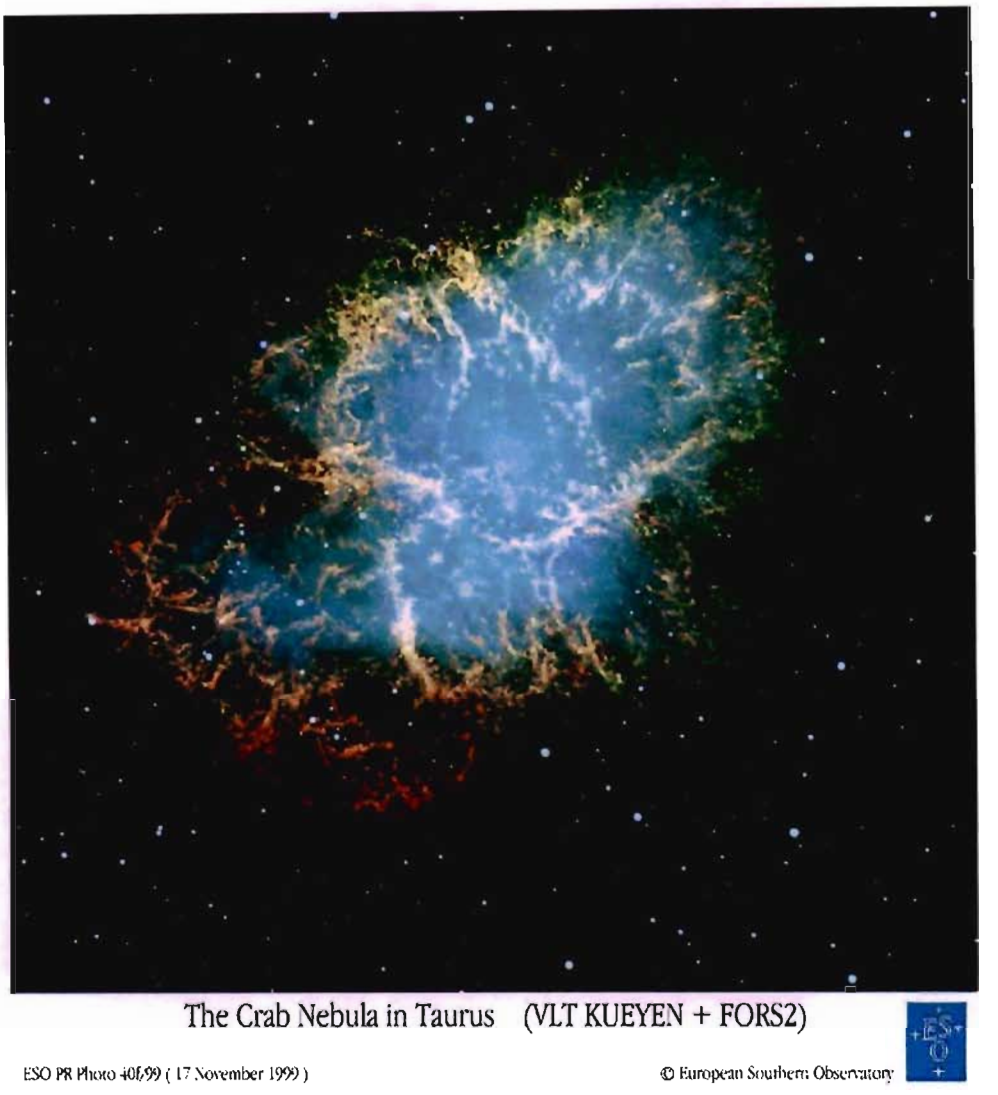

Figure 1.11: This picture shows the Crab Nebula, a remnant of a supernova which exploded in the year 1054 and was observed by Chinese astronomers. The picture was taken with one of the 8.2 m telescopes of the Very Large Telescope of the European Southern Observatory.

could identify the remnant. At the centre of the nebula there is also a pulsar, a very interesting kind of object that cannot really be considered a gas or plasma structure. Two more very bright supernovas were observed in 1572 by Tycho and in 1604 by Kepler and in both cases astronomers have identified the remnant. These are the last two known supernovas in our galaxy. Unfortunately, both were observed just before the invention of the telescope. Judging from the average interval between two supernovas, we should be close to an explosion right now. Of course, the next supernova might explode on the other side of the galaxy, completely hidden by its core. But, even worse, a supernova could explode much closer, bathing the Earth with a shower of harmful radiation. According to some scientists, this could also be the reason of the extinction of the dinosaurs.

Another supernova might have exploded only 700 years ago, but it is a puzzle for astronomers. Two years ago a very young supernova remnant was observed in the constellation of Vela. From the speed of the expansion and the size, the age of the remnant was estimated to be about 700 years. The puzzle is that there are no recorded observations of any supernova in that period. If Europe was going through a dark age that might explain the lack of observations, the same cannot be said about the Chinese astronomers, who were very active.

But supernovas can be brighter than the whole galaxy that host them. So, many times a year supernovas are discovered in other galaxies. That is the reason why the process is quite well known and understood. Even if the

explosion cannot be observed in detail, the light itself carries a wealth of information. Again, many supernovas are discovered by amateur astronomers, even if now there are a few automatic telescopes devoted to this job.

Supernovas are important for many other reasons too. First, when a supernova explodes, its shock wave travels through the surrounding gas, compressing it and triggering the formation of new stars. Then, as we say, stars are the furnaces in which many elements are created, elements that were not present in the primeval universe. These elements can leave their stars only during this kind of explosions. Many more, like gold, can be created only during the explosion itself. This means that most of the matter that makes up the solar system comes from one of these explosions: we are sons of a supernova.

SN1987A

The only well studied supernova in our neighbours is the 1987A, which exploded in the Large Magellanic Cloud in the year 1987. It was denominated 1987A in an excess of optimism, hoping to count again a 1987B. In that case, the evolution of the shocks was studied later and very well thanks to the Hubble Space Telescope, which took some astonishing images of the shocks smashing into the surrounding matter. Indeed, the observation are still repeated every now and then, to follow the evolution of the small nebula created during the explosion. It is actually a pity that the launch of Hubble had been delayed by a few years, because at the beginning it was scheduled

for 1986. As it often happens with this explosions, the behaviour of the shock was quite strange. There are two rings around the stars, the shape of which is still incompletely explained. Probably, the rings were created because the shocks were perturbed by the presence of a small companion star, which is not visible in any image.

Some images of the evolution of the supernova SN1987a are shown in figure 1.12 on the next page. The series of four panels shows the evolution of the SN 1987A debris from February 1994 to February 1996. Material from the stellar interior was ejected into space during the supernova explosion in February 1987. The explosion debris is expanding at nearly 6 million miles per hour. Despite that, the energy carried away by the ejecta is about 1% of the energy produced during the explosion.

This supernova was close enough to study its emission of neutrinos and allowed the astronomers to refine their models of these explosions. It would have been maybe close enough to detect some gravitational waves, but unfortunately most of the detectors around the world were undergoing maintenance after a 1986 collaborative program and therefore were not working.

Only two years ago, again thanks to the space telescope, astronomers have seen for the first time the shocks from the explosion lighting up the rings. This happened a few years ago, but that was only the beginning of the interaction. The space around these stars is also quite often nearly empty, because they have a powerful wind, which pushes away most of the surrounding gas and dust. Then, even before the proper explosion, these

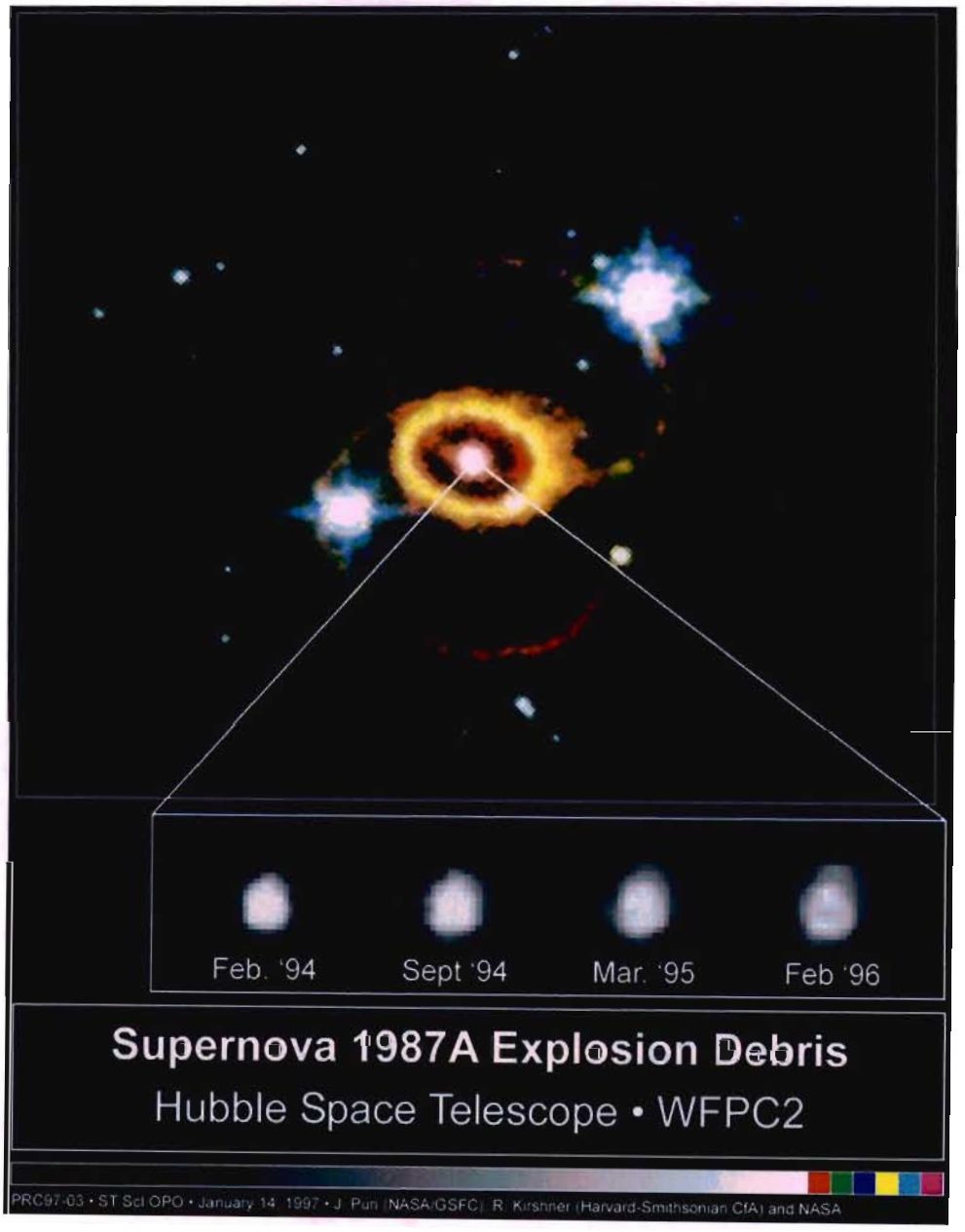

Figure 1.12: Four images of the evolution of the supernova SN1987a during the first ten years since the explosion.

stars emit some weaker shocks. More recently, the new American X-ray observatory, Chandra, has observed directly the hot gas of the shock waves.

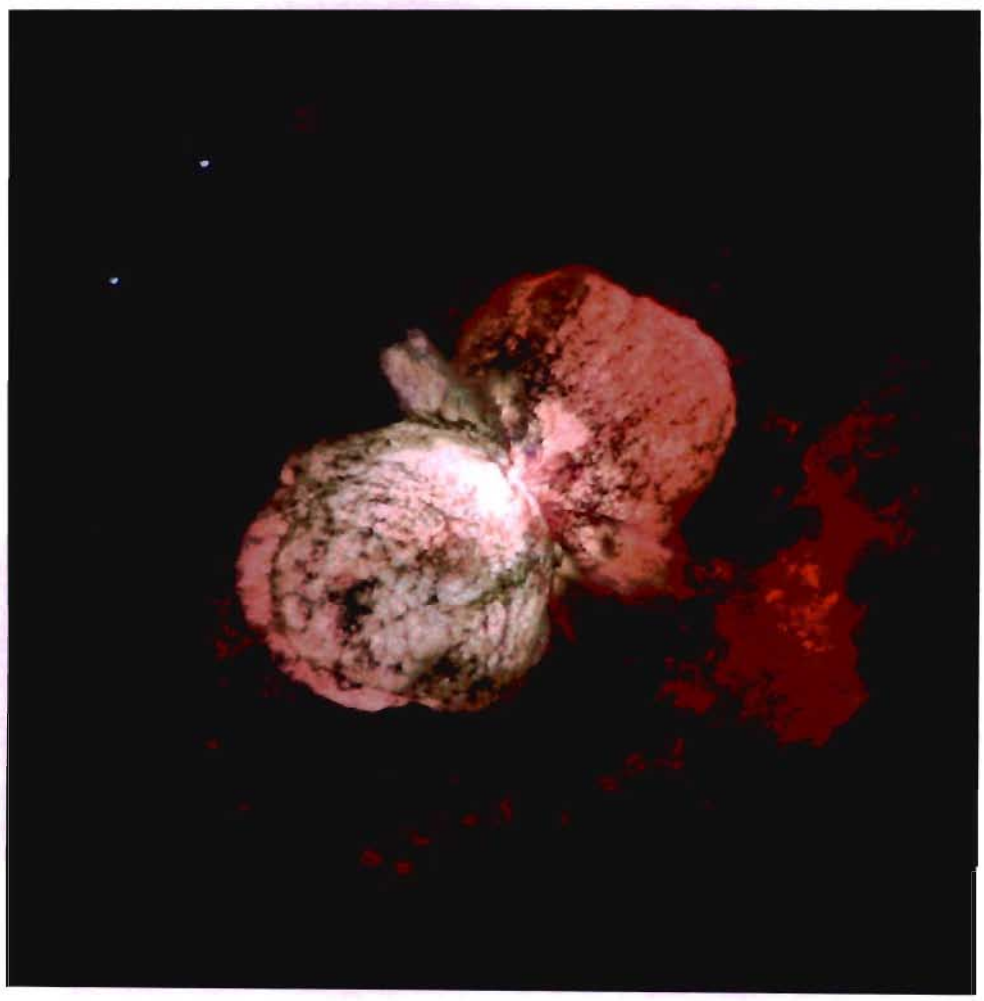

Figure 1.13: Eta Carinae, a good supernova candidate imaged by the Hubble Space Telescope.

Eta Carinae

A very good example of soon to be supernova is the star Eta Carinae, one of the brightest and most massive stars of our galaxy. The mass of this star

is probably fifty times the mass of the Sun. Eta Carinae is only a couple of million years old and probably won't last much more. In order to stay stable, Eta Carinae is burning its mass at a very fast pace, so much that it is five million times brighter than our Sun. This figure was obtained by observing the star in infrared light. It is not the brightest star in the sky only because it is embedded in a nebula that stops most of the visible radiation.

Eta Carina, like most of the stars approaching the end of their lives, has ejected its outermost layers, creating two cones of material that are clearly visible in optical images (see picture 1.13 on the preceding page).

In the past Eta Carinae has gone through a long phase of instability that can not be explained with the current theories of stellar evolution. In particular, during the 19th century Eta Carine had an eruption that increased its brightness by a factor one hundred, up to magnitude -1.

It is interesting to note that the environment surrounding this star is evolving really quickly, on an astronomical timescale. By comparing images obtained only a few decades ago it is possible to see differences in the nebula around the Eta Carinae.

1.6.3 Hypernovas

The last kind of explosion we can consider in our review of the astronomical gas structures created by shock waves are the hypernovas. These objects have been discovered only recently, but are becoming really interesting. They are not very different from the normal supernovas, but the size of the exploding

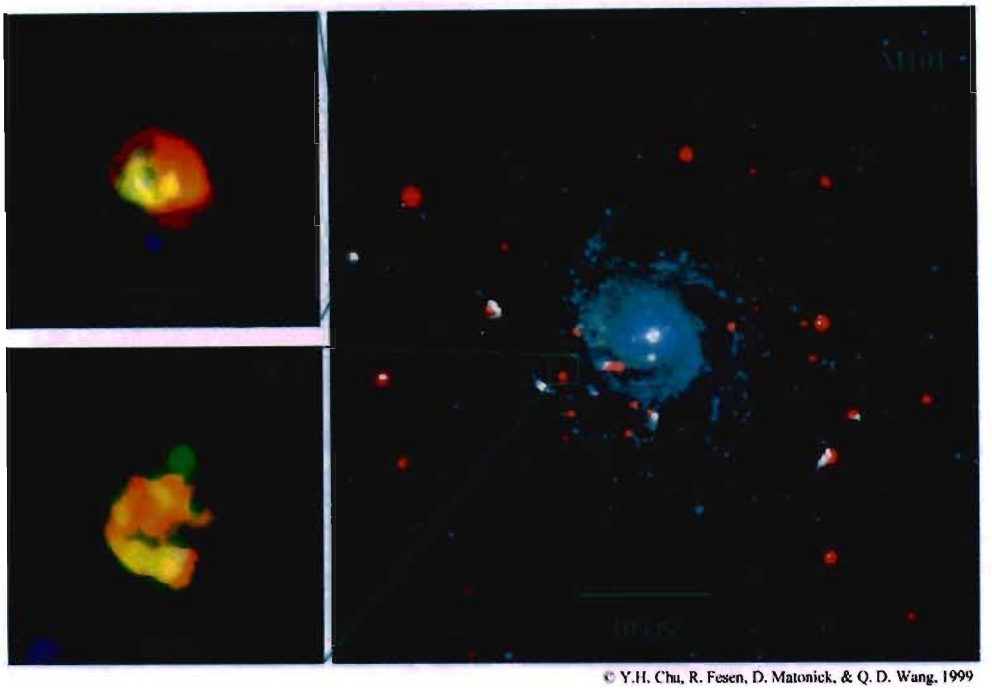

Figure 1.14: Two hypernova remnants observed by the Hubble Space Telescope in the galaxy M101.

star is even bigger, giving birth immediately to a black hole, instead of a neutron star. The first hypernova was identified in April 1998, when the astronomers were looking for counterparts of gamma ray bursts, the most energetic explosions in the universe. What they found was in fact a supernova, which looked normal. What happens in these cases is that the star explodes, and the material sucked by the new-born black hole is responsible for the emission of the gamma rays, usually scarce in these explosions.

In another case, some astronomers have been able to identify two hypernova remnants,shown in figure 1.14 in the M101 galaxy. In the past, these

two nebulae were considered normal supernova remnants, but a new analysis of their X ray emission has shown that there are some very energetic processes going on in them. These two nebulae emit ten times more X rays than the brighter supernova remnant known. Then, one is the biggest planetary nebula known, and the second one has an impressive expansion speed of 160 km/s. The attention of the astronomers was stimulated by the X rays, considering that the galaxy is 25 million light years away, which means that they must be very spectacular from a shorter distance.

1.6.4 Planetary nebulae

When Sun-like stars get old, they become cooler and redder, increasing their sizes and energy output tremendously: they are called red giants. Most of the carbon (the basis of life) and particulate matter (crucial building blocks of solar systems like ours) in the universe is manufactured and dispersed by red giant stars. When a red giant star has ejected all of its outer layers, the ultraviolet radiation from the exposed hot stellar core makes the surrounding cloud of matter, created during the red giant phase glow: the object becomes a planetary nebula. A long-standing puzzle is how planetary nebulae acquire their complex shapes and symmetries, since red giants and the gas/dust clouds surrounding them are mostly round. Hubble's ability to see very fine structural details (usually blurred beyond recognition in ground-based images) enables us to look for clues to this puzzle.

The picture in figure 1.15 on the following page shows the youngest plan-

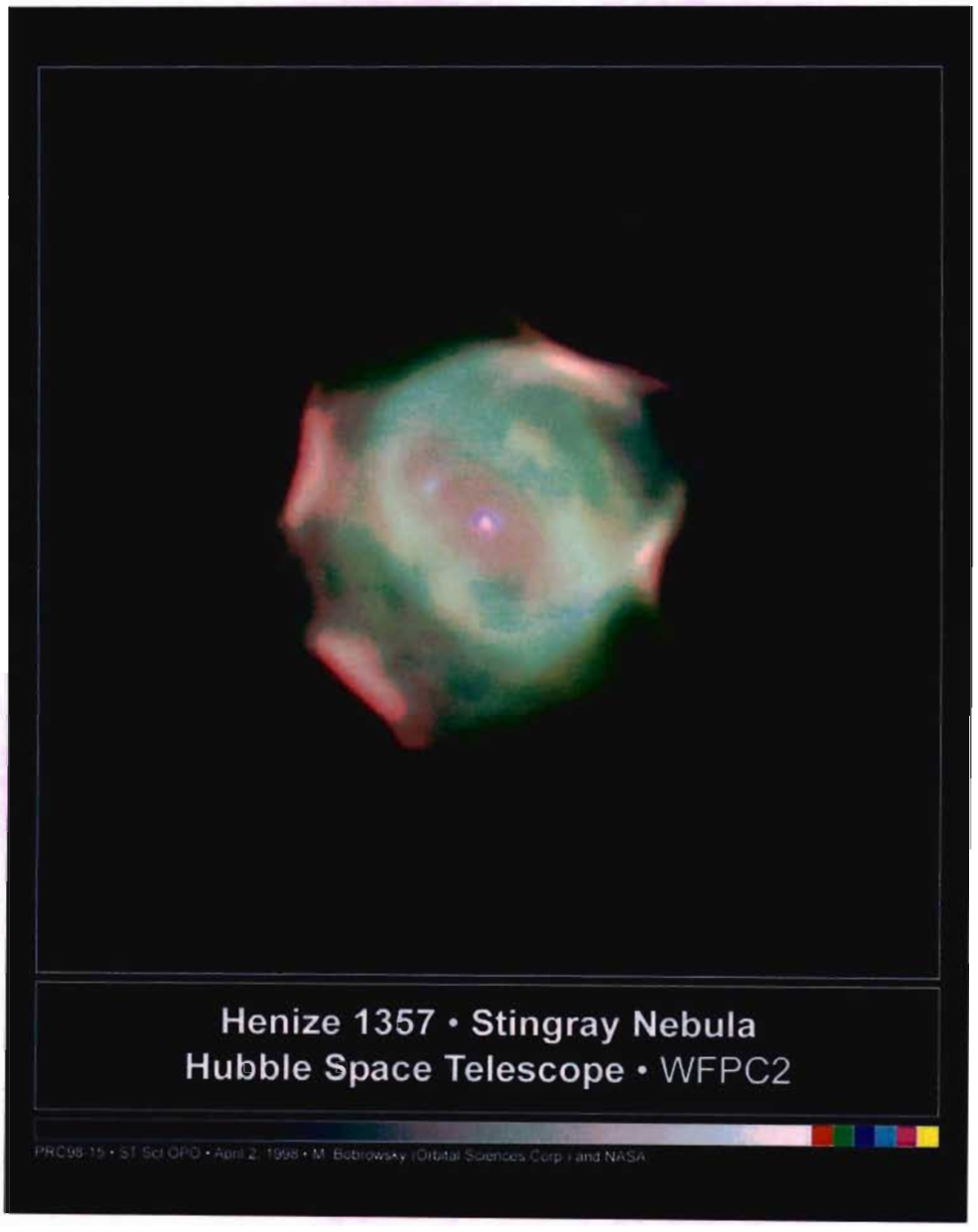

Figure 1.15: Hen-1357, the youngest known planetary nebula.

etary nebula known and was obtained by the Hubble Space Telescope. In the image, the star which built the nebula is in the middle of the green ring of gas. On the left of the central star there is a companion, linked to the main star by a faint bridge of green gas, pulled by the gravity. The red curved lines represent bright gas that is heated by a "shock" caused when the central star wind hits the walls of its bubble. The size of the bubble is $1.2 \cdot 10^{10}$ km, 130 times the size of our solar system.

The picture in figure 1.16 on the next page shows another young planetary nebula. This Hubble image reveals the true shape of MyCn18 to be an hourglass with an intricate pattern of "etchings" in its walls. According to one theory for the formation of planetary nebulae, the hourglass shape is produced by the expansion of a fast stellar wind within a slowly expanding cloud which is more dense near its equator than near its poles. What appears as a bright elliptical ring in the centre might be mistaken for an equatorially dense region. But a closer inspection shows it to be a potato shaped structure with a symmetry axis dramatically different from that of the larger hourglass. The hot star which has been thought to eject and illuminate the nebula, and therefore expected to lie at its centre of symmetry, is clearly off centre. This means that MyCn18, as revealed by Hubble, does not fulfil some crucial theoretical expectations. Hubble has also revealed other features in MyCn18 which are completely new and unexpected. For example, there is a pair of intersecting elliptical rings in the central region which appear to be the rims of a smaller hourglass. There are the intricate patterns of the etchings on the

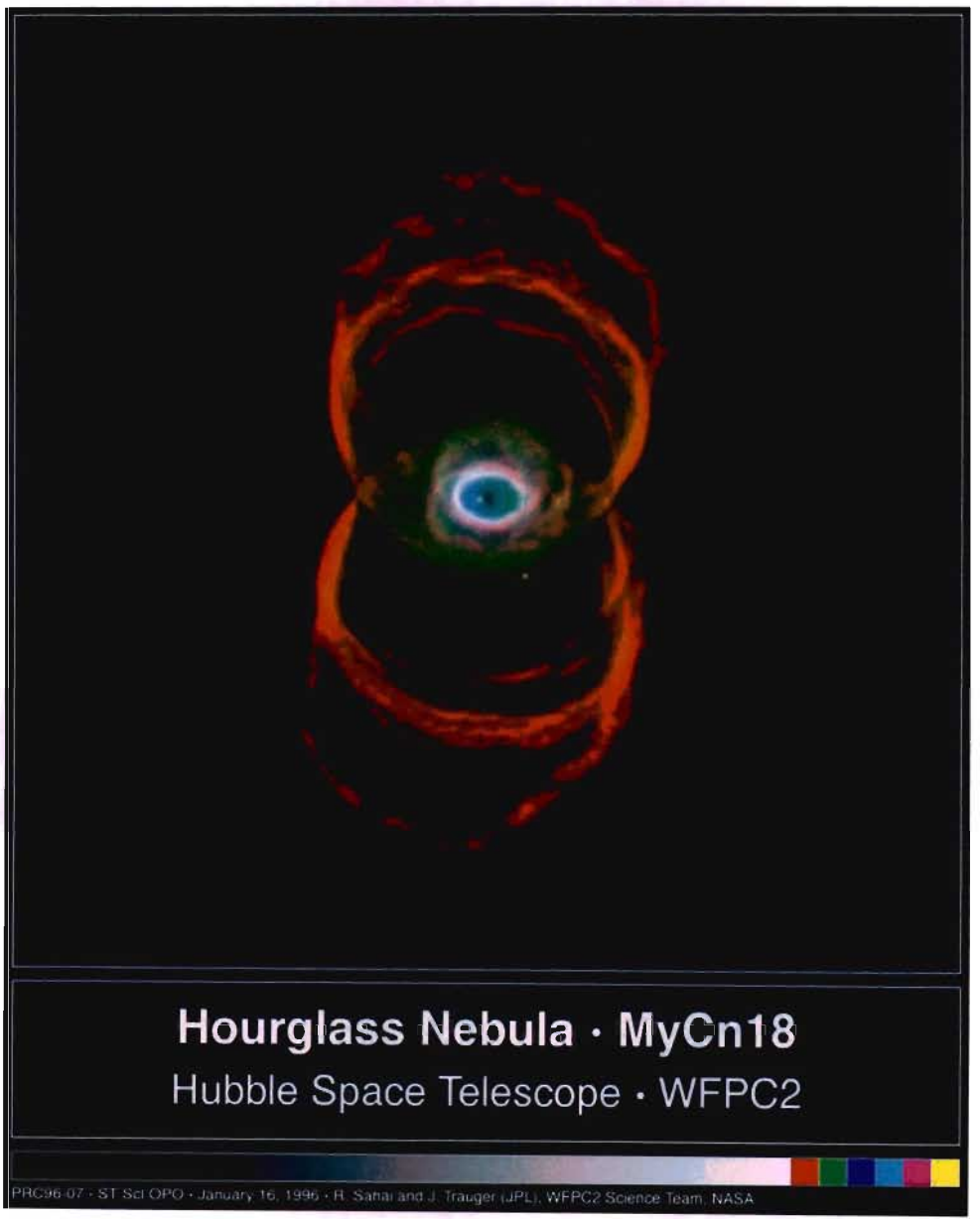

Figure 1.16: MyCn18, known as the Hourglass nebula for obvious reasons.

hourglass walls. The arc-like etchings could be the remnants of discrete shells ejected from the star when it was younger (e.g. as seen in the Egg Nebula), flow instabilities, or could result from the action of a narrow beam of matter hitting the hourglass walls. An unseen companion star and accompanying gravitational effects may well be necessary in order to explain the structure of MyCn18.

Figure 1.17: Another interesting example of planetary nebula.

A tempestuous relationship between an unlikely pair of stars may have created the oddly shaped, gaseous nebula shown in figure 1.17, that resembles an hourglass nestled within an hourglass. Images taken with Earth-based

telescopes have shown the larger, hourglass-shaped nebula. But this picture, taken with NASA's Hubble Space Telescope, reveals a small, bright nebula embedded in the centre of the larger one (close-up of nebula in inset). Astronomers have dubbed the entire nebula the "Southern Crab Nebula" (He2–104), because, from ground-based telescopes, it looks like the body and legs of a crab. The nebula is several light-years long. The possible creators of these shapes cannot be seen at all in this Wide Field and Planetary Camera 2 image. It's a pair of ageing stars buried in the glow of the tiny, central nebula. One of them is a red giant, a bloated star that is exhausting its nuclear fuel and is shedding its outer layers in a powerful stellar wind. Its companion is a hot, white dwarf, a stellar zombie of a burned-out star. This odd duo of a red giant and a white dwarf is called a symbiotic system. The red giant is also a Mira Variable, a pulsating red giant, that is far away from its partner. It could take as much as 100 years for the two to orbit around each other. Astronomers speculate that the interaction between these two stars may have sparked episodic outbursts of material, creating the gaseous bubbles that form the nebula. They interact by playing a celestial game of "catch": as the red giant throws off its bulk in a powerful stellar wind, the white dwarf catches some of it. As a result, an accretion disk of material forms around the white dwarf and spirals onto its hot surface. Gas continues to build up on the surface until it sparks an eruption, blowing material into space. This explosive event may have happened twice in the "Southern Crab". Astronomers speculate that the hourglass-shaped nebulae represent

two separate outbursts that occurred several thousand years apart. The jets of material in the lower left and upper right corners may have been accelerated by the white dwarf's accretion disk and probably are part of the older eruption.

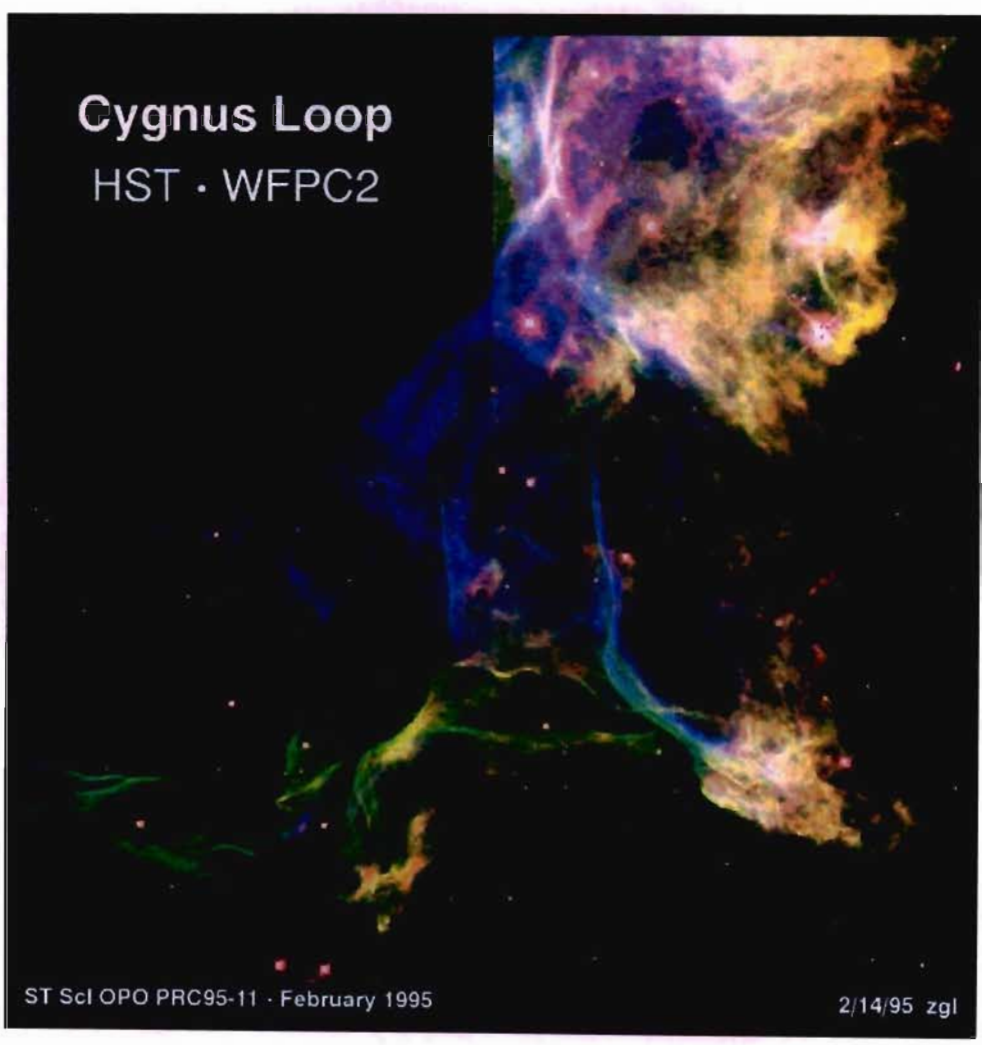

Figure 1.18: The Cygnus Veil.

Another spectacular planetary nebula is the Cygnus Veil, which takes its name from the constellation where it lies. It is an impressive object, which is visible with small amateur telescopes and it is so big that it usually escapes the field of view. The Veil has in fact an angular diameter which is six times that of the Moon. The supernova which gave birth to this object exploded about 15000 years ago and was situated 2500 light years away.

In the image 1.18 on the previous page, the supernova blast wave, which is moving from left to right across the field of view, has recently hit a cloud of denser than average interstellar gas. This collision drives shock waves into the cloud that heats interstellar gas, causing it to glow. In the image, blue shows emission from "doubly ionised" oxygen atoms produced by the heat behind the shock front. Red shows light given off by "singly ionised" sulphur atoms (sulphur atoms that are missing a single electron). This sulphur emission arises well behind the shock front, in gas that has had a chance to cool since the passage of the shock. Green shows light emitted by hydrogen atoms. Much of the hydrogen emission comes from an extremely thin zone (only several times the distance between the Sun and Earth) immediately behind the shock front itself. These thin regions appear as sharp, green, filaments in the image.

Figure 1.19: The famous double spiral M51, in the constellation of Canes Venatici. It is clearly visible the bridge of matter that joins the two interacting galaxies. (Image Hubble Space Telescope)

1.7 Galaxies

The bigger gas structures we can see in space can be considered the galaxies. Of course, they are not made only out of gas and plasmas, but include stars, planets and very often other more exotic objects, like neutron stars. But, as said before, this solid objects account for less than one percent of the mass of a galaxy. Galaxies are huge objects, that rotate with a slow pace. But their rotation hides one of the most intriguing mysteries of modern cosmology. If galaxies had only the mass that we can observe, then they should not be

stable structures, but dissolve in a few million years. Of course, that does not happen. The most likely explanation of this mystery contains another puzzle. If galaxies were surrounded by a big halo of matter containing up to 90% of their mass, that would explain their rotation. The problem is now to discover what that halo is made from. Explanations range from old neutron stars to exotic particles, including "photinos", gravitinos, axions and magnetic monopoles, but none of them has been demonstrated.

1.8 Gas and plasma structures in laboratories

The study of gas and plasma structures as optical system started in the early Sixties[54]. Gas density profiles were produced thermally, dynamically or both to focus or guide a laser beam. The simplest gas lens consists of a heated tube from which the hot air is sucked. This is a lens with a very good quality, but convection limits the aperture to a very small 8 mm. A larger lens can be obtained up to about 3 cm by spinning the tube, but the focal length is too long for most practical purposes, being in the order of a few meters. In our university, a lens of this kind was used to set up a small telescope, as a demonstration of the good quality. Of course, the small diameter does not make it interesting for this purpose, but it is nevertheless amusing to see through a telescope made out of air. Then, the lens can in principle be rescaled to much bigger diameters in space, where convection

does not take place. A much stronger lens, generally negative, is the vortex gas lens; this is the first lens used to drill holes with a laser. The reason for gas lenses is that they can be used for high power lasers, that would damage a conventional glass or quartz lens. For instance, a gas telescope could be useful to transmit the huge powers required to laser propel a satellite into orbit[49].

Many other examples of plasma structure can be found in laboratories. These include all the plasma pinch devices, used mainly for the production of soft X-rays. In these devices, a thin plasma is created by sending a large current pulse through a thin wire.

1.8.1 Magnetically confined plasmas

Other structures can be found in nuclear fusion experiments, where plasmas are confined by means of magnetic and electric fields into a toroidal shape. These structures look very similar to the Van Allen belt of our planet and in fact they are created basically by the same mechanism.

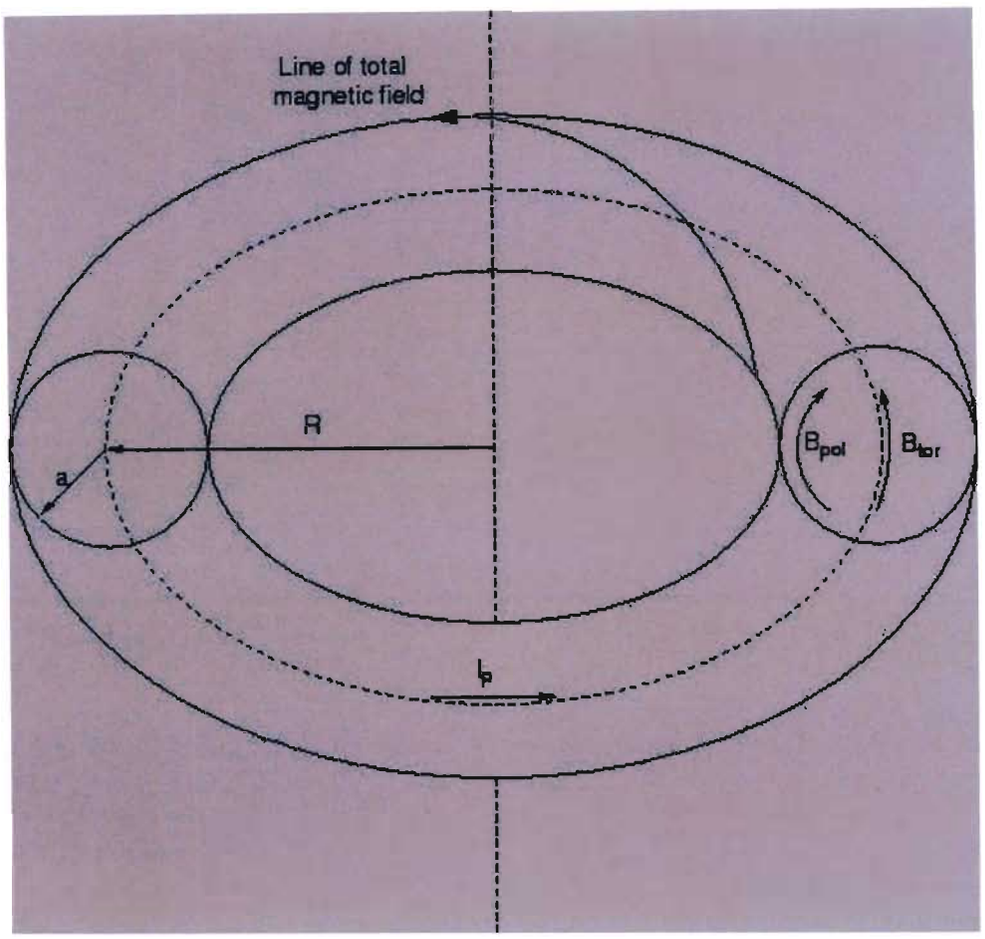

Figure 1.20: Schematic of a toroidal magnetic confinement system showing the basic magnetic geometry. The major and minor radii (R and r) are labelled together with the poloidal and toroidal magnetic field $\vec{B}_{pol}$ and $\vec{B}_{tor}$. A toroidal plasma current may also be present.

A charged particle in a magnetic field tends to move on an helicoidal orbit around the lines of the field. This fact can be used to confine a reacting plasma by means of especially shaped magnetic fields, in order to sustain

the required temperatures for fusion and facilitate the extraction of excess energy. The earliest experiments used "magnetic bottle" configurations, but it became immediately obvious that particle and energy losses are unacceptably high, due to motion along non-closed field lines. Moreover, the plasma rapidly becomes polluted with eroded particles coming from the surface in direct contact with it, further increasing energy loss due to atomic radiation.

In order to avoid energy losses both from open field lines and from contamination, the plasma can be arranged in a toroidal shape. In this way, particles of mass m and charge q are free to move parallel to field lines but are constrained to follow helical orbits of Larmor or gyro-radius $\rho_L = mv_\perp/qB$, with B the magnetic field strength and $v_\perp$the speed perpendicular to the field lines. In this case, collisions lead to radial diffusion by transferring particles from one orbit to another and thus subtracting energy from the plasma.

A device generating a simple solenoidal magnetic field (where field lines are circular and toroidally closed) is not sufficient to confine a plasma. In this configuration, the toroidal field varies as the inverse major radius, $1/R$. The Larmor radii of the particles thus differ as they gyrate, being always smaller in the region of higher field (toward the centre of the torus). This causes a charge-dependent particle drift, whereby electrons and ions move oppositely in the $\vec{B} \times \nabla\vec{B}$ (i.e.vertical) direction. The resulting charge separation then gives rise to an electric field $\vec{E}$ which causes the plasma to drift out of the torus in the $\vec{E} \times \vec{B}$ direction.

In order to counteract this effect, it is possible to supply an additional

poloidal field such that the field lines twist helically around the plasma column. Plasma particles travelling along the field lines thus experience a $\vec{B} \times \nabla \vec{B}$ drift velocity which changes sign as they move around the torus, the net drift effect thus averaging to zero. The way in which the magnetic field 'twist' is generated forms a broad categorisation of confinement devices. A schematic drawing of such a toroidal confinement system is shown in figure 1.20 on page 48.

The Tokamak

The tokamak (derived from the Russian for 'toroidal chamber with magnetic field') has been the predominant line of research on magnetically confined fusion since ts initial proposal by Sakharov and Tamm in 1961[35]. It is an asymmetric device with external coils that generate a large toroidal magnetic field on which a plasma current superimposes the poloidal field necessary for confinement. This plasma current is induced via a transformer action, i.e.by generating a current in a circuit surrounding the plasma column, in which the plasma acts as the secondary winding.

To date, the best fusion plasma parameters ever obtained were those of the JET tokamak experiment in the UK in late 1997. In that experiment JET produced 21.7 MJ of energy, with a peak fusion power of 16 MW using a mixture of deuterium and tritium. This corresponds to a ratio of output to input power of 65%. The JET campaign also demonstrated the feasibility and safety of remote tritium handling techniques which will be a necessary

feature of fusion reactors.

In spite of their relative simplicity and good plasma performance, Tokamaks suffer from some drawbacks regarding suitability as a fusion reactor. Firstly, the high currents required by the transformer action generating the plasma current make impossible to maintain a steady state indefinitely. For this reason, the tokamak is a pulsed device. Another problem with Tokamaks is the so called phenomenon of disruption, where a sudden loss of plasma current occurs, resulting in catastrophic confinement loss and a rapid escape of stored plasma energy. The cause of these drastic events is not yet fully clear. The rapid change in current gives rise to very large inductive forces on the vessel and coils, and thus to enormous mechanical stresses on the machine.

The Stellarator

Another type of fusion confinement device is the Stellarator. The Stellarator was first proposed by Lyman Spitzer at the Peaceful Uses of Atomic Energy Conference in Geneva in 1958[67][1].

The term Stellarator means "star generator" and encompasses non-asymmetric toroidal devices. Unlike the tokamak, the confining field is generated purely by external coils and does not depend on the existence of a toroidal plasma current (although there can be one present). For this reason the plasma can be confined indefinitely without recourse to current drive schemes so that the device is inherently capable of uninterrupted operation, a highly

[1]The original proposal was made in a classified 1951 report for the U.S.Atomic Energy Commission.

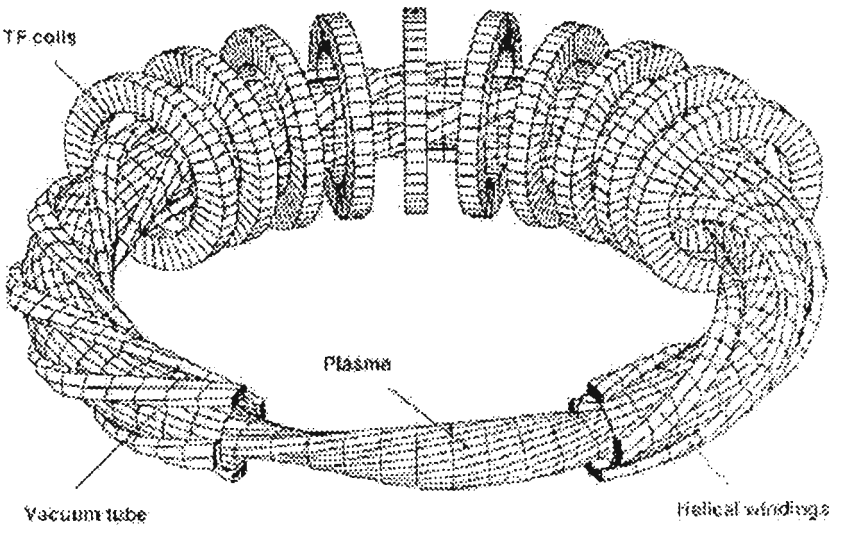

Figure 1.21: Schematic of the Stellarator Wendelstein VII-A.

desirable feature for any reactor concept.

Stellarators are much more complex than Tokamaks and thus the research on these machines has progressed slower. Only recently stellarators have enjoyed increased interest and to date, both of the newest, largest superconducting magnetic confinement devices are stellarators: the Large Helical Device or LHD (which had its first plasma in March 1998) in Toki, Japan and Wendelstein VII-X (currently under construction) in Greifswald, Germany. In spite of their differences, stellarators and Tokamaks share many of the physics issues of fusion plasmas, particularly those concerning the anomalously high rates of energy loss which have baffled scientists in the field for many years.

There are many different kinds of stellarators, depending on the specifics of the magnetic configuration. A common feature of all such devices is the toroidal periodicity. Classical stellarators utilise a system of toroidal field coils and multi-polar helical windings (which generally occur as opposing pairs, with the current flowing in both directions) to generate the confining field. The plasma cross sections of these stellarators tend to be roughly circular, elliptical and triangular in cross-section, respectively. Slightly different machines, the torsatrons, use unipolar helical windings to produce the helical and toroidal fields with a single coil-system. This reduces the number of coils and usually leads to better access for the plasma diagnostics. Such devices require an additional vertical field to complete the confining field.

Chapter 2

Particle acceleration in plasmas

Many applications have been proposed for modern ultra-high intensity and short duration lasers. One of the most promising applications is the acceleration of charged particles, which has already been demonstrated experimentally. In these accelerators, a plasma wave is stimulated by a laser pulse, and a particle beam is simultaneously injected into the plasma. What makes these accelerators very interesting is the fact that the electric field gradient of a plasma wave can be more than 200 GV/m, i.e., four orders of magnitude higher than that of a RF Linac (<20 MV/m). A laser plasma based accelerator would make it possible to reach very high energies in a short space.

A useful guide to Laser Driven Accelerators

Type of acceleration	Process &/or useful equations	Present (2004) experimental parameters	Laser type & Laboratory	other comments e.g. effects of laser guiding
BWA Beat Wave Accelerator	$E_eV = \alpha\sqrt{n_e}(cm^{-3})$ $\nu \simeq q \cdot n_e^{\frac{1}{2}}$ $\omega_1 - \omega_2 \approx \omega_p$	$\omega_1 \approx= \omega_2 \approx 10^{15}\ Hz$ $\omega_1 - \omega_2 \approx 10^9\ Hz$ $I \approx 10^{14} to 10^{16} W/cm^2$ $n_e \approx 10^{18} cm^{-3}$	Two CO_2 lasers (10.6 μm and 9,4 μm) or a YAG and a YLF	Guiding essential to extend Rayleigh interaction length Z_r, otherwise only a few MeV
Inverse Free Electron Laser (F.E.L.)[9]	F.E.L. Gain equations	Split CO_2 laser beams drive two undulators in series: 28 MeV		First Laser Driven Accelerator to demonstrate staging[26].
LWFA Laser Wake Field	Original discovery stimulated by Raman forward scattering: Complicated relativistic equations. Numerical solutions.	$\tau \approx 1\ ps$ $I \approx 10^{18} W/cm^2$ Ionised gas jet: $n_e \approx 10^{19} cm^{-3}$ Early $\epsilon \approx 1 MeV$ Recent $E > 100 GV/m$	Ti-Sapphire (0.5 J in 40 fs, giving approximately 10 TW)	No staging or alternating gradient focusing or phase tuning so far. For "fast ignition" in laser fusion beam is guided into dense fuel region by metal conc.

A useful guide to Laser Driven Accelerators				
Type of acceleration	Process &/or useful equations	Present (2004) experimental parameters	Laser type & Laboratory	other comments e.g. effects of laser guiding
SM-LWFA Self-Modulated LWFA	Intense laser or e^- or e^+ beams → Train of pulses self channeling up to $12Z_R = 0.6mm$	$n_e \approx 10^{19} cm^{-3}$ $25\ TW \rightarrow I > 10^{18} W/cm^2$ 200 MeV but large energy spread.	PW	If particle driven, SM-LWFA guiding problem disappear.
New regime: "bubble" = solitary pl. cavity → monochromatic e^- bunch	$>$ PW laser pulse generates under-dense plasma cavity	$\frac{1}{3} GeV in < 1\ mm$ Demonstrated up to $80 MeV$[16]	Ti-Sapphire (1 J in 33 fs)	Guiding not necessary.
Synchrotron (for comparison)	Multiple passes through radio-frequency cavities, alternating gradient focusing.	$800 MeV$, with a current of 180 μA, a pulse duration of 200 μs and a repetition rate of 50 Hz	n/a	

Two methods for accelerating particles were proposed back in 1979[68] by Toshi Tajima and J.M. Dawson. These methods are called beat wave acceleration (BWA) and laser wake-field acceleration (LWA), respectively. A third method, called self modulated wake-field acceleration (SMLWA), has its roots in Raman scattering, which was observed as an instability in the early eighties by C. Joshi[37]. An experiment followed more than ten years

later[19], when suitable lasers became available.

In all the experiments, laser channelling by plasma can increase the interaction length, especially in combination with a gas pipe, pre-formed as described in chapter 4 on page 89.

Experiments in particle acceleration by means of plasmas and lasers became possible thanks to the enormous increase in peak power of modern lasers, which now reach tens of terawatts, allowing intensities of up to 10^{20} W/m^2 on target. The electric field at the focus of such lasers can be as high as 300 GV/m, compared with the maximum of 100 MV/m obtained in conventional microwave accelerators. Direct use of these electric fields is not straightforward, though, since their direction is perpendicular to the propagation direction of the wave. The Lawson-Woodward theorem [41][70] shows that assuming an infinite interaction length, a relativistic particle and negligible non linear effects, the net acceleration is null. However, it is possible to achieve a considerable energy gain by violating one or more of these assumptions, for example by having the particle in vacuum which escapes the region of the high field before the electric field changes sign.

2.1 Beat wave accelerator

This scheme uses lasers with conventional long pulses ($\sim$100 ps) and modest intensity (I$\sim 10^{14} - 10^{16}$ W/c^{2}m. Two laser pulses are focused in a vessel containing gaseous hydrogen and create a fully ionised plasma. The beating

of the two waves provides a longitudinal electric field which oscillates with the frequency difference of the two lasers. If this frequency difference is equal to the plasma frequency, a resonance effect results, and the charge separation produces a field up to several GV/m. A relativistic particle with the right phase can then catch the wave and gain energy like a surfer.

A plasma has a natural oscillation frequency given by

$$\omega_p = (4\pi n_0 e^2/m)^{1/2} \tag{2.1}$$

where n_0 is the electron density of the plasma and m and e are the mass and charge of the electron, respectively. The ponderomotive force associated with a laser beam is proportional to the gradient of the square of the electric field. The radial intensity profile of the beam expels the plasma electrons from the regions where the laser is more intense, and stimulates the plasma oscillation. In this case, the energy transfer from the laser to the plasma is efficient only if the laser pulse length nearly matches the plasma wavelength λ_p. The field of a linear electron plasma wave is given by

$$E_0 = \frac{m_e \omega_p c}{e} \tag{2.2}$$

where m_e and e are the mass and the charge of the electron, ω_p is the plasma frequency, as in formula 2.1, and c is the speed of light in vacuum. The field is thus proportional to the square-root of the plasma density n_p. This means that a plasma density of $n_p = 10^{18}$ cm^{-3} gives an accelerating gradient of

1 GeV $\cdot$ cm^{-1}. In a nonlinear plasma wave the field is even larger.

The phase velocity of the plasma wave is equal to the group velocity of the laser in the plasma.

$$v_\phi = v_g = (1 - \omega_p^2/\omega_0^2)^{1/2} \tag{2.3}$$

where ω_0 is the plasma frequency. The maximum energy gain of a charged particle injected parallel to the longitudinal wave is

$$\Delta W = 2\epsilon\gamma^2 mc^2 \tag{2.4}$$

where $\gamma = (1 - v_\phi^2/c^2)^{-1/2}$.

2.1.1 Experimental results

The plasma beat wave acceleration was the first method to be proved experimentally, among the ones described here, because it is the one that requires the lowest laser intensity. In order to have the right modulation of the laser envelope, two lasers are used, with frequencies ω_1 and ω_2 such that $\omega_1 - \omega_2 = \omega_p$. This resonance condition can be achieved by tuning the density of the plasma, given fixed frequencies for the laser beams. The first evidence of acceleration was reported from a group by the University of California Los Angeles in 1985[11] using a two frequency CO_2 laser. The same group injected 2 MeV electrons from a Linac and succeeded in accelerating them

up to 30 MeV. The corresponding gradient of that experiment was 3 GV/m over a distance of 1 cm. The most interesting result of this experiment is that it proved that the electrons were actually trapped by the wave. Another group from the university of Osaka, Japan, reported the observation of 10 MeV electrons extracted from the background[27] without any injection.

2.2 Laser wake field accelerator

The laser wake field is a much simpler method, because the plasma wave is excited by mean of a single laser beam with a short duration (< 1 ps) and a high intensity ($> 10^{18}$ W/c^{2}m). In the laser wake field accelerator a plasma wave is driven by the displacement of plasma electrons by the ponderomotive force of the laser light. The ions remain stationary, due to the greater mass, and provide a restoring force while the electrons oscillate creating regions of net positive and negative charge. This electrostatic wake field then propagates with the laser pulse at nearly the speed of light and can trap and accelerate hot electrons. In the case of the laser wake field, the highest energy transfer is obtained when $\omega_p \tau = 4\sqrt{\ln 2}$, where τ is the laser pulse duration at FWHM, a much less stringent resonance condition than the one for the beat wave configuration. The resonant condition can be achieved by adjusting the plasma density. For a 400 fs laser pulse, for example, the resonance requires a plasma density $n_0 = 2.2 \cdot 10^{16}$ cm^{-3}. Before this method could be proved viable, it was necessary to wait for the development of very

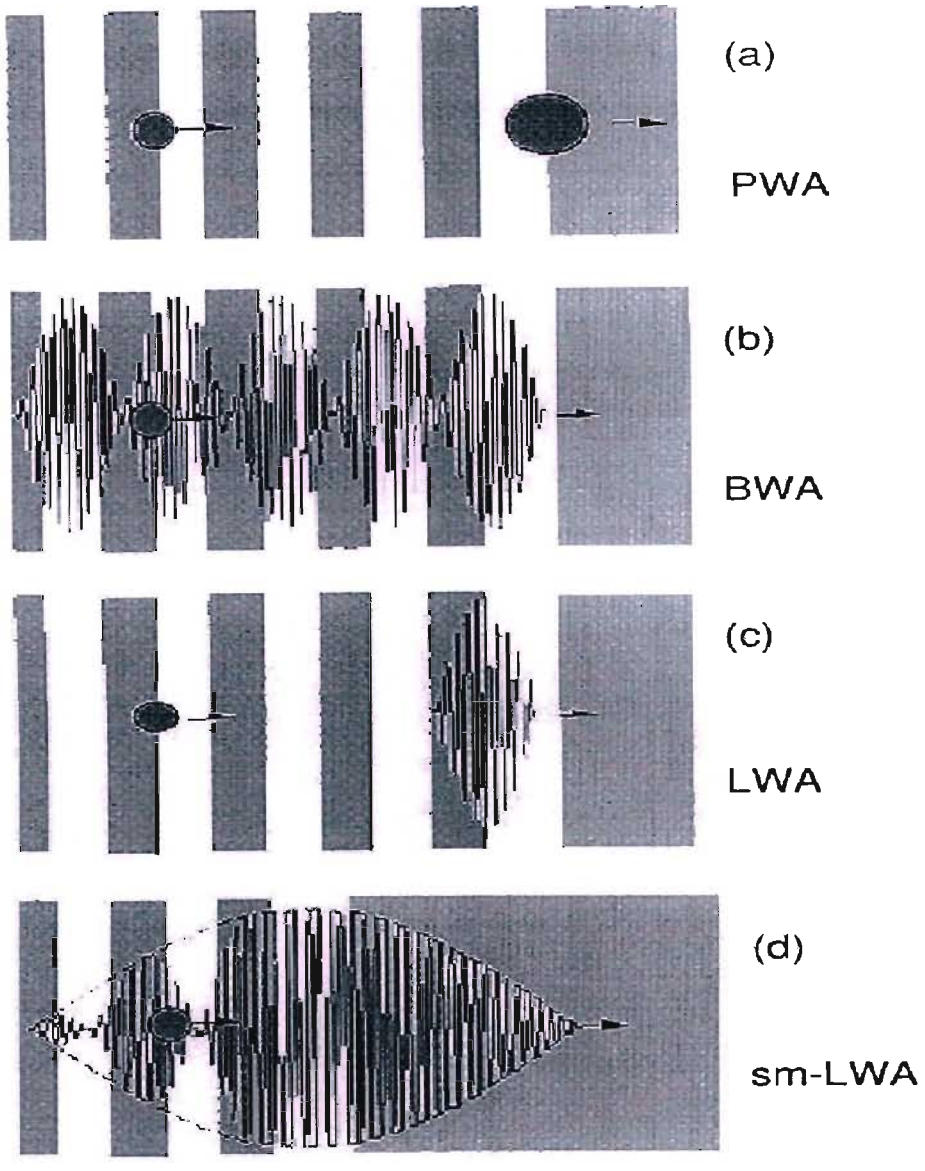

Figure 2.1: This graph from A. Ogata of the National Laboratory for High Energy Physics, Japan, explains clearly the generation of plasma waves in different accelerators. The background intensity shows the plasma density, the balls show the particle bunches and the solid lines show the laser intensity.

high brightness lasers with pulses shorter than one picosecond, to satisfy the resonance condition at a reasonable plasma electron density.

2.2.1 Experimental results

Accelerated electrons by means of laser wake field have been observed for the first time in 1994 by a group from the University of Tokyo, up to 30 MeV[18]. Until 2004, though, electron beam accelerated by mean of laser wake field had a rather large energy spread, that did not make them fit for any applications. Three groups[12][16][23] have recently reported beam of electron accelerated up to 80 MeV with an energy spread of less than 2%. The trick to obtain monoenergetic beams has proved to be that of adjusting carefully the interaction length of the laser with the plasma. In this way, electrons can ride the whole wave from the crest to the foot. Like marbles rolling down a hill, the electrons arrive at slightly different times, but they have all the same energy.

2.3 Self Modulated Laser Wake Field Accelerator (SMLWF)

Another method of accelerating electrons by means of plasmas and lasers is a modification of the wake field idea, which combines stimulated Forward Raman Scattering (FRS) and "sausaging" of the laser pulse envelope. From

an experimental point of view, this method is the simplest, because it does not rely on any resonance condition. FRS describes how a light wave with frequency ω_0 decays into two light waves with frequency $\omega_0 \pm \omega_p$ and the plasma wave ω_p. The forward Raman scattering was firstly identified as a plasma instability, but with the development of very high energy lasers it is now seen as a mean to accelerate particles. In order to allow the FRS to grow, the plasma density must be much higher than with the normal wake field accelerator.

2.3.1 Experimental results

The first experimental proof of self modulated laser wake field was obtained in 1995[10] by a group of LLNL/UCLA, which observed 2 MeV electrons from background using a 5 TW laser. Later, another group using the 25 TW laser Vulcan, at the Rutherford Appleton Laboratory, observed 100 MeV electrons[13].

2.4 Laser guiding

Normally, the acceleration length is limited to twice the Rayleigh length, defined as

$$L_R = \pi\sigma_0^2/\lambda \tag{2.5}$$

where σ_0 is the laser spot size and λ is the laser wavelength. With a typical spot size of 10 μm and the wavelength of a Neodymium laser ($\simeq$ 1 μm), $L_R \simeq 0.6\ mm$. This is mainly due to the fact the the laser beam is focused into a very small spot, in order to reach the required high intensity.

In order to achieve the right conditions for the acceleration, the laser pulse must be trapped and guided through a pre-formed channel. For optical guiding of laser pulses in plasmas, the radial profile of the refractive index must have a maximum on the axis, causing the wavefront to curve inward and the laser beam to converge.

Guiding a laser pulse in a plasma with the required intensity is not easy. A very promising method relies on the ponderomotive self channelling, already described[25]. This method of creating the central depression involves the use of another laser. If a laser pulse with a long duration is sent into a plasma, the laser ponderomotive force expels electrons from the axis and prevents their return, despite the Coulomb attraction, which arises from charge separation. If the laser pulse is long, ions start to move as well, as a result of the Coulomb force and gain momentum during the process. After the pulse is gone, electrons return to neutralise the charge of the ions which keep moving out. This leads to a plasma density depression on the axis[2][42]. For the self channelling to occur, the laser intensity must exceed the critical value of $17(\omega_0/\omega_p)^2 GW$[20]. In this case, the beam extends and forms a second focus. Increasing further the power leads to the formation of multiple foci, which eventually merge into a single channel. A channel formed in this

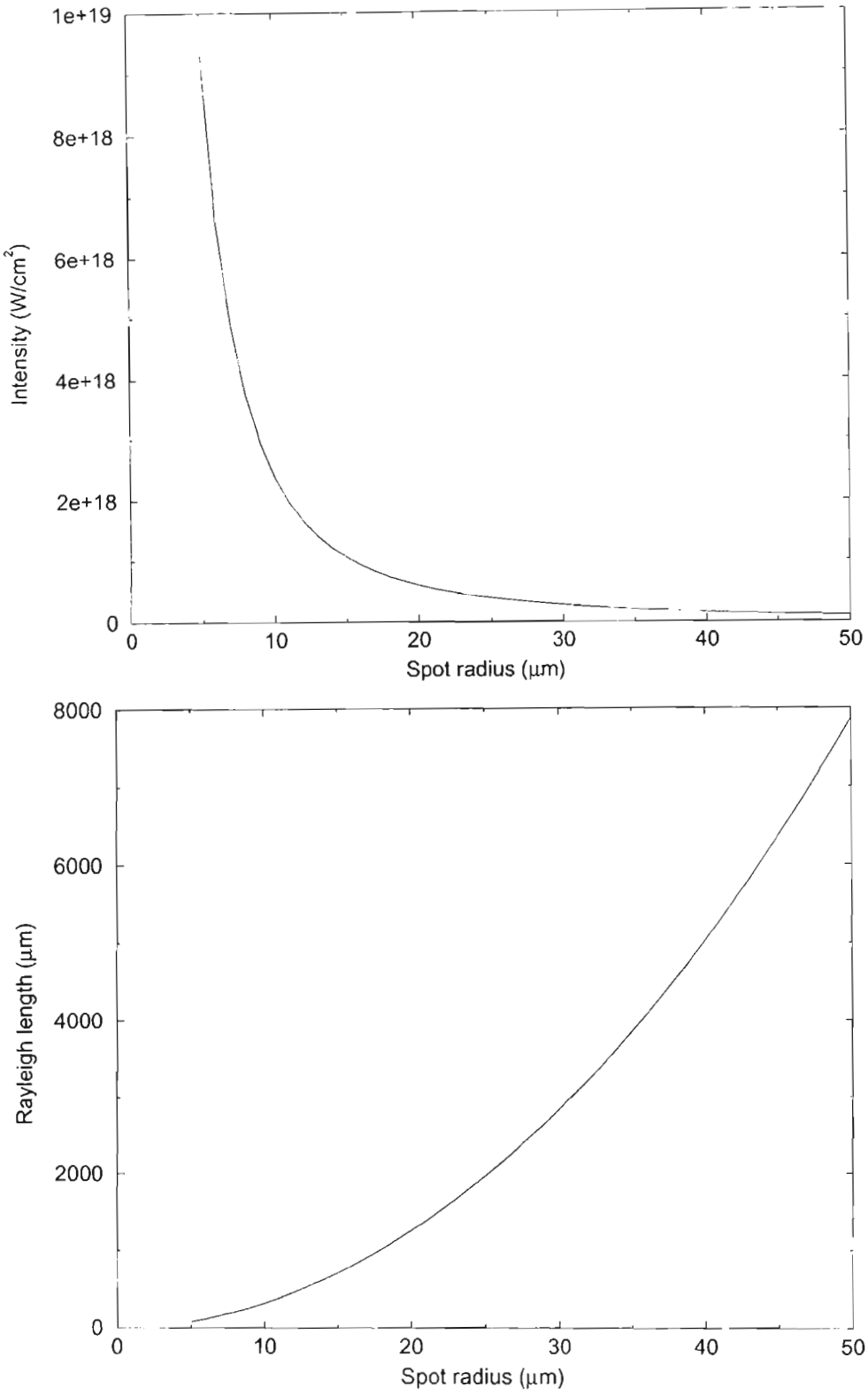

Graph 2.1: These two graphs show the behaviour of the intensity onto the target and the Rayleigh length for a typical laser pulse of 3 J, with a duration of 400 fs and a wavelength of 1 μm.

way has the advantage of having a small size, usually smaller than 30 μm, a high plasma density and the ability to sustain high laser intensities. The short interaction length is then the result of the diffraction.

2.4.1 Experimental results

Many experiments have already reported a laser self channelling by ponderomotive forces up to twelve times the Rayleigh length[15]. In all the experiments, the laser is focused onto the side of a helium gas supersonic jet a few millimetres long. By focusing the beam onto the side of the jet one can use the highest possible density gradient. The jet provides the right density profile for the laser channelling but not over a long distance and many groups reported this limit[22].

2.4.2 Improved laser guiding

Although to my knowledge no actual experiments have been performed on this topic, previous experience with conventional accelerators indicates that the following type of improved laser guiding should be studied. This is an optical analog of the well known alternating gradient focusing used in most large accelerators (the general principle is made understandable by the inverted pendulum experiment [63]). In the alternating gradient scheme for electron and heavy ion beams, the diameter of the beam is considerably reduced by applying a series of converging and diverging magnetic lenses. A

much less well known fact is that in the early sixties a similar beam diameter reduction was obtained with laser light. This was also done with a series of converging and diverging optical lenses at Bell Laboratories. Together with my supervisor, we suggest here that a series of converging and diverging virtual capillaries could be used to shrink both the particles beam and the laser beam in laser driven accelerators.

Another improvement not easily realisable with solid state capillaries is the tuning of the central density of the laser channel to the relativistic changing mass of the electrons. This changing mass leads to dephasing of the acceleration process.

Potential applications of Laser Driven Accelerators		
Realm	Specific application & method	Required beam energy
Medicine	Positron emission tomography. Tumour differentiation and heart disease. Requires local e^+ production due to short $\frac{1}{2}$ life of e^+ emitters. C^{11} 20 min, N^{13} (2 min), O^{15} (110 min)	e.g 5 MeV deuteron, 10 MeV protons
	Proton irradiation: range varies with beam energy, but is well defined by "Bragg peak" in human tissue.	$E < 200MeV$
	Neutron irradiation for deep tumours. Possibly the most effective form or radiation as it destroys both DNA strands: no mutations.	neutrons from spallation
	Hard X-rays. A range of energies could become accessible from T cubed laser driven accelerators.	X-rays energies of same order as beam energy (line and bremsstrahlung)

Potential applications of Laser Driven Accelerators		
Realm	Specific application & method	Required beam energy
Biology	At higher energies a laser driven accelerator X-ray undulator could replace international facilities such as Grenoble (France) and Diamond (UK).	Diamond: $E_{beam} \approx 3GeV(300\ mA)$
Solid State pharmacology research	Likewise biology, existing neutron spallation sources at international facilities could be powered by laser driven accelerators.	
Laser driven T-N fusion	Fast ignition from...eV electrons generated by PW laser focused deep in target with gold cone.	eV
Rubbia thorium burner	Proton injection into pure thorium generates neutrons and reactions: $Th_{90}^{232} + n_0' \rightarrow Th_{90}^{233} \rightarrow Pa_{91}^{233}\beta \rightarrow U_{92}^{233}$ $U_{92}^{233} + n_0' \rightarrow fission + 2n_0'$ No isotope separation necessary. Short $\frac{1}{2}$ life of decay products. Safe (accelerator dependent) reactor.	Initial experiment: 115 MeV protons (2 mA)
Particle physics	In the very long term laser driven accelerators might compete with LHC and Tevatron. In medium term, XXXX propose positron or electron driven "after burner."	SLAC beam

2.5 Conclusion

The principle of particle acceleration by means of laser stimulated waves in plasmas have already been demonstrated in several experiments. At least three different schemes, i.e., beat wave, laser wake field and self modulated

laser wake field, have actually been used to accelerate particles. With future development, this methods may be used to build small table top accelerators for medical use, for example, which would be almost impossible and too expensive with traditional methods. A 1 GeV accelerator based on the LWFA concept is already possible with the technology available now, with lasers able to deliver 25 J pulses in 120 fs.

A multi-stage accelerator is then mandatory in order to reach energies of several TeV, which would make these accelerators interesting for particle physicists. The difficulty of operating a multi-stage system is that phase control is a non trivial problem. In every stage the particles have to be in phase with the wave produced by the plasma.

A new and alternative method to produce a pre-formed gas channel with a length up to several centimetres is proposed in the chapter 4 on page 89 of this thesis.

Chapter 3

Experimental setup

Our experimental setup was rather simple, using mainly devices that where built within the university, some by me . This was due to a lack of funds, which forced us to be creative and make the best out of what we had.

Our first experiment, described in chapter 4 on page 89, was an attempt to produce a pipe with over-dense walls and an under-dense core. This can be obtained by means of colliding cylindrical shock waves. The aim of the second experiment, described in chapter 5 on page 127, was to produce a colliding shock lens with a useful diameter, up to 1 cm. This device makes use of spherical shocks to create a gas structure that works as a lens.

Since we performed two different experiments, we had two setups. The only difference between them was in the shock production, because the diagnostics were almost identical in both cases.

3.1 Production

The main issue in any experiment with gas structures or colliding shock lenses is the production of the shocks. In our experiment we used two methods of production, which depended on the kind of structure required. The idea behind is always to store the energy in a big capacitor and discharge it at once through a suitable device.

3.1.1 Spherical shocks

When we need spherical shocks, as in the case of the colliding shock lens, we obtain them by breaking down the air contained between two pins in front of each other, as in figure 3.1 on the following page. The breakdown is controlled by means of a spark gap. In this case, the explosion is always a sudden one, because the resistance drops quickly to zero during the breakdown. This ensures the good quality of the shocks, which are sharp, fast and travel for long distances without weakening too much. At the beginning of the experiment, the pins were connected in parallel using different capacitors. This method allows the use of a much lower voltage (a few kV as opposed to 20 kV); however, small differences in the electrode separation corresponds to different break down times, and therefore the shocks arrive to the centre unevenly and do not produce a working lens.

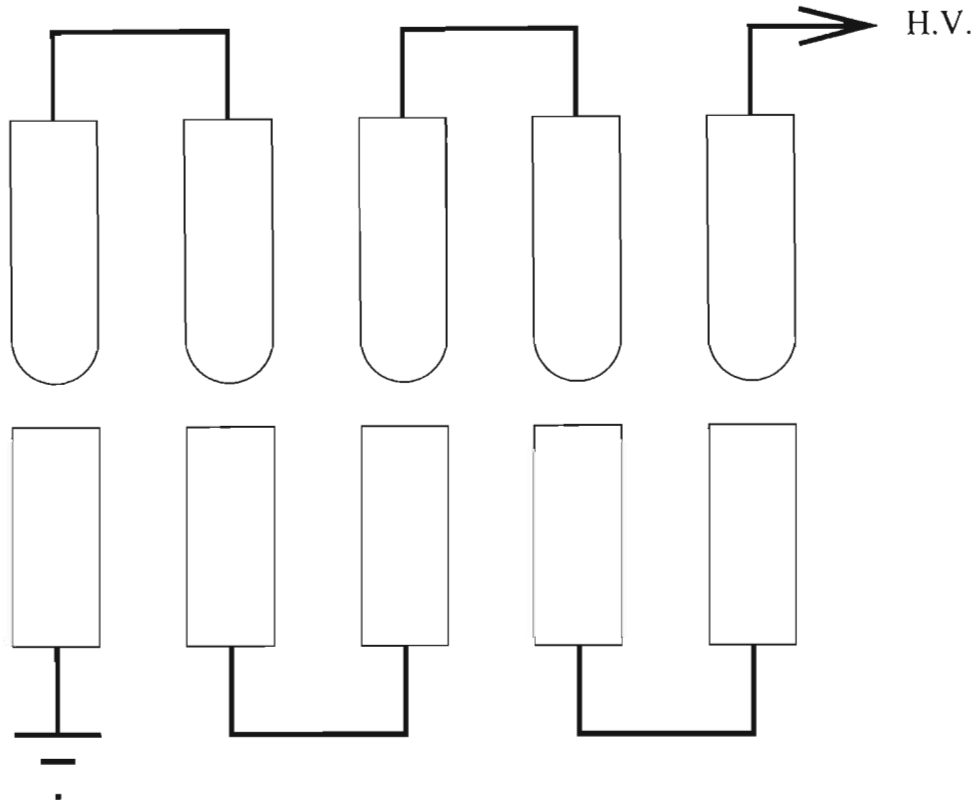

Figure 3.1: Shock wave production by means of facing pins. It can be noted that all but the first and the last pins are left floating. The voltage is applied between the first and the last pin by mean of an inductor or a resistor (see figure 3.10 on page 88). The voltage propagates by induction to the other pins. The pairs could be driven in parallel, but this makes more difficult to synchronise the discharges. When the discharge is very fast, each arc is like a small explosion and produces a shock wave.

3.1.2 Cylindrical shocks

Two different systems can be used to produce the cylindrical shocks, depending on the needs of the experiment. If a high repetition rate is required or the experiment is performed in a closed environment, the best way is to use a row of small spark gaps connected in series. Due to Mach addition, the several shocks would then merge into a cylindrical one. By the process of Mach Addition, two or more shock waves that collide at a shallow angle generate a new wave, which travels between the two original directions.

A cylindrical shock can be obtained in another way: by discharging a big capacitor through a very thin wire it is possible to explode it producing a high quality cylindrical shock. Of course, the time needed to replace the wire makes this system unsuitable for experiments which must be operated in repetition mode. In this case, the thickness of the wire is the most critical factor for the quality of the shock. A thin wire has a higher resistance and breaks down more quickly. Also, the thinner the wire, the smaller the amount of material, and hence the amount of energy required to explode it. Moreover, having less material leads to the production of fewer debris, which can be dangerous for some experiments (see section 4.4.1 on page 109).

Using the data in graph 3.1 on the following page, it is possible to estimate the explosion time, that can be compared later with the observed one. The time needed to explode the wire may be approximated by the time needed to heat a piece of the same wire to boiling temperature, including the latent heat of melting and vaporisation. As a simplification, we may regard the

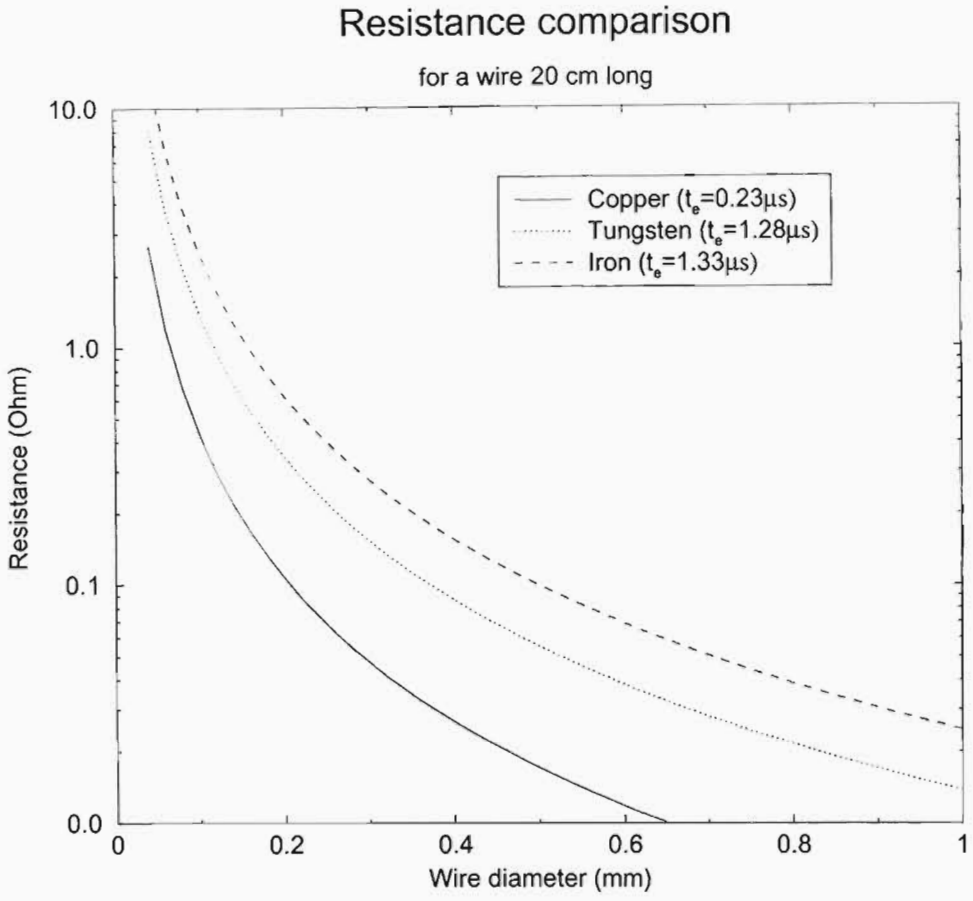

Graph 3.1: Resistance of three materials vs wire diameter.

specific heat as being constant and equal to the one of the solid phase. The explosion time is then

$$t_e = \frac{E}{P} \tag{3.1}$$

where P is the power available and E is the energy required to heat and vaporise the wire.

The available power depends on the voltage of the capacitor used in the

circuit and on the resistance of the exploding wire, because the heat production is due to Joule effect. Again, for the sake of simplicity we regard the capacitor as a battery with a constant voltage. As we shall see later, this assumption is a sensible one, because the energy needed to vaporise the wire is much less than the one available in the capacitor.

Because the wire is heated by Joule effect, the power available is

$$P = RI^2 = \frac{V^2}{R} \tag{3.2}$$

where R is the resistance of the wire, V is the voltage across the capacitor and I is the current flowing through the wire. For a wire of a given material, the resistance is equal

$$R = \frac{\rho L}{\pi r^2} \tag{3.3}$$

where ρ is the resistivity of the wire material, and L and r are the length and the radius of the wire, respectively. It should be noticed that the resistivity of a metal increases with the temperature (for carbon, for instance, it decreases), but we assume it constant.

The energy required to vaporise the wire depends on its mass, on its boiling temperature and on its thermodynamic properties, and is

$$E = \pi r^2 L(\delta C_p T_b + L_f + L_v) \tag{3.4}$$

where r and L are again the radius and the length of the wire, respectively,

δ is the density of the material, C_p is the specific heat, T_b is the boiling temperature of the material and L_f and L_v are its fusion and vaporisation heats, respectively.

The exploding time then becomes

$$t_e = \frac{\rho\delta L^2(C_pT_b + L_f + L_v)}{V^2} \tag{3.5}$$

From the equation it may be noted that the explosion time does not depend on the radius of the wire. This is simply a consequence of the assumption we made of the infinite capacitor. This assumption makes sense if and only if the energy required to explode the wire is much smaller than the energy stored in the capacitor. In the case of a copper wire 30 cm long and with a diameter of 50 μm, for instance, the exploding energy is 20 J, to be compared with the 200 J stored in a 1 μF capacitor at 20 kV (typical of our experiment).

Using the data in table 3.1 on page 78, considering a wire 30 cm long and a voltage of 20 kV, the explosion time becomes:

	Copper	Iron	Tungsten
Time (μs)	0.23	1.33	1.28

Despite our crude approximation, these times are comparable with those observed during the actual experiment (see figure 3.2 on the following page). Of course, in the actual experiment there are other factors to be taken into account, like the radiative dissipation of energy.

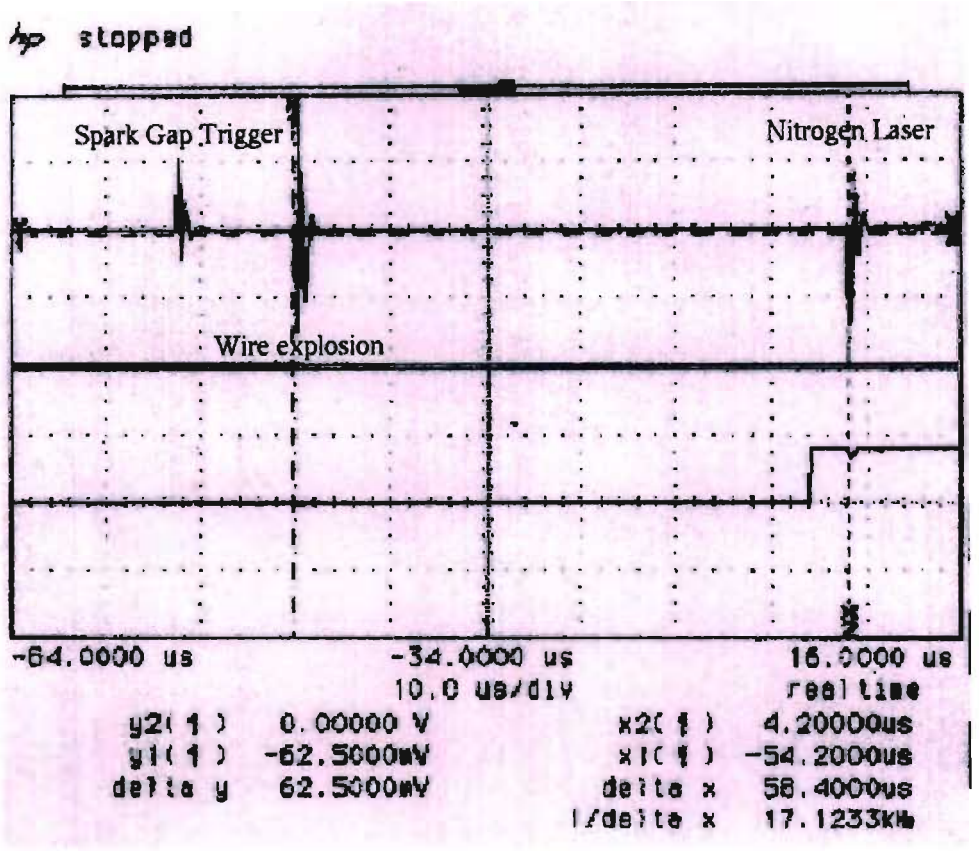

Figure 3.2: An oscilloscope trace of one of our pipe experiments. The actual explosion is the second peak from the left in the top trace. It is interesting to note that, despite our wire was made with an unknown alloy, the explosion time is comparable with the calculated ones.

3.2 Propagation

The propagation of the shocks is a critical part of the experiment. One has to ensure that the shocks are not only produced with a high quality, but also that they maintain it until they can interact. The first easy and obvious rule is that shock become broader and weaker as they travel. Of course, one has

	Copper	Iron	Tungsten
Density (kg/m^{-3}	8960	7860	19250)
Specific Heat J/kgK	385	444	135
Boiling point (K)	2843	3023	5828
Heat of Fusion, L_f (kJ/kg)	205	250	190
Heat of Vaporisation, L_f (kJ/kg)	4730	6200	4390
Resistivity (Ωm)	$1.72 \cdot 10^{-8}$	$9.71 \cdot 10^{-8}$	$5.51 \cdot 10^{-8}$

Table 3.1: Elements data

to take into account the angle at which the shocks collide. If the angle is too sharp, they go through each other unmodified, as when the energy is too low, and do not merge by Mach addition.

The shock is a discontinuity in the pressure, a compression wave, that travels through the medium. The behaviour of colliding shocks is mainly ruled by their M_0 (Mach) number, which is the ratio between the speed of the shocks and the speed of sound in the medium and depends on the size of the discontinuity. Different Mach numbers correspond to different regimes for the shocks. For $\Delta P/P < 5\%$ we may consider the flow incompressible and the waves are normal acoustic ones. For higher discontinuity ratios, the shocks travel faster than sound. In most of our experiments $1.2 < M < 1.6$.

The right Mach number is necessary in order to ensure the formation of the right structure. Shock waves with a Mach number close to unity are not useful, because when they collide they simply pass unmodified through each other. For higher Mach number, shocks merge together, losing some information on their origin and producing a bigger common shock, which generally has a slightly higher speed; this process is called Mach addition

and many experimental examples of it are shown later. This is the regime used in all our experiments. For even higher values of M, say $M > 1.6$, the collision of the shocks leaves behind only turbulence and the resulting structure becomes unusable, at least in our experiments. The situation is made more complicated by the energy dissipation of the shocks on the shock front. This makes the shocks weaker (i.e., it reduces their M number) and wider. In fact, when shocks have to travel for a long distance, it is possible to produce them with $M > 1.6$ without having turbulence problems, as far as they interact with a lower M.

3.3 The image acquisition system

At the beginning of the experiment, the acquisition system was a CCD camera connected with a computer through a digitising board. Unfortunately, these cameras are very sensitive to the electromagnetic noise produced in our experiments. This means that most of the time the image was lost because of the noise. This happened either because the noise triggered the camera at the wrong time or because the image was unreadable. For this reason, despite the many advantages offered by the video-camera, after a while we moved to a much simpler imaging system, namely photographic paper. Photographic paper is very sensitive to the ultraviolet light emitted by our nitrogen laser and can be developed at once. But photographic paper has many disadvantages too. The most important problem is that the high intensities of laser

light saturate immediately any photographic paper. In our experiments we used Ilford paper number 1 (i.e. with the lowest possible contrast), but still most of the images are really only in black and white. This did not allow a quantitative comparison of the laser intensity in different parts of the image. The idea of calibrating the paper in order to obtain some more quantitative data was not pursued for many reasons. First of all, most of the time the development of the images was tailored to what we wanted to see. This means that in the dark room, very often the development was stopped and the image fixed as soon as we could see the features we were interested in. Moreover, chemical films or paper calibration is not a trivial topic. I have worked in the past on soft X-ray spectroscopy and I have some experience of film calibration, that used to be a hot topic[34], before the CCD era. Part of the problems comes from that fact that every time paper or films is produced, there are small differences. As an amateur photographer, I used to buy several films with the same production number and do some tests on one one of them and treat the others according to the results. Moreover, the density of the images depends on many parameters, like the temperature of the bath, it's exact composition and the developing time. Controlling all of them at the same time over several months without a proper professional developing machine is not possible.

A more important problem with the paper is a safety issue. Our experiment is performed on an optical bench, where the diagnostic laser and the "detector" lies at the ends and the CSL, or the pipe, is in the centre. This

means that changing the photographic paper involves going very close to the high voltage power supply and the capacitors. This can be very dangerous, because at the end of the experiment the capacitors are still charged up to 1 kV and a special care must be taken to avoid touching them. Since photographic paper must be kept in darkness, at the beginning of our experiment we used to switch off the lights. Later, after a few near misses, we had a red light installed, but the laboratory remained still quite dark, and dangerous of course.

Figure 3.3: The "detector" used during our experiments. The photographic paper is placed into the box. On the right, a lens focuses the beam into a little hole and the light is then filtered through a UV filter. In this way, we avoid the light from the explosion of the wire.

3.4 The optical setup

The optical line was different according to the experiment performed. For the CSL, a single lens was normally used to expand the beam. In this way, the magnification of the system may be adjusted only by changing the distance of the photographic paper. This make sense because the device is small and the beam does not diverge very much while going through it. When trying to get images on the far field, we had to set up a small telescope to collimate the beam. In this case it is very important to have a parallel beam, because of the weakness of the colliding shock lens. An advantage of the CSL is that it does not require a very precise alignment.

Much more critical is the experiment with the pipe. First of all, in this case the divergence of the beam must be as small as possible, and so a telescope must be used. Then, the alignment is very critical, because the light must be free to travel all the way through the pipe, for diagnostic purposes. To align the pipe we used two plastic disks with small holes, placed at the extremities of the holder. A second problem with this experiment is the fact the the explosion is very bright and the paper must be protected from its light. Unfortunately, a filter for the laser wavelength proved insufficient. So, a lens was place at the end of the device, in order to send the laser beam through a little hole. On the other side of the hole, the beam was free to expand and again the magnification could be chosen simply by moving the paper.

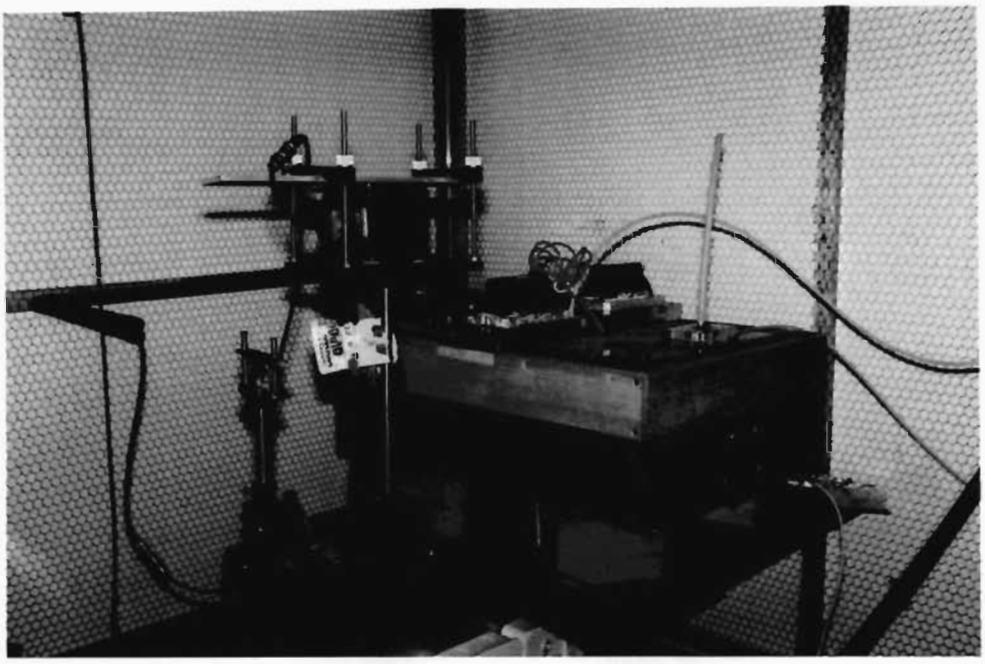

Figure 3.4: The diagnostic nitrogen laser used in our experiment. We had to put a small shutter in front of it because it often self triggers.

The last part of our optical equipment was a small shutter in front of the laser, lifted by an electromagnet. This was important because our nitrogen lasers often fire spuriously, untriggered, and if the paper is in position then it needs to be changed before running the experiment.

3.5 The circuit

The electric/electronic part of the experiment can be divided into two well separated sections. On one side, we have the high voltage circuit, on the other, the trigger and diagnostics.

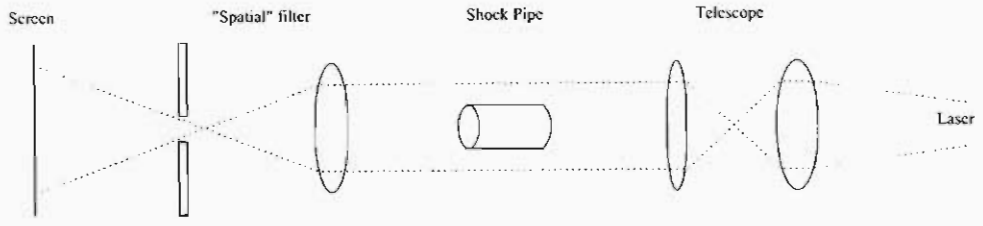

Figure 3.5: The simple optics of the experiment. The two lenses of the beam collimator, on the right, have a focal length of 5 cm and 50 cm respectively. The lens used for the filter has a focal length of 10 cm.

The high voltage section is quite simple. Figure 3.9 on page 88 shows the circuit used for the pipe experiment, which is the simpler of the two. For the CSL, in fact, we have to put a coil in parallel to the pins, as in figure 3.10 on page 88. The coil is necessary because the pins are an open circuit and it is necessary to charge the spark gap; of course, with the DC voltages used to charge the capacitor, the coil is a good conductor, but becomes almost an open circuit at the high frequencies of the discharge.

The HT power supply is remotely controlled from the control room. We can operate the experiment without being in the room where the dangerous high voltages are. Between the power supply and the experiment there is a resistor (400 Ω) and a coil, to protect the PS from extra voltages during the main discharge. The voltage across the capacitor is measured with a multimeter connected to a 1:1000 high voltage probe.

The rest of the circuit, which controls both the trigger and the diagnostics, is described in figure 3.7 on page 86. The main signal to run the experiment comes from the main trigger, which is a small box that delivers a 5 V square

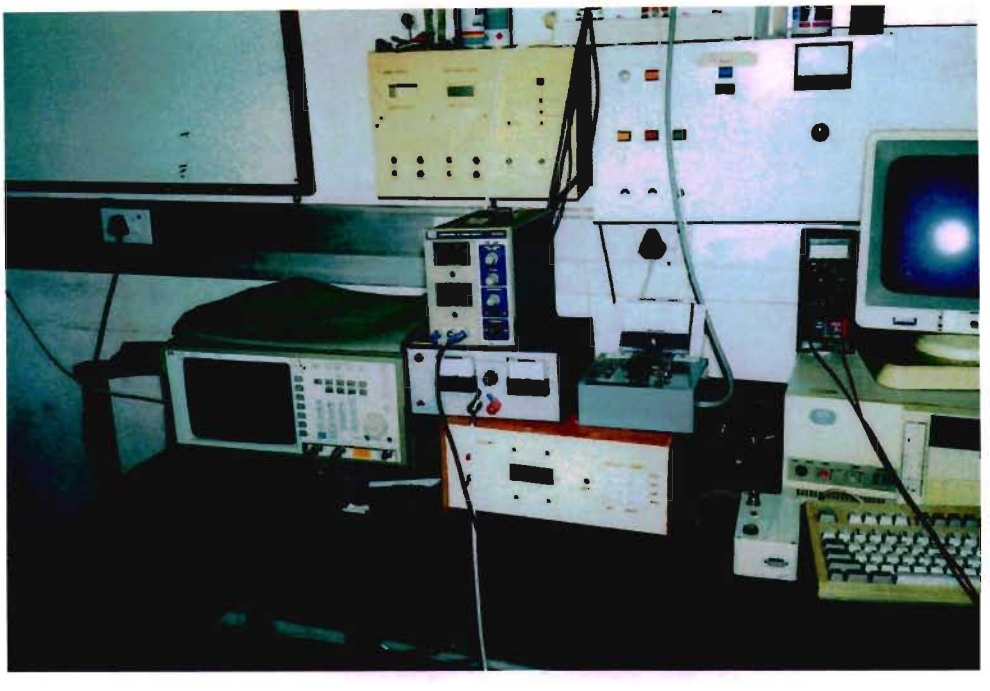

Figure 3.6: The main remote controls of the experiment. The orange box is our delay box and, above it, there are the power supply of the optical trigger and the controls of the power supply.

pulse. This pulse is sent both to the oscilloscope and to the high voltage trigger of the spark gap. Once the spark gap opens and the device (either the CSL or the wire experiment) fires, an optical trigger picks up the light and sends a signal to a delay box. The delay box then triggers the laser with the appropriate delay, in accordance with the requirement of the experiment. A coil in the screened room then picks up the noise both from the main experiment and from the laser, allowing one to measure precisely the delay, without relying on the value set on on the delay box.

All the devices used in these experiments were made in this university,

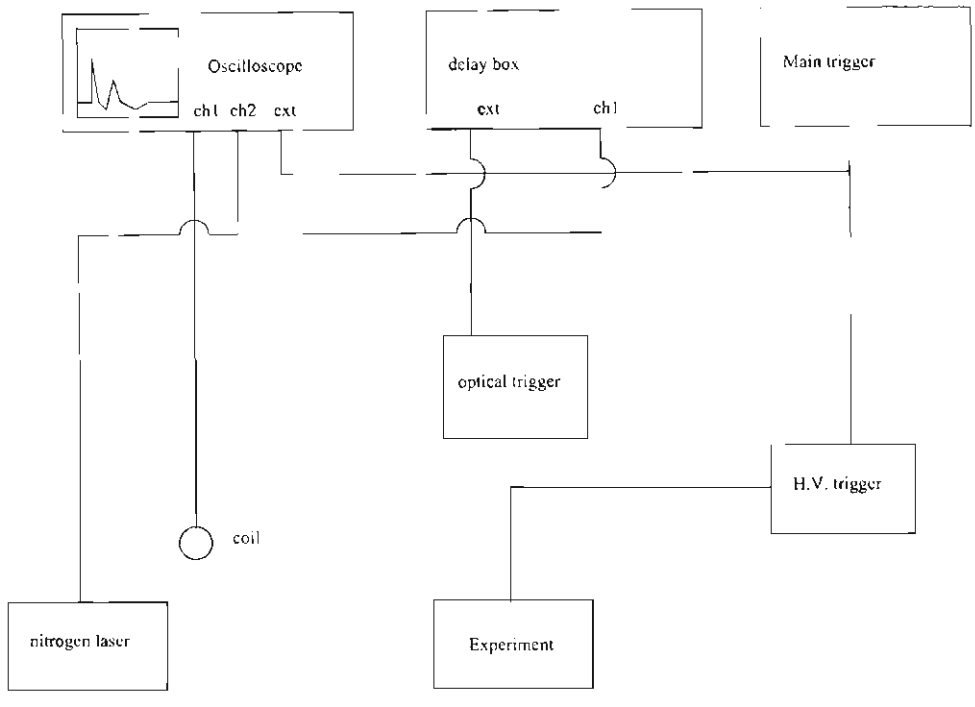

Figure 3.7: The main circuit of the experiment.

apart from the Oscilloscope (Hewlett Packard 54510B 300 MHz Digitising Oscilloscope 1 GSa/s) and the H.T. power supply (A.L.E. Systems Inc., model PS 102 30KV POS).

In particular, most of our diagnostics were based on nitrogen lasers constructed in our laboratory, described later in chapter 6 on page 169.

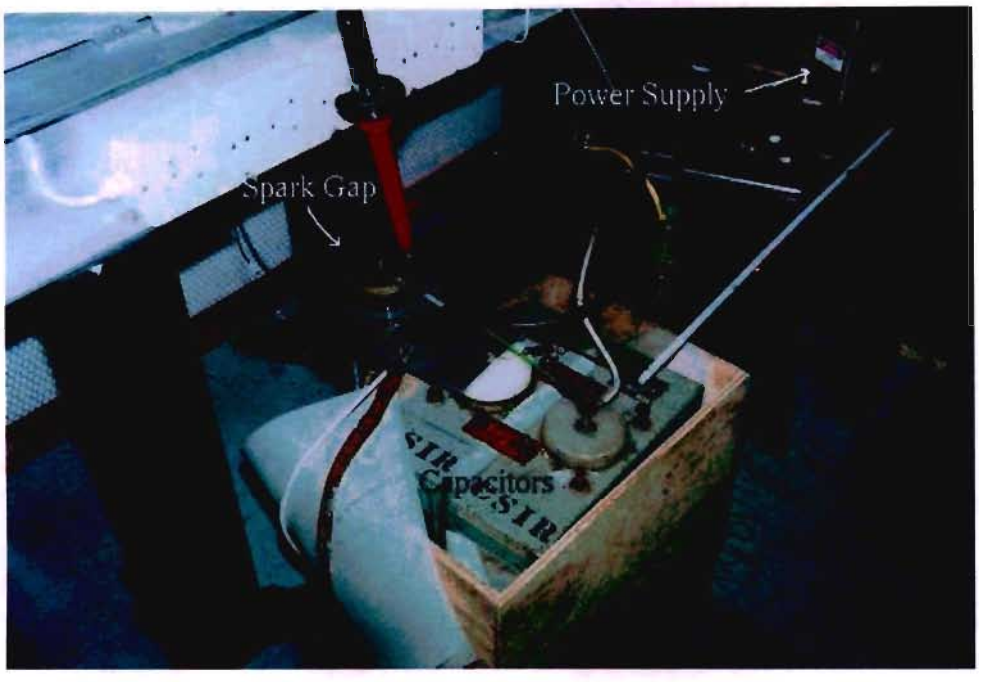

Figure 3.8: The circuit used in most of our experiment. The power supply is in the top right corner of the picture. It can be seen that the power supply is connected to the capacitor through two resistors and a "pan cake" inductor used as protection. The spark gap is above the capacitor and the high voltage probe (red) can be seen.

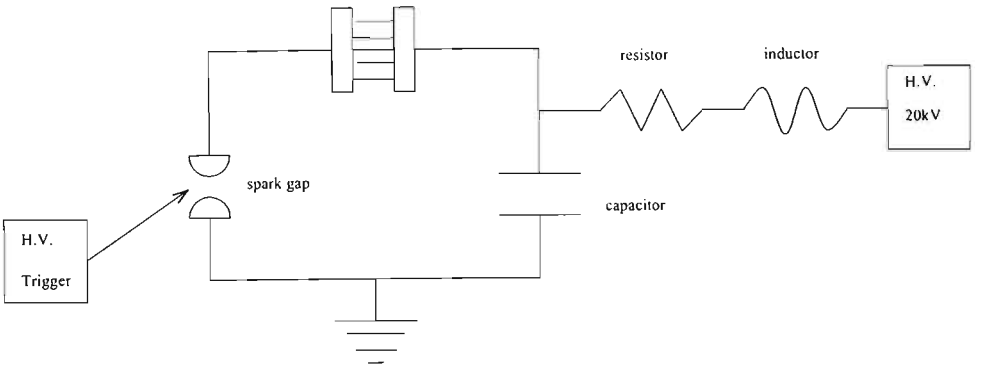

Figure 3.9: The High Voltage circuit of the pipe experiment. The inductor and the resistor are there only to protect the power supply from the high voltage spikes generated during the discharge. Their value is not important and has not been recorded. The value of the capacity was 1 μF.

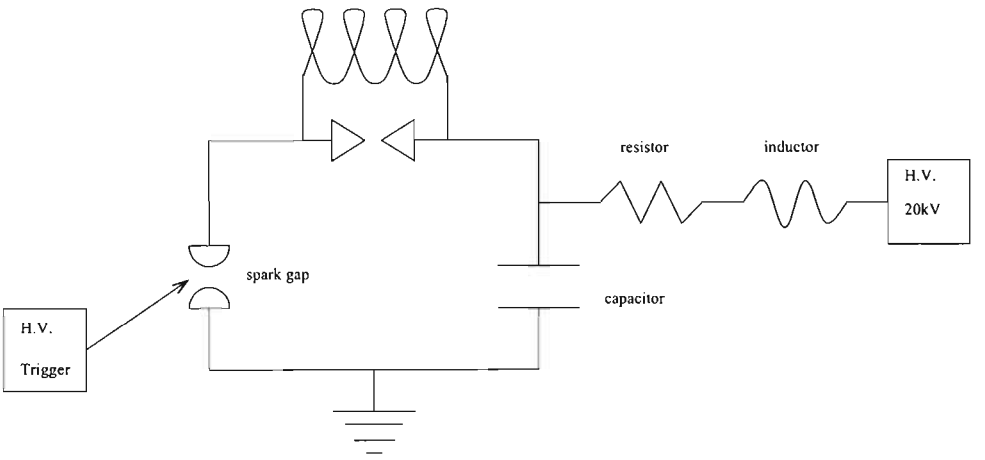

Figure 3.10: The High Voltage circuit of the CSL experiment. It can be noted this circuit is almost identical to the pipe experiment circuit (figure 3.9) and, as in that case, the values of the resistor an the inductor has not been recorded. The only difference is that in this case there is a coil connected in parallel to the CSL. The coil carries the voltage across the device, that otherwise would be an open circuit. For the capacity we used values of 1, 4 and 8 μF

Chapter 4

Gas pipes

By using shock waves it is possible to manipulate a gas to create many kinds of useful structures, like the colliding shock lenses, described in chapter 5 on page 127. Such versatility comes from the fact that the shocks themselves may be cylindrical or spherical, they may arrive from different directions and with a specific timing and, moreover, their number may be different from time to time.

The particular structure described in this chapter promises to be of interest for another kind of physics experiments, namely the acceleration of charged particle in plasmas (see chapter 2 on page 54). Particle acceleration is obtained by sending a femtosecond laser beam through a pre-formed plasma. The laser stimulates electrostatic waves with a very strong electric field. These waves actually travel through the plasma and a beam of parti-

cles can be injected in phase with them. For the time being, even if there have been some very successful experiments, the results are still modest and the energies far from those obtained with the big traditional accelerators. One of the problems with plasma based accelerators is that the plasma must have the right density profile, in order to guide the laser beam over a long distance. If the density of the plasma is uniform, then the laser suffers from focusing and defocussing problems. Once these problems are solved, laser plasmas accelerators can reach energies that are practically impossible with traditional accelerators, because they would need machines that would be far too long.

The proper pressure profile for the acceleration is a hollow of under-dense plasma, surrounded by higher density walls. This density profile can be created in many different ways, but all those used so far have in common the fact that they all produce a short pipe. In particular, many experiments succeeded in accelerating particles by shooting the laser onto the edge of a supersonic gas jet a few millimetres long.

The main part of our experiments was an attempt to create an air pipe with high density walls and a low density core by means of supersonic shock waves. To create a pipe it is necessary to have cylindrical shock waves, which may be produced either by exploding several wires or alternatively with a series of small sparks; we chose the former option.

Exploding wires have been used in the past in pinch machines to produce X rays[24]. As far as we are aware, this is the first time exploding wires have

been used to create a "wall-less" gas capillary, that can be the starting point for a light guide for laser pulses.

4.1 Electron density gradient

The radial gradient of the refractive index is the most important quantity to be taken into account in guiding a high intensity laser pulse though a plasma. If the refractive index has a maximum in the centre, the laser beam is curved inward and forms a uniform channel, as described in chapter 2 on page 54.

For a laser beam travelling through a plasma, the index of refraction is given by[21]

$$n(r) = \left(1 - \frac{\omega_p^2}{\omega_0^2}\right)^{1/2} \tag{4.1}$$

where ω_0 is the frequency of the laser, ω_p is the plasma frequency, given by

$$\omega_p = \sqrt{4\pi e^2 n_e / \gamma m_e} \tag{4.2}$$

The factor $\gamma(r)$ is the relativistic factor associated with the electron's motion transversal to the laser propagation and depends on the laser intensity. The maximum along the axis can be achieved by modifying $\gamma(r)$ and/or $n_e(r)$. The intensity of the laser always decreases away from the axis of the beam and, for a Gaussian beam, it has been calculated and proved experimentally that self channelling of the beam occurs if the power exceeds a critical

threshold given by $P_c = 17(\omega_0/\omega_p)GW$[20].

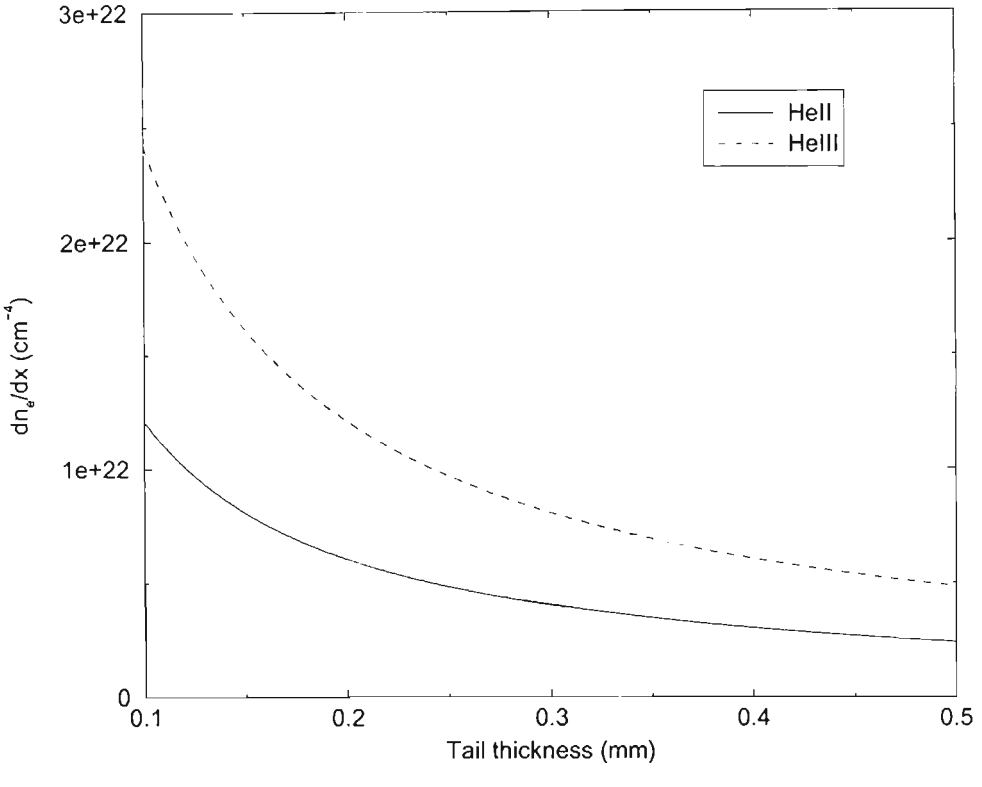

Graph 4.1: Electron density gradient in a Helium plasma as a function of the shock tail thickness (see equation 4.5 on page 94) for different ionisation states of the plasma. A peak pressure of 500 kPa is assumed. From this graph and the following one, it is clear that by preforming a channel by means of shock waves it is possible to achieve a gradient of electron density suitable for laser guiding.

Using shock waves it is possible to pre-form a channel with a high gradient of the electron density n_e, comparable with the one of $\sim 5 \cdot 10^{22}$ cm^{-4} obtained during self channelling[65]. Let us use an idealistic model of a shock with a peak pressure P_0 that falls to zero in the tail over a distance x_0. This

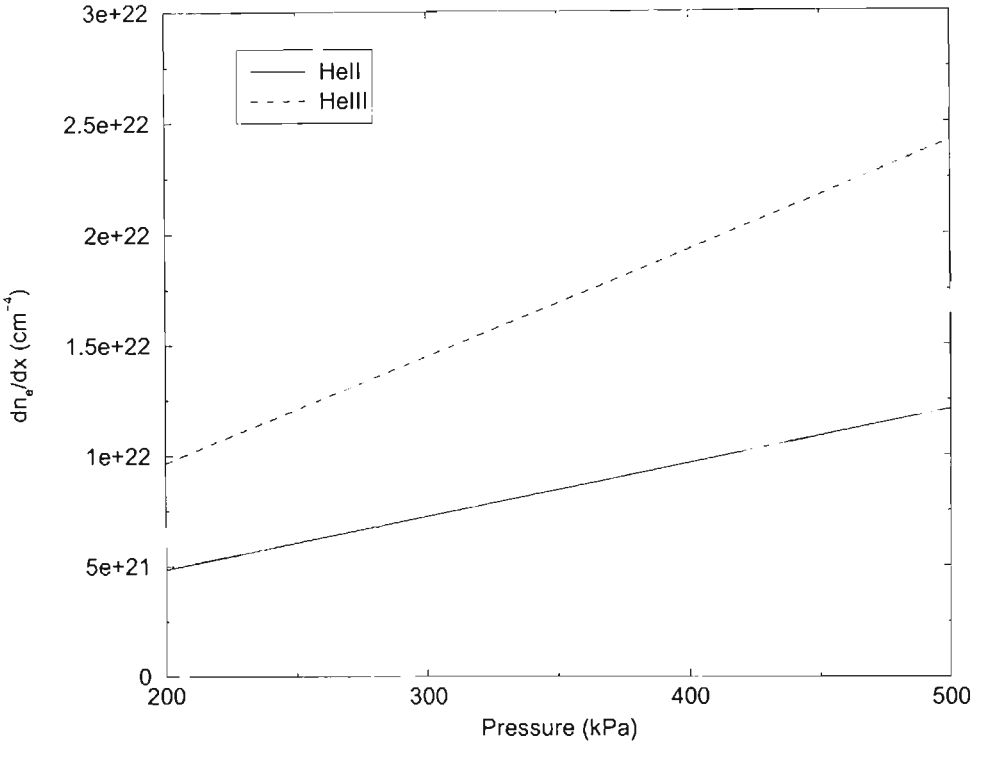

Graph 4.2: Electron density gradient in a Helium plasma as a function of the peak pressure of the shock (see equation 4.5 on the next page) for different ionisation state of the plasma. A tail thickness of .1 mm is assumed.

is a shock wave propagating in a neutral gas. The tail of the shock is the interesting part for laser channelling, because the pressure drops almost to vacuum over a short distance. If we model the pressure changing linearly, the pressure in any point is given by

$$P = \frac{P_0}{x_0} x \tag{4.3}$$

The number of moles in a specific unit volume of gas, in the ideal gas ap-

proximation, is given by

$$n = \frac{P_0}{RTx_0}x \tag{4.4}$$

where R is the universal gas constant, equal to 8.3145 J/molK and T is the absolute temperature. Let us assume now that the shock has been fully ionised by mean of a laser or a flash lamp. Considering a Helium plasma, the gradient of the electron density becomes

$$\frac{dn_e}{dx} = N_a I \frac{dn}{dx} = \frac{P_0}{RTx_0} \tag{4.5}$$

where N_a is the Avogadro constant and I is the ionisation number of the atoms ($0 < I <= 2$, in the case of Helium), considered in only one state for the sake of simplicity. As can bee seen in graph 4.1 on page 92, assuming a fully ionised shock in helium with a tail 0.1 mm thick, an electron density gradient of about $2.5 \cdot 10^{22} \frac{dn_e}{dx} cm^{-4}$ can be obtained.

Although all our experiments were done in neutral gas, it is clear that in a real-life laser accelerator the neutral gas would need to be ionised, as stated above.

4.2 Experimental set up

The circuit used for the experiment has been already described in section 3.1.2 on page 73. In the case of the pipe experiment, we used a 1 μF capacitor

and the voltage was in the range between 16 kV and 20 kV. This particular experiment is very sensitive to the energy stored in the capacitor. If the voltage is too low, the explosion is weak and almost no shock production is observed. If the voltage is too high, after the collision of the shocks there is turbulence and no pipe is observed.

4.2.1 Cylindrical shocks

A very good cylindrical shock can be obtained by exploding a piece of thin wire, as described in section 3.1.2 on page 73. The idea is to store energy into a big capacitor and then discharge it quickly through the wire and ensuing plasma using a triggerable spark gap (or a Thyratron, if available). The circuit is simpler than in the case of the CSL, because it does not require any coil (see figure 3.9 on page 88 and 3.1 on page 72). In fact, the voltage is carried to the spark gap by the wire itself. The absence of the coil makes the experiment less noisy from an electromagnetic point of view.

One critical factor for this experiment is the resistance of the wire. If the resistance is too small, the plasma forms very quickly, when there is still plenty of energy in the capacitor. In this case, once the plasma has formed the resistance drops to almost zero and the circuit oscillates radiating away a large amount of energy. The optimal resistance is the one that allows the circuit to dissipate most of the energy into the wire during the first cycle of the oscillation. The resistance of the wire depends on the material and on the thickness. If the wire is very thin, the resistance can be very high and

also the amount of debris is reduced.

In our experiments we used a copper wire 150 μm thick. For the eight-shocks experiment described in section 4.3 on page 104, the wire was 50 cm long, with a total resistance of 8 Ω.

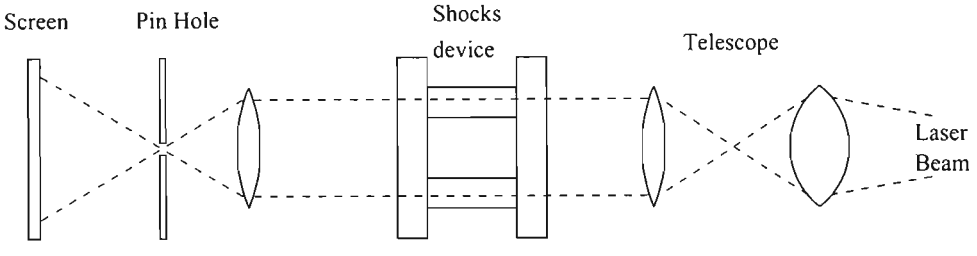

Figure 4.1: The diagnostic setup for the pipe experiment. From the left, the two lenses used for the telescope have a focal length of 5 cm and 50 cm. The lens used for the "spatial filter" has a focal length of 10 cm.

For the diagnostic of the shock waves we used a nitrogen laser, described in chapter 6 on page 169, of the square electrode type. The laser beam is sent through the pipe and produces shadowgrams of the shock waves. The refractive index of the shocks is so high that they just refract the light out of the collecting optics. Since the exposed film is a "negative," the regions corresponding to the shocks therefore appear "white," against an undisturbed "black" background.

The set-up of the experiment is shown in figure 4.1. The small telescope on the right is necessary to compensate for the divergence of the laser beam. In this experiment, in particular, the beam has clearly to be parallel and aligned with the pipe. The "spatial filter" on the left was used to eliminate the light of the explosion, which is very bright. In addition to that, when

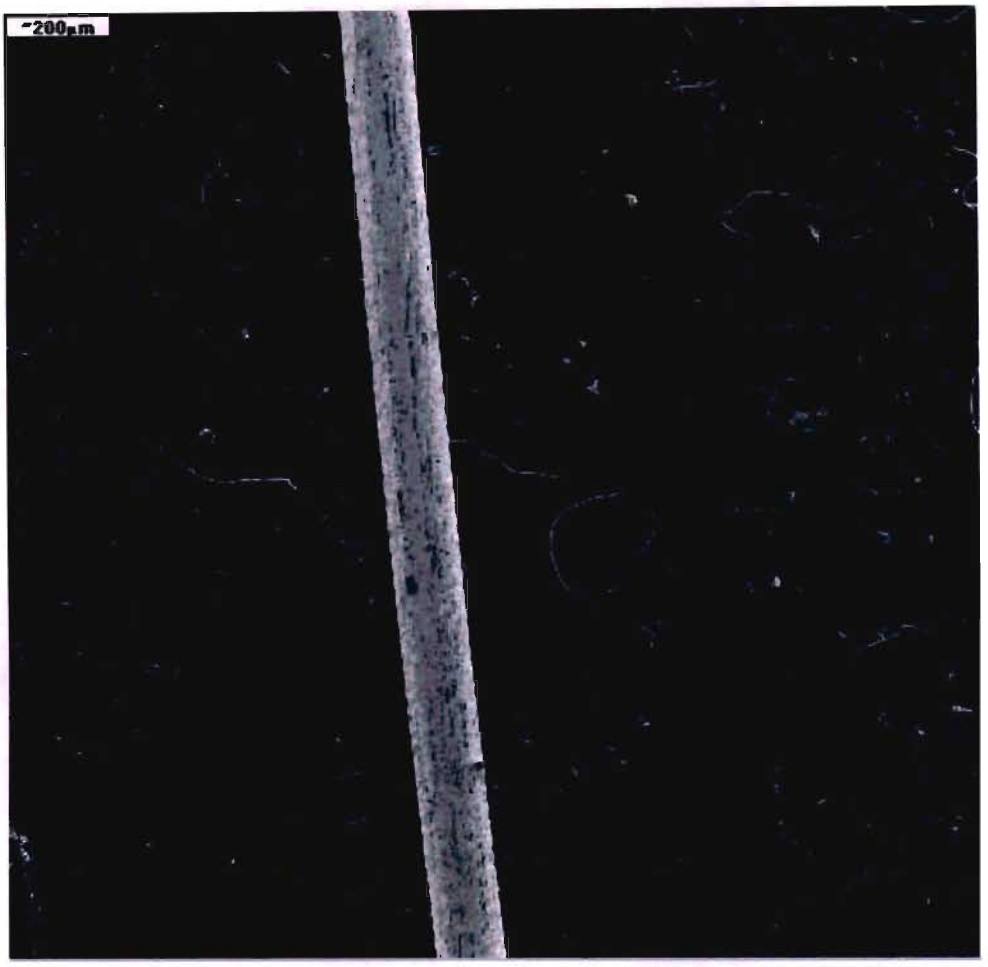

Figure 4.2: A SEM image of a piece of the wire used during the experiment. It can be noted that the wire has a thickness of about 130 µm. In order to be sure that the thickness of the wire was uniform, we took several images of different pieces of wire.

the photographic paper was very close to the device, a UV filter was used to let through only the light of the laser. The single lens detector also offers the possibility of changing the magnification of the image only by moving the detector, i.e., the photographic paper. This is true only if the detector is in the near field, where the effects due to the lensing of the pipe can be neglected. The magnification itself can be measured afterwards by imaging an object of known size.

Our first unsuccessful attempt to create a pipe was made by exploding a coil of wire. Unfortunately, the wire is so thin that it needs to be supported. In our case, we used a cylinder of very thin paper, on which the wire was wound. The idea was that the paper would have been blown away by the explosion without affecting the shock waves, but the first experiments showed only a very strong shock coming from one side of the experiment, from the bottom in figure 4.3 on the next page. What happened was that the discharge jumped across the coils, instead of flowing through the whole wire, probably helped by some skin conduction effect due to the paper.

The second attempt was made using six short pieces of wire connected in parallel. The wires were held between two metal disks, to which the high voltage was applied. With this approach, we could get all the wires to explode, but not at the same time. In this case, the formation of the pipe does not take place because the shock waves arrive at different times. This system may probably work, but one has to be sure that the wires are strictly identical in both length and thickness. In our case, we did not have any

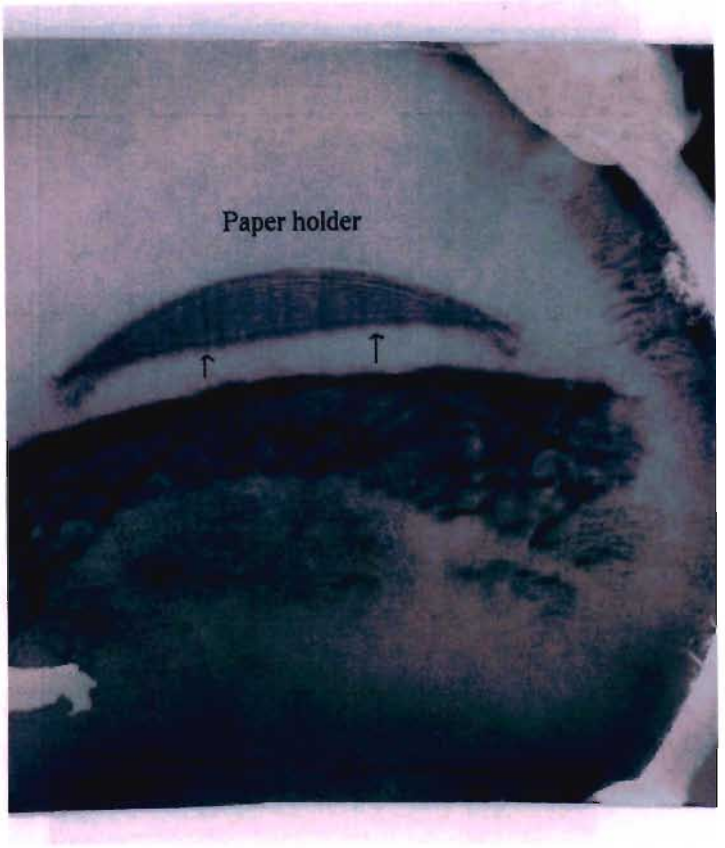

Figure 4.3: The single strong shock coming from the coil, due probably to the jumping of the arc across the coils. The shock is travelling toward the top of the picture. Turbulence left behind by the shocks is clearly visible. This is a clear sign of the energy being too high. The white circle is the cylinder of paper used to hold the wire, that is usually blown away by the explosion. It should be noted that all our pictures have a negative grayscale, so the highest light intensity corresponds to the blackest parts of the image.

means to tighten the wires, which had therefore a slightly different length and even small kinks.

The third way is the only one which allowed us to obtain some good results. Instead of using separate wires, we used only one long piece, going up and down between two insulating holders. In this case, the explosion has to occur everywhere at the same time. With this technique we obtained some good quality pipes as long as 2.5 cm. In principle, given enough energy, there is no limit to the length of the pipe. The main problem, in this case, was that our particular holder was not built with enough precision, leading to some differences in the arrival time of the shocks, which travel at speeds approaching 1.5 times the speed of sound.

4.2.2 Different foci

In the first experiment we started using only two wires, in order to check that the shocks were really arriving in the centre at the same time, as far as allowed by the precision of the holder. The experiment was very successful and led to the production of a lenticular light guide, which quite strongly focuses the light in the centre, producing a sort of line focus. However, two shocks are not enough to produce a proper pipe. Moreover, in this case we had a number of secondary shocks, sometimes strong enough to produce a focus of their own. Considering that in this case the wire is short and has a very little resistance, the secondary shock probably is only an oscillation of the circuit, before all the energy is dumped and the plasma recombines. The

Figure 4.4: The line focus with two shocks. The shocks have already collided in the centre. Many secondary shocks are visible.

low resistance of the wire does not in fact allow the energy to be dumped into just one cycle, as could be seen in the oscilloscope traces.

In the following experiment we used the same technique as with the single wire, but this time producing four shocks instead of two. Even in this case the experiment was successful and led to the formation of a channel, but with a square shape. This happens because the angle at which the shock waves collide is too wide to allow Mach addition to take place. In some cases, the square pipe worked as a very strong lens, producing a bright spot. The pictures of the square pipe are shown in figure 4.5 on the following page. Unfortunately, the photographic paper is not a good detector. What happens is that the paper saturates quite quickly and does not show the real difference between different parts of the picture. Only when developing the pictures in the dark room it is possible to see a dark spot (the images are negative) forming in the centre much earlier than the rest of the picture. Attempts were made to stop the development at an early stage, but without any results. For this experiment the delays were unknown, because the oscilloscope was not working properly.

The square pipe does not look very useful, but it is an interesting proof of the versatility of gas structure produced in this way. Given the right geometry of the experiment, many different shapes may be produced.

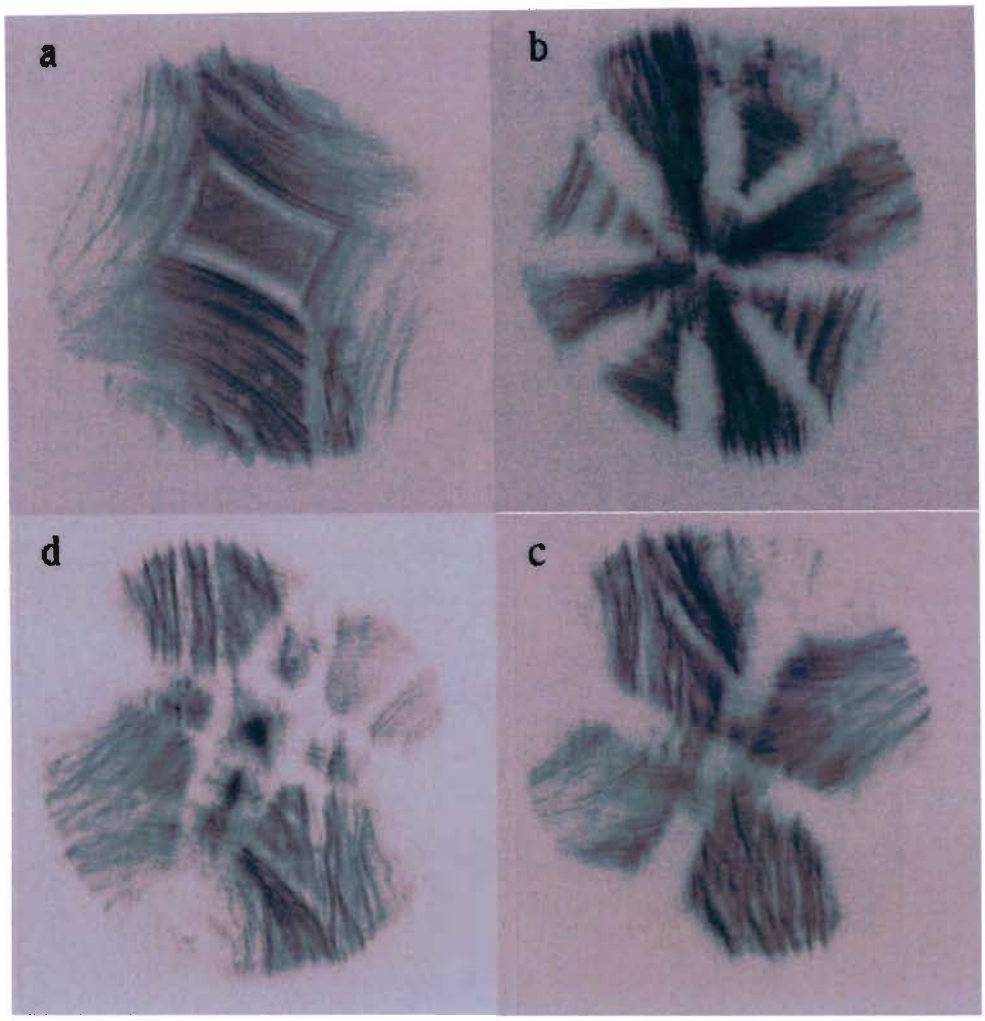

Figure 4.5: Four pictures of the square pipe. a) the four shocks coming to the centre; b) the short side of this square pipe is about 5 mm long. c) The moment of the collision; the pipe is not visible, as the shocks collide in the centre at the same time. d) The moment immediately after the collision. The square pipe focusing the light; the light is refracted to the centre of the image, which appears darker. Between the first and the last image, the delay is about 6 μs.Though square pipes are unlikely to be useful, this demonstrates the ability of colliding shocks to produce channels.

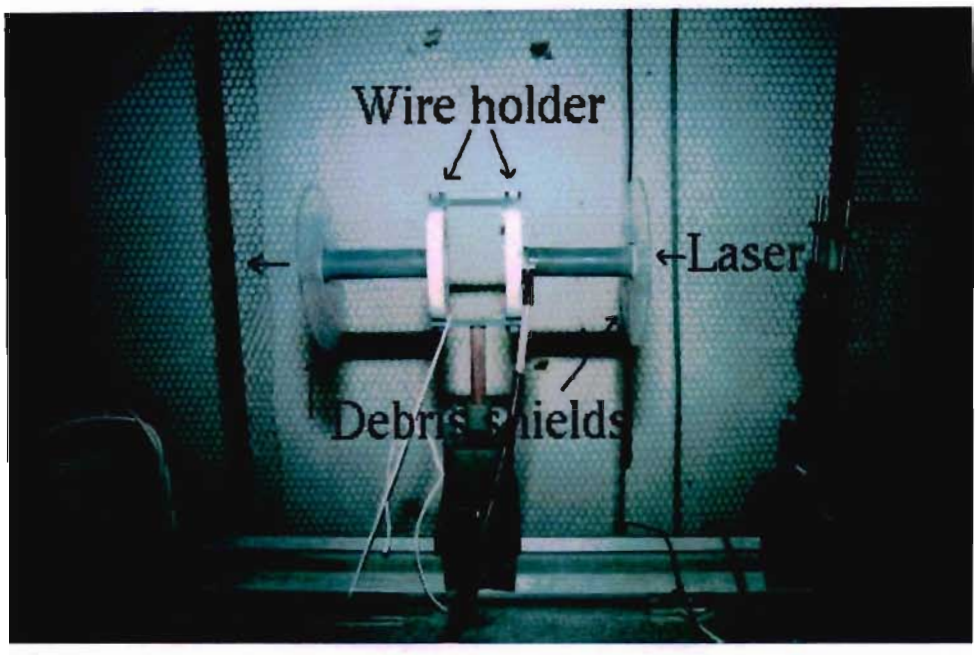

Figure 4.6: The wire holder used for the experiment. The two disks on both sides protect the optics from the debris ejected by the exploding wire.

4.3 The cylindrical gas pipe

A real cylindrical gas pipe was eventually obtained by using eight parallel wires. The eight wires were all part of a single wire threaded through 16 holes. The first results of this experiment are shown in the figures 4.7 on page 106 and 4.8 on page 107.

Experiments where conducted with different voltages ranging from 16 to 23 kV, corresponding to energies from 128 to 265 J. With the lowest voltage, the explosion is very weak and there is no shock formation. With some experience, the quality of the shocks can be judged by the noise heard in the

laboratory. With the lowest voltage, almost no noise can be heard. With the highest voltage, a good channel can be seen before collision, but after collision there is only strong turbulence. Even if the quality of the pipe may be good before collision, this is not the structure that we want, because even though the walls may be at high pressure, the core is made of unperturbed air at atmospheric density.

All the images up to figure 4.7 on the next page were obtained with a capacitor of 1 μF charged to a voltage of 23 kV, which corresponds to an energy of 265 J. The images taken after the collision of the shocks show only turbulence. This means that the energy was too high. Nevertheless, before collision we observed a channel as small as 500 μm, which is shown in figure 4.8 on page 107. A densitometry of the same picture is shown in graph 4.3 on page 108. Probably the real channel was even smaller, but the holder moved every time a new wire was inserted and this prevented a good alignment of the laser.

Our holder allows us to place the wires at three different radii (1, 2 and 3 cm). Our experiment showed that the larger distance is unusable, because the shocks become too broad and two weak, before they reach the centre, and the pipe has a poor quality, i.e., a small gradient of the density. The smaller diameter is unusable as well, in this case because the ends of the wire are too close to each other and there is an electric arc between them, instead of exploding the wire. In our subsequent experiments, the distance between the wire and the centre was fixed to be 2 cm.

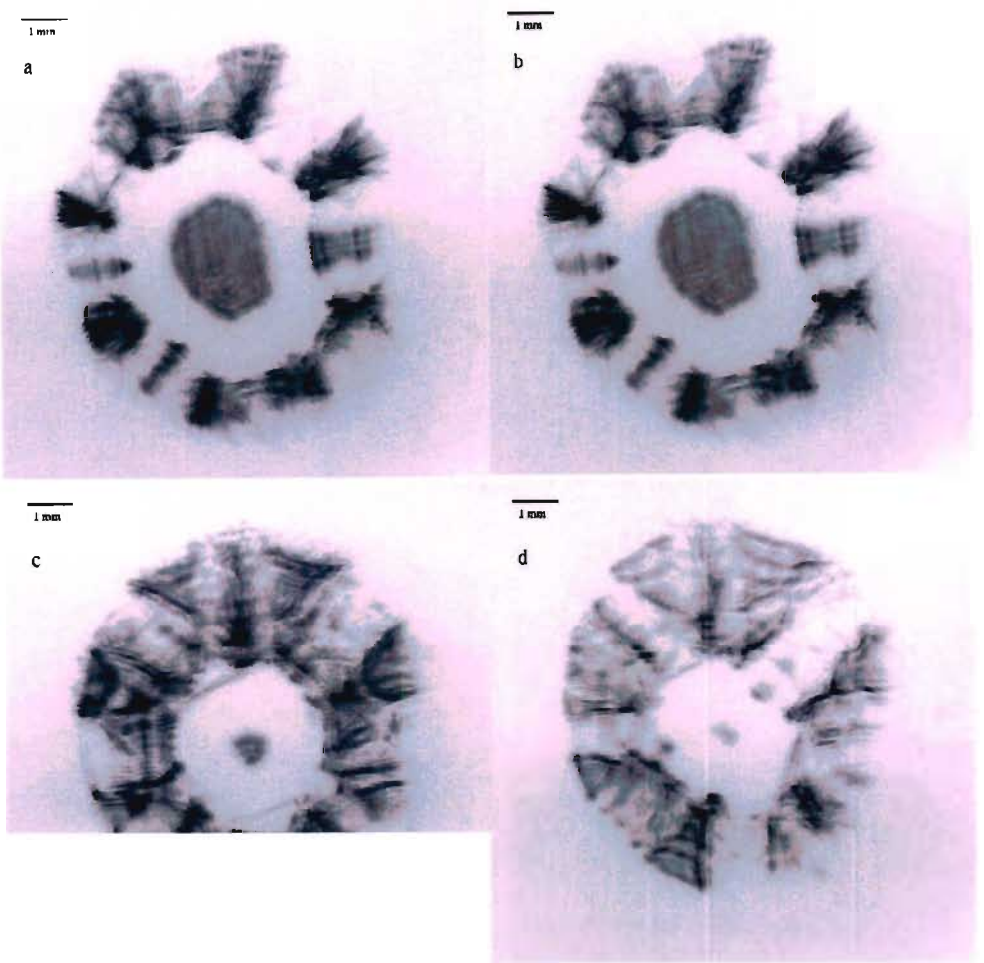

Figure 4.7: Four pictures of an early series of experiments with eight wires. All these images were obtained before the shock waves collided in the centre. This pictures were obtained with too much energy (265 J) and it was never possible to observe a pipe after collision. The delay between (a) and (d) about 5 μs.

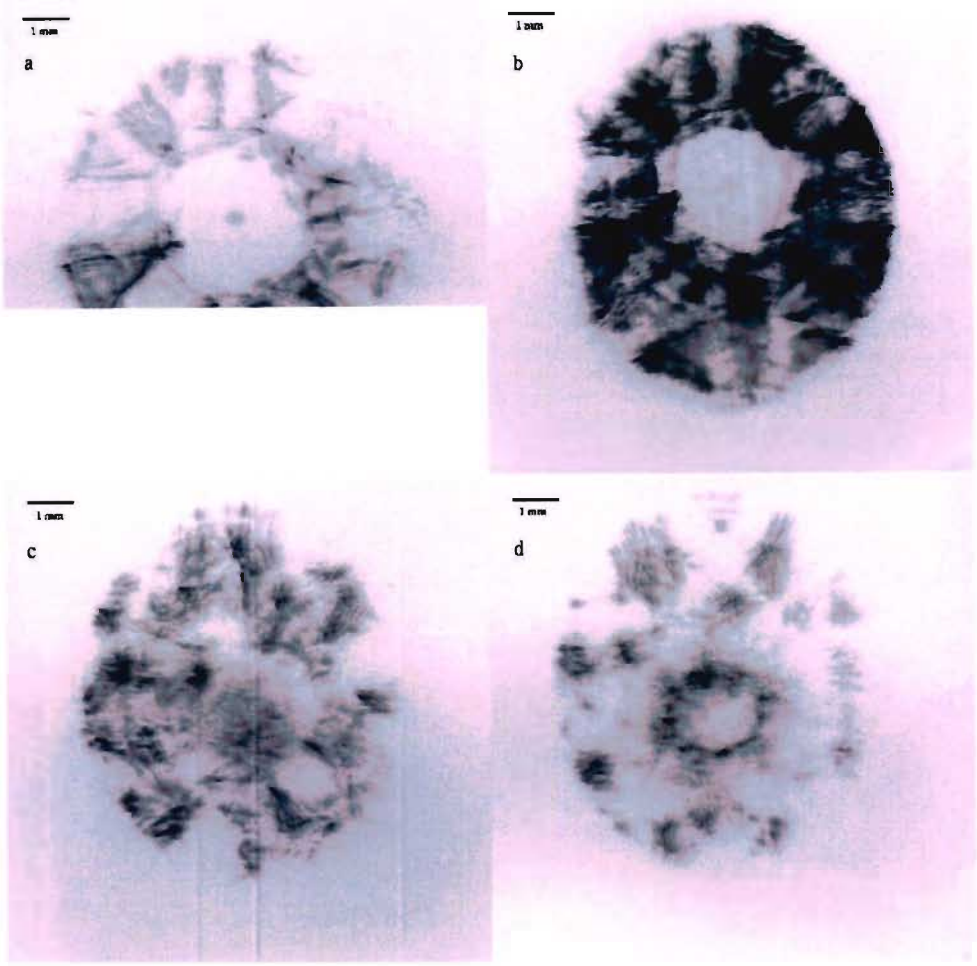

Figure 4.8: Four more pictures from an earlier series of experiments performed with too much energy (265 J). (a) was taken just before collision, whilst (b) during and (c) and (d) after. It is clear that there is no channel formation after collision, because of the turbulence. The delay between the first and the last image is about 5 μs.

From shot to shot we noticed that the voltage left in the capacitor after the explosion was different and in two different ranges. We isolated fast shots, in which the remaining voltage was lower than 300 V, and so more energy was sent through the wire, producing faster shocks. In the case of the slow shots the voltage left across the capacitor was about 1 kV.

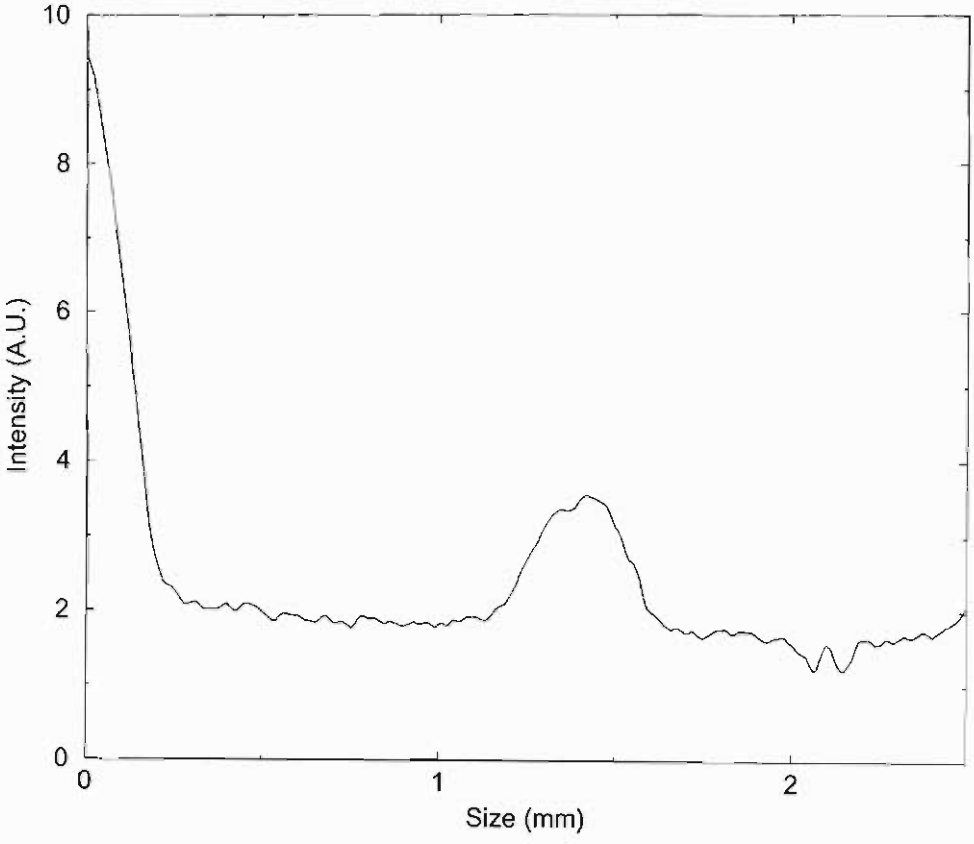

Graph 4.3: Densitometry of the smallest channel obtained during the pipe experiment (see picture 4.15 on page 116). This picture was obtained before the collision of the shocks, therefore the channel does not have the right density profile for particle acceleration.

The results of a later series of experiments are shown in figure from 4.9 on the following page. In this case, the voltage was decreased to 19 kV, and therefore the energy to 180 J. This voltage reduction allowed us to reduce the turbulence as well. In this experiments we observed for the first time a channel after the collision, with the correct density profile for laser acceleration.

4.4 Experimental problems

Problems in operating this kind of device are numerous. The first one is the fact that the wire has to be changed after every shock. In the case of our holder, this has to be done manually and takes a few minutes. Nevertheless, this problem may be solved in two different ways. The holder is a very cheap device, so many of them may be prepared already pre-loaded with the wire, ready to be inserted into the experiment. A better way is the use of a row of small sparks, already mentioned in section 3.1.2 on page 73. This second approach is the only one that can be used, for instance, in a helium filled chamber, that cannot be opened after every shot.

4.4.1 Debris

An exploding wire produces a large quantity of debris, which may jeopardise the experiment to be performed using the gas structure. In our case, the only problem we had was that the debris from the wire outside the holder was

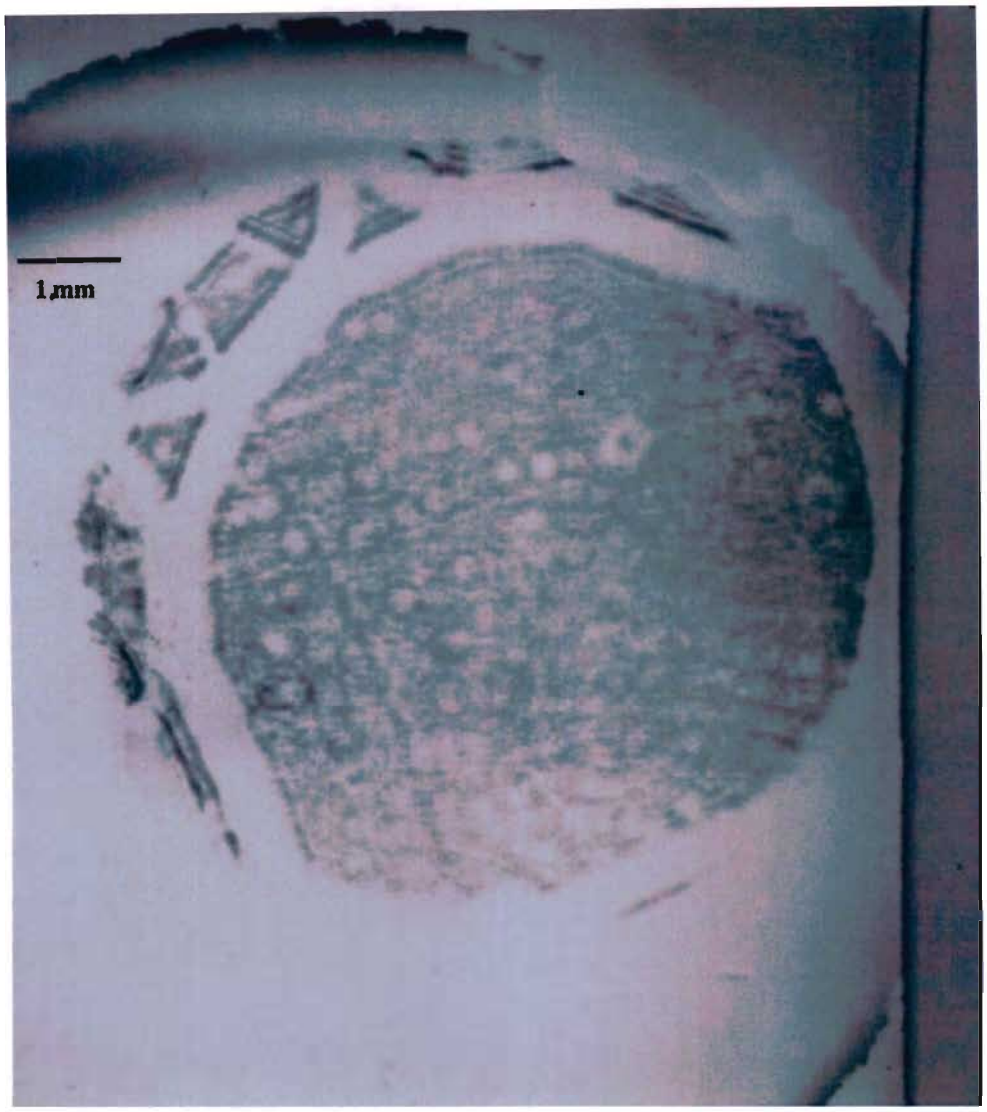

Figure 4.9: Image of a circle well before the collision of the shocks. The delay between the explosion and the diagnostic laser is 49.8 μs. This picture is a good example of Mach addition, because the shocks are creating a uniform common shock with a circular shape. The uneven background is due to defects of the lens used to collimate the laser. $W_{bank} = 180$ J.

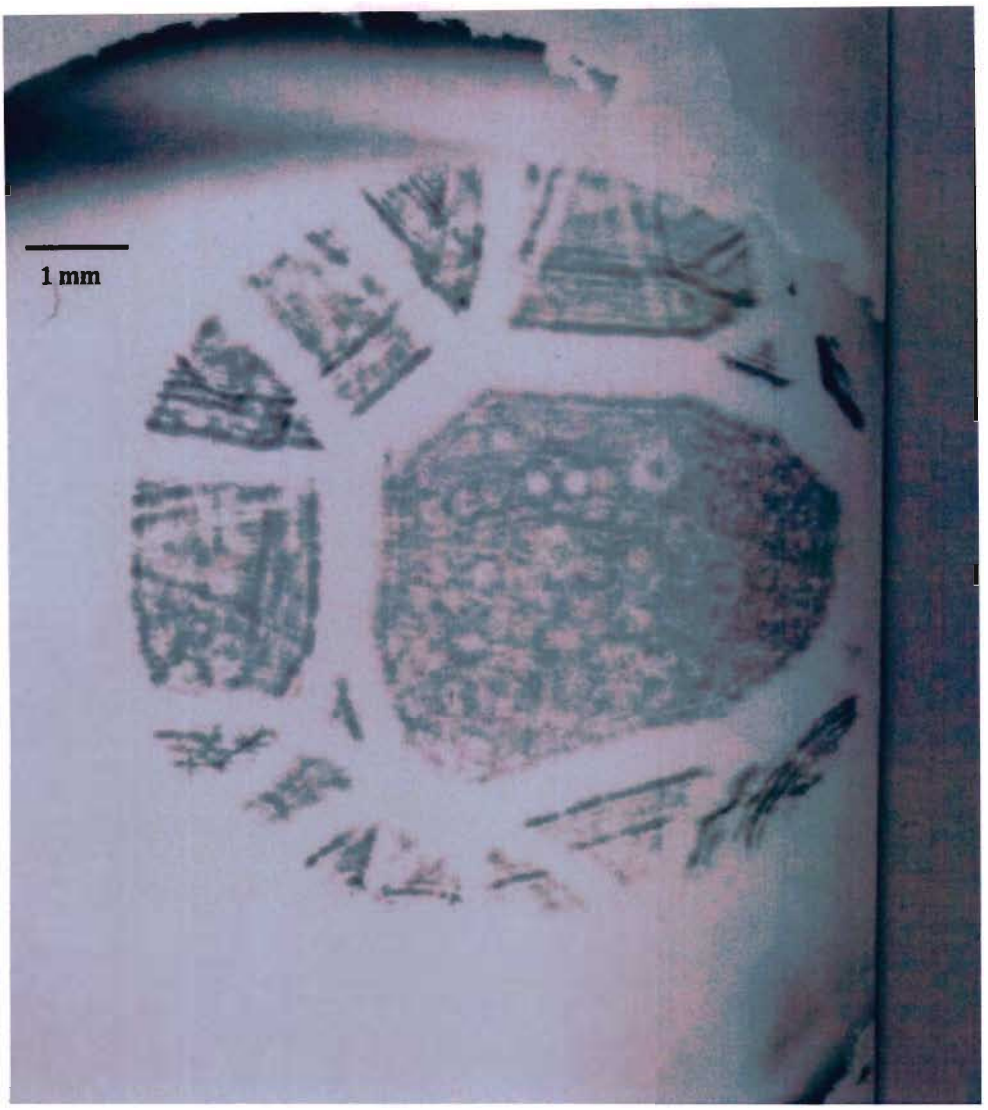

Figure 4.10: Image of a gas pipe before the collision of the shocks in the centre. The delay between the explosion and the diagnostic laser is 52.8 μs. The circle is not perfect, probably due to small errors in the position of the wire. It can be noted that there is no turbulence behind the shocks. $W_{bank} = 180$ J.

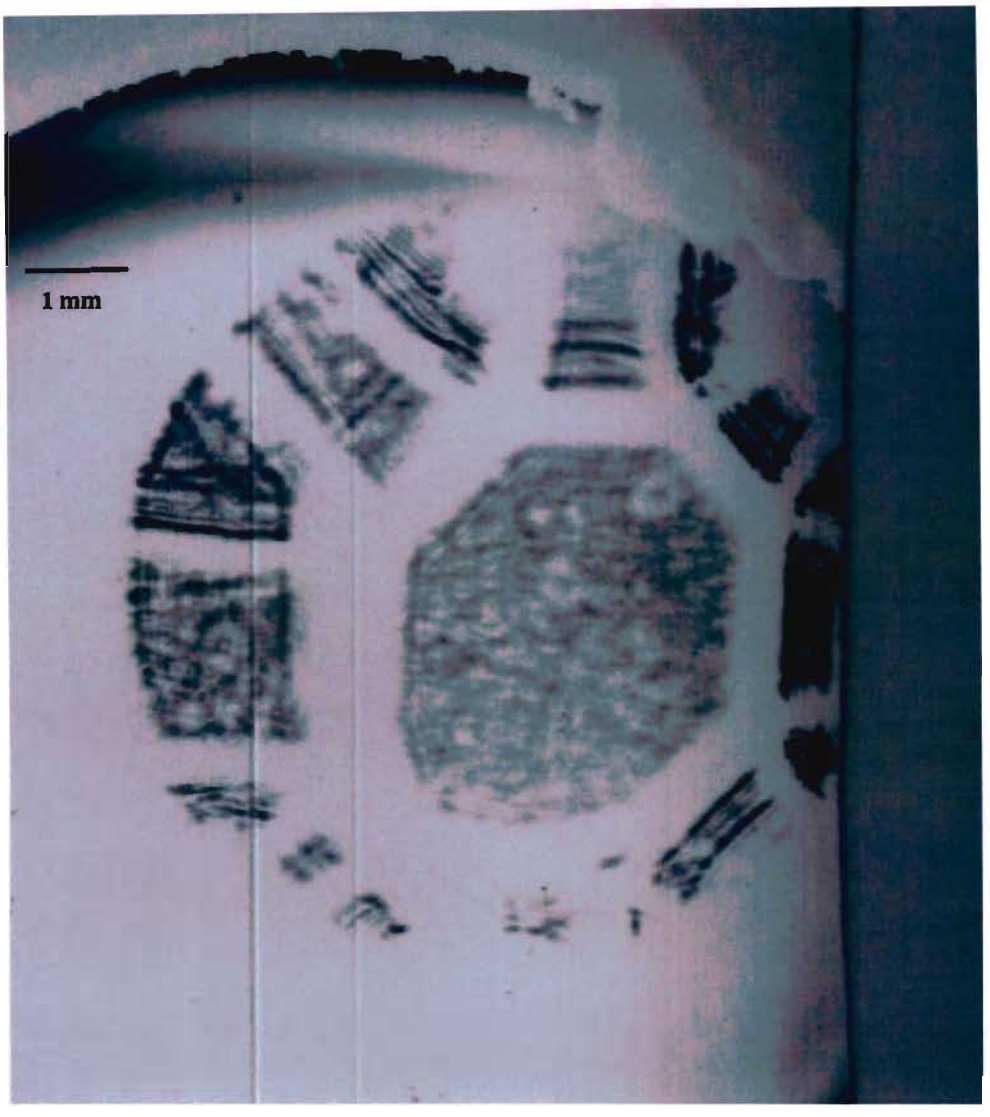

Figure 4.11: Image of a big pipe before the collision of the shocks. The delay between the explosion and the diagnostic laser is 56.6 μs. The pipe has now a diameter of about 1 mm. $W_{bank} = 180$ J.

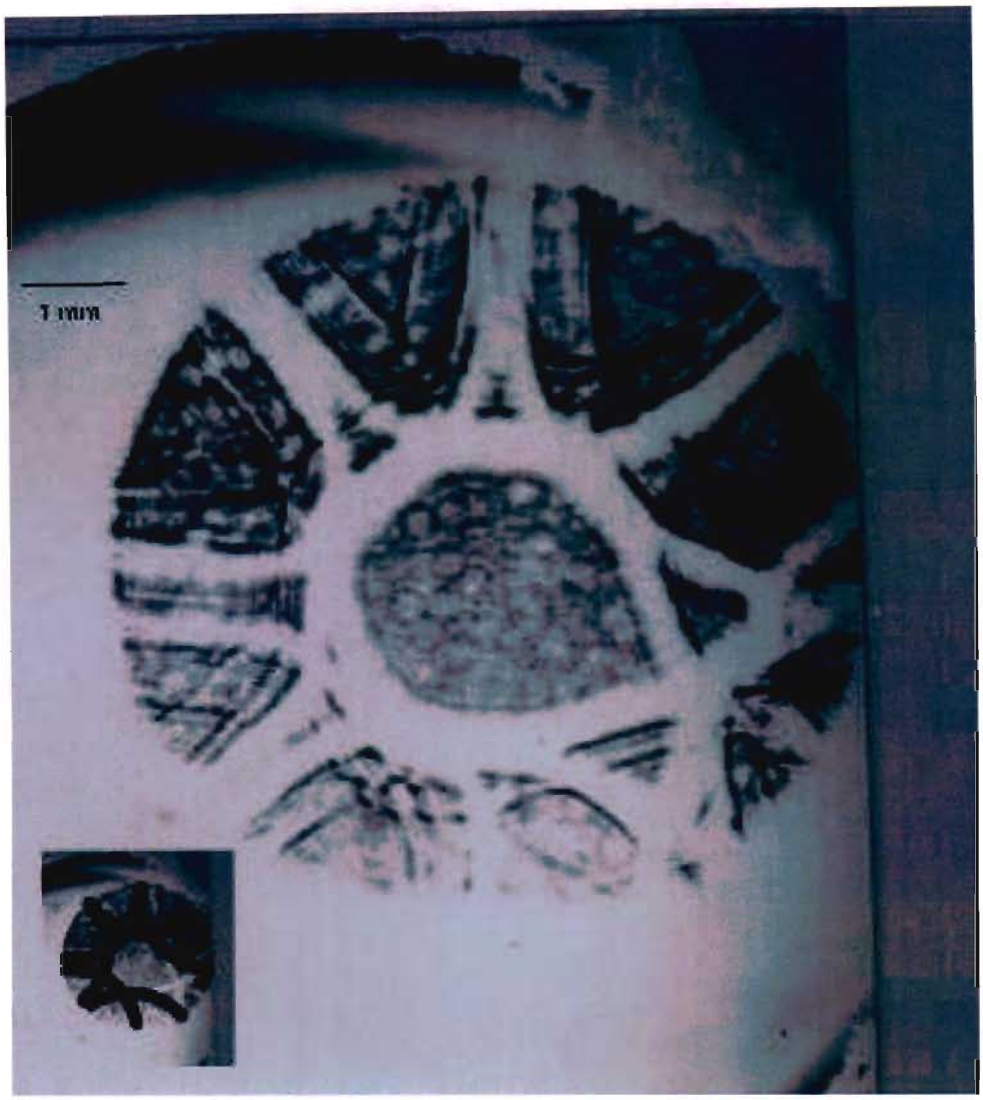

Figure 4.12: An example of a quasi perfect pipe, with a delay of 61.2 μs. Only two shots are arriving later, without affecting the shape of the pipe too much. The inset shows a schematic drawing of the shock waves. One can see that six shocks are almost perfectly on time. It is not clearly understandable what the two on the right are doing. Probably, distortions like this one are smoothed by Mach addition after collision. Indeed, we noted that the pictures after collision tend to show more regular shapes than the ones before. $W_{bank} = 180$ J.

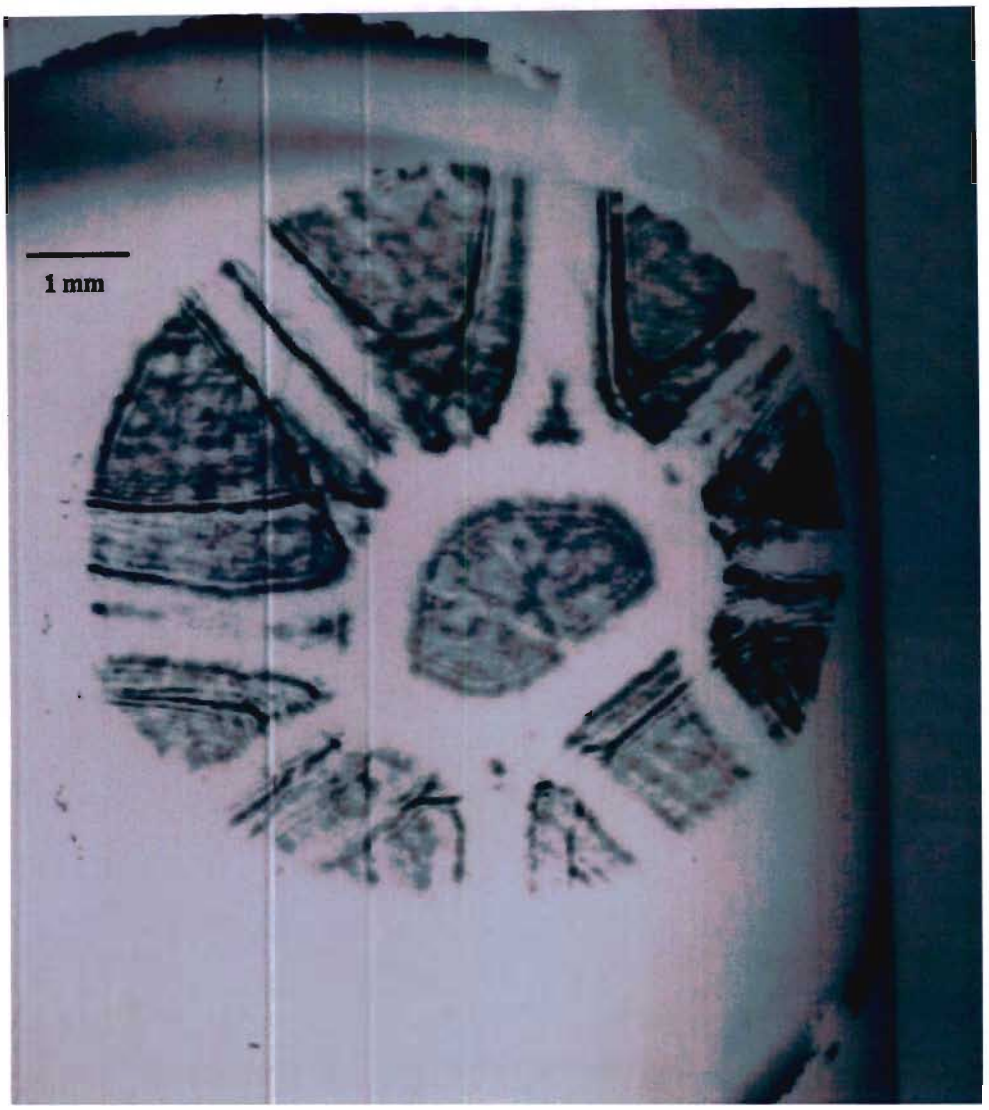

Figure 4.13: A fast shot. Despite the delay of 57.4 μs the inner diameter of the pipe is now smaller. As the time between the explosion and the firing of the laser is measured on the oscilloscope, this can only mean that the shocks were faster. Indeed, from shot to shot the residual energy left in the capacitor, and therefore the energy gone into the shock, is different. $W_{bank} = 180$ J.

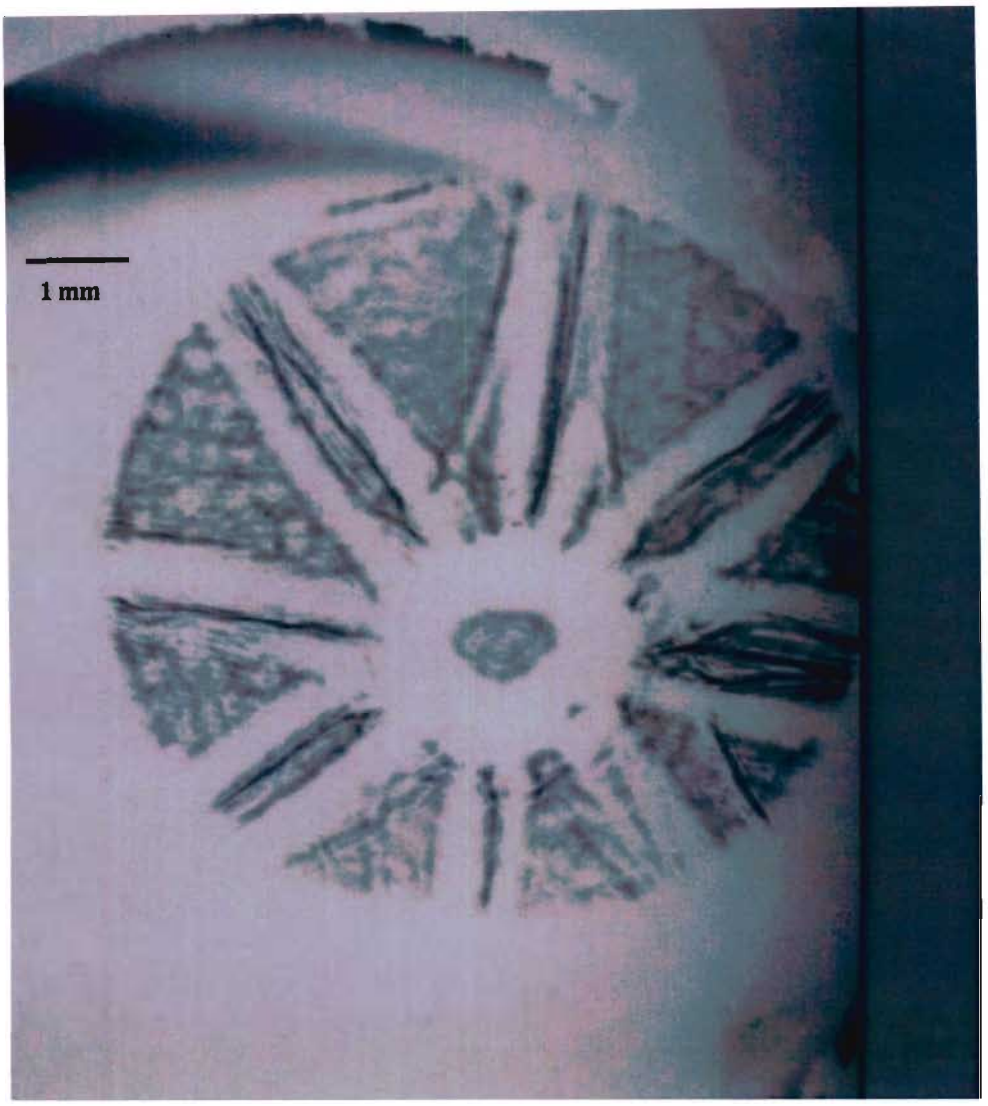

Figure 4.14: An even faster shot. After 55.8 μs the shocks have already merged through Mach addition. Despite the delay is smaller than in picture vrefpict:s32, the circle is smaller, which means the shock waves travelled faster. The circle is now smooth and the single shocks cannot be recognised anymore. $W_{bank} = 180$ J.

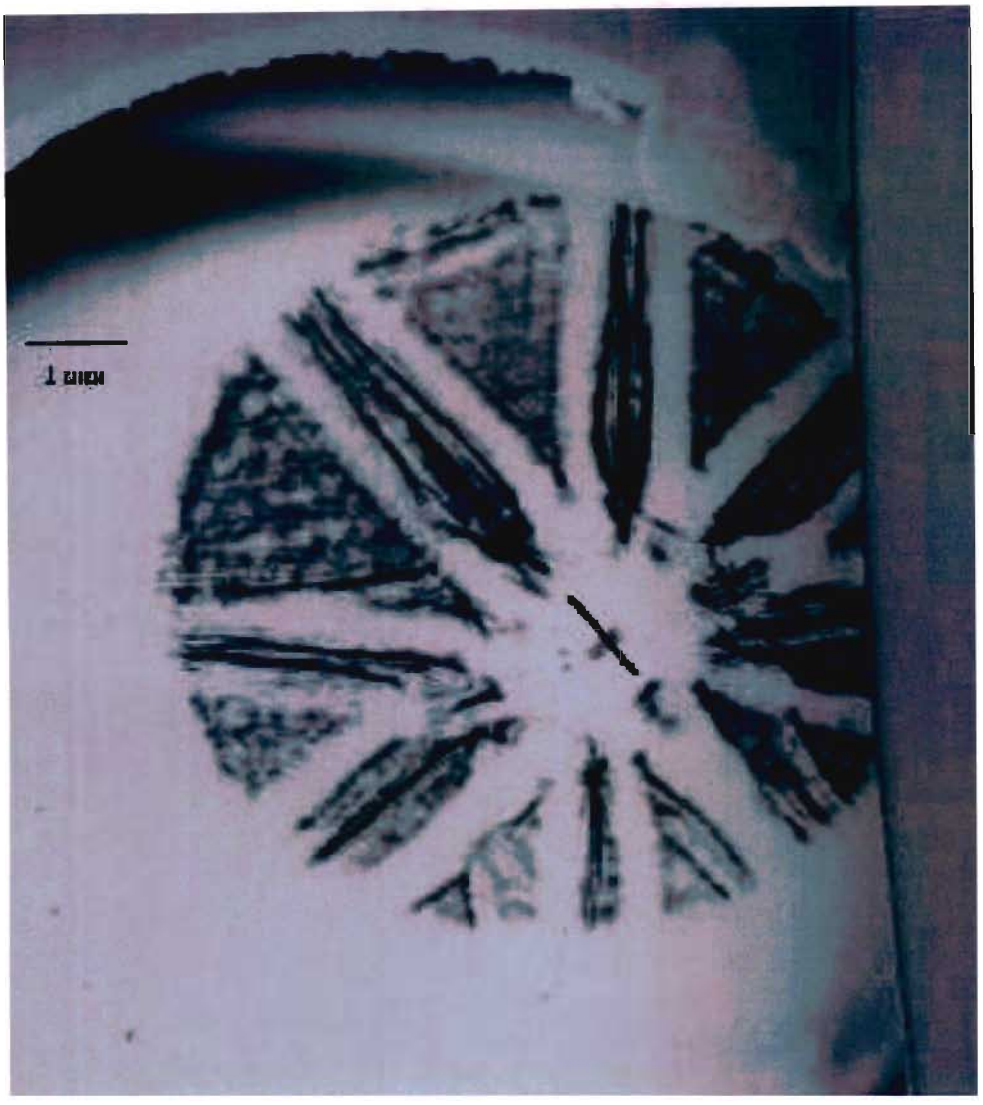

Figure 4.15: This picture with a delay of 57.0 μs shows the smallest pipe we have observed before collision. It can be noted that the pipe is not perfectly circular but has an elongated shape. The line shows the path of the densitometry in graph 4.4 on the following page. $W_{bank} = 180$ J.

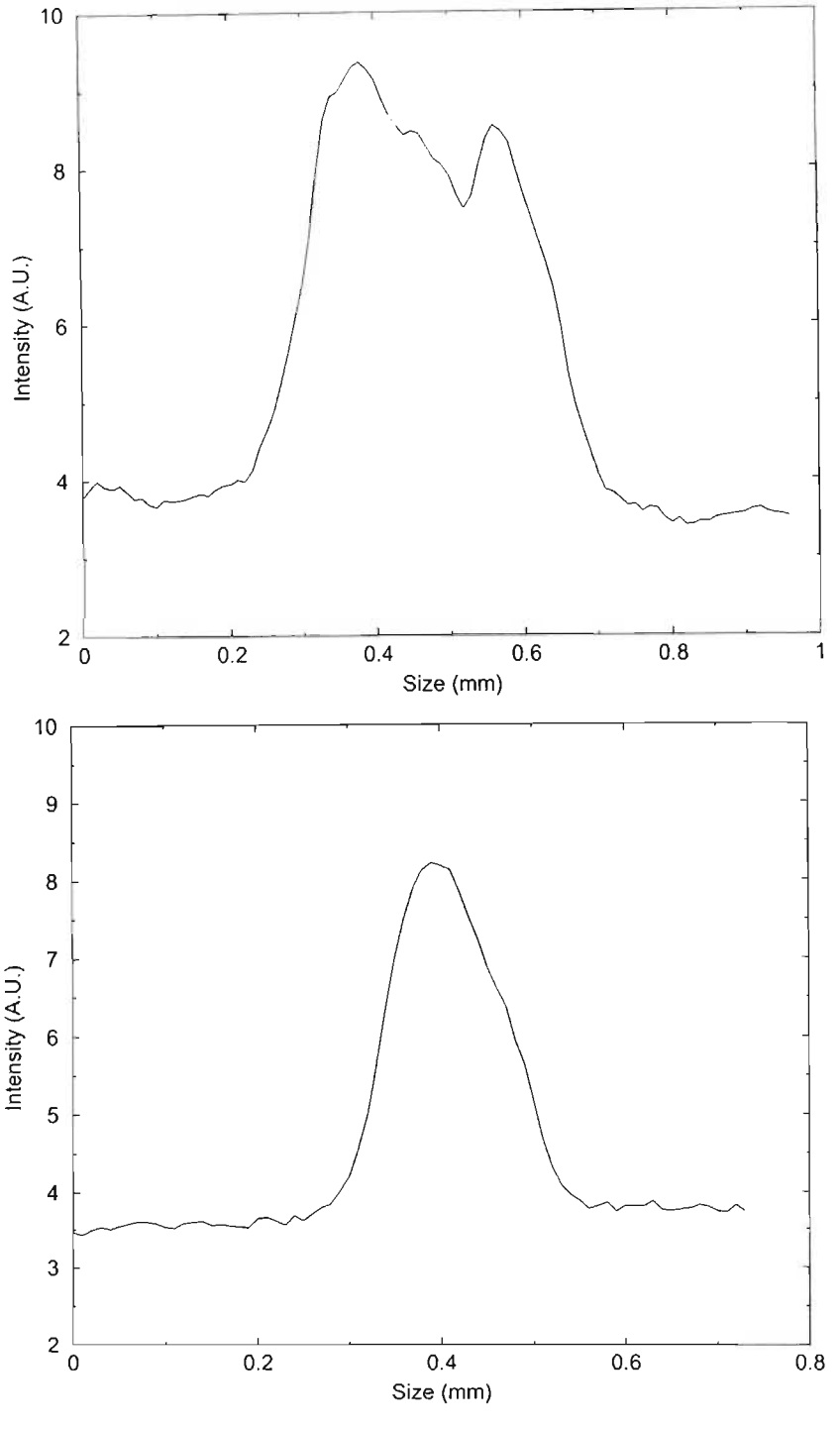

Graph 4.4: Densitometries of the picture 4.15 on the preceding page. The top graph shows the densitometry along the longest side of the pipe, the other one along the shortest side. The density, obtained with a computer scanner, is in arbitrary units. $W_{bank} = 180$ J.

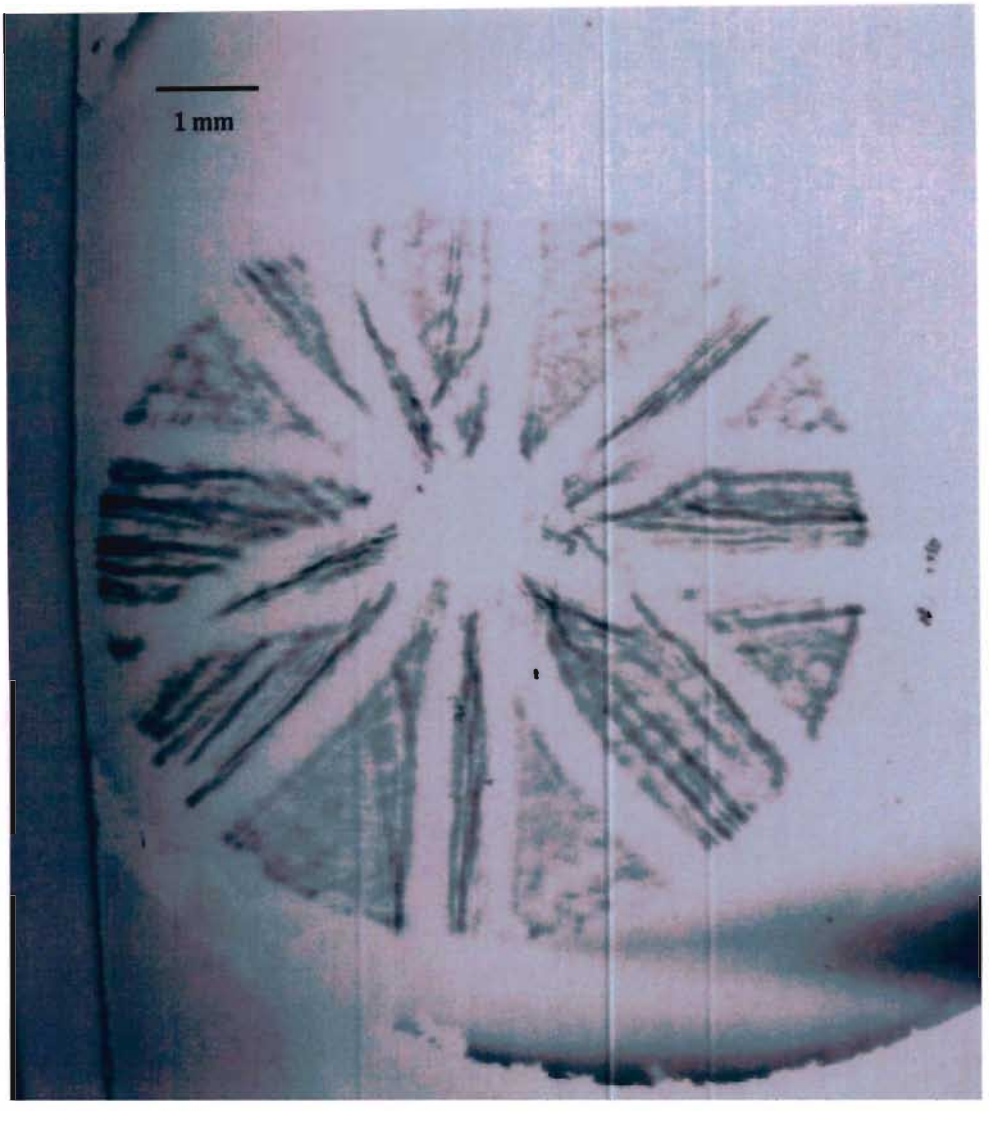

Figure 4.16: In this picture with a delay of 62.2 μs the shock are colliding in the centre. In the centre there might be a solid column of gas or a very small and slightly misaligned pipe, so that no light is getting through. W_{bank} = 180 J.

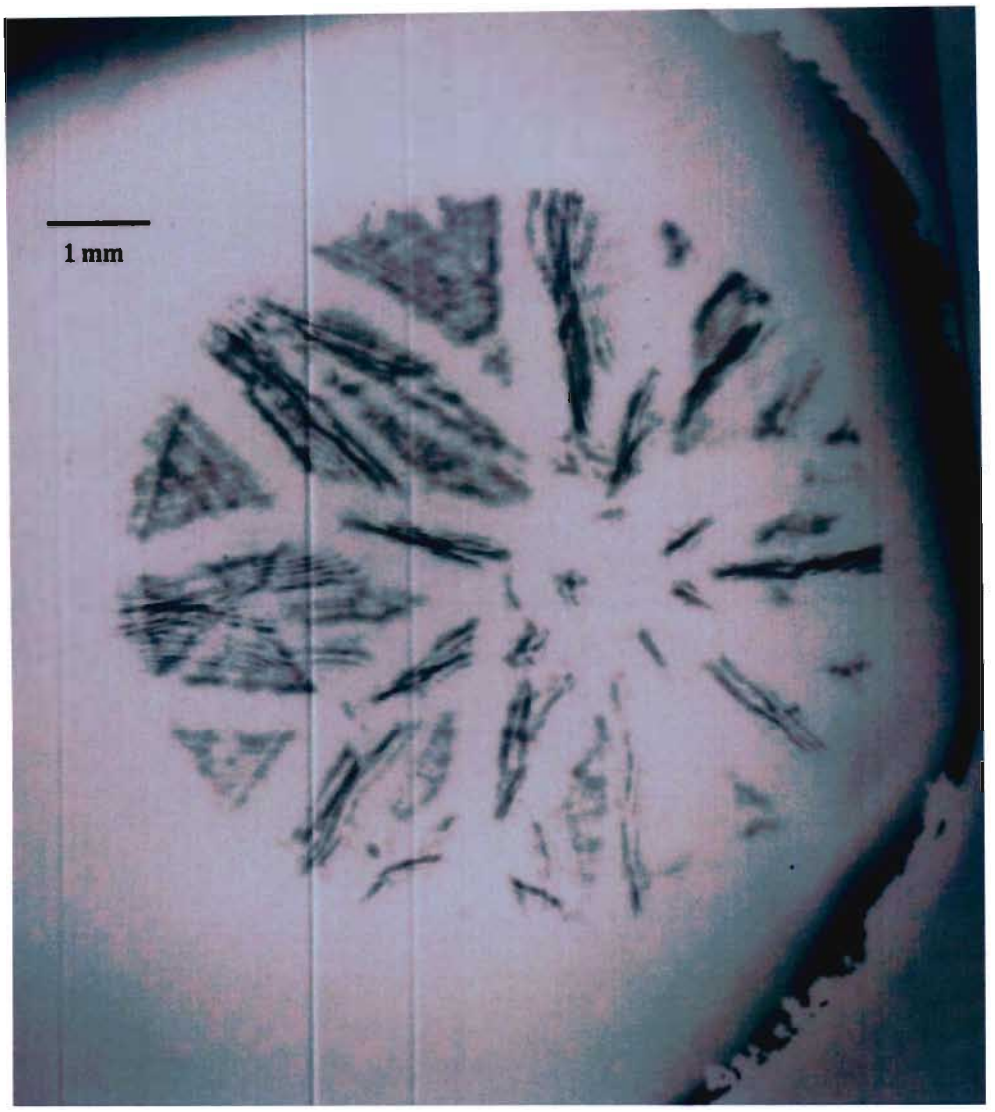

Figure 4.17: This picture, obtained with a delay of 54.6 μs shows the smallest pipe we obtained after collision. The pipe is not perfect because of some turbulence, but the size is very small. The central black dot should be noted. This corresponds to light refracted inward by the rebounding shock waves. Is is the desired result for colliding shock lenses. It may also be the optimum time for colliding pipe formation. $W_{bank} = 180$ J.

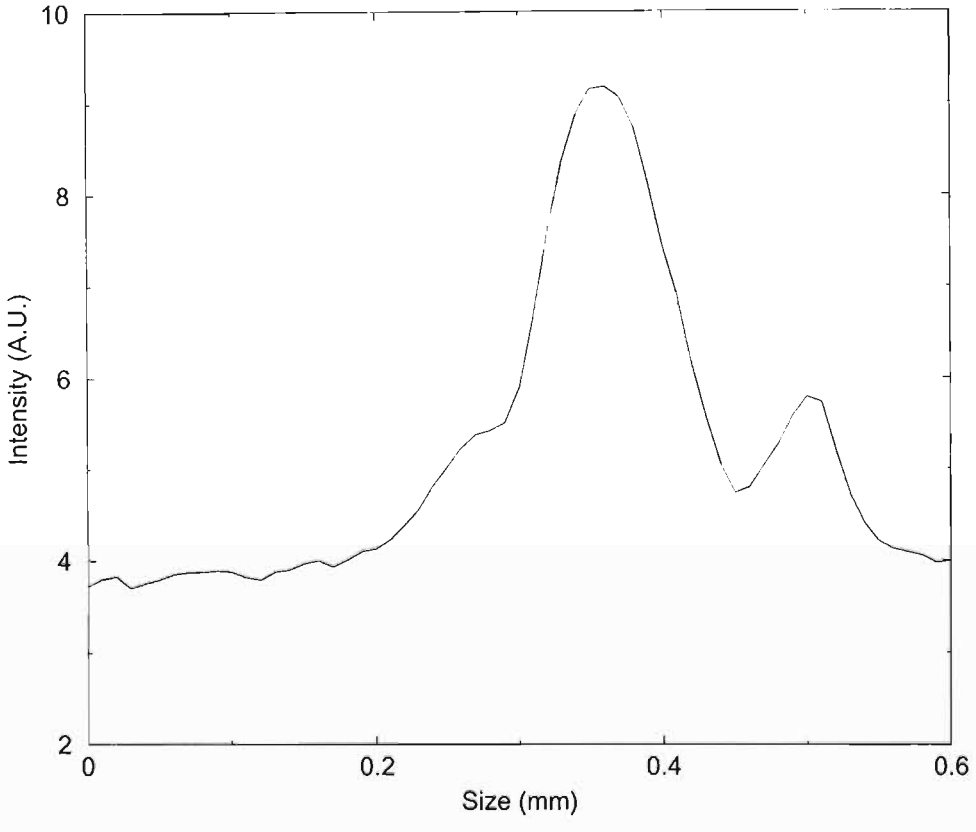

Graph 4.5: A densitometry of the picture in figure 4.17 on the preceding page. It can be noted that the bright spot in the centre has a size of $\sim$ 100 μm (FWMH). In order to have a focus reasonably close to the lens, the laser beam was not parallel, but converging 5 m after the device, by means of a quartz lens. $W_{bank} = 180$ J.

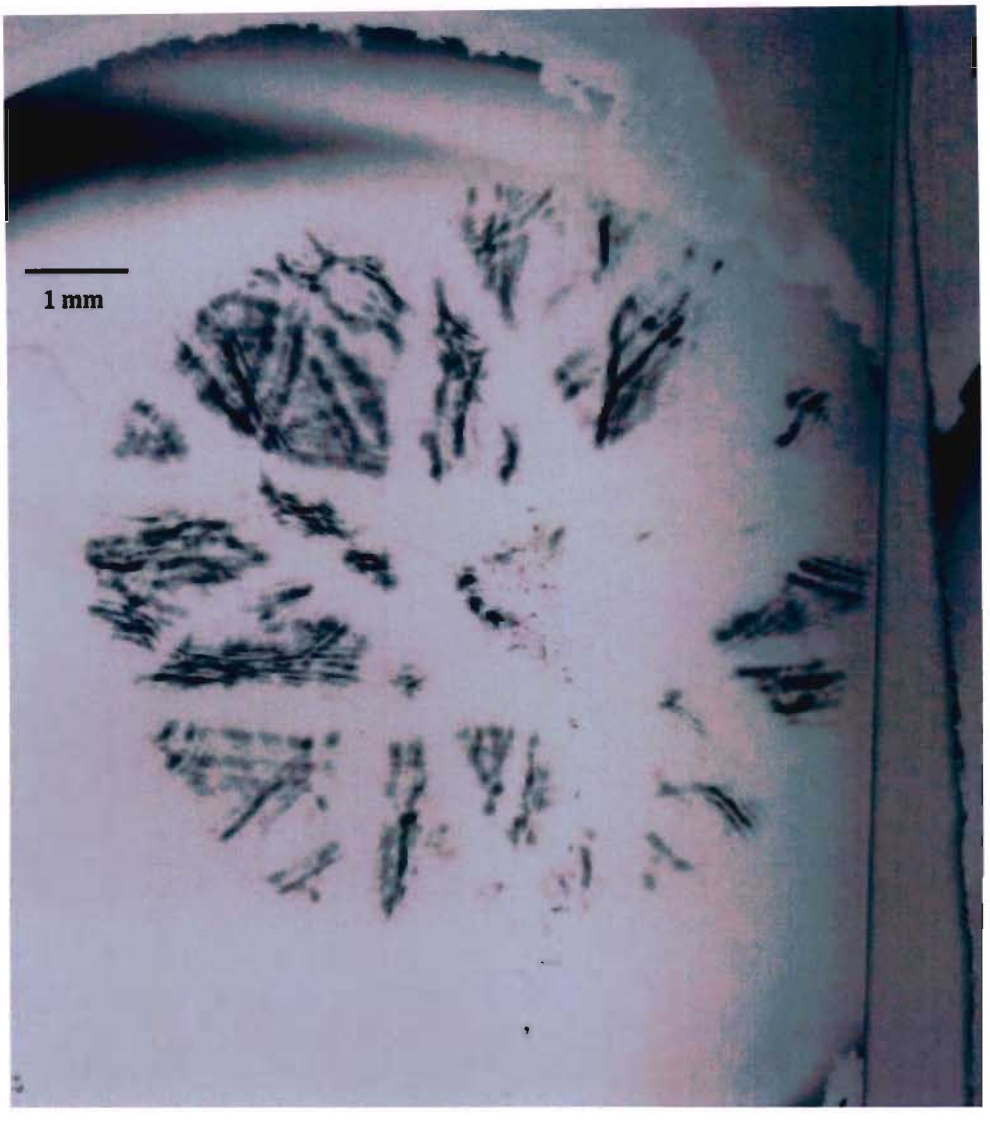

Figure 4.18: Another shot immediately after the collision of the shock in the centre. The circle has already a diameter of about 5 mm. Unfortunately, the delay is unknown because the oscilloscope did not record the trace. The small dots close to the centre are foci created by the intersection of the shock waves. $W_{bank} = 180$ J.

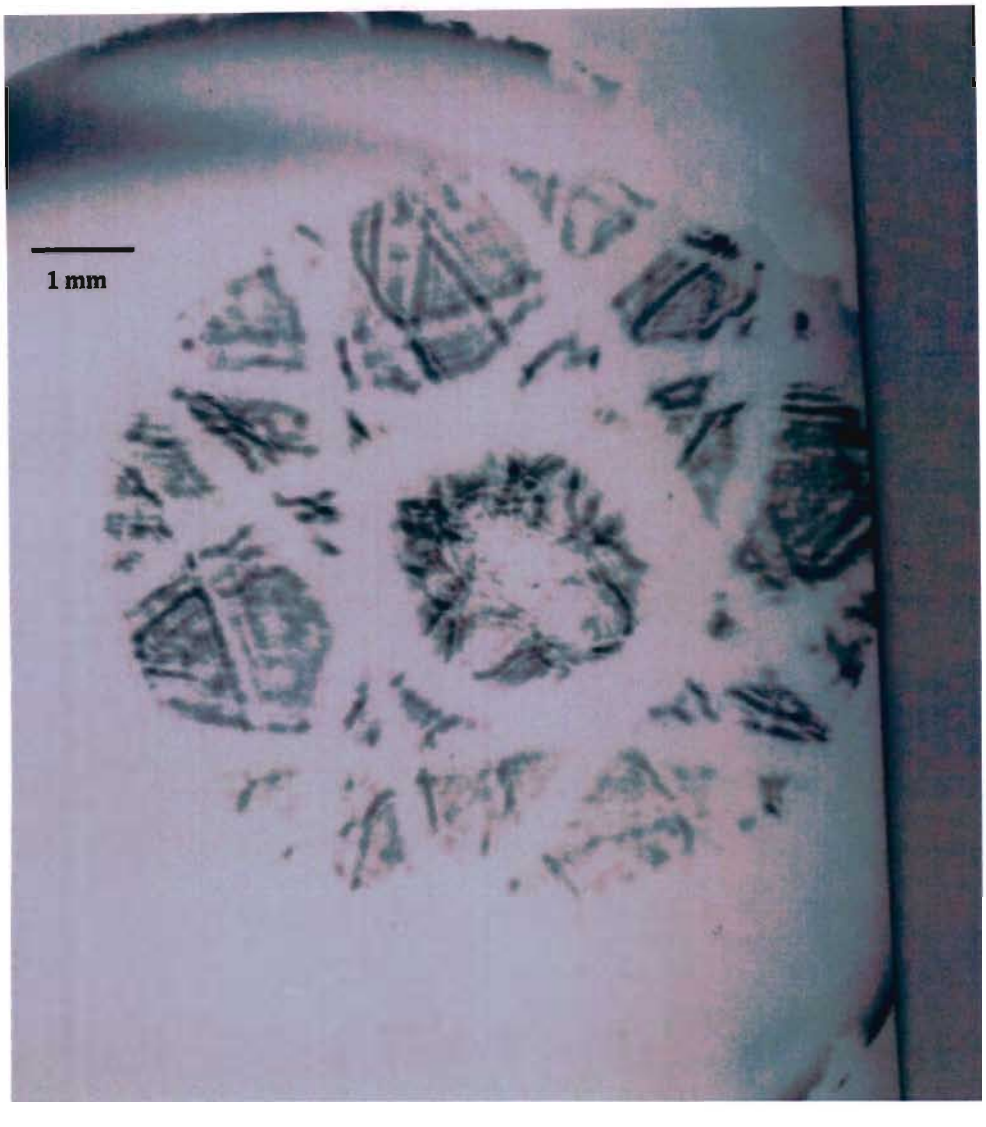

Figure 4.19: In this fast shot after collision with a delay of 65.2 μs the shocks have expanded more. Now the circle has expanded up to more than one centimetre in diameter and no focus is observed in the centre. It is interesting to notice in any case that there is no light in the centre. $W_{bank} = 180$ J.

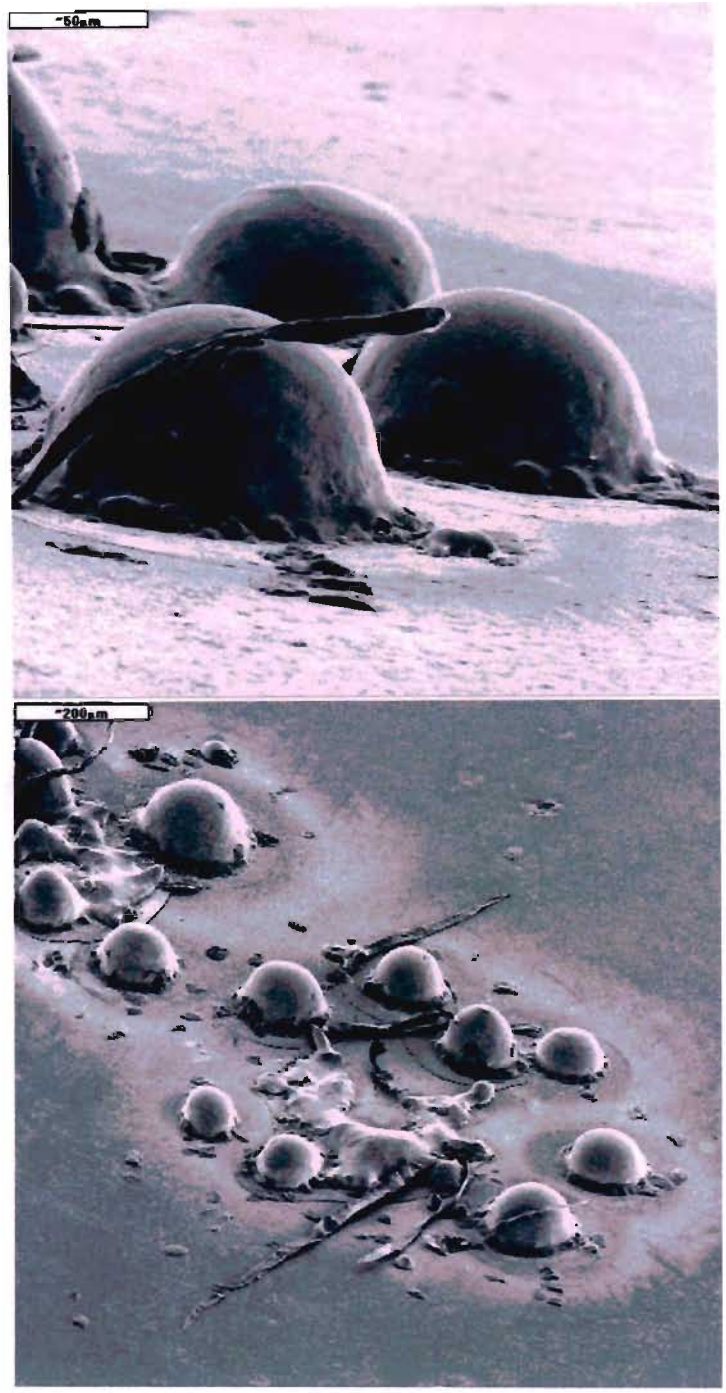

Figure 4.20: SEM pictures of copper droplets from the melted wire on the lens surface.

damaging the lens we were using to focus the laser beam. The SEM pictures in figure 4.20 on the preceding page show tiny droplets (smaller than 100 μm) on the lens. Since the debris are travelling slower than the shock wave, they should not have a bearing on particle acceleration experiments, in which the centre of the interaction chamber is empty.

4.5 Conclusions

Colliding shock waves proved to be a viable way of producing a uniform pre formed channel for a laser pulse. As shown in our experimental results, there are many parameters to be taken into account.

Our device is far from perfect. First, we do not have any means of tightening the wire. As a result, there are small kinks in it, which then induce non-uniformities in the pipe. If in our case this was not a problem, but the pipe needed for an electron acceleration experiment must be much more uniform. Moreover, the position of the wires in our device cannot be controlled very well. The wire goes through a hole 1 mm wide. Since the goal is to obtain a pipe smaller than a few hundreds of microns (if not less) the attainable precision is not sufficient. This may be seen in the form of small differences from shot to shot. Nevertheless, small difference are probably going to be compensated after the collision by Mach addition. It is true that the pipe gets usually more uniform after collision. All these problems can be easily overcame by a better design of the holder.

Moreover, our equipment was affected by many problems, the first one being a large amount of jitter. This is why results like that shown in picture 4.17 on page 119 were not at all easy to reproduce. This is because we could measure precisely the delay between the explosion of the wire and the firing of the laser, but we had little control on the actual delay.

The pipe described in this chapter may be seen even as a wall-less micro-capillary. In this case, this structure can become interesting for experiments dealing with soft X-rays lasers. In the Rocca scheme[17], an electrical discharge is sent trough a capillary filled with gas. In other experiments the capillary walls were covered with the lasing medium, that is ablated during the first part of the discharge. In both schemes, after a number of shots the capillary deteriorates and has to be replaced. In another scheme[14], a laser beam is sent through the capillary and, in this case, after a while the capillary mouth melts. In order to be of interest for these experiments, a gas capillary must be as small as 100 μm. In our laboratory, we have produced capillaries with an internal diameter of 500 μm, which is not very far from this limit.

Non coherent capillary discharges are also a potential source of EUV radiation for the so-called Next Generation Lithography[6][69][32][48]. Again, shock waves could be a good means of preforming a capillary that can then sustain the discharge. In this way there would be no need of replacing the capillary stopping the production every now and then.

For special application it is also possible to bend the pipe (e.g. if at a later

stage of laser accelerator development, gently curved trajectories in strong magnetic fields are required). In our case, this cannot be done, because our wire is not stiff enough to hold itself in position and we did not have enough energy to explode a thicker one.

Chapter 5

Colliding shock lenses

Colliding shock lenses[59][1] (CSL) are one of the better known applications of gas structures[8][45][40][29][58]. They are real optical elements, sometimes with a very good quality, and are made out of air. CSLs are of course dynamic lenses, which last for a few microseconds and are always evolving. Because these lenses are intended to be used with pulsed lasers, this is not a problem. Most modern lasers are in fact pulsed with a pulse duration almost always below 1 μs, often by many orders of magnitude. The main advantage of a CSL is the fact that it cannot be destroyed nor damaged. If the laser pulse to be focused has too much energy, it ionises the air and the lens stops working but without any damage. Traditional glass lenses instead suffer damage, usually due to thermal effects. Lenses need therefore to be replaced, increasing the cost of any laser machinery.

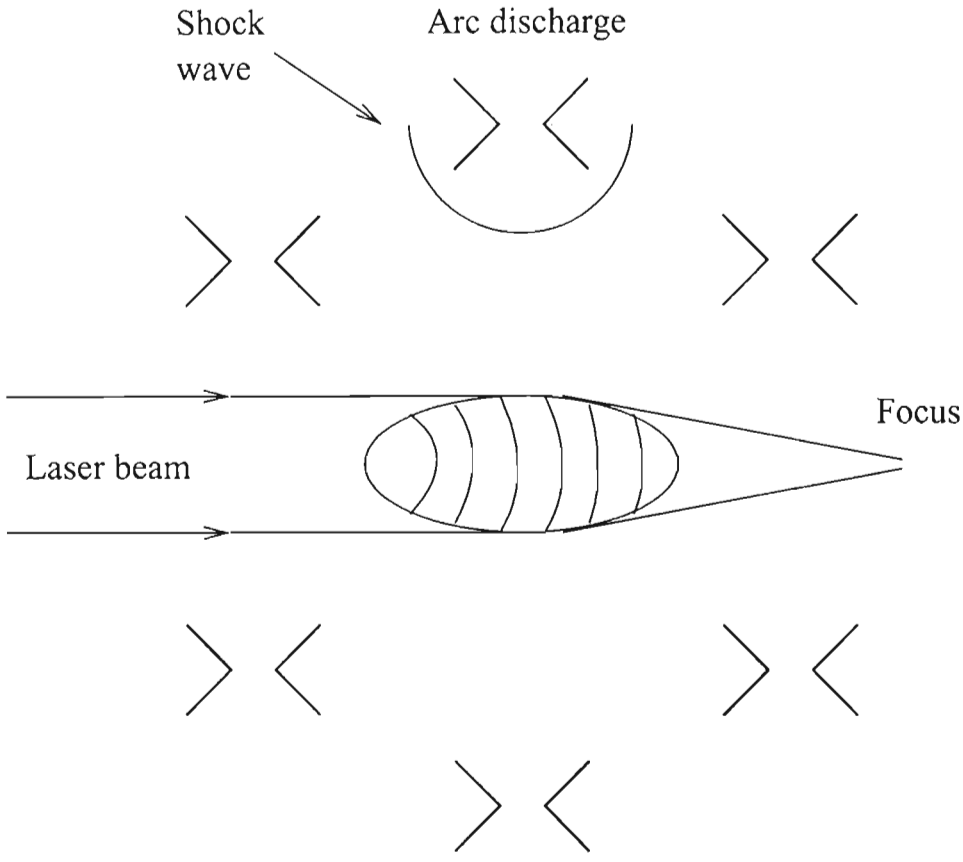

Figure 5.1: The working principle of a colliding shock lens. A hot cigar of air left behind after the collision of the shock wave focuses the light inward.

But CSLs have another characteristic that can make them interesting for some applications[61]. These lenses have a very long focal length, in comparison with their small diameter. For example, a lens with a diameter of 1 cm can have a focal length of several metres, something quite difficult to make out of glass because of the very small curvature. This means that the cone of light hitting the target, if there is any, can be very sharp. In case of laser drilling, this allows a better quality hole.

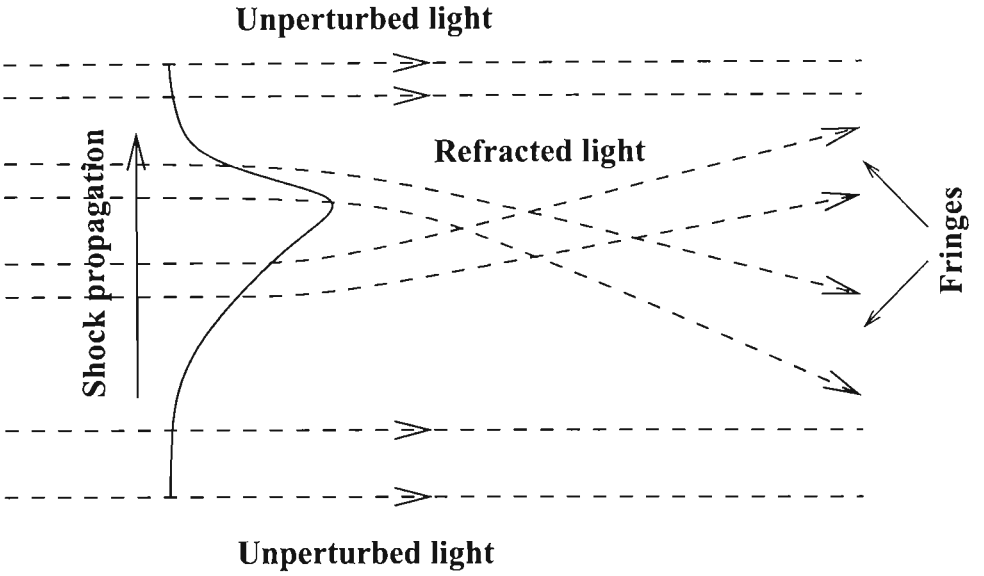

Figure 5.2: The fringes produced by a single shock wave. If there is a steep pressure gradient in air, light is refracted toward the denser medium. Steeper gradients bend the light more. In a single shock we have a front, with a very steep gradient and a tail, which is less steep. Both, the front and the tail refract light that interferes with the unperturbed light propagating on the side of the shock to create fringes. The fringes produced by the tail, visible in the pictures in front of the shock, are finer[64][50].

CSLs can be used in a repetition mode. In our laboratory, a CSL with a

diameter of 4 mm was operated up to a repetition rate of 1 kHz (G. Turner, unpublished) without any noticeable loss of optical quality. This means that the relaxing time for the air is very short. Of course, this can be difficult to obtain on a big lens, where the energy required for every shot can be of several hundreds joules. Looking at the results for our 1 cm lens, the minimum energy required for every shot is 800 J. This means that running such a lens at 100 Hz would require 80 kW of electrical power. But a solution can be found using a resonant device, in which the shocks bounce on the wall and receive another portion of energy. In this case, the repetition frequency of the lens depends on the speed of the shock waves and on the diameter of the device. In our case, with a 30 cm lens and the shocks travelling at a measured speed of 1.6 Mach, we could have a lens operating at 1100 Hz. Of course, this is the repetition rate of the lens, the laser can fire at a lower frequency, keeping synchronised with the lens firing.

CSLs have also many disadvantages. The first one is that any spark in air is usually very noisy, both from an acoustic and an electromagnetic point of view. The acoustic problem can probably be neglected, because high power lasers have usually a high level of acoustic noise of their own. Unfortunately, in any case, a CSL can not be acoustically isolated without enclosing it with optical windows, which would be subjected to the same sort of damage as a glass lens, making the device pointless. The electromagnetic noise is a much more serious problem. The device is quite noisy during normal operations, up to the point where the use of ear-plugs is recommended. Sometimes the

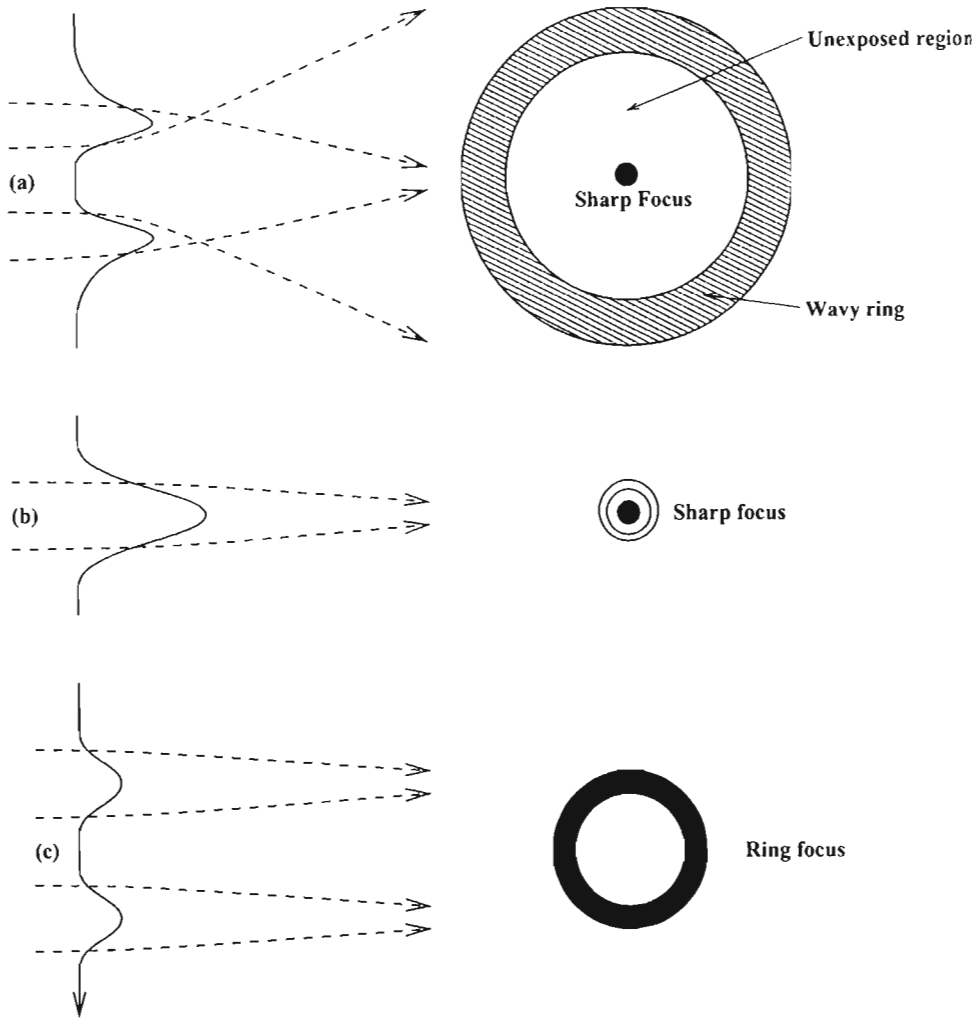

Figure 5.3: Evolution of a CSL with the corresponding images. In a), before collision, the light is refracted both by the head and by the tail of the shock, producing a sharp focus in the centre and a weaker ring focus. In b), at collision time, the light is refracted only toward the centre, creating a sharp focus. After collision, in c), the shocks are smoother, the pressure gradient is similar on both side of a shock and a sharp ring focus is produced.

pins do not breakdown and all the energy goes into the coil, which acts like an antenna, radiating most of the energy in a large burst of noise. This noise can affect, or even damage, computers and sensitive devices normally present in laboratories or factories. The figures 5.8 on page 139 and 5.9 on page 140 show a comparison between a normal oscilloscope trace and one recorded when the pins did not break down.

The second problem is that the electrodes of the CSL are eroded by the arc, even if the lens itself cannot be damaged. In our case, the problem was particularly serious. In order to make the alignment of the pins easy, we used a flat electrode in front of a spherical one. After several shots, the eroded flat electrode becomes concave, and the gap has to be decreased to allow the breakdown. This adjustment changes the geometry of the pins and makes it impossible to control where the arc takes place. In our case, the problem was made worse by the fact that the electrodes were made of normal steel and not of tungsten, which would be more resistant but much more expensive and difficult to machine.

Unfortunately some important measurements that could be expected in a work on lenses, like the focal length, are missing. This is due mainly to limitations of our equipment and limitations in what was actually available. For instance, erosions on the electrodes during every discharge made the CSL and its firing characteristics change slightly. This changed the energy that could go into the shocks themselves and therefore their speed. We could verify in shocks taken exactly at the same time after discharge that the position of

the shocks can vary quite substantially. In this device, unfortunately, this translates into a change of the focal length and this means that without a simultaneous check of what happens to the shocks and at the focal plane, it is impossible to know where exactly the focus is. Such measurement would have been possible by using some beam splitters along the optical path, but such optics were not available. This problem could be solved in a production device. Erosion can be limited by using a device faster than a spark gap, like a thyratron (which was nor available nor affordable in our laboratory), and reducing the energy. Moreover, steel electrodes could be replaced with harder (and more expensive) tungsten ones.

5.1 Experimental set-up

The CSLs obtained until now in our laboratory had optical apertures of up to only 5 mm, too small to find a real application. Our next aim was to obtain a useful aperture, at least of 1 cm. Of course, in order to have such a lens, the device itself must have a bigger diameter, to allow the shocks to meet in the centre with a larger radius of curvature, necessary to obtain Mach addition. Then, since the shock waves have to travel a longer distance, the energy must be increased, to allow Mach addition to take place and to avoid a serious broadening of the shocks themselves.

The device we use (see the picture 5.4 on the following page) has a diameter of 30 cm and has sixteen pairs of pins, in order to increase the optical

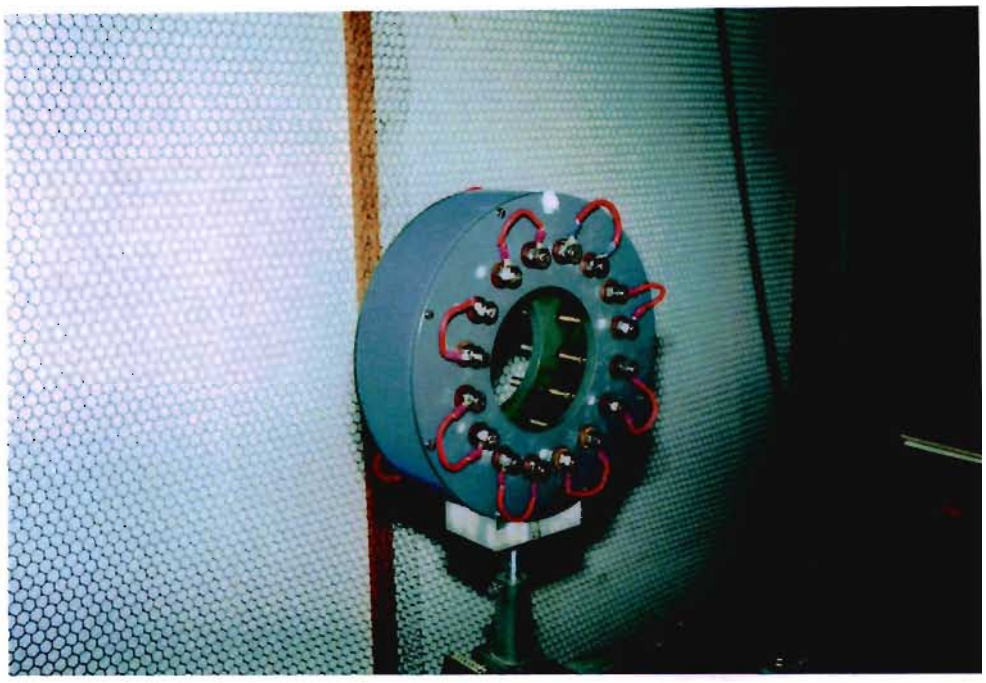

Figure 5.4: The lens used in the experiments. The frame is made out of plastic because the pins have to be insulated from each other.

quality of the lens by generating a smooth circle. At the beginning, we tried to operate the lens with the pins connected in parallel, usually in pairs. Working in this way the voltage across the capacitors can be reduced, allowing the use of a cheaper and simpler power supplier and reducing the H.T. dangers in the laboratory. After a few experiments, it became clear that this configuration leads to a large difference in the breakdown time of the pins, which yields a distorted lens which does not work.

The electrodes for the discharge are a flat surface and a sphere, as shown in figure 5.7 on page 138. Two tips or two spheres would probably facilitate

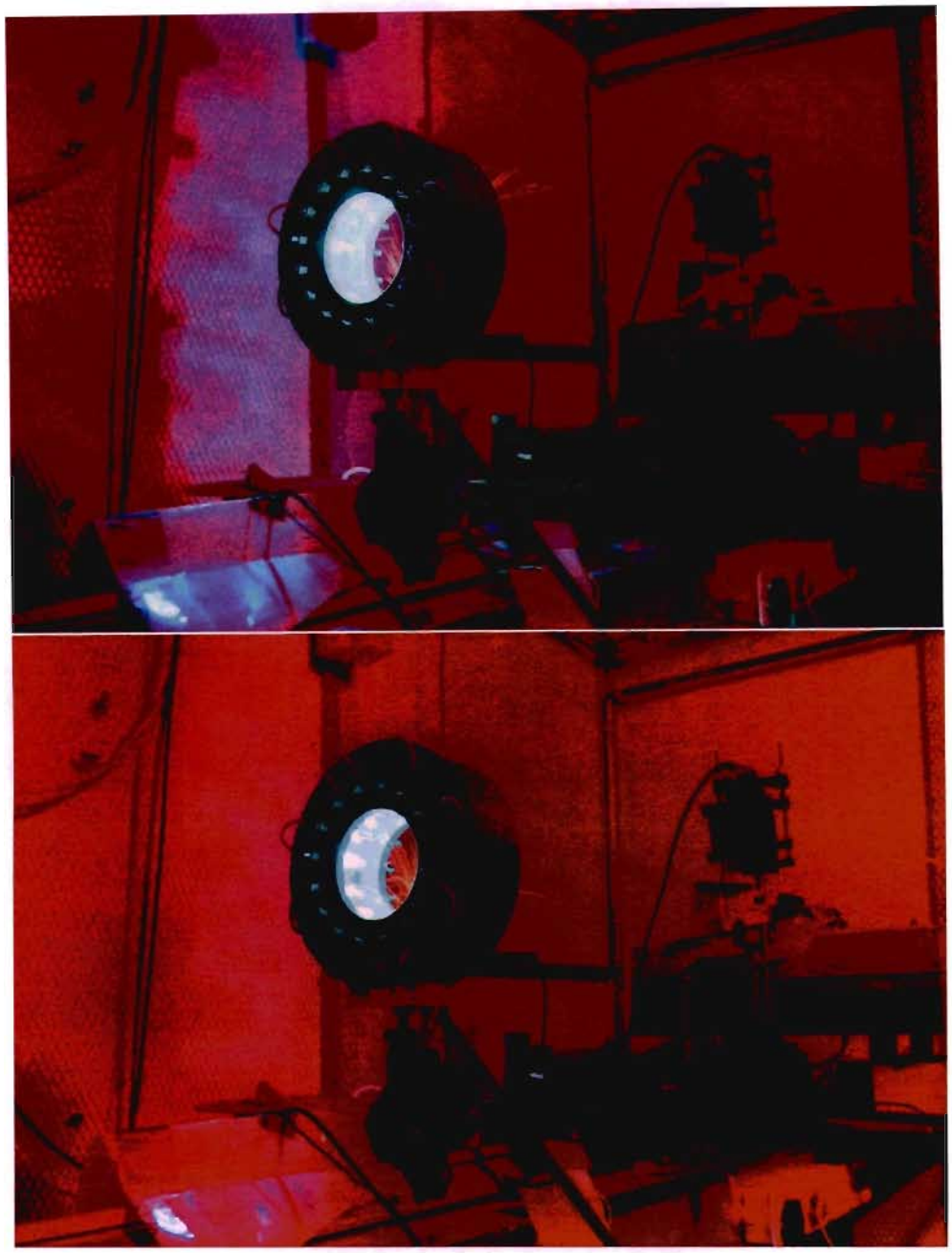

Figure 5.5: Two pictures of the lens during a shot. It is possible to see the light coming from all the pairs of pin. The sparks leaving the pins are debris from the electrodes, a clear sign of the erosion of them taking place.

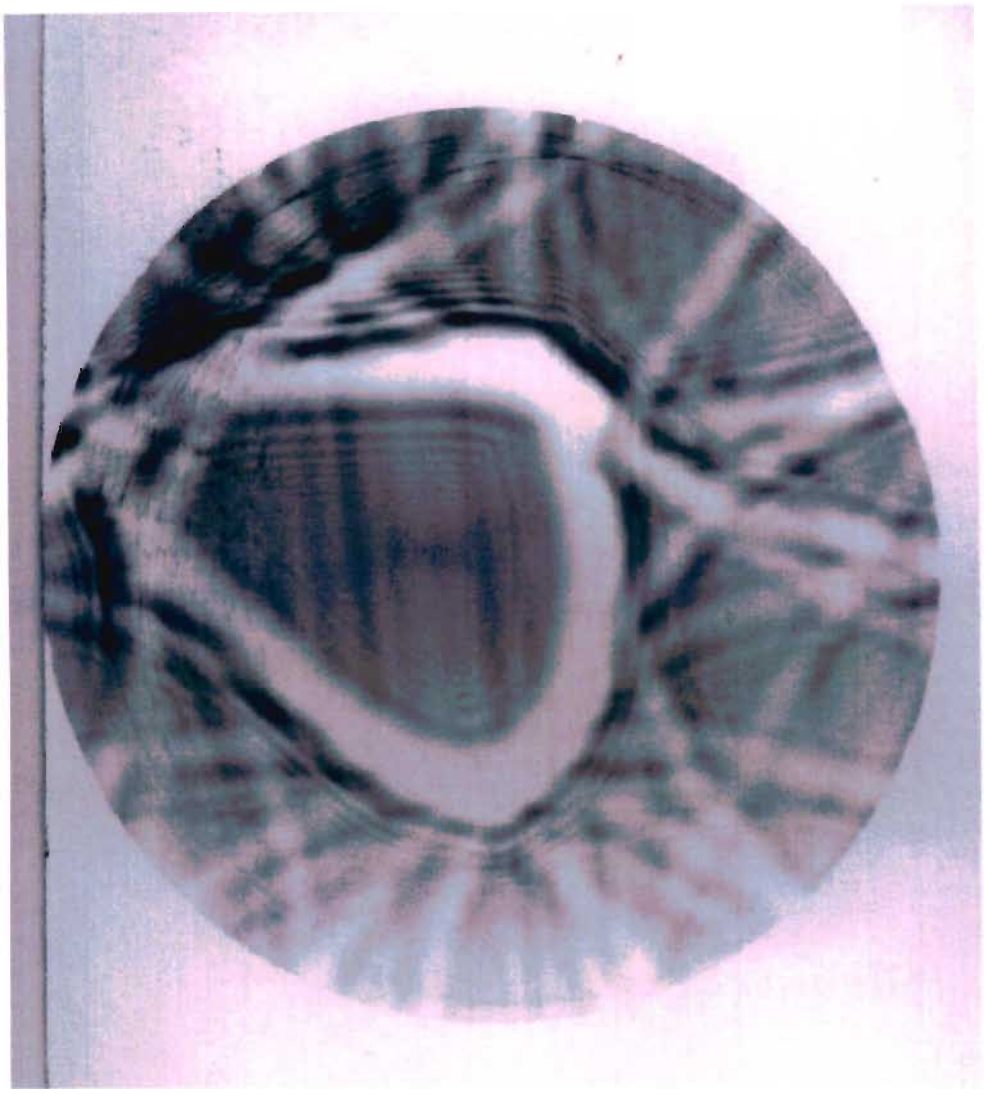

Figure 5.6: An image of a lens in which part of the shocks are completely missing. In this case, the resulting structure is a circle with a missing part. Such a lens can still work, but of course the optical quality is very poor and the focus is not circular.

the breakdown, but they would be more difficult to align. The separation between the single couples of electrodes was around 0.1 mm, in order to have a safe breakdown at the voltage required to operate the lens, which is of the order of 20 kV. The separation of the electrodes is very important. First of all, it must be small enough to ensure the breakdown, in order to avoid the generation of a large amount of electromagnetic noise. Also, if the electrode separations are different from one another, then it is very likely to obtain a lens distorted by a single shock much stronger or much weaker that the others, as shown in the picture 5.6 on the preceding page.

The circuit is like the one shown in figure 3.1 on page 72, except that there are sixteen pairs of pins, connected as in figure 5.7 on the following page.

Then, another factor which has to be taken into account is that the shock waves have to travel a very long distance, before they get to the centre. A fair amount of energy must be provided, otherwise the shocks weaken too much before they collide, and do not create the lens.

Unfortunately, in our laboratory we have only one capacitor capable of handling 30 kV, with a capacity of 1 μF, and a few more rated up to 20 kV, but with a much bigger capacity of 8 μF. This means that we cannot continuously change the energy used in our experiment. Moreover, another constraint is that in most of our experiments the minimum voltage depends on the setup or on the energy required for the device, and cannot be chosen arbitrarily.

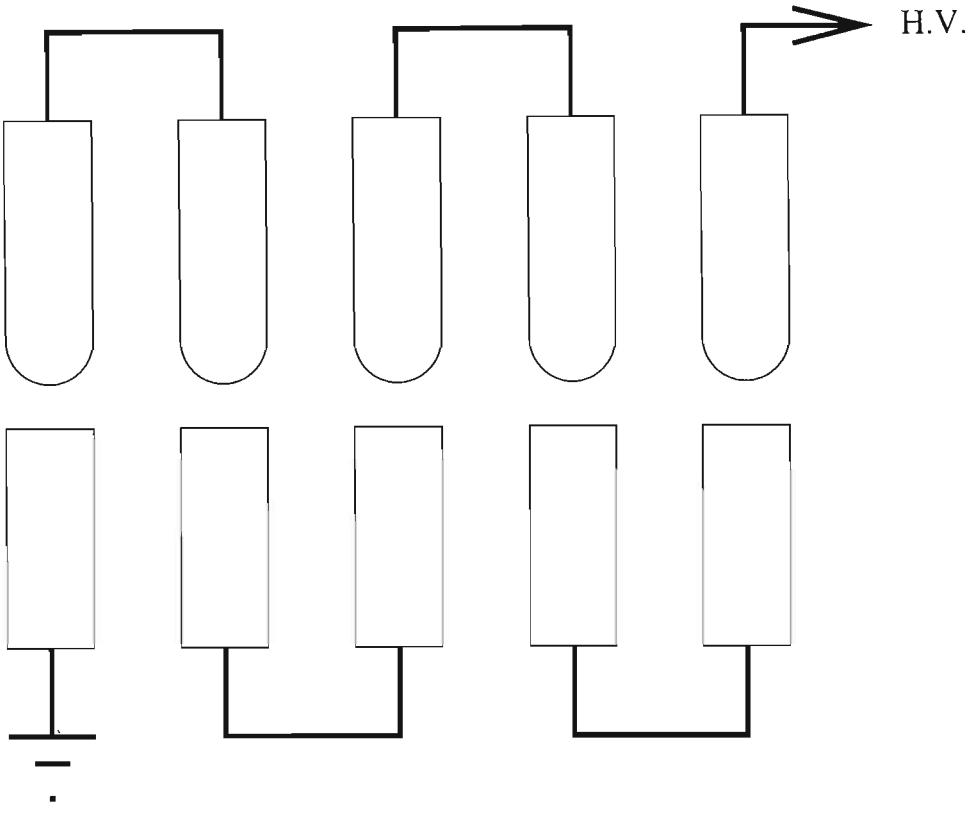

Figure 5.7: Connection of the pins (only 10 are shown for sake of simplicity). It can be noted that the middle segments of the circuit are all floating. This is the reason why we had to put a coil in parallel to the lens, in order to carry the voltage to the spark gap. As in the drawing, each pair has a flat surface in front of a semi-spherical one

In principle, it should be possible to change the energy by putting an arbitrary number of 8 μF capacitors connected in series and parallel. Unfortunately, in our case this is not true, because this kind of connection increases the impedance of the circuit, which in turn slows down the discharge, thereby

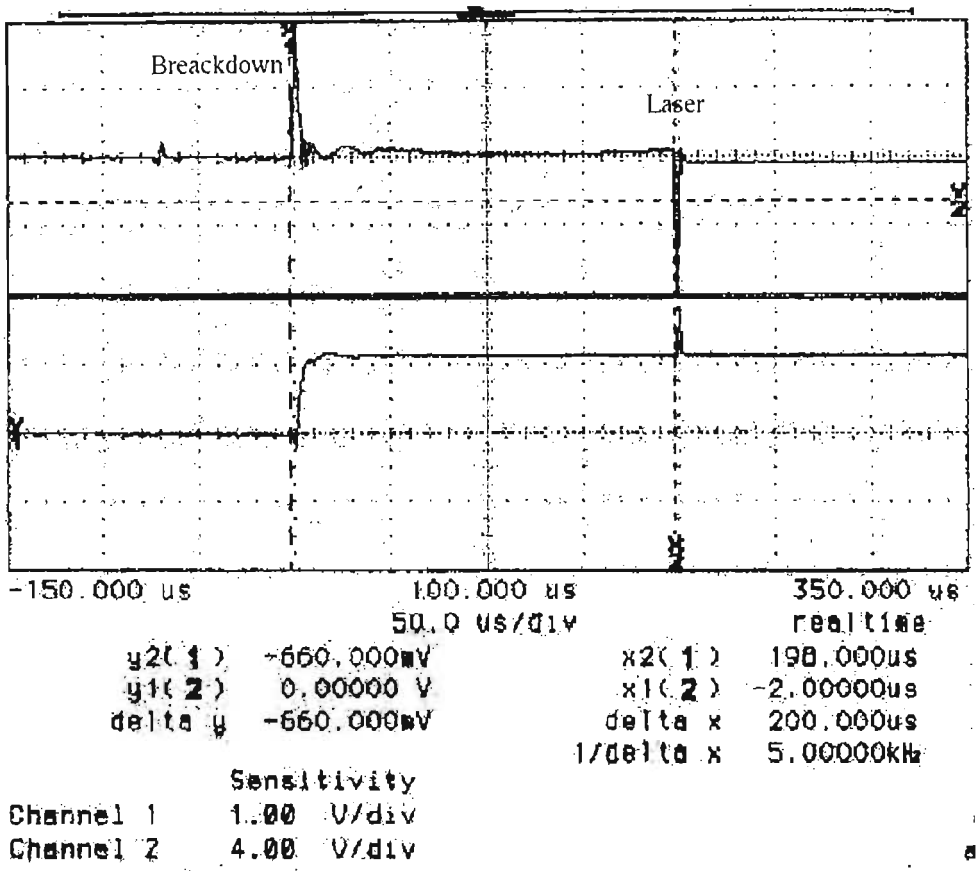

Figure 5.8: Oscilloscope trace of a normal experiment. The top trace shows the noise from a coil close to the device. The first high peak from the left is the breakdown of the pins; the second is the firing of the laser. The bottom trace is the signal from the optical trigger.

reducing the quality of the shocks. In fact, we managed only to connect only two capacitors in series, using the circuit with the lowest possible impedance, which is shown in figure 5.10 on page 141. This kind of connection dramatically reduces the impedance of the circuit, but it is potentially dangerous. Both the cases of the capacitors have in fact half of the voltage used in the

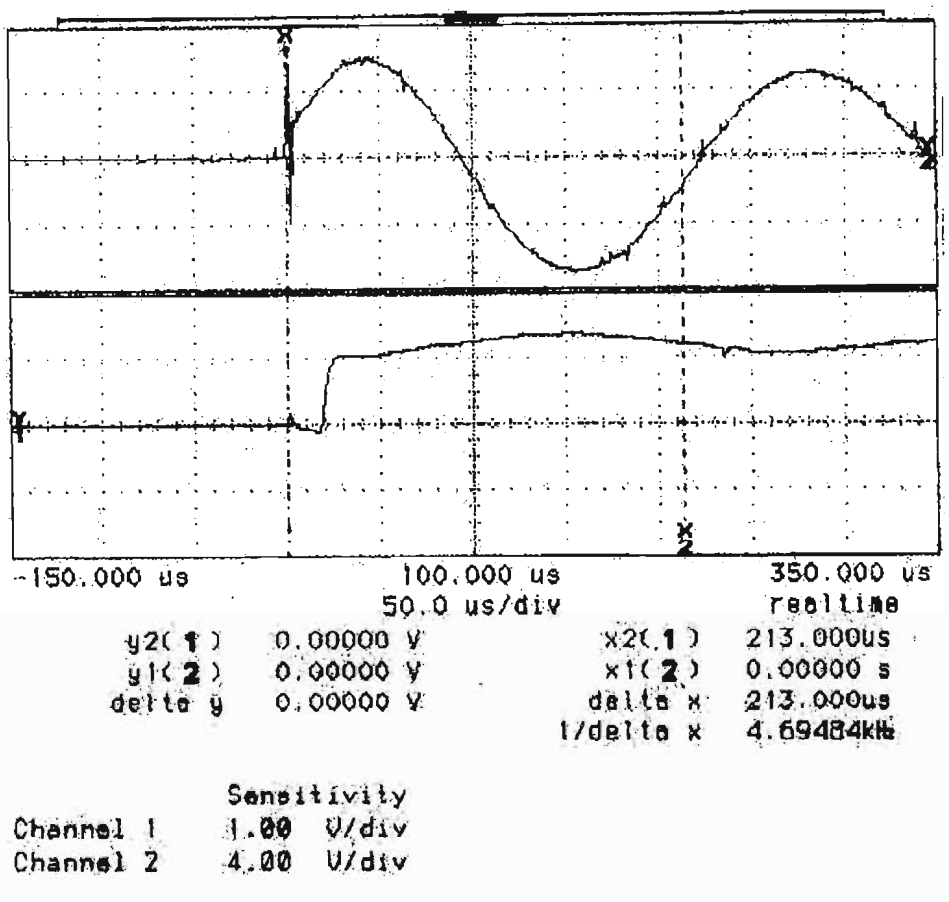

Figure 5.9: Oscilloscope trace of the experiment when the pins do not break down. In this case most of the energy is radiated as electromagnetic noise. This noise can be seen in channel 1, at the top. It should be noted that the oscilloscope settings were the same as in in figure 5.8 on the preceding page. The bottom trace shows that the optical trigger is activated by this noise.

experiment, which is usually several kilovolts. In experiments with three capacitors we saw only weak shocks.

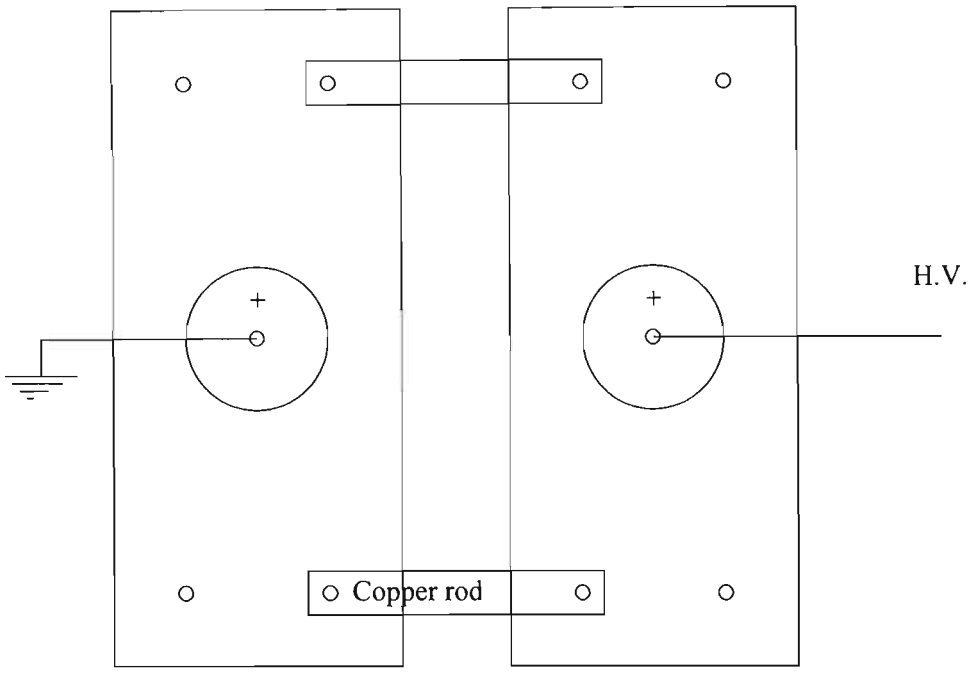

Figure 5.10: The figure on top represents the connection that we used to put two high voltage capacitors in series without increasing the impedance of the circuit very much. It should be noted that the two capacitors do not have a polarity. Normally the electrode in the centre (labelled +) is connected to the high voltage and the case to ground, for safety reasons. Having used the capacitors this way, both the cases where at half the charging voltage. Two resistors, not shown in this diagram, were put in parallel to each capacitor to divide the voltage.

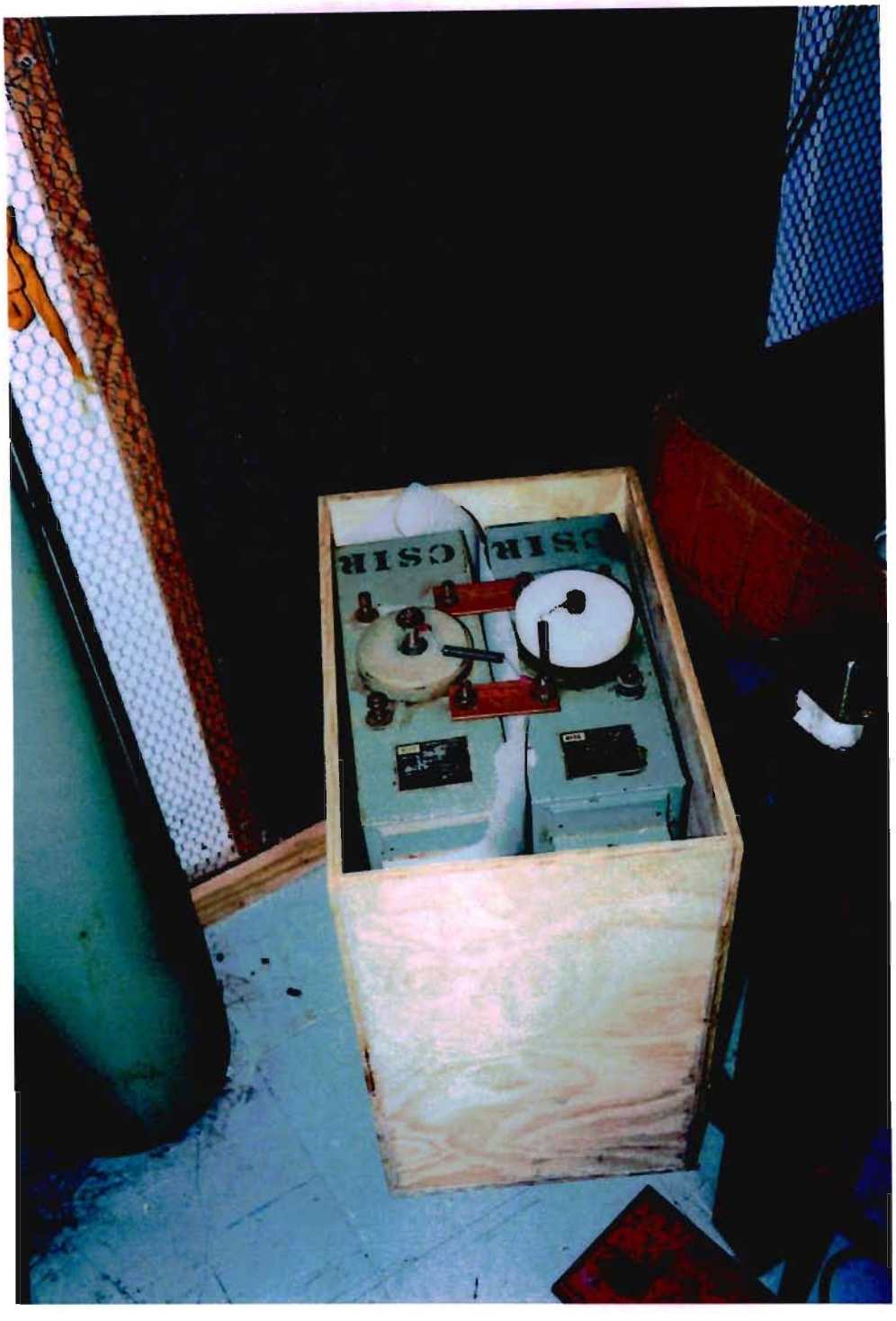

Figure 5.11: An actual picture of the capacitors connected as described in figure 5.10 on the previous page. The resistors (a few hundreds kiloohms) partitioning the voltage are clearly visible, as well as other components of the circuit.

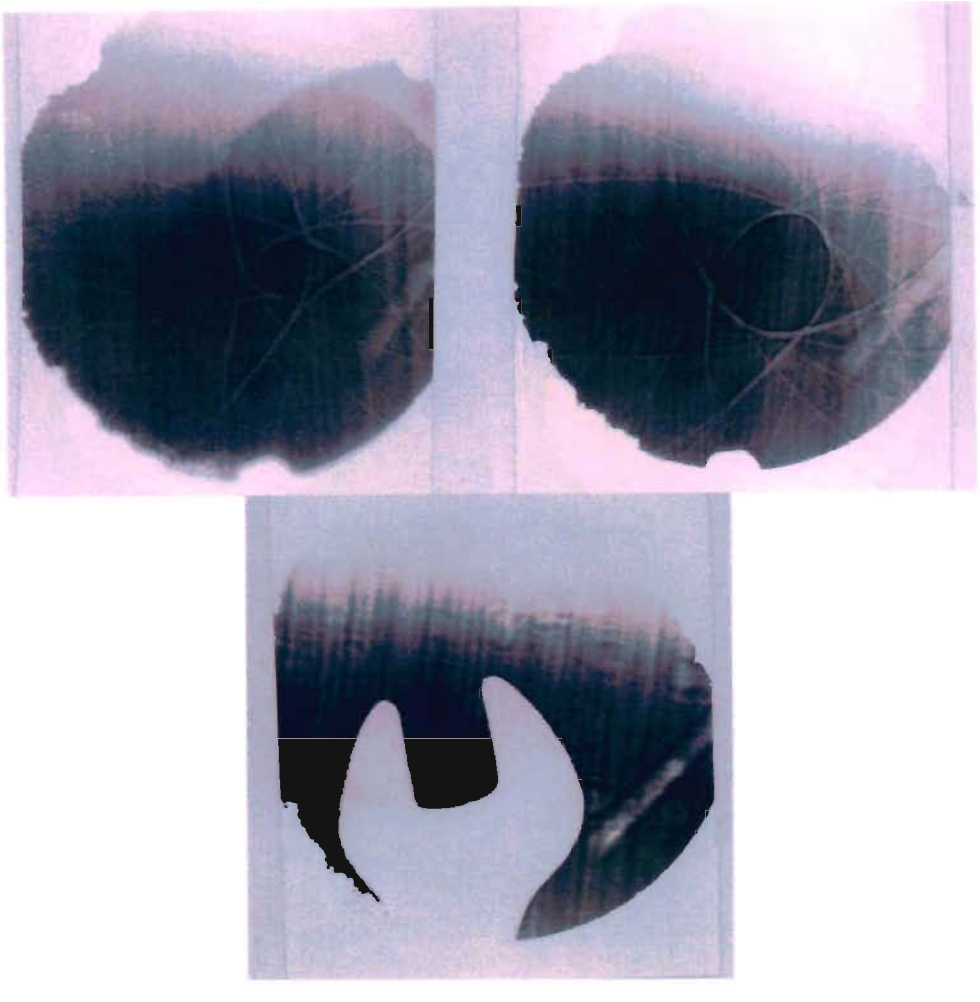

Figure 5.12: The two picture used to measure the speed of the shock waves. The reference object on the bottom has a size of 6 mm and the two lenses have a radius of 1.9 mm and 3.9 mm and the delay between them is 5 μs.

5.1.1 Speed measurement

In order to know the size of the lens corresponding to every delay, we had to measure the speed of the shock waves. This was easily done by measur-

ing the diameter for two known delays, after checking the reliability of the system over a few shots. Because the lens is not always perfectly circular (see figure 5.12 on the preceding page), we measured the area of the lens and calculated the diameter approximating it to a circle. The resulting speed, with a voltage of 20 kV, and an energy of about 800 J was 1.6 Mach.

5.2 Experimental results

The first results were obtained using an energy of 300 J. In this case, our shadow-grams showed good circles with diameters up to 12 mm. Nevertheless, we could not observe any lensing for diameters larger than 6 mm. This happened because the energy was not enough to get Mach addition. In this case, the shocks pass through each other unmodified and do not create the cigar of dense air, heated by compression, that is the actual lens.

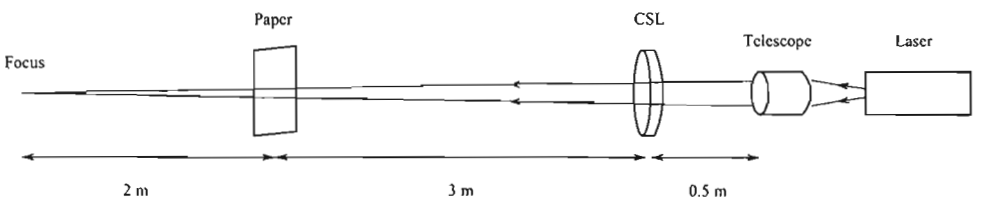

Figure 5.13: The scheme of the first experiment with the CSL. The telescope was adjusted in order to have the beam focused 5 m after the CSL. In this case it is like having two lenses in series and when the CSL works the focus moves closer to the laser.

The first series of good results was obtained with an energy of 800 J and the results are shown in the figures from 5.14 on the next page to 5.3. In

this case the telescope in front of the laser was adjusted in order to have the beam converging 5 m from the lens (see figure 5.13 on the preceding page). This was useful, because the rail where the experiment is set up is not very long. This could be also and idea of how to use CSLs. In some cases, a high energy laser pulse can be focused to a small size with a normal lens, keeping the energy density low in the glass, and then focused yet again to a very small spot with a CSL.

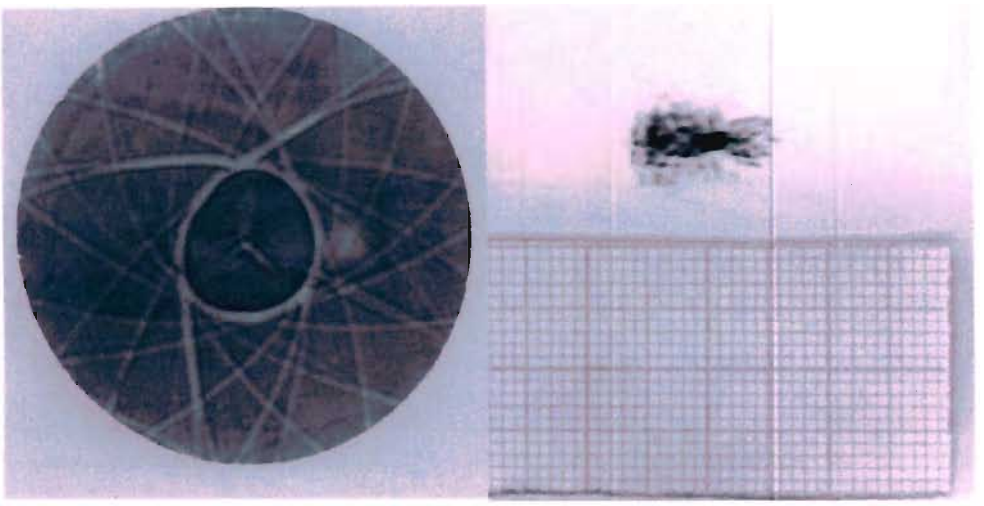

Figure 5.14: An image of the lens and of the corresponding focus, obtained in a different shot. The diameter of the lens is 7.2 mm. It should be noticed that the two images were taken in different shots (we can not simultaneously image the shocks and the laser spot in the far field). The photographic paper was 3 m far from the CSL and the densitometry (see figure 5.1 on page 149) shows that the focus is still rather large. Later experiments showed that the focal length of our CSL is around 15 m, which means that the focus was probably 3.75 m from the lens. A comparison between an actual experiment and an image showing only the laser can be seen in figure 5.15 on the following page.

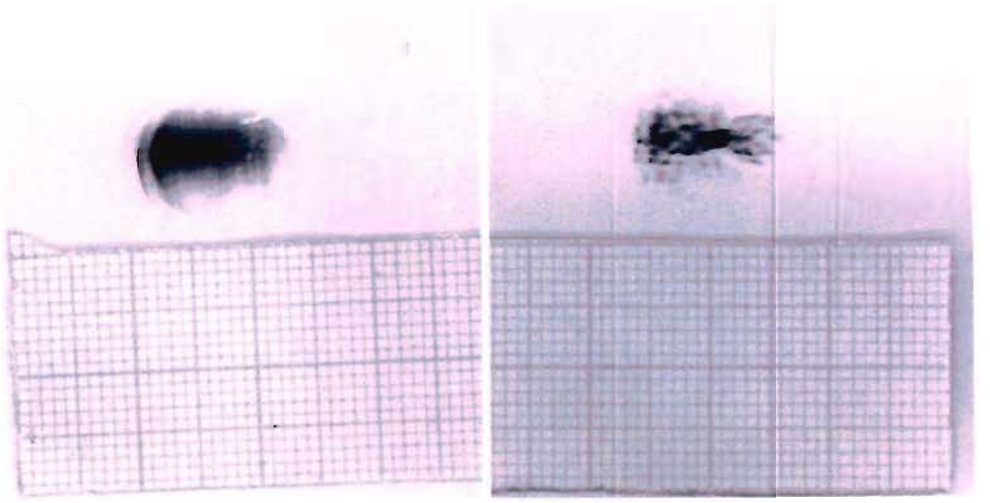

Figure 5.15: A comparison of a blank image (left), obtained firing only the laser and one firing the CSL too. It is clear that the CSL is really focusing the beam. The image on the right is the same as in figure 5.14 on the preceding page

The effect of Mach addition may be observed by comparing the pictures in figure 5.18 on page 154, obtained before the collision of the shocks, with the ones obtained later after it. All the pictures before collision show a very irregular shape, which, in most of the shots, is later smoothed after the collision itself into a nearly perfect circle.

Another series of results is shown in figures from 5.20 on page 156. In this case, the telescope was adjusted to have a parallel beam and focus it only with the CSL, without the aid of any additional lens.

It can be noted that for small delays after the collision of the shock in the centre, a strong small lens can be observed with a focal length shorter than 2 m (see figure 5.19 on page 155).

The two pictures 5.22 on page 158 and 5.23 on page 159 show the size of the lens in the near field in two shots with the same delay. Unfortunately small differences in the behaviour of the circuit result in a different speed of the shocks. This explains the difference of 10% in size between the two images. Assuming that the focal length is directly proportional to the diameter of the lens, the corresponding fluctuation in the focus position can be as high as 2 m. This can mean that the quality of the focus can be actually better than what we measured, i.e., the focal spot might be smaller. Unfortunately, we could not get images of the near and far fields at the same time, in order to know the size of the lens in every shot. This can in principle be done using a beam splitter placed immediately after the device, but it requires more laser energy than we have available.

The image in figure 5.24 on page 160 was obtained very close to the CSL, only 3.3 m apart. It is clear that the lens is focusing but the focus is still very far. Images taken at distances in the range between 5 m and 10 m show similar results.

The images from figure 5.26 on page 162 to 5.31 on page 167 show the results obtained with the lens at a distance of 15 m. The size of the focus is quite big, but rings can be seen around it in many images to prove the quality of the lens. All the images were taken with the same delay, but being unable to measure the actual diameter of the lens we could not be sure the lens was really always the same. That means the results must be considered as a lower limit of the quality of the lens.

The formula

$$r_m = 1.22\frac{\lambda L}{2a} \tag{5.1}$$

gives the diameter of the first diffraction minimum for a circular aperture of diameter a, where L is the focal length of the lens. In our case, considering the ideal case of a diffraction limited beam and a lens of 10 mm, the diameter of the smallest possible theoretical spot becomes $\sim$ 0.5 mm, which is comparable with our results (see figure 5.31 on page 167 densitometry trace indicating five times diffraction limited spot).

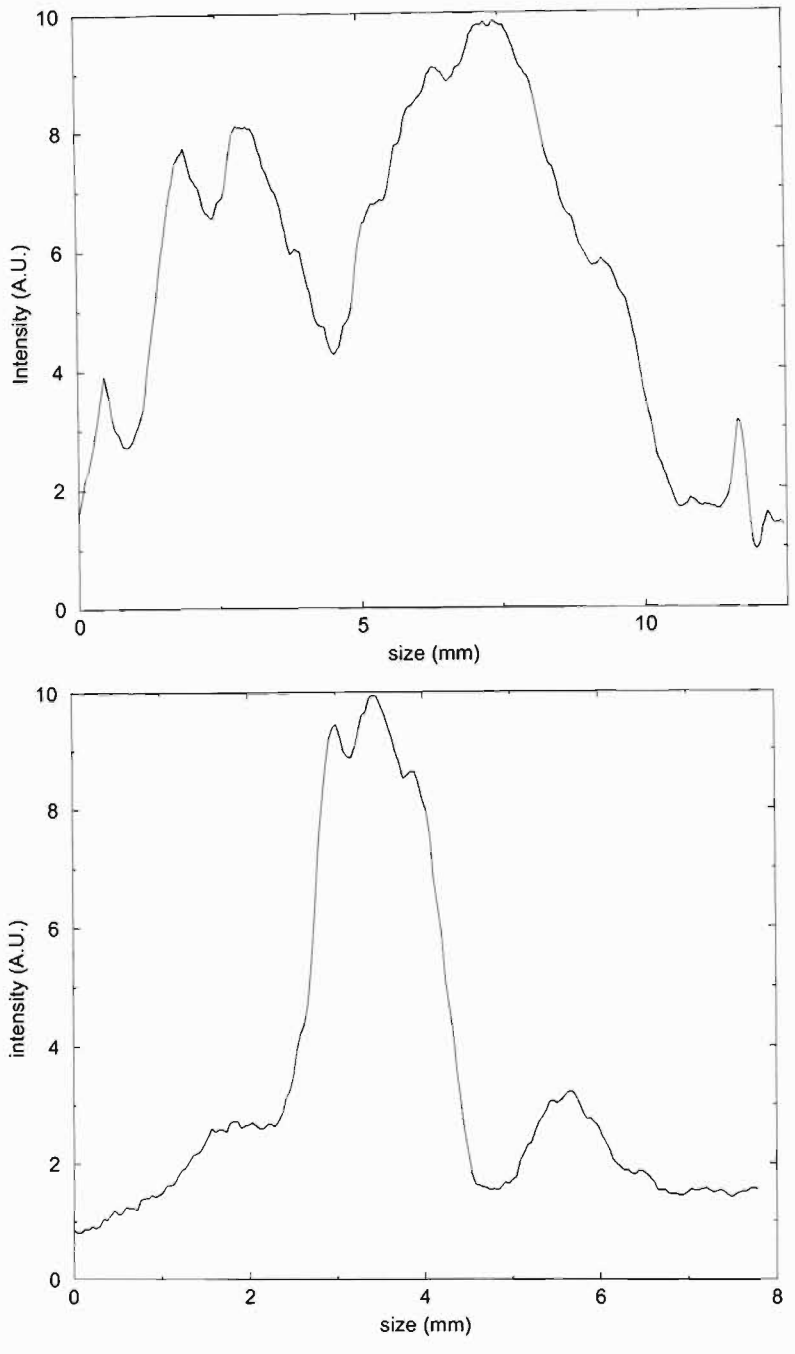

Graph 5.1: Horizontal and vertical densitometry of figure 5.14 on page 145. It can be seen that the actual size of the focus is quite large in the horizontal direction. The difference between the horizontal and vertical profiles might be due to the asymmetry of the laser beam or to the multiple laser beams described in subsection 5.2.1 on page 168. In any case, it cannot be due to the lens itself, which is quite symmetric.

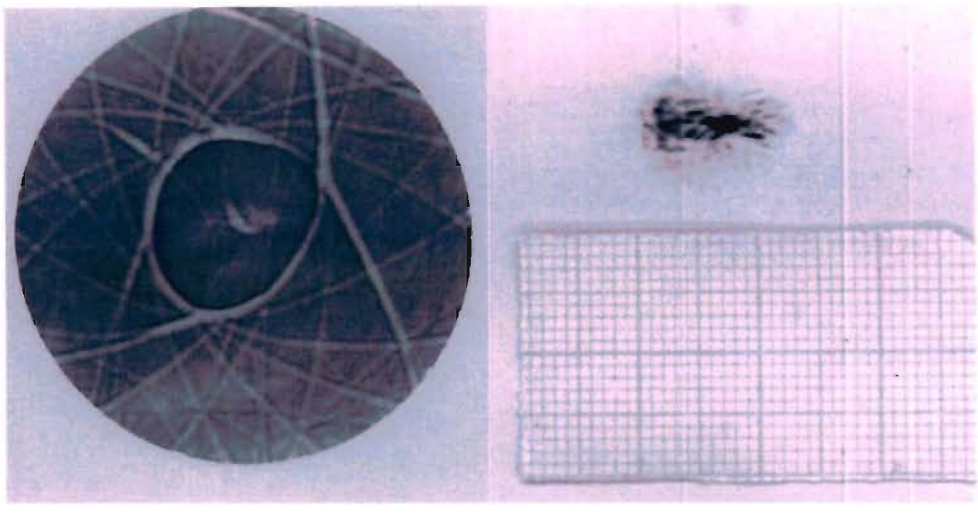

Figure 5.16: An image of a 9.0 mm lens and the corresponding focus, 3 m far from the CSL. It should be noticed that the images were taken in different shots.

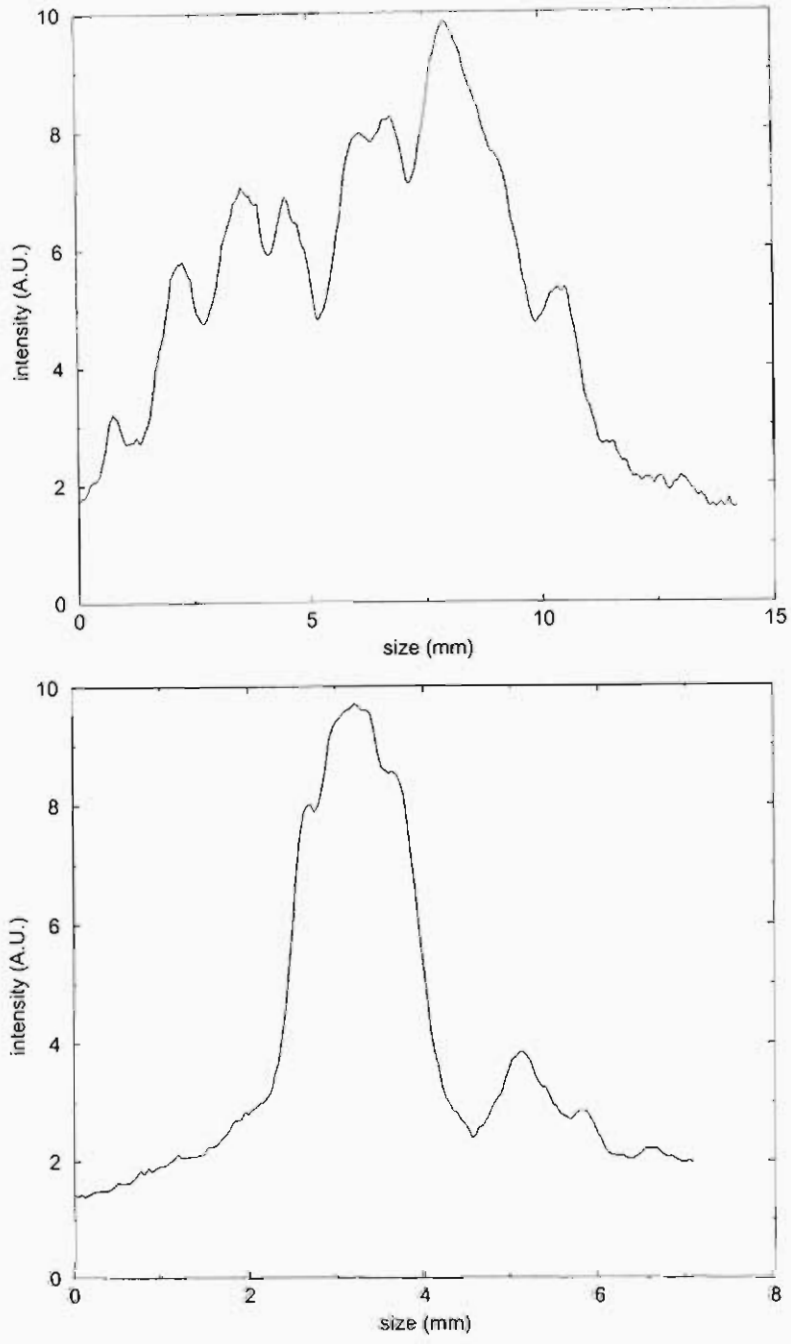

Graph 5.2: Horizontal and vertical densitometry of figure 5.16 on the previous page. It can be noted that the focus size on the vertical axis is less than two millimetres.

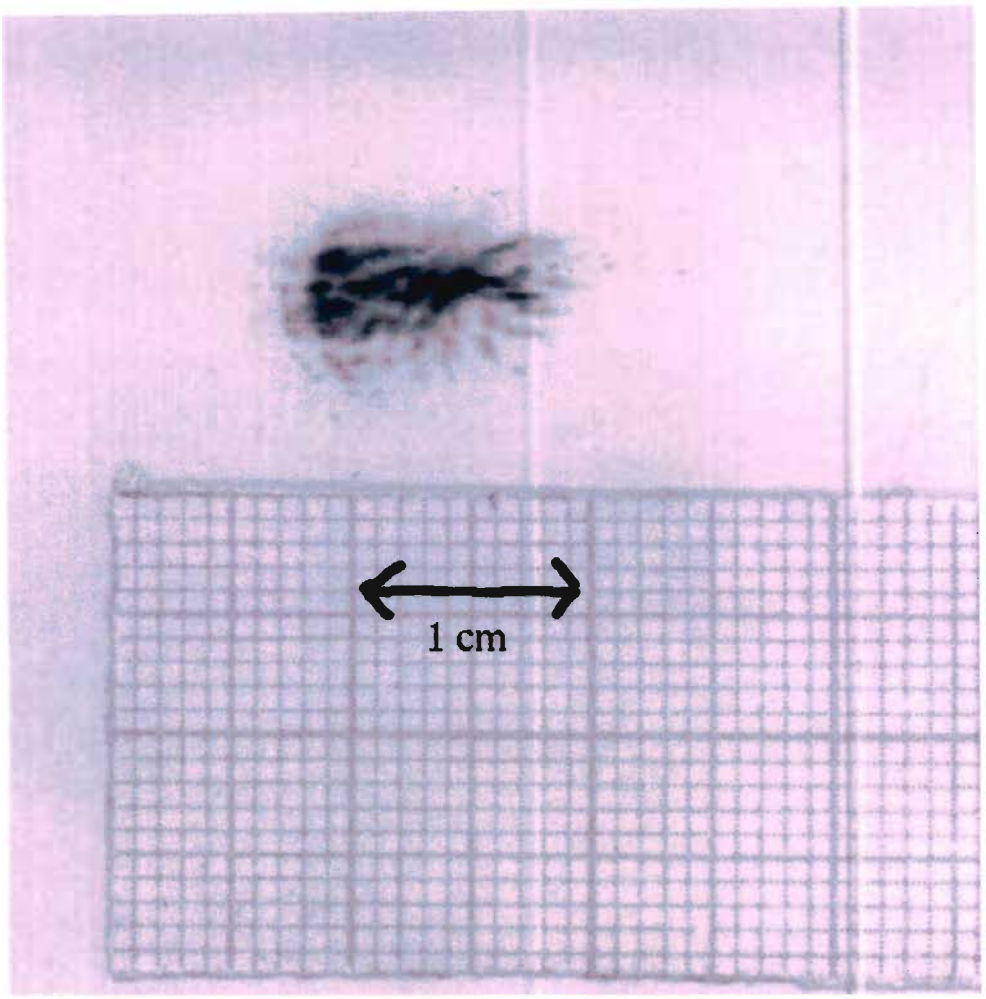

Figure 5.17: One of the best foci obtained during our experiment. The diameter of the lens was in this case 10 mm. The focus is smaller than 1 mm. As in the previous case, the focus is probably better than this, but our detector, the photographic paper, was too close to the lens.

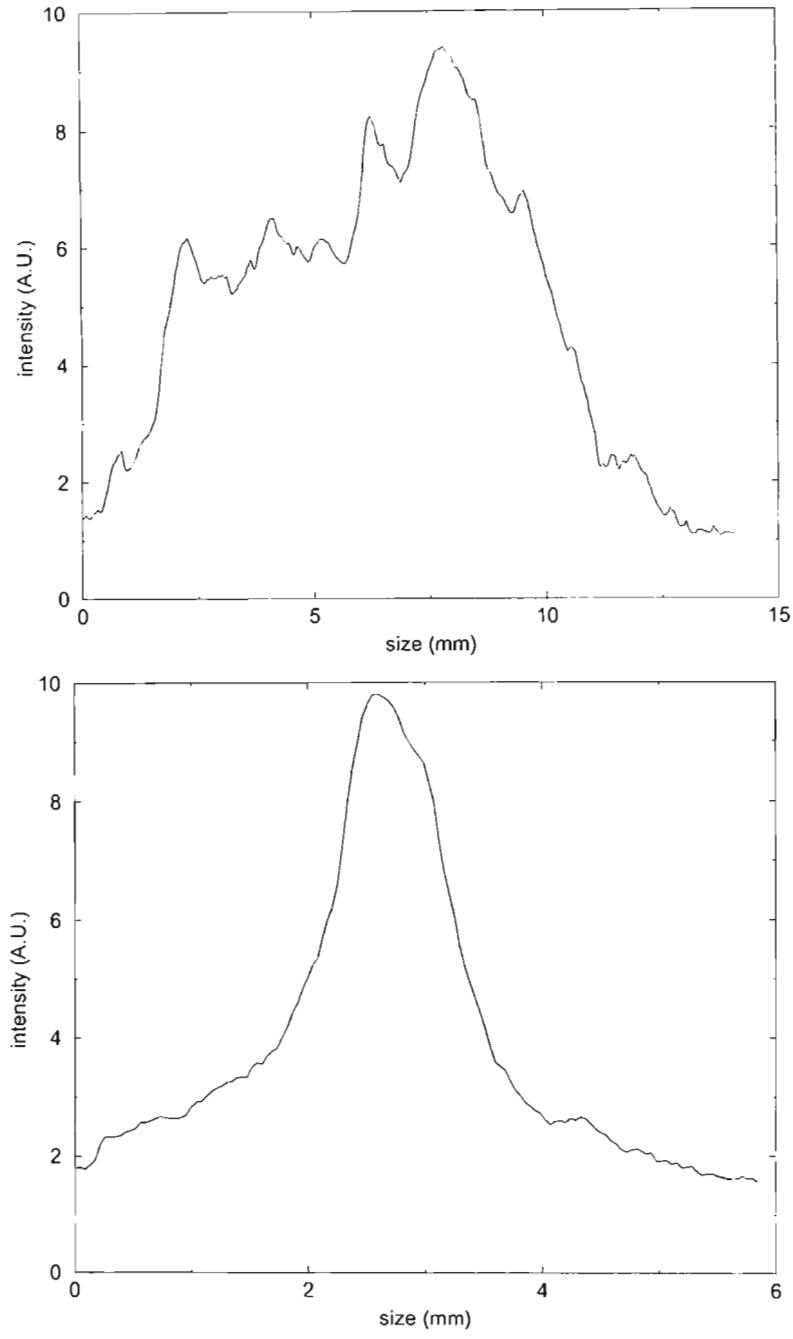

Graph 5.3: Horizontal and vertical densitometry of figure 5.17 on page 152.

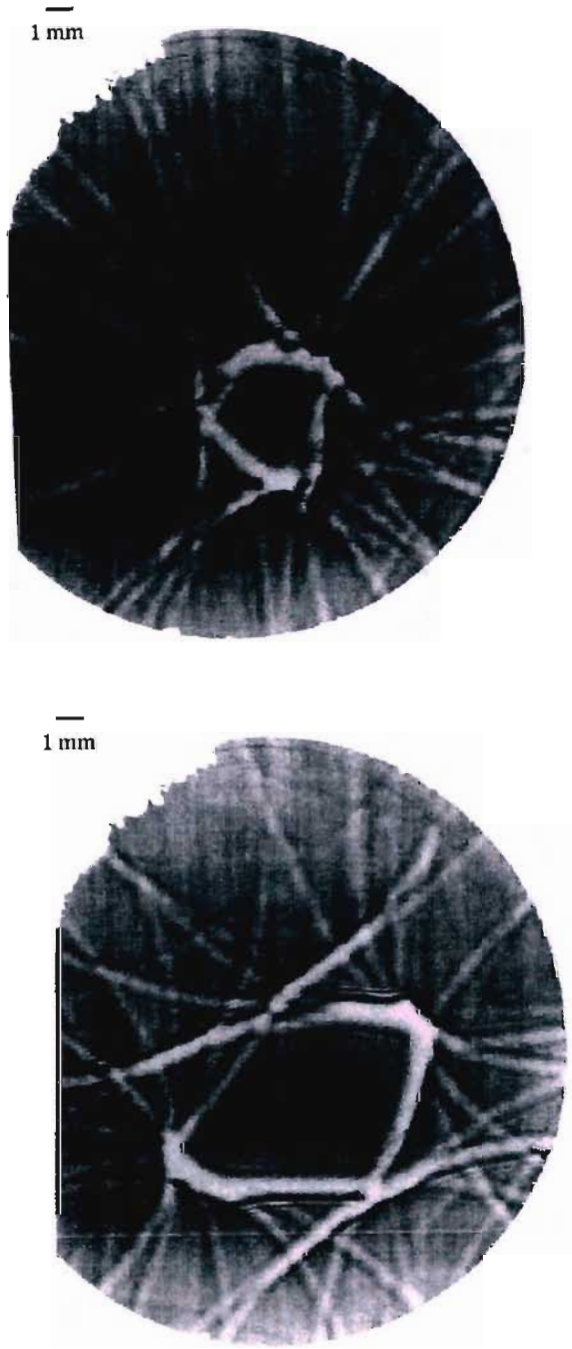

Figure 5.18: Two images of the shock obtained before the collision in the centre. It is interesting to note how all the images before collision show an irregular shape, which is smoothed into a circle after the collision due to the Mach addition.

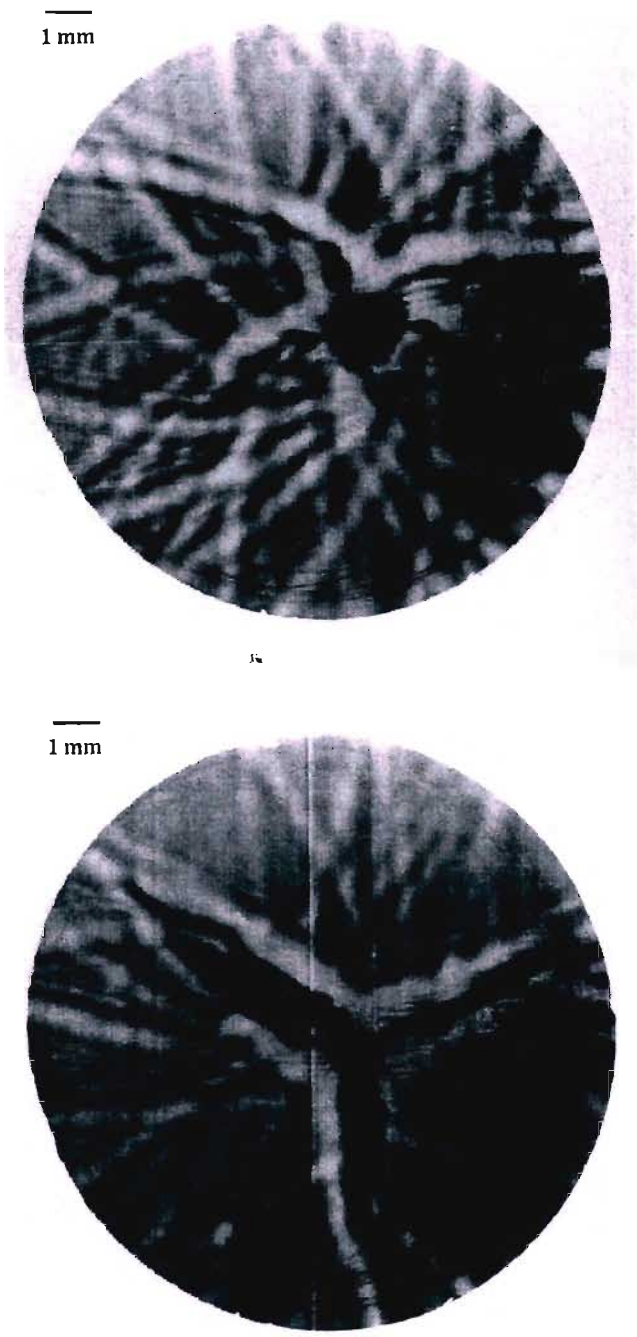

Figure 5.19: Two images of small lenses (i.e. with a short focal length) obtained immediately after collision, when the lens has still a very small diameter. Such lenses have a much shorter focal length, but their size does not make them interesting for practical applications.

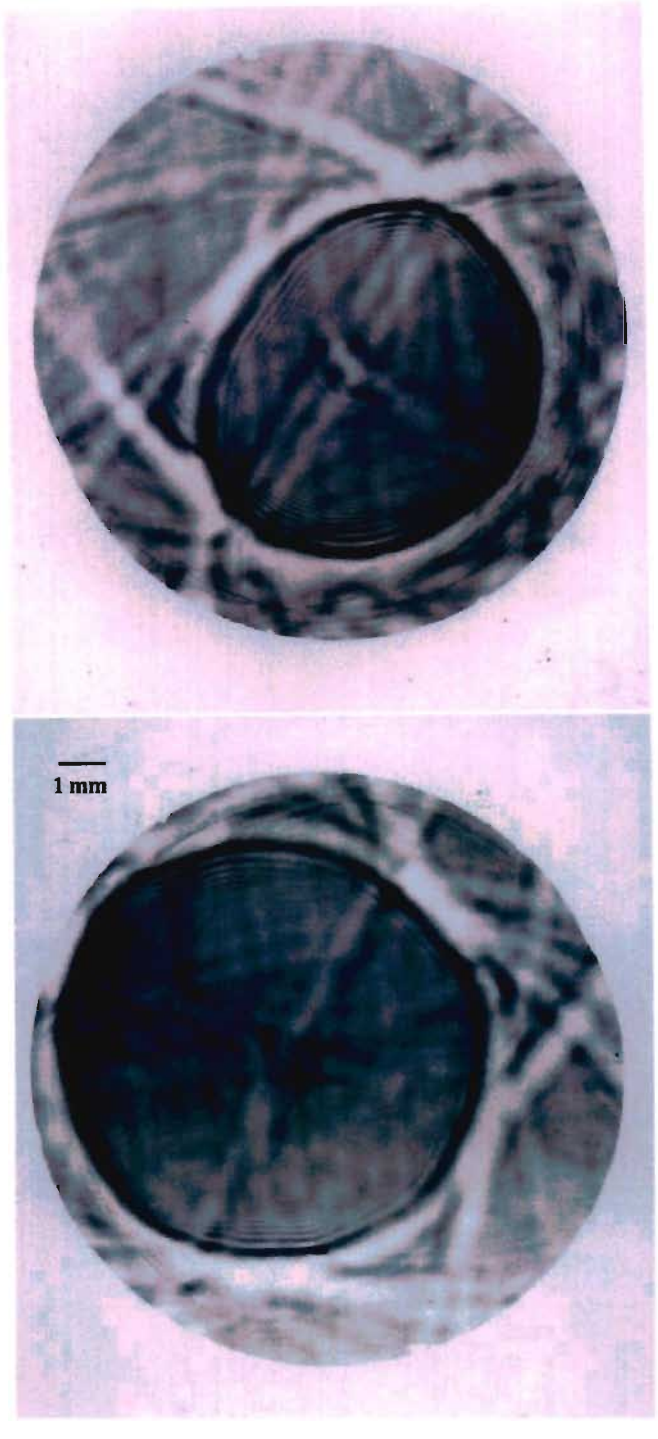

Figure 5.20: Two images of lenses of good quality, obtained with an energy of 600 J. In this case the lens has an almost perfect circular shape. Many refraction fringes are observable.

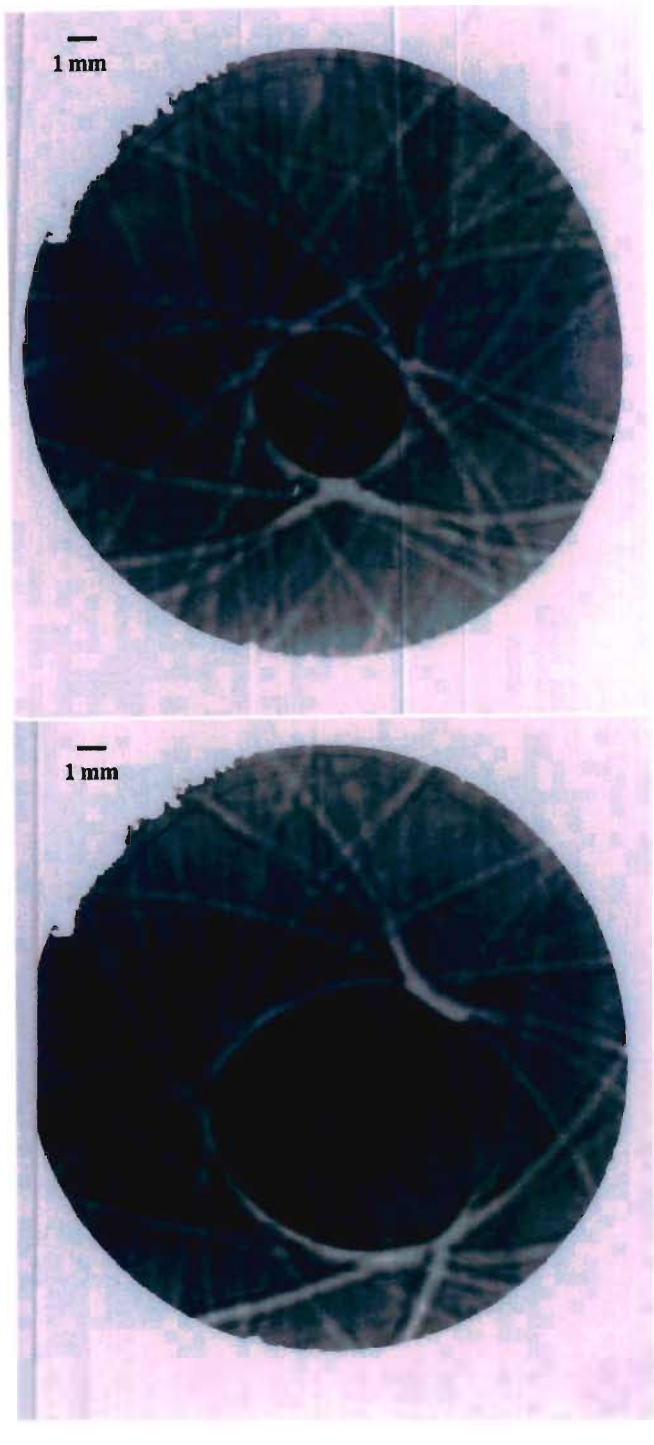

Figure 5.21: Two images of lenses of good quality, obtained with an energy of 600 J. In the bottom image a part of the lens is missing. Such an incomplete lens might be expected to give a poor focus.

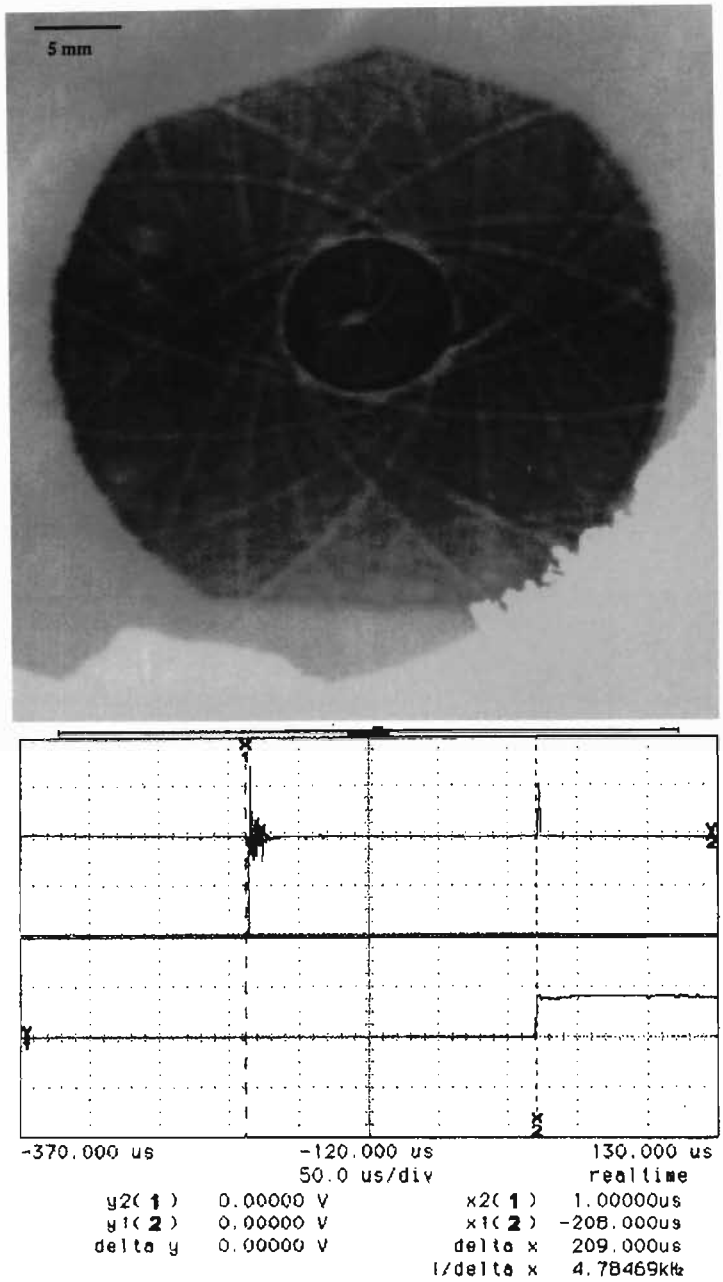

Figure 5.22: Image of the lens obtained in the near field, 91 cm far from the device. The diameter of the lens is 9.0 mm. At the bottom is reported the oscilloscope trace. In this image, and in the following ones, the telescope was adjusted in order to have a parallel laser beam.

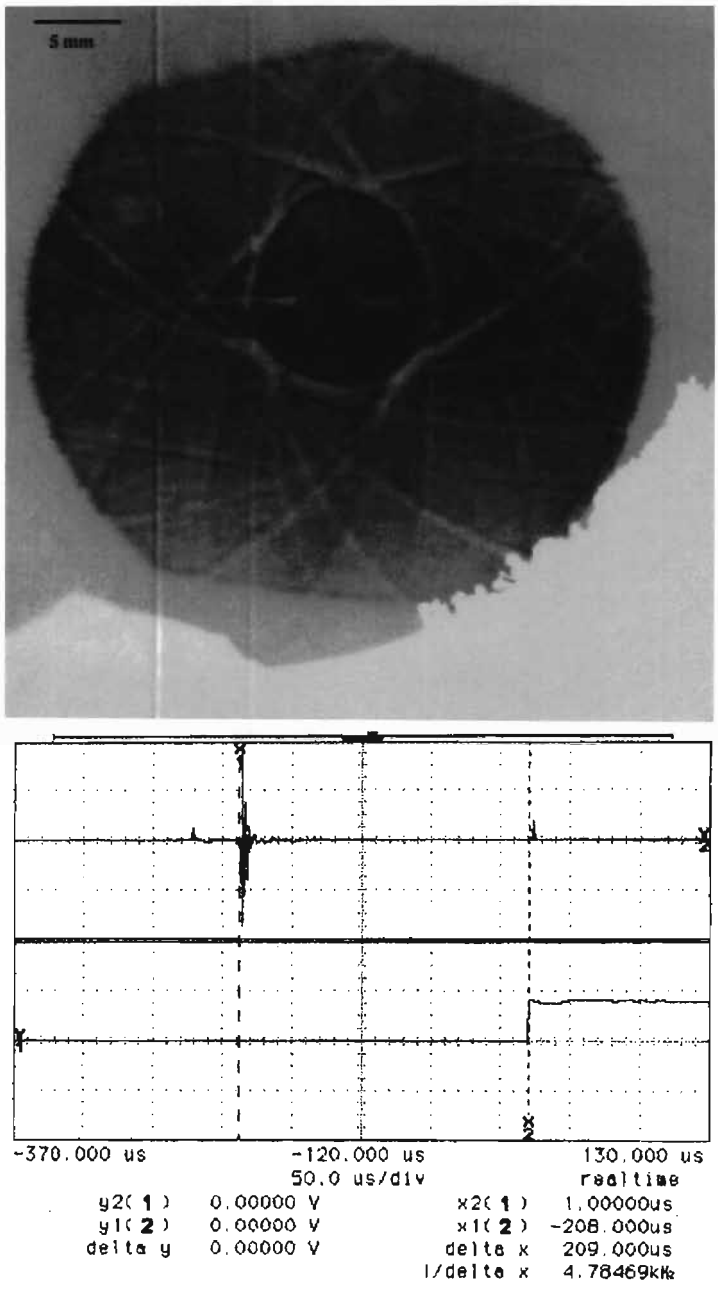

Figure 5.23: Another image of the lens obtained in the near field, 91 cm far from the device. The diameter of the lens is 10.3 mm. At the bottom is reported the oscilloscope trace.

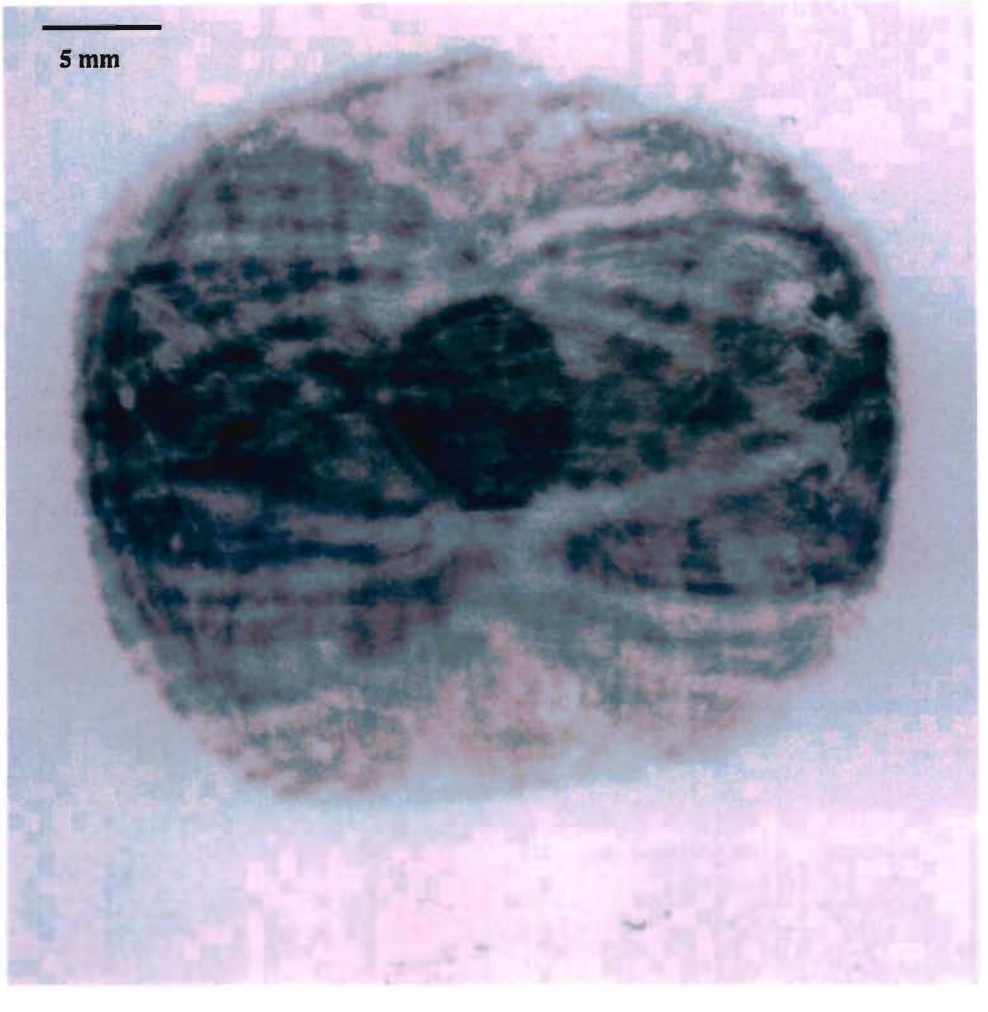

Figure 5.24: Image of the converging beam of a 10 millimetres CSL at a distance of 3.3 m. From our measurements we know that such a large (as far as CSLs go) lens has a focal length of around 10 m. This means that the darker circle in the centre is light converging into a focus that is still far away.

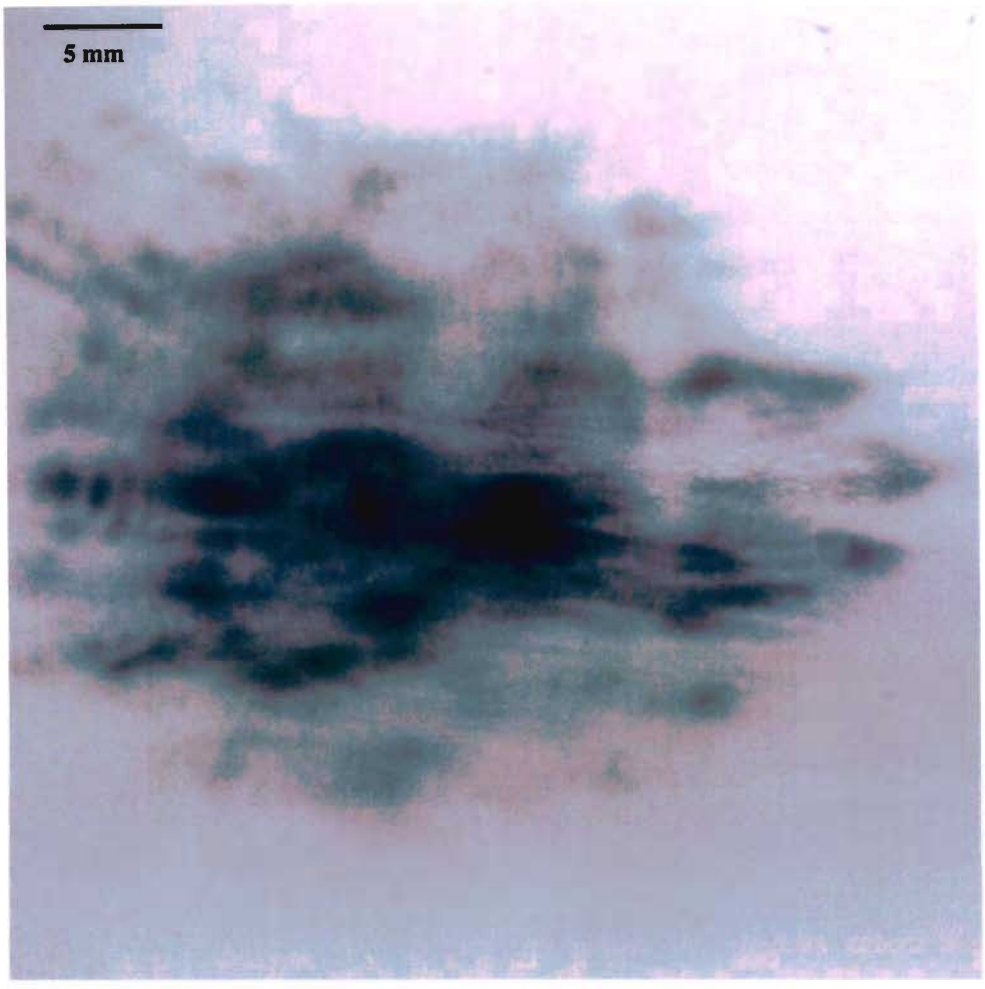

Figure 5.25: Another image of the focus obtained on the far field at more than 10 m from the lens. The size of the focus can be compared with the 0.5 mm expected for a diffraction limited beam. It must be considered that our beam has a very low optical quality. Moreover, in order to image the laser beam at such distances we had to use two mirrors (respectively at 4 and 8 metres from the CSL) to relay the beam.

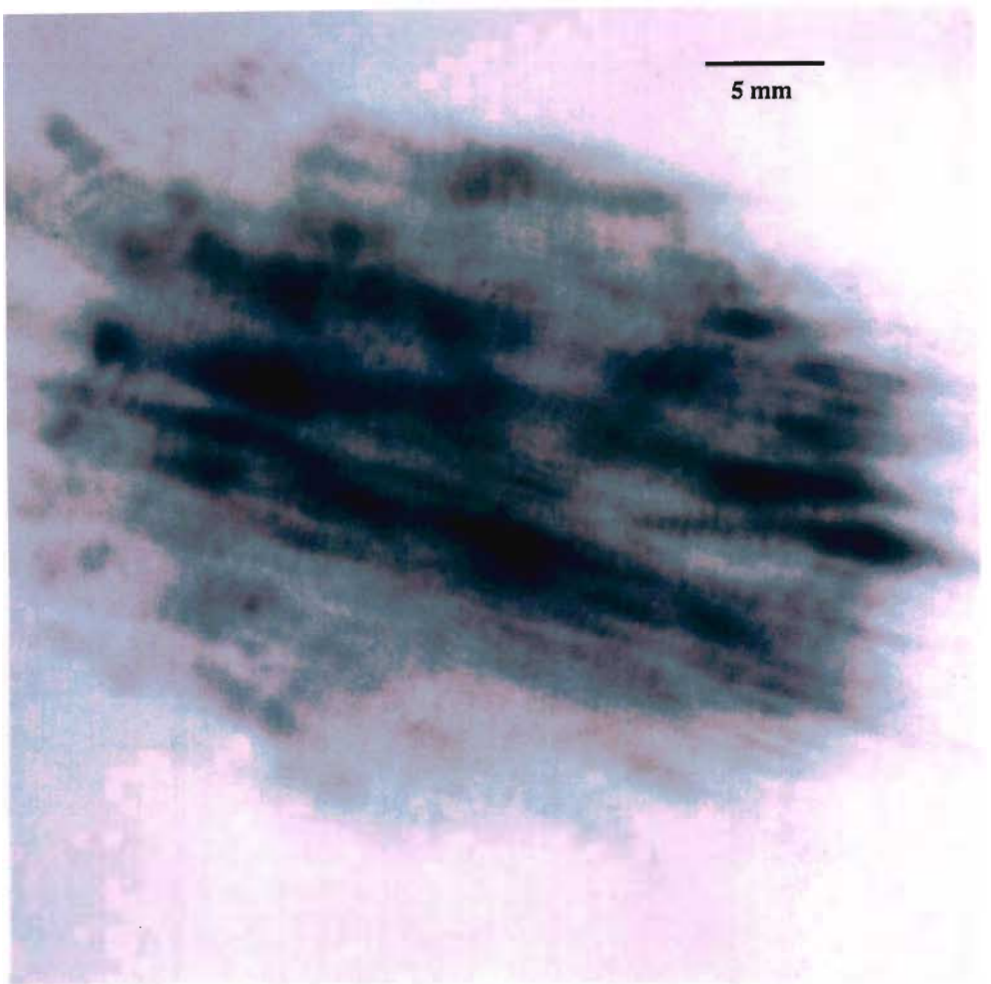

Figure 5.26: Image of the focus obtained in the far field, about 15 m far from the lens. Part of the poor quality of the focus derives from the fact that our laboratory was not long enough and we had to use two mirrors to be able to take images so far from the lens.

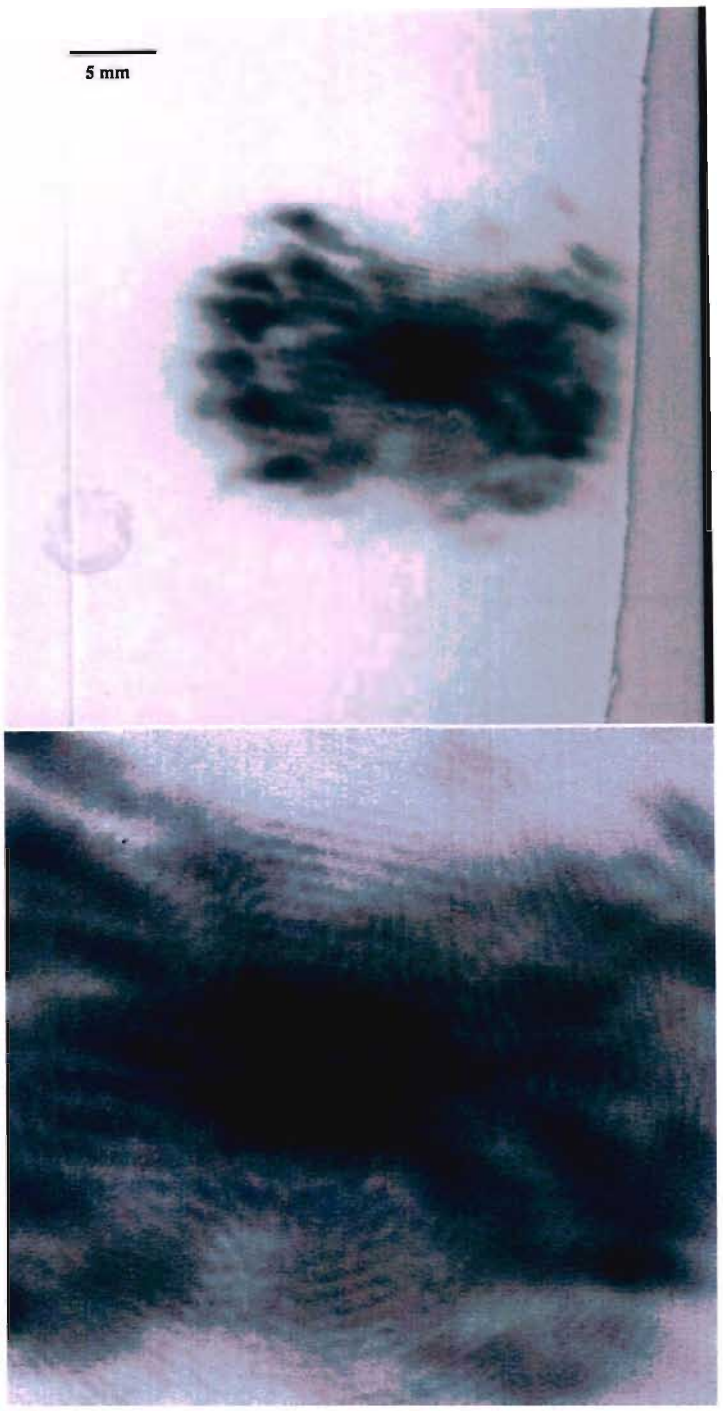

Figure 5.27: Image of the focus obtained 15 m far from the CSL. The bottom image shows a magnification of the centre, processed, increasing the contrast, in order to make visible the Airy rings.

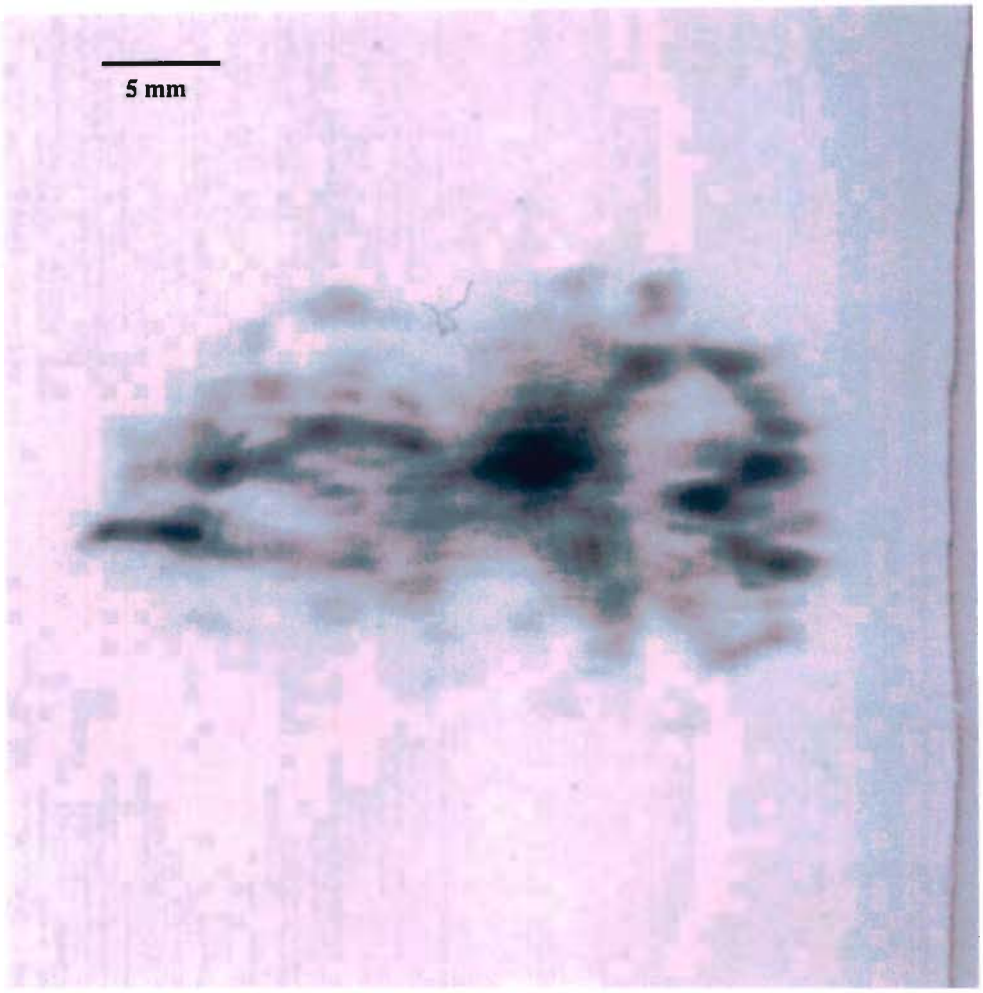

Figure 5.28: Image of the focus obtained 15 m far from the CSL. Despite the fact that the delay and all the other parameters of the experiment were the same as in the previous one, in this case the focus has a poorer quality, i.e., size.

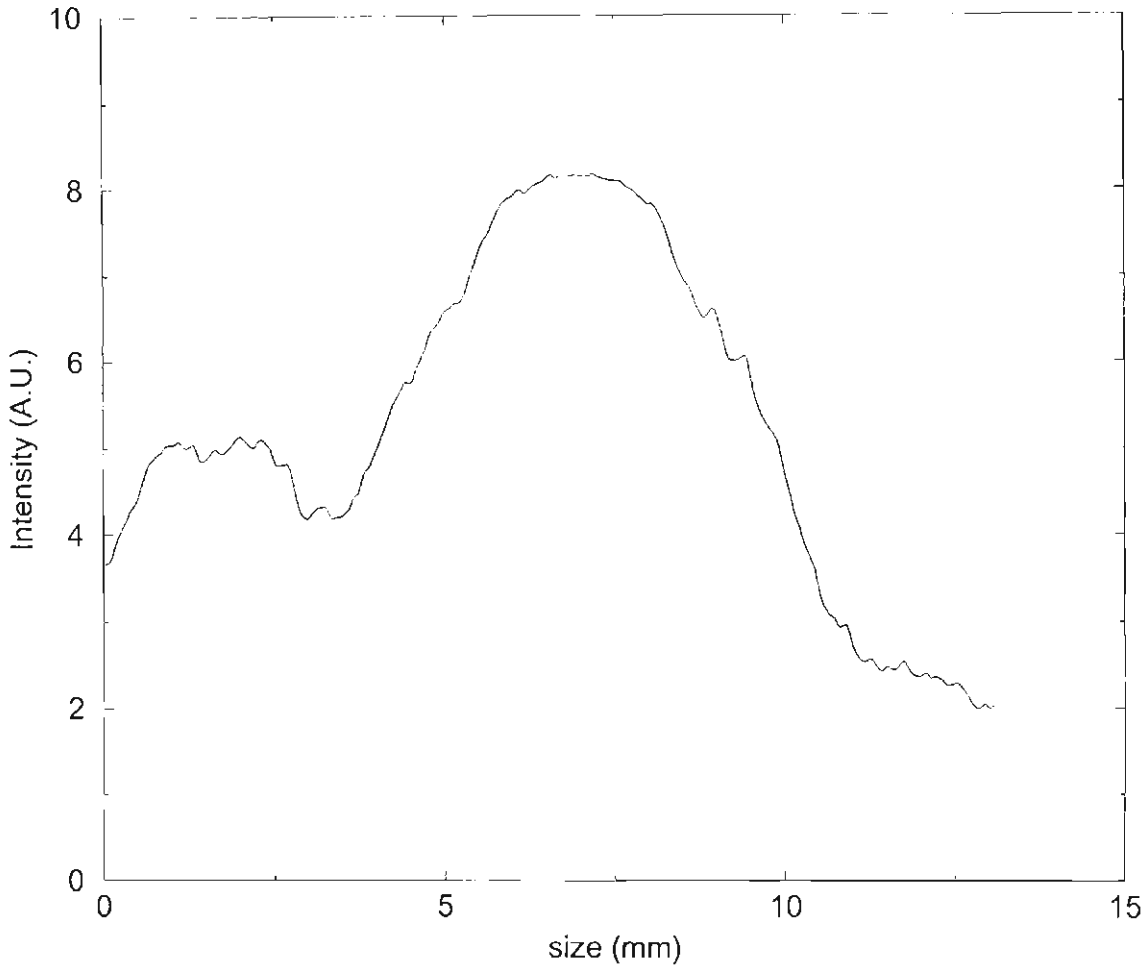

Figure 5.29: Densitometry of image 5.28 on page 164. In this case, the lens did not work very well and the focus is larger than 5 mm.

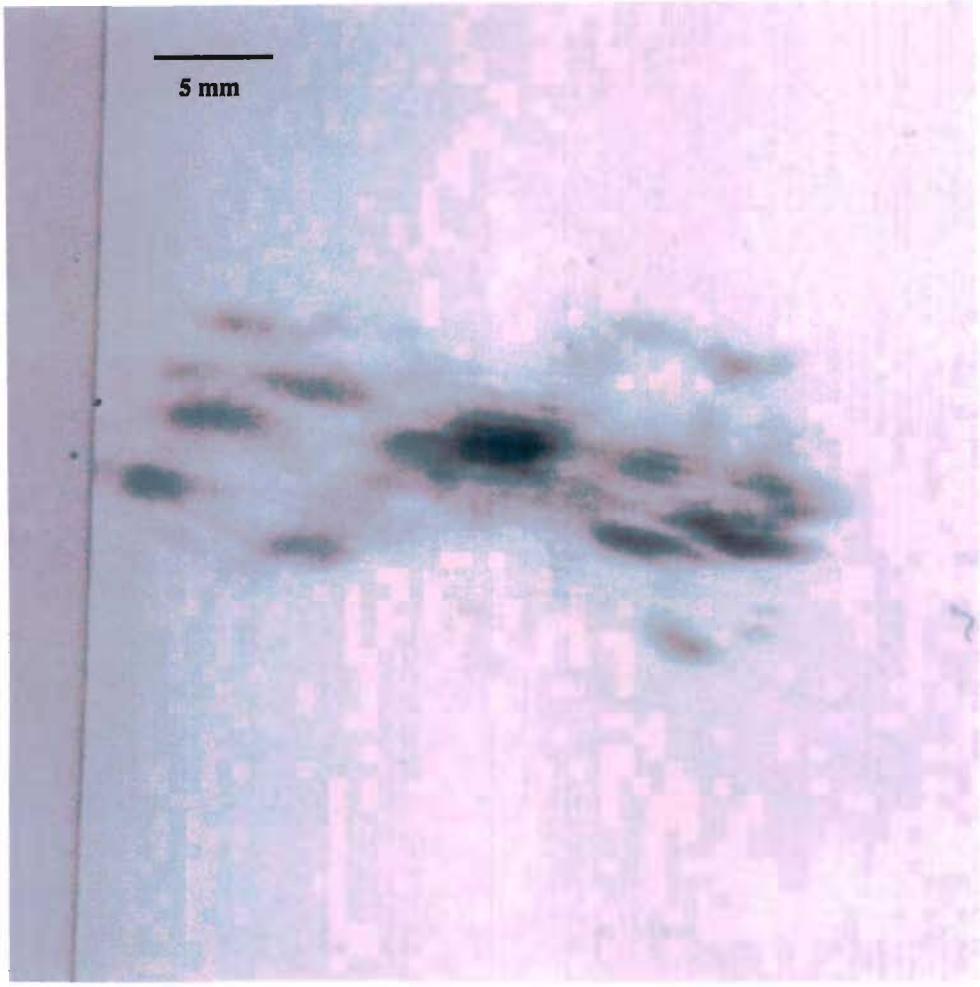

Figure 5.30: Image of a good focus, obtained in the same conditions of the previous ones.

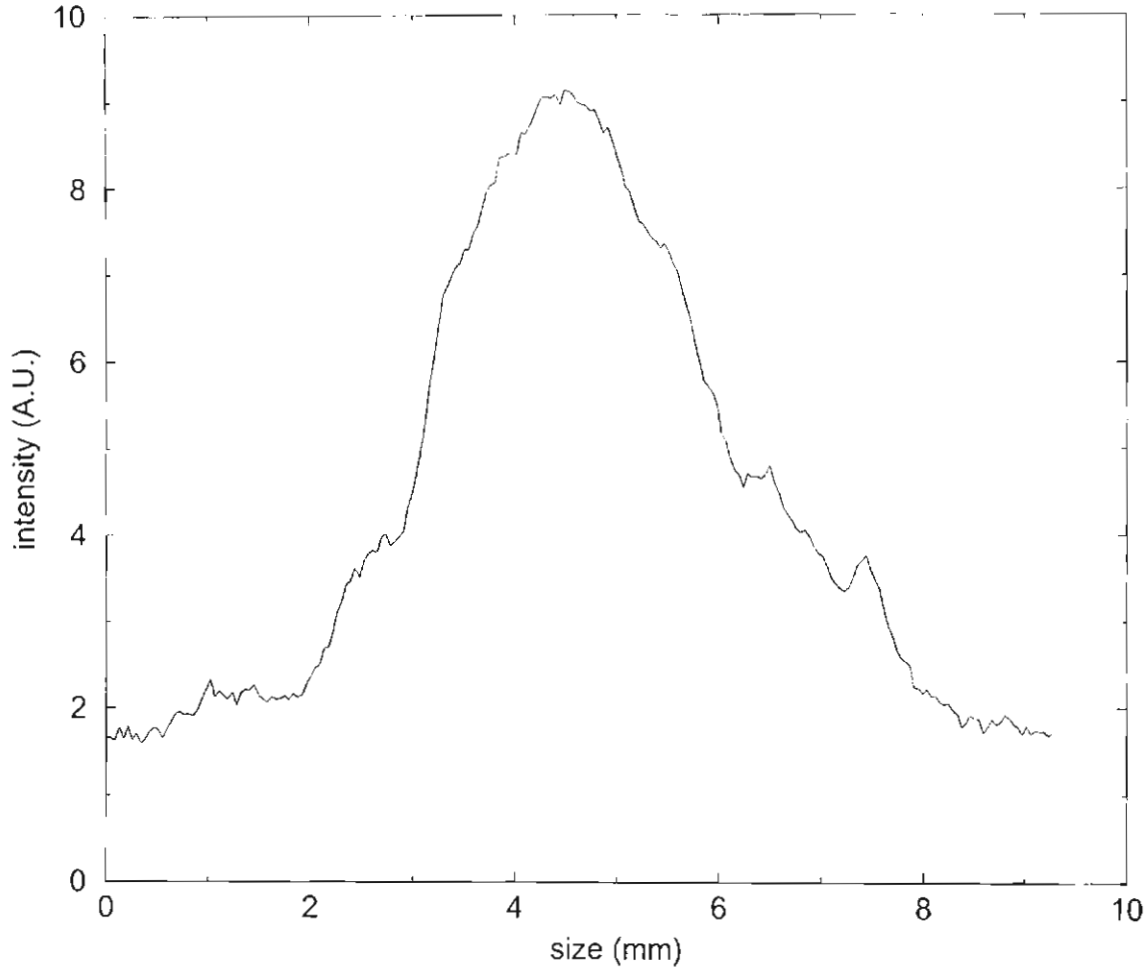

Figure 5.31: Densitometry of image 5.30 on page 166, taken across a vertical path.

5.2.1 Laser anomaly

During this series of experiments it was noted that the image in the far field was showing two weaker ghosts. After checking carefully that they were not due to internal reflection of the mirrors, we put a 100 μm pinhole into the telescope, thus obtaining a spatial filter. The secondary images disappeared at once, thus proving that they were separated beams produced in the laser itself.

5.3 Applications

Thanks to the latest results, in which we showed the feasibility of a CSL with a diameter of 1 cm, this kind of device is now ready for an application[53]. Of course, the device now needs a fair amount of work to be engineered into a reliable lens, as problem free as possible. Possible applications could be found in any field where the power of the laser damages the optics used to focus the beam. Among this kind of applications we can mention laser drilling, or any kind of laser machining, and laser welding. In particular, laser drilling through a thin aluminium foil has been already demonstrated[52]. Colliding Shock Lenses can also be used as an intra-cavity Q-Switch in lasers[46].

Chapter 6

The nitrogen laser

In all our experiments we used successfully a very simple diagnostic tool, which is a nitrogen laser. Nitrogen lasers are perfect in our case for many reasons. First of all, they emit ultraviolet light, which can be used to pump a dye laser and converted to visible wavelength. Moreover, normal photographic paper is very sensitive to UV radiation and it makes a good and cheap detector. Then, the duration of the pulse is very short, ranging usually around 1 ns, allowing us to freeze the movement of almost everything. Moreover, even if the pulse energy is quite low, less than 50 μJ, the peak power can be very high, 50 kW in our case.

On the other hand, nitrogen lasers, especially if home made, do not have a high reproducibility and are affected by environmental factors, like humidity. Being completely open to the atmosphere, there is always a layer of humidity on the laser electrodes, which can modify the behaviour by increasing disper-

sion and thus by lowering the voltage. In our case, this resulted in a much lower charging voltage, and therefore energy, in rainy days. Apart from that, another problem with nitrogen lasers is that they have a very large optical divergence (up to a few degrees), which is not too serious in our case, but can be a limiting factor for other experiments.

One serious problem with the nitrogen lasers is their very poor optical quality. In particular, these lasers can have a very high divergence, that can be limited by making a longer discharge channel. The divergence limit set by the geometry of the laser is

$$div = 2\arctan(\frac{d}{l}) \tag{6.1}$$

Where d is the separation between the electrodes and l is their length. For one of our most common lasers, with 35 cm long electrodes and a separation of 2 mm, the divergence is around 11 mrad. The graph 6.1 on page 171 shows that divergence can be improved by making a longer laser, but this solution is not always practically viable.

6.0.1 The classic laser

The most common nitrogen laser has another advantage in its cheapness and in the fact that it can be made easily out of a normal double sided circuit board. This kind of laser has a limited lifetime, as after a while the dielectric breaks down. The damage could be in principle repaired, but most of the

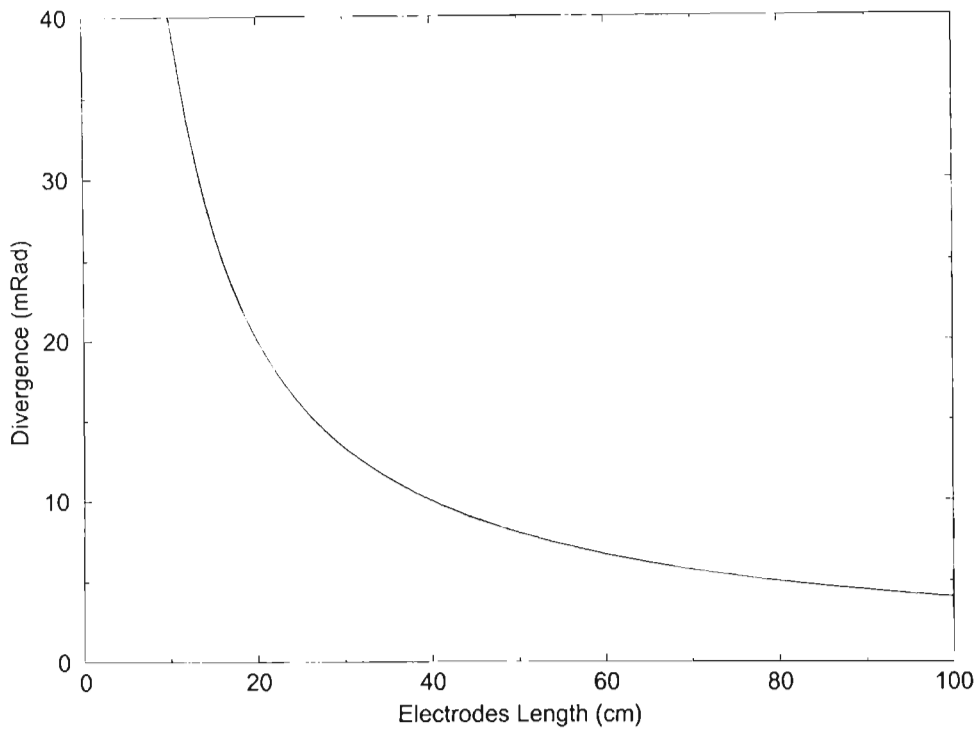

Graph 6.1: Geometrical divergence for a nitrogen laser with an electrodes separation of 2 mm.

time it is impossible to locate it. For this reason, we made several of these lasers, so that there was always a new one available to carry on with the experiment.

We made several lasers, in order to counteract their tendency to have a limited life time by replacing them rather often.

The basic idea of the laser is to keep the impedance as low as possible, because a nitrogen laser needs to have most of the energy delivered in the shortest possible time. The circuit normally used is called Blumlein[51]

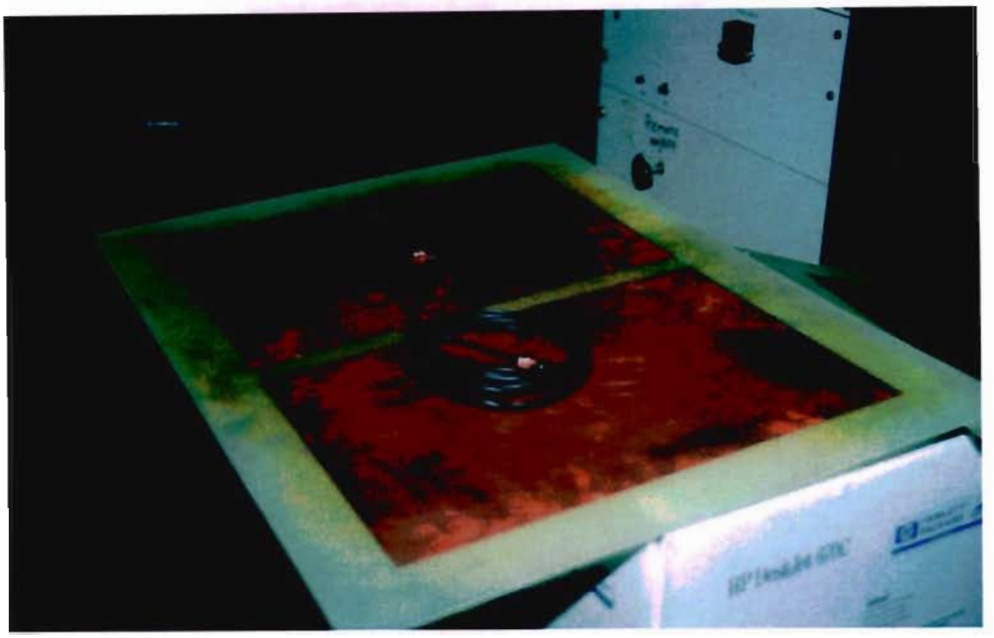

Figure 6.1: One of our square nitrogen lasers, in this picture without both the electrodes and the spark gap.

(British patent 461324, obtained in 1937) and becomes the one in figure 6.2 on page 173 when adapted to the circuit board.

In this circuit, the power supply charges the laser, which basically consists of two capacitors in parallel, connected by an inductor. During the charging process, the inductor behaves as a closed circuit, allowing both the capacitors to be connected with the power supply. Then, when the spark gap opens, the high frequencies of the discharge causes the inductor to act as an open circuit, and the discharge occurs transversally between the two electrodes. The electrodes themselves are made of aluminium, and enclosed in a Plexiglas frame to contain the nitrogen that flows between them.

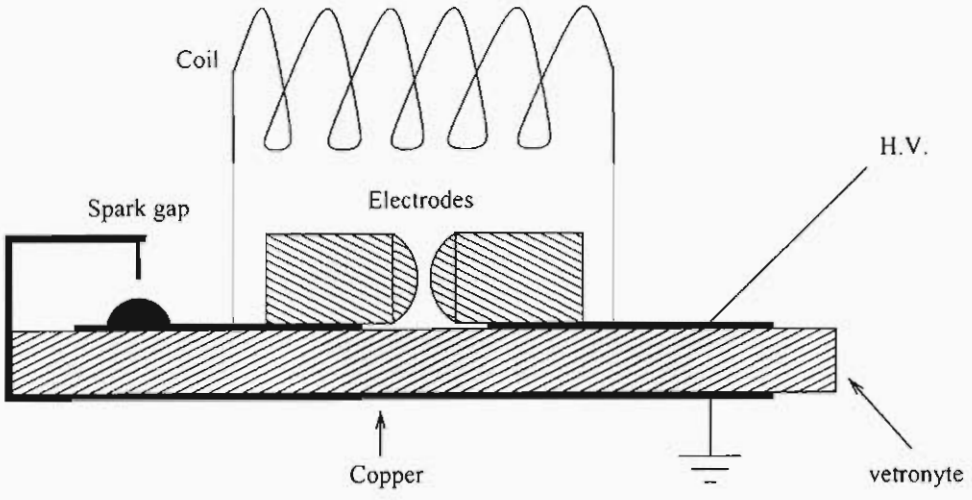

Figure 6.2: Cross section of the nitrogen laser.

As can be easily seen in figure 6.1, the high voltage surface of the laser is in open air. This make the laser sensitive to the environment and also means that it has to be used carefully, to avoid touching a capacitor charged to 20 kV.

6.0.2 The parabolic laser

Because nitrogen lasers where so important in our experiment, we decided to study them for a while, in order to increase their performance, in particular the energy output was very poor. The normal square laser, figure 6.6 on page 178 has in fact an average output of 50 μJ (measured with the instrument described in section 6.1 on page 178). Considering a capacity $\sim$ 10 nF and a voltage of 17 kV, this means an efficiency of $\sim 3.5 \cdot 10^{-5}$.

One reasons of the poor efficiency can be found in the very shape of

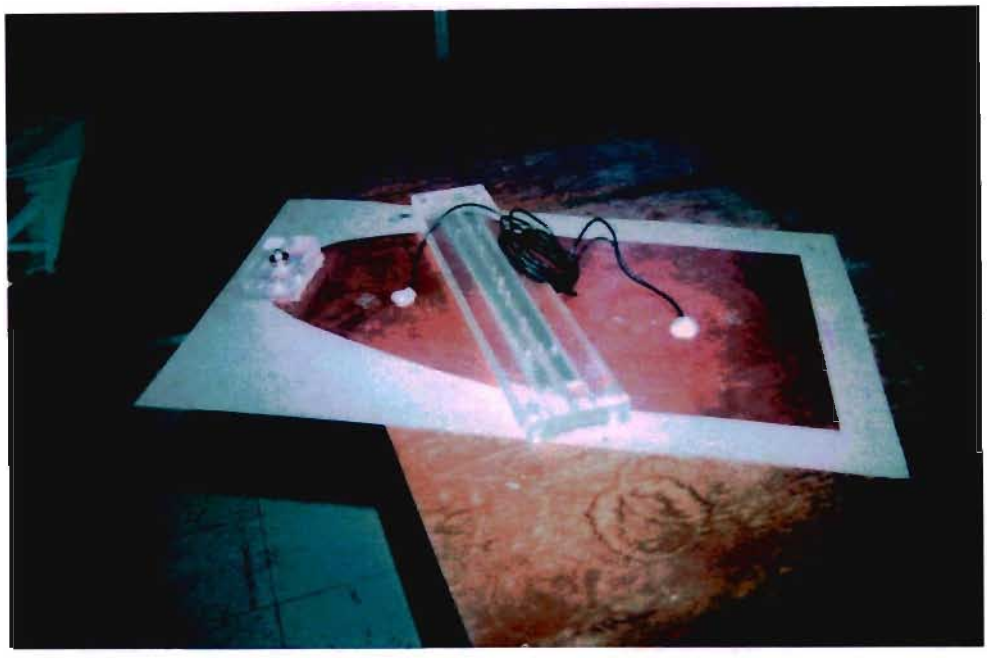

Figure 6.3: One of our parabolic nitrogen lasers. It is clearly visible the slope of the electrodes, included in a Plexiglas frame. In this case, the spark gap is of the pressurised triggerable type.

the laser. With the original laser, figure 6.4 on page 175, the electrodes are rectangular. In this case, there is a circular "discharge wave" that propagates through the dielectric medium (vetronyte). Because the speed of the photons in the discharge pipe is (nearly) equal to the speed of light, and the speed of the discharge wave is something like one third of it, the photon packet after a while is ahead of the discharge and is not amplified anymore. This sets a practical limit to the length of the discharge and so to the energy that can be obtained.

If we shape the electrode that contains the spark gap as a parabola, see

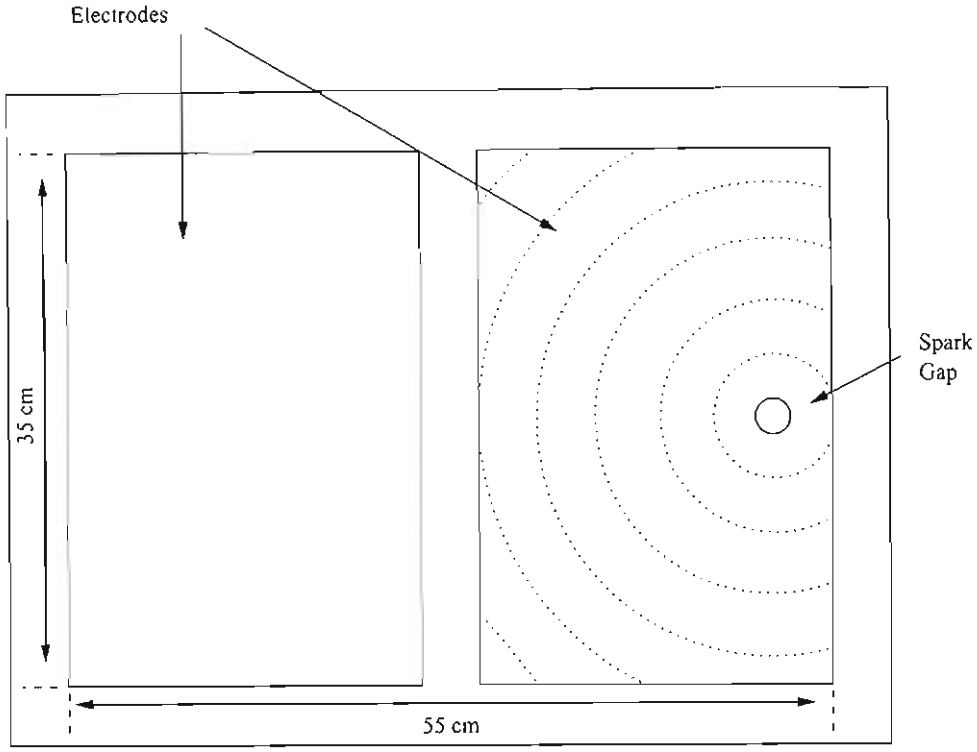

Figure 6.4: The rectangular nitrogen laser.

figure 6.6 on page 178, after reflection the discharge wave is turned into a plane wave. In this case, by changing the angle of the discharge pipe, it is possible to have the photons travelling always with the discharge and always in an active medium with the maximum gain. For this idea to work, it is necessary to insert a screen to prevent a primary circular discharge wave from reaching the discharge channel (the screen was formed by removing a small strip of copper between the spark gap and the electrodes). The screen also makes a shadow in the electrical wave (considering the diffraction, it is not as sharp as it is shown in the drawing, for sake of simplicity), which

usually obscures a few percents of the laser channel. The advantages of this system are two. Firstly, the photons always travel in the best possible gain, and second there is no limit, beyond a practical one, to the length of the discharge pipe.

The slope of the discharge channel can be calculated easily, looking at the figure 6.5 on page 177. The speed of the discharge wave travelling through the laser is equal to $c/\sqrt{\epsilon}$, where c is the speed of light and ϵ the permittivity of the medium. So, the difference of the travelling time between the path y_1 and y_2 must be equal to the time it takes for the photons to travel along the segment d. Considering that x can be neglected, because the wave travels in opposite directions, the equation for the angle is hence

$$\frac{\sqrt{\epsilon}}{c}(y_1 - y_2) = \frac{d}{c} \tag{6.2}$$

But

$$d = \frac{y_1 - y_2}{\sin(\alpha)} \tag{6.3}$$

Hence

$$\alpha = \arcsin\left(\frac{1}{\sqrt{\epsilon}}\right) \tag{6.4}$$

In our case, the permittivity of the vetronyte (epoxy resin impregnated glass cloth) used in the circuit board is equal to 4.5 (http://www.g8cyerichmond.freeserve.co.uk/data.htm the speed of the wave is $c/2$ and the angle is about 28 degrees.

The circuit of the laser remains, obviously, the same as for the normal

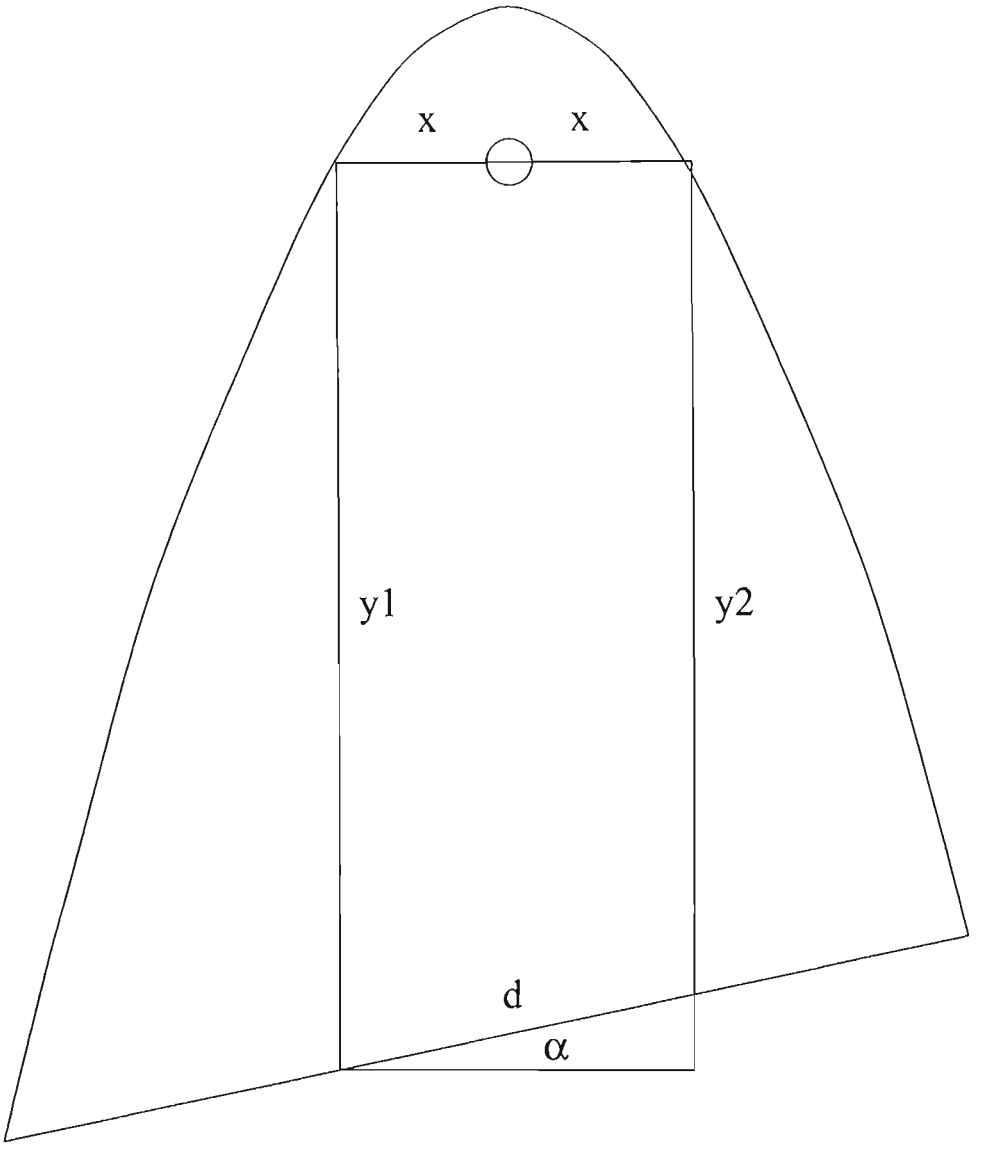

Figure 6.5: Calculation of the angle of the discharge pipe for a parabolic nitrogen laser.

square laser.

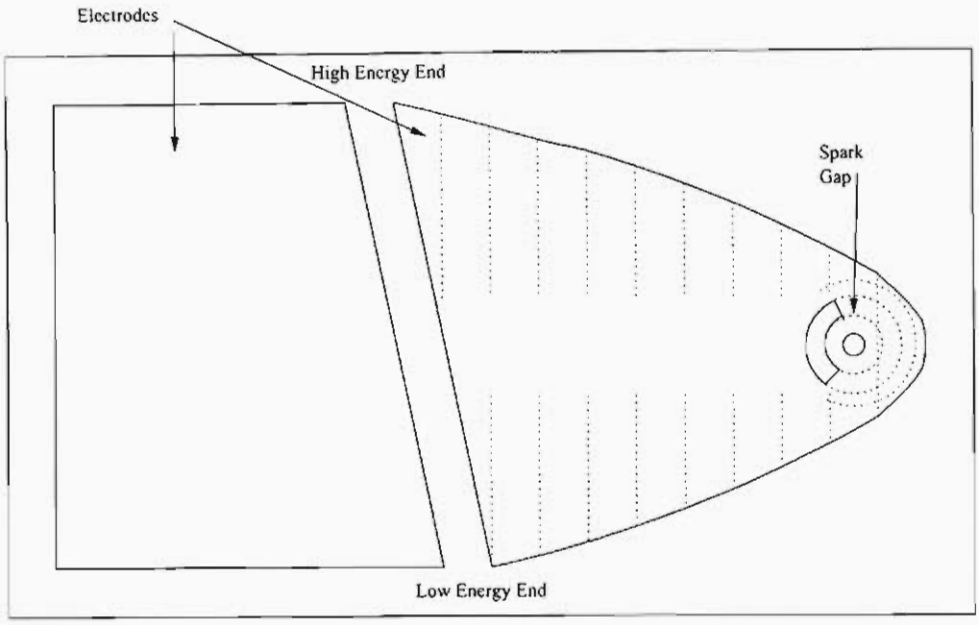

Figure 6.6: The parabolic nitrogen laser.

6.1 Experimental results

In order to investigate the efficiency of the parabola, we built several lasers and for each one we measured the output on both sides with a pyroelectric Nova energy-meter (model PE25), made by Ophir. This instrument turned out to be very sensitive to the typical acoustic noise made by the spark gaps and had to be properly shielded against it. This happens because the instrument is triggered by any pulse of energy absorbed by the detector, including that of acoustic waves. Moreover, the instrument is very sensitive,

being able to measure only a few microjoules. For these measurements, all the lasers were equipped with a simpler spark gap, not triggerable and free running. This spark gap is basically a hole which connects the electrodes of the capacitor; an adjustable screw allows us to change the gap and, so, adjust the discharging voltage of the laser. This kind of spark gap is not very reliable and the laser fires at different voltages (normally between 14 kV and 17 kV). This means that reliable measurements can be obtained only by integrating over a series of shots.

The shape of the laser is not the only parameter that affects the energy output. The other two most significant parameters are the flux of the nitrogen and the separation of the electrodes. The latter, in particular, affects the amount of active medium of the laser, but also the density of the pumping energy. The graph 6.2 on page 180 shows the behaviour of the output versus the nitrogen flux (i.e., the speed of the gas). It is clear that the curve has a maximum around 6 L/min, which was observed for all lasers of this size. As we will see later, the optimum flux depends on the size of the laser.

The first measurements considered the difference in output between the two ends of the laser. Of course, in the event of the whole idea of the parabola being wrong, the two ends must have almost the same energy output. As can be seen in the same graph for the pressure, 6.2 on the following page, on average the low end[1] has half of the energy of the high one. but this ratio is

[1]With high and low end I mean respectively the end with the highest energy output and the end with the lowest one.

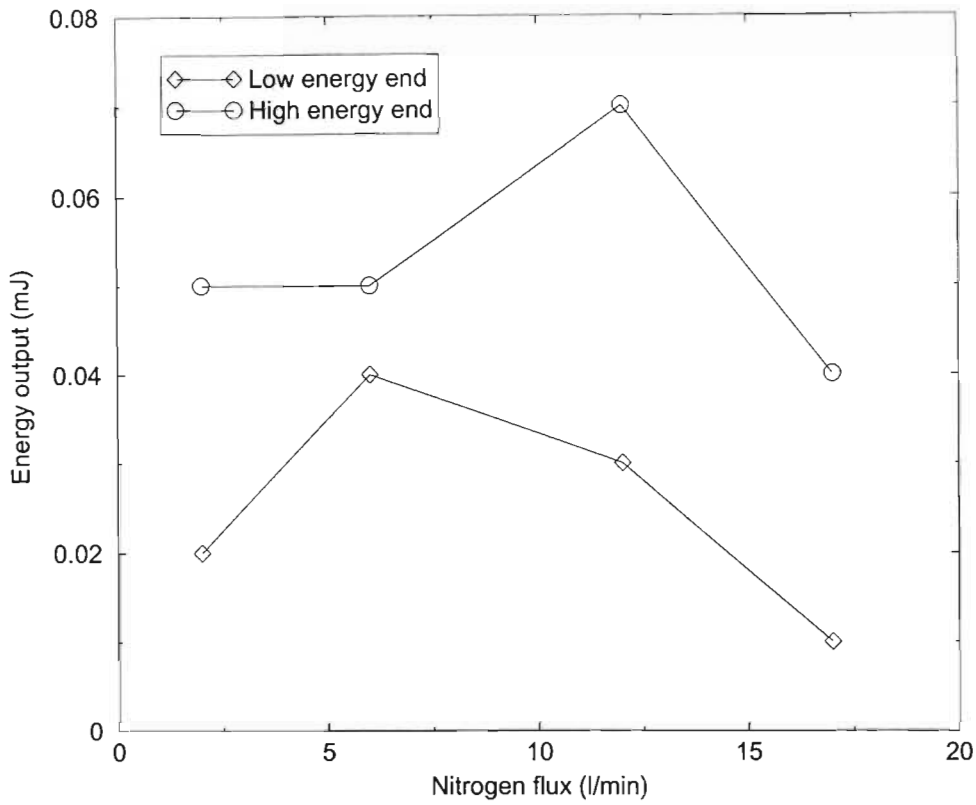

Graph 6.2: Energy versus nitrogen flux in a parabolic nitrogen laser. The flux was measured with a flux-meter connected between the gas cylinder and the laser.

sensitive to the configuration of the laser and can be optimised.

The first parabola we made had a total measured capacity of 13.13 nF, and was used with to a power supply capable of delivering up to 17 kV. Using an electrodes separation of 2 mm, the output with a nitrogen flux of 6 L/min, the best output we could obtain from the laser was 0.1 mJ, twice as much as with the normal square laser. It has to be noted that we did not optimise the electrodes separation.

With a nitrogen flux of 6 L/min, the output from the high energy end was 0.107 ± 0.002 mJ. From the high energy end, the output was less than half of that, 0.039 ± 0.001 mJ, averaged over 10 shots. From these numbers we can calculate the efficiency of the laser. Considering that the total energy stored in the capacitor was 1.897 J, the efficiency is $5.6 \cdot 10^{-5}$ for the high energy end.

After this results, a bigger laser was made, with a total capacity of 47.5 nF and an electrode length of 35 cm. In this case, the highest output was obtained with the smallest measurable nitrogen flux, which was 2 L/min. The high energy end output, averaged over ten shots, was 0.265 ± 0.001 mJ, and the low energy end output was 0.122 ± 0.004 mJ. In the case of this laser, the efficiency at the high energy end was lower, $3.8 \cdot 10^{-5}$.

The graph 6.3 on page 182 shows the energy output as a function of the nitrogen flux. In the case of the big laser, it is clear that the best results are obtained with the slowest possible flux and that the output can be improved with a different flux regulator.

The next laser we made has almost the same capacity, 48.4 nF, but was built in a way to maximise the area of the parabola itself, reducing the other side of the capacitor. The area of the parabola was in fact 4949 cm^{-2}, instead of the 3200 cm^{-2} of the previous case. In principle, the expected output would be the same, considering that they store the same amount of energy. The output from the high energy end was in this case higher than before, 0.30 ± 0.01 mJ, with a peak of 0.35 mJ. It in interesting to point out

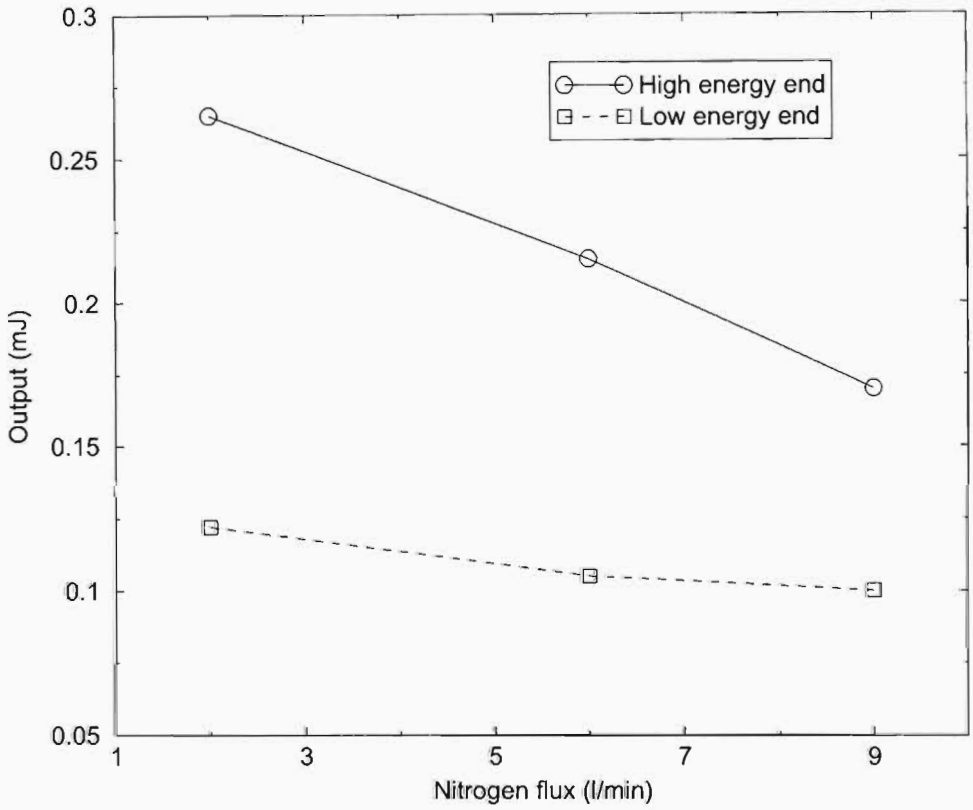

Graph 6.3: Energy versus nitrogen flux in the big parabolic nitrogen laser

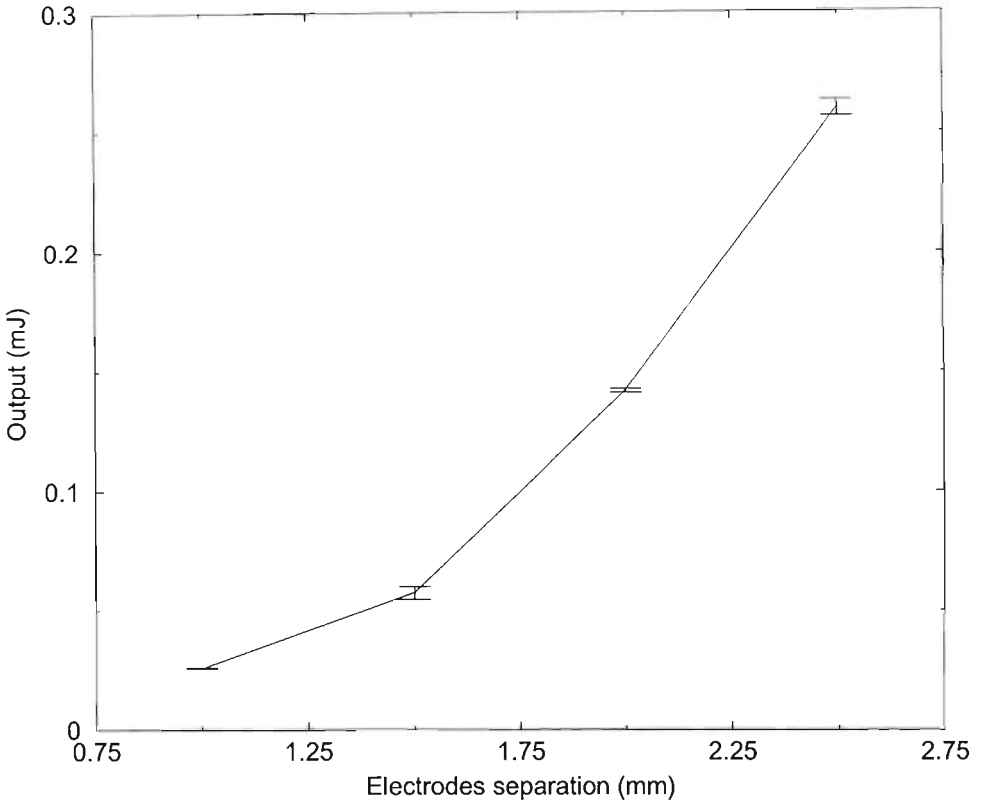

Graph 6.4: Energy versus electrodes separation for a big parabolic laser

that the output from the lower end was in this case 0.075 ± 0.005 mJ, only 25% of the high end, the best ratio that we had. Even the efficiency was higher, $4 \cdot 10^{-2}$, which is a very good result for a gas laser. Again, in this case, the energy can be improved by using a slower nitrogen flux.

The graph 6.4 on page 183 shows the dependence of the output, for the last parabolic laser on the separation between the electrodes. In this case, the separation can be increased, thanks to the improved energy stored in the laser itself. Increasing the channel increases the volume of active medium

allowing more energy to be extracted from the laser. At a separation greater that 2.5 mm, the discharge becomes uneven and no laser emission is observed. In this case, the energy is not enough to ionise uniformly the active medium.

The last experiment was done using a different kind of electrodes, closed in a pipe to allow the nitrogen flux to be at low pressure. In this case, using the last parabola, the energy output from the high end was 0.097 ± 0.002 mJ, but that from low end was only less than 0.01 mJ, less than 10% of the high end. The low pressure solution, even if it leads to an energy loss of 40%, offers another practical advantage, because the acoustic noise of the discharge is greatly reduced (sensed physiologically).

6.2 Multilayer laser

Another idea we tried, is to use a multilayer laser, with more than one capacitor connected in parallel directly to the electrodes in order to increase the stored energy. Even though the principle is easy, making the actual laser proved to be a challenge. The problem is how to connect the capacitors in such a way not to increase the impedance and slow down the energy transfer to the nitrogen. After much thinking and several attempts, we built a laser as shown in figure 6.7 on page 185. In this case, on one side of the laser, and only one, there are many layers, the bottom one made normally out of copper, the other ones made with aluminium foil. In order to avoid arcs between the layers, between each one there is an insulating layer (mylar). In our lasers,

we had the high voltage sides of the capacitors compressed together below the electrode. The ground layers where connected to the bottom of the laser, simply by folding them around it.

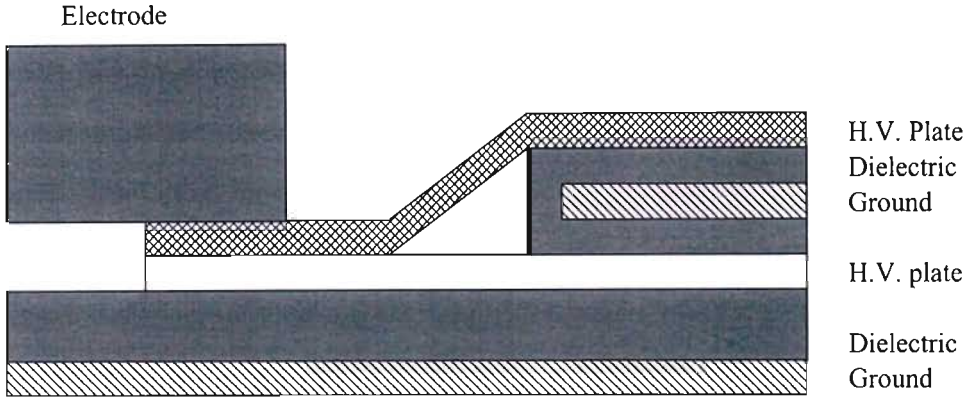

Figure 6.7: Cross section of the multilayer nitrogen laser.

This laser creates new problems, the main one being the fact that sometimes the dielectric between the two copper sheets gets burned and develops a hole. In this case, all the energy goes into the hole and the laser can't fire anymore. Other problems arise trying to use a triggerable spark gap, instead of a free running one. In this case, apart from the troubles in setting up a multilayer spark gap, after a while the discharge digs a hole through the dielectric itself, and become free to fire regardless of the trigger signal. We are not able to estimate the average life of one of these devices, but it is not very long.

The laser as we made it suffers from another problem. Because the layers are not compressed, the electrical forces move them and suck air in, decreas-

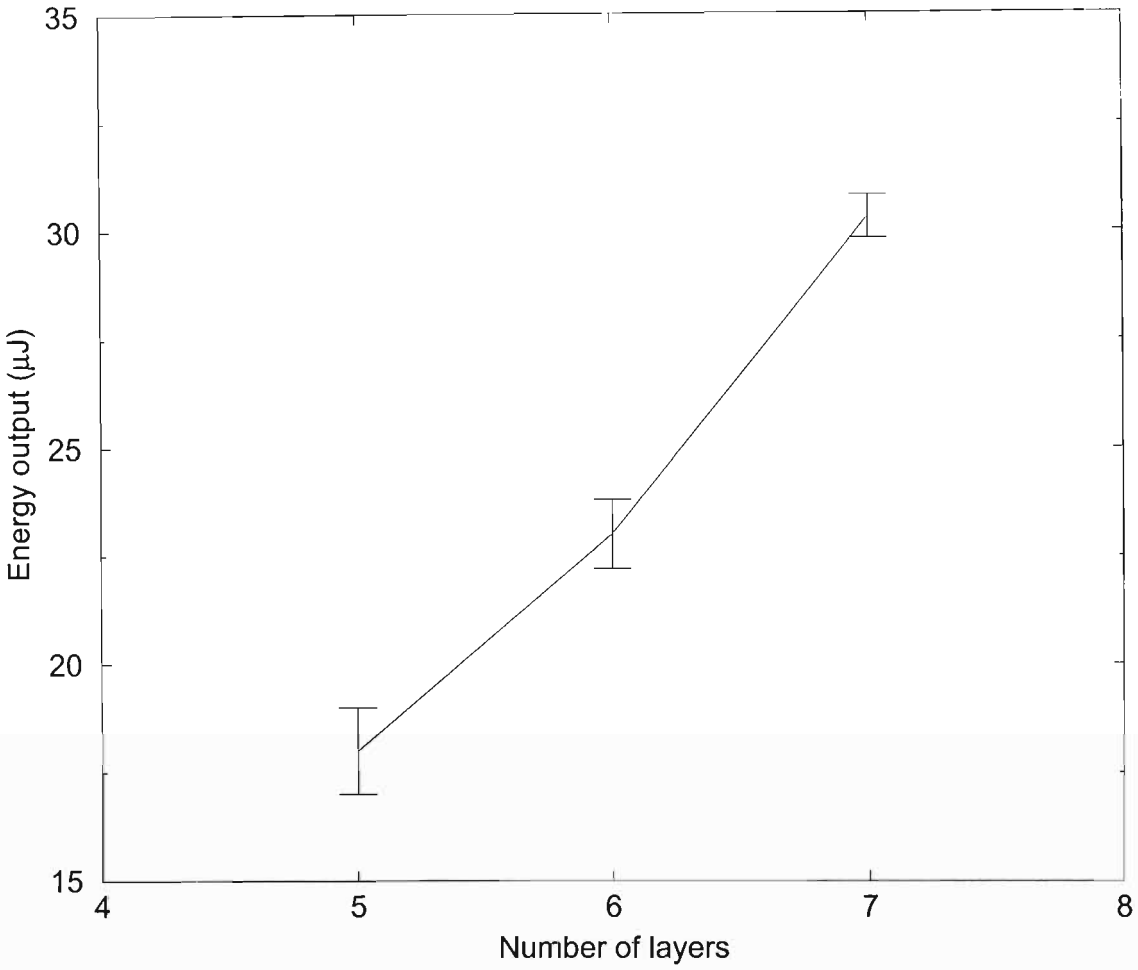

Graph 6.5: Output for a multilayer square laser.

ing the total capacity and hence the energy output.

The graph 6.5 on page 186 shows the results for a multilayer laser, as a function of the number of the layers. The data are obtained averaging the first ten shots, before the energy decreases too much (by a factor of around 3). As an be seen, the graphs proves that the multilayer idea really increases

the output. Going to a higher number of layers proved to be impossible for us, because electrical losses prevented the capacitor from getting fully charged and there was no laser output.

In conclusion of this section, the making of the standard single layer laser is quite simple, especially for the conventional square type: we used a mask to cover the parts of the sheet where we want to erase the copper. The mask is made out of a thick mylar sheet (200 μm). Spray paint is then applied to cover the regions where the copper will remain. Once the mask is removed, the board can be etched.

Chapter 7

Simulations

In order to understand better our results, some simulations were done, not of the shock-waves themselves, but of the effects of them on the laser light. A ray tracing program called LightPipes, from Oko Technologies[1], which has been released for free in April 1998 was used. This is a powerful tool, which allows simulation the propagation of a laser beam through many different optical elements, including any three-dimensional distribution of refractive index and absorption coefficient. The refractive index matrices were created with a series of small programs written in Fortran77 or Perl.

A big difference between the actual experiment and the simulation is that the former allows us, in different shots, to study the temporal evolution of the shocks. During the experiment we take many images with different

[1]P.O. Box 581, 2600 AN, Delft The Netherlands, Tel: +31-62-2794647, Fax: +31-15-2574233, E-mail: oko@okotech.com, Web site: www.okotech.com

delays to see how they evolve at a certain precise distance from the device. In the case of the simulation, we can decide to freeze the shock waves in a certain position and configuration, and move the screen to see how the image evolves with the propagation of the laser beam. This could be done in principle during the experiment too, but would require too many images and the behaviour of the shocks is not reliable enough. The optical scheme used for the simulation (see figure 7.1 on page 189) is simpler than the actual one of the experiment.

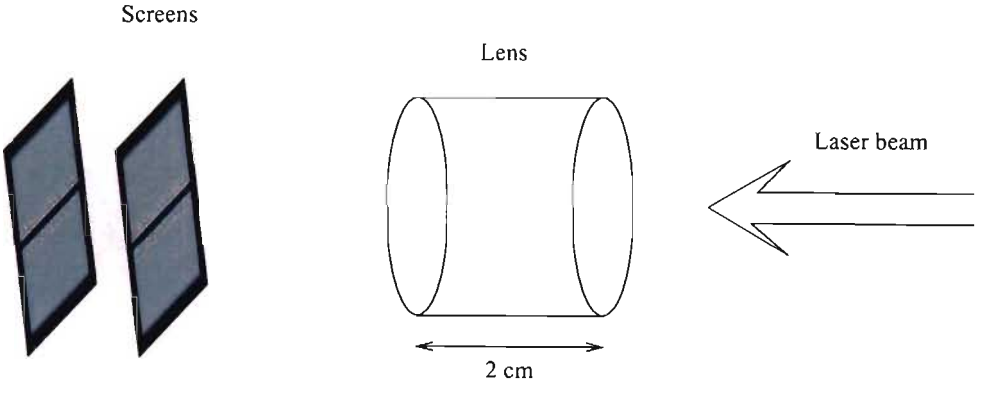

Figure 7.1: The simple optical scheme used for the ray tracing.

With LightPipes, only perfect Gaussian beams can be used. Our nitrogen laser beam is very different from a Gaussian beam, but the results of the ray tracing are important to understand what kind of image a gas structure can generate.

7.1 Ray tracing

The LightPipe ray tracing program offers three different methods for the propagation of the beam. Among them, only one is suitable for our simulation because it allows one to input a complex three-dimensional distribution of both the refractive index and the absorption coefficient; the latter is not of interest for our calculations.

For the calculation, the propagation of a field U in a medium with a complex refractive coefficient $A(x, y, z)$ is described by the differential equation

$$\frac{\partial^2 U}{\partial x^2} + \frac{\partial^2 U}{\partial y^2} + 2ik\frac{dU}{dx} + A(x, y, z)U = 0 \tag{7.1}$$

This equation can be written as a system of finite difference equations:

$$\frac{U^{h+1}_{i+1,j} - 2U^{h+1}_{i,j} + U^{h+1}_{i-1,j}}{(\Delta X)^2} + \frac{U^{h}_{i,j+1} - 2U^{h}_{i,j} + U^{h}_{i,j-1}}{(\Delta Y)^2} + 2ik\frac{U^{h}_{i,j} - 2U^{h}_{i,j}}{\Delta x} + A^{h+1}_{i,j}U^{h+1}_{i,j} = 0 \tag{7.2}$$

By collecting the terms it is possible to obtain a standard three-diagonal system of linear equations, which solution describes the complex amplitude of the light field in the layer $Z + \Delta Z$ as a function of the field defined in the layer Z:

$$-a_i U^{h+1}_{i-1+j} + a_i U^{h+1}_{i,j} - b_i U^{h+1}_{i+1,j} = f_i \tag{7.3}$$

where, with $\Delta X = \Delta Y = \Delta$:

$$a_i = b_i = -\frac{1}{\Delta^2} \tag{7.4}$$

$$a_i = A_{i,j}^{h+1} - \frac{2}{\Delta^2} + \frac{2ik}{\Delta Z} \tag{7.5}$$

$$f_i = \frac{2ik}{\Delta Z} U_{i,j}^h - \frac{U_{i,j+1}^h - 2U_{i,j}^h + U_{i,j-1}^h}{\Delta^2} \tag{7.6}$$

The linear system 7.3 can be solved using the method described in [3]. This scheme is absolutely stable (this variant is explicit with respect to the index i and implicit with respect to the index j). One step of propagation is divided into two sub-steps: the first sub-step applies the described procedure to all rows of the matrix, the second sub-step changes the direction of elimination and the procedure is applied to all columns of the matrix.

The main advantage of this approach is the possibility to take into account uniformly diffraction, absorption (amplification) and refraction. For example, the model of a waveguide with complex three-dimensional distribution of refraction index and absorption coefficient (both are defined as real and imaginary components of the (three-dimensional in general) matrix $A_{i,j}^h$ can be built easily.

This propagation method is implemented in the *step* routine of LightPipes.

A second propagation method is used after the arbitrary distribution of refractive index for the propagation into the far field. In this case, LightPipes offers the routine *forvard*, which performs a FFT propagation (spectral method).

Let us consider the wave function U in two planes: $U(x, y, 0)$ and $U(x, y, z)$. Let us also suppose that $U(x, y, z)$ is the result of the propagation of $U(x, y, 0)$

to the distance z, with the Fourier transforms of these two (initial and propagated) wave functions given by $A(\alpha, \beta, 0)$ and correspondingly $A(\alpha, \beta, x)$.. In the Fresnel approximation, the Fourier transform of the diffracted wave function is related to the Fourier transform of the initial function via the frequency transfer characteristic of the free space $H(\alpha, \beta, x)$, given by[30] and [66]:

$$H = \frac{A(\alpha, \beta, x)}{A(\alpha, \beta, 0)} = \exp(-ikz(1 - \alpha^2 - \beta^2)^{1/2} \tag{7.7}$$

where

$$A(\alpha, \beta, 0) = \int\int_{-\infty}^{\infty} U(x, y, 0) \exp(-ik(\alpha x + \beta y))dxdy \tag{7.8}$$

$$A(\alpha, \beta, z) = \int\int_{-\infty}^{\infty} U(x, y, z) \exp(-ik(\alpha x + \beta y))dxdy \tag{7.9}$$

The last three expressions provide a symmetrical relation between the initial and diffracted wave functions in the Fresnel approximation. Applied in the order 7.8 $\Rightarrow$ 7.7 $\Rightarrow$ 7.9 they result in the diffracted wave function, while being applied in the reversed order they allow for reconstruction of the initial wave function from the result of diffraction. We shall denote the forward and the reversed propagation operations defined by the last three expressions with operators L^+ and L^- respectively.

The described algorithm can be implemented numerically using Fast Fourier Transform (FFT)[66][4] on a finite rectangular grid with periodic border conditions. It results in a model of beam propagation inside a rectangular waveguide with reflective walls. To approximate a free-space propagation, wide

empty guard bands have to be formed around the wave function defined on a grid. To eliminate the influence of the finite rectangular data window, Gaussian amplitude windowing in the frequency domain should be applied. The simplest and fastest LightPipes command for propagation is forvard. It implements the spectral method described by 7.7, 7.8 and 7.9.

In our case, we used the *step* routine for the propagation through the device, i.e., the shocks, and the *forvard* routine for the propagation in the far field.

7.2 Shock shape

The first problem to solve, not knowing the actual shape of the shock is to make some reasonable assumption about it, and compare the ray-tracing results with the experimental images. This procedure applies not only to the shock shape, but also to its peak pressure, which is not known.

The shapes used are quite simple and consist of two half sines with different periods, in order to model the front of the shock steeper than the tail. The different shapes are shown in figure 7.1 on page 194.

As could be expected, the best results are obtained using the profile with the steepest front, as can be seen in figures 7.2 on page 195 and 7.3 on page 196. In fact, judging by the speed of the shocks, which is well above the speed of sound, the profile cannot be a broad one. In the images, the fringes coming from the side of the field of view are due to reflection from the light

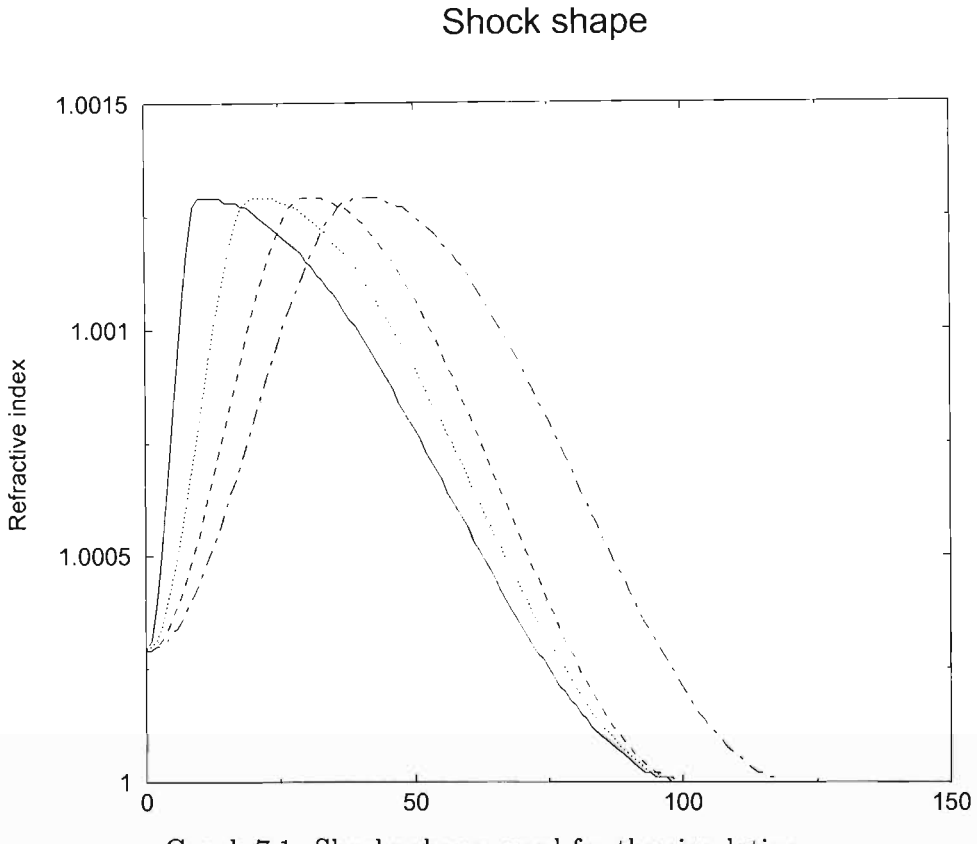

Graph 7.1: Shocks shapes used for the simulation.

guide the program uses for the propagation. Even if there is a *built in* filter which cuts 90% of the light close to the border, there is enough to interfere with the propagating beam. This problem can be solved by using a smaller grid, but at the expenses of the precision (or increasing the resolution, which would lead to a much longer computational time).

A shock with a tail, that could be expected for the actual experiment, does not give a good results. Probably, in our case the explosion is so sharp that we have a very sharp shock.

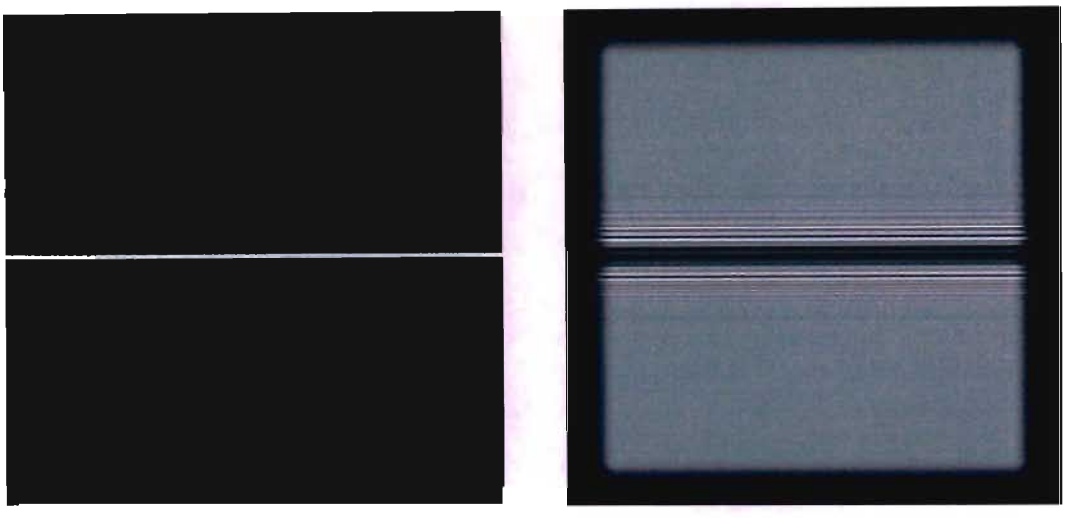

Figure 7.2: The results of the simulation, for a shock 1 mm wide and a grid of 10 mm. In this case, the profile of the shock is the first one of the graph 7.1 on page 194, with the steeper front. The picture on the left is the input matrix of the refractive index, the one on the right shows the result of the ray tracing 50 0cm after the pipe. The shock is travelling from the top to the bottom.

Then, we still have a free parameter, which is the pressure of the shock. Again, using the first profile, I tried different pressures (i.e. refractive index) to see which one compare the best with the images.

The next step in the simulation, not having a proper simulation of the shocks, we went on with the simulation of a perfect circle made using the same shock profile of before. In this case, we have some sort of a lens, which can be used to predict the results of the experiment, and not only to understand them. The results of this work are still very preliminary and, although interesting, are not included in this thesis.

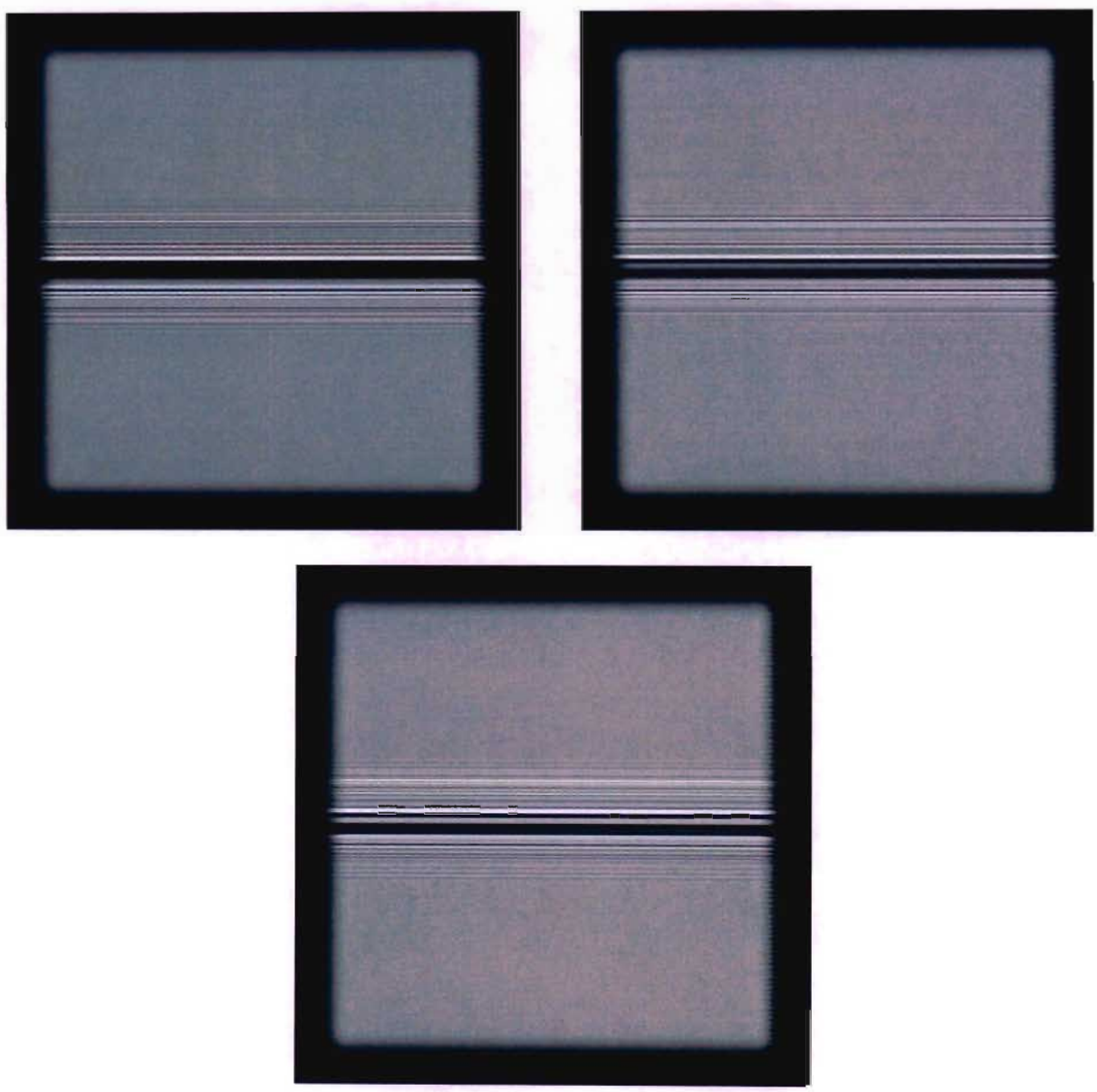

Figure 7.3: The results of the simulation with the other shapes for the shock. Clockwise, the shapes are the second, third and fourth of the graph 7.1 on page 194

Chapter 8

Conclusions

Astronomy, as probably just any other science, has seen a real revolution in the last few tens of years. The result is nothing less than a rather deep change in the way people try to understand our universe. At the beginning, astronomy was just a way of studying how planets and other different bodies move, basically in order to measure the flowing of time, the calendar. This is what astronomy has been for a few thousands years. Much more recently, the focus has moved to the understanding of the object themselves and their structure. This is no longer astronomy, but astrophysics. Among the results of this new science, we can mention the discovery of what happens in the Sun, the energy source of the Solar System. But both astronomy and astrophysics are very similar in the way they hunt for their data, i.e. by observing objects that are almost always very distant. Now these observations concern the whole electromagnetic

spectrum, but there is still a limit on what can be inferred on objects that can be millions of light years away. But now astrophysics seems to be moving toward a different phase, where many data will come from the laboratory. This new era has been opened up by big lasers. By means of these lasers matter can be compressed to densities approaching those of white dwarfs, opening a window to study these objects in a laboratory.

Other interesting experiments have tried to create molecular clouds in a terrestrial laboratory, to study the formation of organic compounds. In this case, the simulation is much simpler than in the case of ultra high pressure matter. In fact, some of these experiments have already led to the creation of compounds like amino-acids ([31]). These experiments have profound implications in other fields, apparently very far from astrophysics. According to many scientists, the real origin of life on the Earth should be looked for in space, and not in hydrothermal vents or other earthly places. The theory, first proposed by Fred Hoyle in 1981[28] has a still growing support from the scientific community. In any case, the understanding of the chemistry of these clouds is very important on its own.

But there are astronomical observations that might have several strong links with part of the laboratory work described in this thesis. One of the most intriguing mysteries of the universe is the observation of ultra high energy cosmic rays. They are particles that smash into our atmosphere with incredible energies of over 10^{20} eV and where observed for the first time in 1962[43]. More recently, the first result of the AMANDA neutrino detec-

tor, presented by Francis Halzen at the International Astronomical Union, July 15, 2003, clearly hints the presence of some sort of cosmic accelerator. It is interesting to note that, among the many proposed explanations, few involve the most impressive explosion of the universe and their relativistic blast waves[71]. These are the Gamma Ray Burst, first observed in 1969 by the Vela 5a and Vela 5b satellites[62]. These bursts are observed daily and come from the deepest cosmic spaces. They have probably at least two different sources, one being almost normal supernovas and the other being collisions and merging between exotic objects like pulsars and black holes. Again, the mechanisms behind all these accelerators might very well be understood by studying similar mechanisms for earthly accelerators. Recent results[7], already described in chapter 2 on page 54, do indeed prove that similar accelerators work.

Well, what is then the point behind this thesis? More than one. The first one is the idea that even the gas structures studied in our little laboratory might one day be discovered in space. As the mathematicians often devise structures that are discovered in nature many decades later. So our gas structures could be the key to understand complex structures like those of planetary nebulae (see 1.6.4 on page 37).

The second point is that, although plasma based accelerators are far from reaching the energy levels of the traditional ones, there is enormous growth potential[39] for laser driven accelerators. In fact, the energy level achieved with these machines has increased by an order of magnitude every *five years*.

In particular, by the Ecole Polytechnique in France, an experiment with the Laser Wakefield Accelerator scheme has achieved a 200 MeV peak energy in less than 1 mm. This raises the point of the major limit of these experiments, that is the length of the acceleration achievable by mean of gas jets. All the laser driven acceleration scientists agree that some method of extending the interaction length between the laser beam and the plasma must be found. Possibly the most popular method is a discharge in a solid state capillary. This discharge automatically generates a hollow plasma density profile. Unfortunately the solid state capillaries can only be used for a limited number of shots. We have proved that shock waves can form wall-less capillaries with the right density profile over a distance of several centimetres. The hope is that this technique, described in chapter 4 on page 89, might one day advance this promising and exciting field.

Wall-less capillaries might also find an application in EUV sources for the next generations lithography. At the moment, there still two competing sources for this application, namely laser produced plasmas and capillary discharges. The main disadvantages of the latter, the limited time life of solid capillaries and the debris coming from their erosion, would be both solved by my wall-less capillary.

We have also demonstrated that the aperture of the colliding shock lens can be scaled up to the centimetric range, albeit at considerable energetic expense. In the past it had been predicted that such devices could not reach a size larger than the physical thickness of the shock[44][60], i.e. about two

millimetres. A centimetric CSL has a large number of potential applications, as do wall-less capillaries.

All in all colliding shocks structures are full of research and industrial promise.

Bibliography

[1] R. Buccellato, M.M. Michaelis, A. Prause and P.F. Cunningham. Pulsed gas lenses. *Optics & Laser Technology*, 25(4):247–250, 1993.

[2] A. Pukhov and J. Meyer-Ter-Vehn. Relativistic magnetic self-channeling of light in near-critical plasma: Three-dimensional particle-in-cell simulation. *Physical Review Letters*, 76:3975–3978, 1996.

[3] A.A. Samarskii and E.S. Nikolaev. *Numerical Methods for Grid Equations*, chapter Direct methods. Birkhäuser Verlag, 1989.

[4] A.E. Siegman and E.A. Sziklas. Mode calculations in unstable resonators with flowing saturable gain: 2. fast fourier transform method. *Applied Optics*, 14:1874–1889, 1975.

[5] J.M. Beckers. Adaptive optics for astronomy: Principles, performance, and applications. *Ann. Rev. Astron. Astrophys*, 31:13–62, 1993.

[6] Bernard Fay. Advanced optical lithography development, from uv to euv. *Microelectronic Engineering*, 61-62:11–24, 2002.

[7] Robert Bingham. Accelerator physics: In the wake of success. *Nature*, 424:258 – 259, 2003.

[8] R. Buccellato. *Refractive Effects in Phase Objects and Associated Phenomena*. PhD thesis, University of Natal, Durban, South Africa, 1994.

[9] E.D. Courant, C. Pellegrini and W. Zakowicz. High-energy inverse free-electron-laser accelerator. *Physical Review A*, 32(5):2813–2823, November 1985.

[10] C. Coverdale et al. Propagation of intense subpicosecond laser pulses thtough underdense plasmas. *Physical Review Letters*, 74:4659, 1995.

[11] C.E. Clayton et al. Relativistic plasma-wave excitation by collinear optical mixing. *Physical Review Letters*, L54:2343, 1985.

[12] C.G.R. Geddes, Cs. Toth et al. High-quality electron beams from a laser wakefield accelerator using plasma-channel guiding. *Nature*, 431(7008):538–541, September 2004.

[13] D. Gordon et al. Observation of electron energies beyond the linear dephasing limit from a laser-excited relativistic plasma wave. *Physical Review Letters*, 80:2133–2136, 1998.

[14] D. Korobkin et al. Soft x-ray amplification at 26.2 nm with 1 Hz repetition rate in a table-tob system. *Physical Review Letters*, 82:1607, 1998.

[15] H.M. Milchberg et al. Development and applications of a plasma waveguide for intense laser pulses. *Physics of Plasmas*, 3:2149, 1996.

[16] J. Faure, Y. Glinek et al. A laser-plasma accelerator producing monoenergetic electron beams. *Nature*, 431(7008):541–544, September 2004.

[17] J.J. Rocca et al. Demonstration of a discharge pumped table-top soft-x-ray laser. *Physical Review Letters*, 73:2192–2195, 1994.

[18] K. Nakajima et al. A proof-of-principle experiment of laser wakefield acceleration. *Physica Scripta*, T52:61–64, 1994.

[19] K. Nakajima et al. Observation of ultrahigh gradient electron acceleration by a self-modulated intense short laser pulse. *Physical Review Letters*, 74:4428, 1995.

[20] P. Monot et al. Experimental demonstration of self-channeling of a multiterawatt laser pulse in an underdense plasma. *Physical Review Letters*, 74:2953, 1995.

[21] R. Wagner et al. *Advanced Accelerator Concepts*. AIP Press, New York, 1997.

[22] R. Wagner et al. Electron acceleration by a laser wakefield in a relativistically self-guided channel. *Physical Review Letters*, 78:3125, 1997.

[23] S.P.D. Mangles, C.D. Murphy et al. Monoenergetic beam of relativistic electrons from intense laser-plasma interactions. *Nature*, 431(7008):535–538, September 2004.

[24] S.V. Lebedev, J.P. Chittenden, S.N. Bland, D.J. Ampleford et al. Effect of discrete wires on the implosion dynamics of wire array z-pinches. In *AIP Conference Proceedings*, volume 651, pages 65–70. AIP, AIP, 2002.

[25] S.Y. Chen et al. Evolution of a plasma waveguide created during relativistic-ponderomotive self-channeling of an intense laser pulse. *Physical Review Letters*, 80:2610–13, 1998.

[26] W.D. Kimura et al. Detailed experimental results for laser acceleration staging. *Physical Review Special Topics - accelerators and beams*, 4(101301):1–12, October 2001.

[27] Y. Kitagawa et al. Beat-wave excitation of plasma wave and observation of accelerated electrons. *Physical Review Letters*, 68:48, 1992.

[28] F. Hoyle and N.C. Wickramasinghe. *Evolution from Space.* Simon and Schuster, New York, 1981.

[29] A. Forbes. *Photothermal Refraction and Focusing.* PhD thesis, University of Natal, Durban, South Africa, 1997.

[30] J.W. Goodman. *Introduction to Fourier Optics.* McGraw-Hill, 1968.

[31] M.P. Bernstein, J.P. Dworkin, S.A. Sandford, G.W. Cooper, and L.J. Allamandola,. Racemic amino acids from the ultraviolet photolysis of interstellar ice analogues. *Nature*, 416:401–403, 2002.

[32] L.R. Harriott. Next generation lithography. *Materials Science in Semiconductor Processing*, 1(2):93–97, September 1998.

[33] W.J. Humphreys. *Physics of the Air.* McGraw-Hill, New York, third edition edition, 1940.

[34] G.J. Tallents, J. Krishnan, L. Dwivedi, D. Neely, I.C.E Turcu. Film calibration for soft x-ray wavelengths. In George A. Kyrala, Jean-Claude J. Gauthier, editor, *Applications of X Rays Generated from Lasers and Other Bright Sources*, volume 3157, pages 281–190. SPIE, 1996.

[35] Igor Yevgenyevich Tamm and Andrei Sakharov. *Plasma physics and the problems of controlled thermonuclear reactions*, volume 1, chapter Theory of a magnetic thermonuclear reactor. Pergamon Press, Oxford, 1961.

[36] M.M. Michaelis, P.F. Cunningham, R. Cazalet, J.A. Waltham and M. Notcutt. Gas lens applications. *Laser and Particle Beams*, 9:641–655, 1991.

[37] C. Joshi, T. Tajima, J.M. Dawson. Forward raman scattering and electron acceleration. *Physical Review Letters*, 47:1285, 1981.

[38] J.M. Pernter and F.M. Exner. *Meteorologische Optik*. Wilhelm Braumller, Wien und Leipzig, second edition edition, 1922.

[39] Joshi Chandrashekhar and Thomas Katsouleas. Plasma accelerators at the energy frontier and on tabletops. *Physics Today*, pages 47–53, June 2003.

[40] M. Kuppen. *On the Interaction of Laser Beams with Air*. PhD thesis, University of Natal, Durban, South Africa, 1996.

[41] J.D. Lawson. Lasers and accelerators. *IEEE Trans. Nucl. Sci.*, NS-26:4217, 1979.

[42] L.C. Johnson and T.K. Chu. Measurements of electron density evolution and beam self-focusing in a laser-produced plasma. *Physical Review Letters*, 32:745, 1974.

[43] J. Linsley. Evidence for a primary cosmic-ray particle with energy 10^{20}eV · *Physical Review Letters*, 10:146–148, 1963.

[44] N. Lisi. Private communications.

[45] N. Lisi. *Optical Properties and Laser Applications of Non-Uniform Gas Distributions*. PhD thesis, University of Natal, Durban, South Africa, 1995.

[46] N. Lisi, M.M. Michaelis, R. Buccellato, M. Kuppen and A. Prause. The colliding shock lens as an intracavity q-switch. *Applied optics*, 6(34):942–945, 1995.

[47] M.M. Michaelis, M. Notcutt and P.F. Cunningham. Drilling by gas lens focused laser. *Optics Communications*, 5(59):369–374, 1986.

[48] R.S. Mackay. The future of lithography after 193 nm optics. *Microelectronic Engineering*, 41-42:71–74, March 1998.

[49] M.M. Michaelis and C.R. Phipps. Private communications.

[50] J.A. Waltham, P.F. Cunningham, M.M. Michaelis and M. Notcutt. The application of the refractive fringe diagnostic to shocks in air. *Optics & Laser Technology*, 19(4):203–208, 1987.

[51] R.S. Kunabenchi, M.R. Gorbal and M.I. Savadatti. Nitrogen lasers. *Progress in Quantum Electronics*, 9(4):259–329, 1984.

[52] M.M Michaelis, M. Kuppen, G. Turner, A.C.K. Mahlase, A.R. Prause, A. Conti, N. Lisi. Limitations and applications or the colliding shock lens. In *High Power Laser Ablation*, volume 3343, pages 228–241. SPIE, April 1998.

[53] M.M. Michaelis, M. Kuppen, A. Prause, N. Viranna and N. Lisi. Progress with gas lenses. *Laser and Particle Beams*, 3(14):473–485, 1996.

[54] M. Notcutt. *Gas Lenses.* PhD thesis, University of Natal, Durban, South Africa, 1989.

[55] M. Notcutt, J.A. Waltham, M.M. Michaelis, P.F. Cunningham and R. Cazalet. Gas lens laser-produced plasma. *Applied Optics*, 28(13):2464–2465, 1989.

[56] M. Notcutt, M.M. Michaelis, P.F. Cunningham and J.A. Waltham. Spinnig pipe gas lens. *Optics and Laser Technology*, 20(5):243–250, 1988.

[57] M.M. Michaelis, C.A. Dempers, M. Kosch, A. Prause, M. Notcutt, P.F. Cunningham and J.A. Waltham. A gas-lens telescope. *Nature*, (353):547–548, October 1991.

[58] A. Prause. *Applications of Optical, Plasma and Laser Focusing.* PhD thesis, University of Natal, Durban, South Africa, 1994.

[59] R. Buccellato and M.M. Michaelis. Colliding shock gas lens. *Optics Communications*, 101:350–355, 1993.

[60] M. Kuppen, M.M. Michaelis, R. Buccellato and N. Lisi. Scaling up the colliding shock lens. *Review Scientific Instruments*, 9(66):5037ff, 1995.

[61] M.M. Michaelis, N. Lisi, R. Kuppen, R. Buccellato and A. Prause. Applications of the colliding shock lens. *Laser and Particle Beams*, 12(3):001–008, 1994.

[62] R.W. Klebesadel, I.B. Strong, R.A. Olson. Observations of gamma-ray bursts of cosmic origin. *Astrophysical Journal*, 182, L85, 1973.

[63] R.P. Feynman, R.B. Leighton and M.L. Sands. *They Feynman Lectures on Physics*, chapter 29. Addison-Wesley, Massachussets, 1964.

[64] M. Bacon, R.N. Campbell and M.M. Michaelis. Refractive fringe diagnostics of sparks in air. *Journal of Applied Physics*, 66(3):1075–1079, 1989.

[65] G.S. Sarkisov-1999. Self focusing, channel formation and high energy ion generation in interaction of an intense short laser pulse with a he jet. *Physical Review E*, 59(6):7042–7054, June 1999.

[66] W.H. Southwell. Validity of the fresnel approximation in the near field. *J. Opt. Soc. Am.*, 71:7–14, 1981.

[67] Lyman Spitzer. The stellarator concept. *Physics of Fluids 1*, (253), 1958.

[68] T. Tajima and J.M. Dawson. Laser electron accelerator. *Physical Review Letters*, 43:267–270, 1979.

[69] Wolfgang Arden. Review key challenges. *Materials Today*, 6(5):40–44, May 2003.

[70] P. Woodward. A method of calculating the field over a plane aperture required to produce a given polar diagram. *J. IEEE*, 93:1554–1558, 1947.

[71] Y.A. Gallant and A. Achterberg. Ultra-high-energy cosmic ray acceleration by relativistic blast waves. *Monthly Notices of the Royal Astronomical Society*, 305, 1999.